

DEVELOPMENT AND CONTROL OF A SINGLE ROD ELECTRO  
HYDROSTATIC ACTUATOR

A THESIS SUBMITTED TO  
THE GRADUATE SCHOOL OF NATURAL AND APPLIED SCIENCES  
OF  
MIDDLE EAST TECHNICAL UNIVERSITY

BY

HAKAN ÇALIŞKAN

IN PARTIAL FULFILLMENT OF THE REQUIREMENTS  
FOR  
THE DEGREE OF DOCTOR OF PHILOSOPHY  
IN  
MECHANICAL ENGINEERING

SEPTEMBER 2015



Approval of the thesis:

**DEVELOPMENT AND CONTROL OF A SINGLE ROD ELECTRO  
HYDROSTATIC ACTUATOR**

submitted by **HAKAN ÇALIŞKAN** in partial fulfillment of the requirements for the degree of **Doctor of Philosophy in Mechanical Engineering Department, Middle East Technical University** by,

Prof. Dr. Gülbin Dural Ünver  
Dean, Graduate School of **Natural and Applied Sciences**

\_\_\_\_\_

Prof. Dr. Tuna Balkan  
Head of Department, **Mechanical Engineering**

\_\_\_\_\_

Prof. Dr. Tuna Balkan  
Supervisor, **Mechanical Engineering Dept., METU**

\_\_\_\_\_

Prof. Dr. Bülent E. Platin  
Co-Supervisor, **Mechanical Engineering Dept., METU**

\_\_\_\_\_

**Examining Committee Members:**

Prof. Dr. Samim Ünlüsoy  
Mechanical Engineering Dept., METU

\_\_\_\_\_

Prof. Dr. Tuna Balkan  
Mechanical Engineering Dept., METU

\_\_\_\_\_

Prof. Dr. Yücel Ercan  
Mechanical Engineering Dept., TOBB ETU

\_\_\_\_\_

Assoc. Prof. Dr. Yiğit Yazıcıoğlu  
Mechanical Engineering Dept., METU

\_\_\_\_\_

Assist. Prof. Dr. S. Çağlar Başlamışlı  
Mechanical Engineering Dept., Hacettepe University

\_\_\_\_\_

**Date:**

11.09.2015

**I hereby declare that all information in this document has been obtained and presented in accordance with academic rules and ethical conduct. I also declare that, as required by these rules and conduct, I have fully cited and referenced all material and results that are not original to this work.**

Name, Last name : Hakan ÇALIŞKAN

Signature :

## **ABSTRACT**

### **DEVELOPMENT AND CONTROL OF A SINGLE ROD ELECTRO HYDROSTATIC ACTUATOR**

Çalışkan, Hakan

Ph.D., Department of Mechanical Engineering

Supervisor: Prof. Dr. Tuna Balkan

Co-Supervisor: Prof. Dr. Bülent E. Platin

September 2015, 276 pages

In this thesis a variable speed pump controlled electro hydrostatic drive system for a single rod actuator is developed. The problem of the single rod actuator in hydrostatic applications is the differential flow rate which is formed due to the asymmetric structure of the piston rod assembly. The hydraulic circuit solutions proposed in the literature commonly suffer from undesired pressure oscillations, which are named as system internal instability. This thesis, addresses the stability problem of the pump controlled asymmetric hydraulic actuators, proposes a physical to solution to this problem and introduces a novel single rod electro hydrostatic actuator (EHA) which demonstrates a high dynamic performance and efficiency.

The system under consideration utilizes a shuttle valve to compensate for the differential flow rate. For the stability analysis a simple linear model of the system, which constitutes of load pressure and actuator velocity states, is derived. It is shown that there exists a critical load pressure region in which any equilibrium point requiring a partially opened spool position is unstable during the retraction of the actuator. It is proposed that an underlapped shuttle valve provides a stable operation region up to certain retraction speed. Theoretical findings are validated by both numerical simulations and experimental tests.

The deficiency of the underlapped shuttle valve solution, which is the circulating leakage flow over the spool pre-openings, is investigated. An inverse kinematic model of the system is developed to compensate the effects of flow losses and verified with numerical simulations. The circulating leakage losses are physically eliminated by a novel shuttle valve spool structure, which provides asymmetric orifice pre-opening. The theoretical stability analysis is extended and a numerical program is developed, which is suitable to investigate all possible spool structures. The effects of several valve parameters on system stability are investigated and second novel valve solution is proposed, which provides symmetric pre-opening, removes the spring pre-loading and increases its stiffness. The first valve solution, with asymmetric orifice pre-opening, is manufactured and implemented on the electro hydrostatic actuator (EHA). A combined feedback and feedforward position control system is designed, based on a linearized model that includes the servo motor and hydraulic actuator dynamics. The developed single rod EHA is tested experimentally on a previously developed load simulator test set up and its performance is evaluated in terms of positioning, set point tracking and disturbance rejection.

**Keywords:** Fluid Power Control, Electro Hydrostatic Actuator, EHA, Stability, Variable Speed Pump, Energy Efficiency, Shuttle Valve, Combined Feedforward and Feedback Control

## ÖZ

### TEK MİLLİ ELEKTRO HİDROSTATİK EYLEYİCİ GELİŞTİRİLMESİ VE DENETİMİ

Çalışkan, Hakan

Doktora, Makina Mühendisliği Bölümü

Tez Yöneticisi: Prof. Dr. Tuna Balkan

Yardımcı Tez Yöneticisi: Prof. Dr. Bülent E. Platin

Eylül 2015, 276 sayfa

Bu tez çalışmasında tek milli eyleyiciler için, değişken devirli pompa denetimli elektro hidrostatik bir sürücü sistemi geliştirilmiştir. Tek milli eyleyicilerin hidrostatik sistemlerde kullanımında karşılaşılan sorun, piston mil bütününün asimetrik yapısı nedeni ile oluşan fark debisidir. Mevcut durumda fark debisinin giderilmesi için önerilen hidrolik devre çözümlerinde sistem kararsızlığı olarak adlandırılan istenmeyen basınç salınımları oluşmaktadır. Bu tez çalışmasında, pompa denetimli asimetrik hidrolik eyleyicilerin kararsızlık sorunu konu edilmekte, bu soruna fiziksel çözüm önerilmekte ve yüksek dinamik başarımlar gösteren yeni bir tek milli elektro hidrostatik eyleyici tanıtılmaktadır.

Çalışmaya konu olan sistemde fark debisinin giderilmesi için mekik valfi kullanılmıştır. İlk aşamada, kararsızlık analizi yük basıncı ve eyleyici hızı durumlarından oluşan basitleştirilmiş doğrusal model kullanılarak yapılmıştır. Hidrolik eyleyicinin geri çekilmesi sırasında, valf makarasının kısmi açık konumda olmasını gerektiren bir denge noktasının kararsız olduğu bir kritik yük basıncı bölgesinin varlığı gösterilmiştir. Kısmi orifisi açıklıklarına sahip bir valf kullanıldığında kararlı bir çalışma bölgesi elde edilebileceği önerilmiştir. Teorik bulgular, numerik benzetim ve deneysel testler ile doğrulanmıştır. Önerilen çözümde,

valf makarasının ön açıklıkları üzerinden oluşan valf sızıntı debisi sorunu incelenmiştir. Sızıntı kayıplarının etkilerini gidermek için sistemin ters kinematik modeli oluşturulmuş ve numerik benzetimlerle doğrulanmıştır.

Valf sızıntı kayıplarını fiziksel olarak gidermek için, asimetric orifisi açıklıkları olan, yeni bir mekik valfi makara yapısı önerilmiştir. Teorik kararsızlık analizi geliştirilmiş ve bütün olası makara yapılarını incelemeye uygun bir numerik program oluşturulmuştur. Mekik valfi parametrelerinin sistem kararlılığına olan etkileri incelenmiş ve ikinci valf çözümü önerilmiştir, bu çözümde simetrik orifis ön açıklığı sağlanmakta, yayın ön yüklemesi kaldırılmakta ve sertliği arttırmaktadır. Elektro hidrostatik eyleyici (EHA) üzerinde asimetric orifisi ön açıklığına sahip olan ilk valf çözümü üretilerek uygulanmıştır. Servo motor ve hidrolik eyleyici dinamiğini yansıtan doğrusallaştırılmış bir model kullanılarak, birleşik yapıda ileri ve geri besleme bir konum denetleyicisi tasarlanmıştır. Geliştirilen tek milli EHA önceden tasarlanmış olan bir kuvvet simülatörü test düzeneğinde test edilmiş ve başarımı konumlama, istek sinyali takip ve bozucu etkileri giderme açılarından değerlendirilmiştir.

**Anahtar kelimeler:** Akışkan Gücü Kontrolü, Elektro Hidrostatik Eyleyici, EHA, Kararsızlık, Değişken Devirli Pompa, Enerji Verimliliği, Mekik Valfi, Birleşik İleri ve Geri Beslemeli Kontrol

## ACKNOWLEDGEMENTS

I would, first of all, like to thank to Prof. Dr. Tuna Balkan and Prof. Dr. Bülent E. Platin for their guidance, suggestion and support throughout the thesis study.

I would specially like to thank to Suat Demirer for his financial support and suggestions. He financed the construction of the load simulator test rig for the development of the EHA. Furthermore, he financed all the required electronic and hydraulic components.

I would specially like to thank to Gökalp Ecin, for his great support during the manufacturing of the hydraulic manifolds, and modification of the shuttle valve spools.

I would like to thank to my colleague Ulas Akova, who worked for the development of the load simulator test set up as his M.Sc. thesis. I would also like to thank to my colleague Salih Alan.

I would like to thank to Scientific and Technological Research Council of Turkey (TÜBİTAK) for the scholarship with the code BİDEB 2211.

And my dear family,

I would like to thank to my father and mother, brothers, and my wife Nagihan for their endless support and patience.

At last I would like to thank to my dear daughter Bilge ÇALIŞKAN. This year she is starting pre-school. This is a relay race and now it is time to hand off the baton.

Good luck Bilge☺.

**BİLGE**  
**İÇYİĞİ**

## TABLE OF CONTENTS

ABSTRACT .....	v
ÖZ .....	vii
ACKNOWLEDGEMENTS .....	ix
TABLE OF CONTENTS .....	xi
LIST OF TABLES .....	xvi
LIST OF FIGURES .....	xvii
LIST OF SYMBOLS .....	xxiv
CHAPTERS	
1 INTRODUCTION.....	1
1.1 Research Motivations and Challenges .....	7
1.2 Objective of the Thesis .....	10
1.3 Thesis Outline.....	11
2 REVIEW OF PUMP CONTROLLED HYDRAULIC SYSTEMS .....	13
2.1 Pump Controlled Systems .....	13
2.2 Closed and Open Circuit Pump Control.....	14
2.3 History of Hydrostatic Systems with Valve Control.....	16
2.4 Conventional Hydrostatic Circuit with Symmetric Actuator .....	17
2.5 Single Rod (Asymmetric) Hydrostatic Actuators.....	25
2.5.1 Multiple Pumps and Transformers.....	26
2.5.2 Single Pump Solutions .....	29
2.6 Conclusion.....	38

3 MATHEMATICAL MODELING OF THE EHA .....	39
3.1 Working Principle.....	39
3.2 Mathematical Modeling.....	43
3.2.1 Hydraulic Actuator Model .....	44
3.2.2 Pump Model .....	47
3.2.3 Shuttle Valve Model.....	50
3.2.4 Electric Motor Model .....	57
3.2.5 Hydraulic Accumulator .....	63
3.3 Simulation Model .....	79
3.4 Experimental Test Set Up.....	81
3.4.1 Control System Hardware Components .....	83
3.4.2 EHA Test System Components.....	85
3.4.3 Prototype EHA .....	86
3.5 Simulation Model Validation .....	88
4 STABILITY ANALYSIS OF THE EHA .....	91
4.1 Simplified Shuttle Valve Model and Flow Continuity Equations.....	91
4.2 Linear Model .....	94
4.3 Critical Load Pressure Region.....	95
4.4 Equivalent Flow continuity equations .....	97
4.5 State Space Representation.....	99
4.6 Stability Analysis.....	100
4.7 Stability Analysis of Partially Opened Shuttle Valve Circuit .....	102
4.7.1 Proposition 1 .....	103
4.7.2 Proposition 2 .....	103
4.7.3 Proposition 3 .....	103

4.7.4	Proposition 4 .....	104
4.8	Determination of the Valve Underlap .....	104
4.9	Simulation Results .....	108
4.10	Experimental Tests .....	111
4.11	Experimental Results with Closed Center Valve.....	112
4.12	Experimental Results with Underlapped Valve.....	114
4.13	Conclusion .....	116
4.14	Proofs of the propositions .....	117
4.14.1	Proof of Proposition 1 .....	118
4.14.2	Proof of Proposition 2 .....	119
4.14.3	Proof of Proposition 3 .....	120
4.14.4	Proof of Proposition 4 .....	121
5	DEVELOPMENT OF HYDRAULIC CIRCUIT SOLUTIONS .....	125
5.1	Simplified Kinematic Model .....	126
5.1.1	Calculation of Orifice Opening.....	130
5.1.2	Calculation of Orifice Area.....	132
5.2	Transformer Ratio and Dead Pump Speed .....	133
5.2.1	Circulating Leakage Flow Region .....	142
5.2.2	Dead Pump Speed Required to Move the Actuator .....	144
5.3	Inverse of the Kinematic Model.....	146
5.3.1	Numerical Simulations.....	152
5.4	Asymmetric Shuttle Valve Spool Solution.....	159
5.5	Extended Stability Analysis .....	164
5.5.1	Linearized Valve Coefficients with Linear Orifice Geometry.....	165
5.5.2	Linearized Valve Coefficients with Non-Linear Orifice Geometry ..	170

5.6	Linearized State Equations .....	174
5.6.1	Without Shuttle Valve Dynamics.....	174
5.6.2	With Shuttle Valve Dynamics.....	176
5.7	Numerical Stability Analysis Program.....	179
5.7.1	Underlapped Shuttle Valve .....	181
5.7.2	Asymmetric Spool Shuttle Valve.....	184
5.8	Second Shuttle Valve Solution and Comments on Stability .....	187
5.9	The Proposed Shuttle Valve Solutions .....	192
5.10	Conclusion .....	193
6	LINEARIZED SYSTEM MODEL .....	197
6.1	Electrical and Rotational Mechanical System.....	198
6.2	Hydraulic and Translational Mechanical System.....	199
6.3	State Space Representation of the Open Loop Plant, $G_o$ .....	204
6.4	Servo Motor Control System.....	205
6.5	State Space Representation of the Motor Speed Controlled Plant, $G_p$ .....	207
6.6	Comparison with Non-linear Simulink Model .....	209
6.7	Investigation of the Root Locations.....	209
6.8	Simplified Plant Model.....	214
6.8.1	State Space Model with Fully Opened Valve Considerations .....	215
6.8.2	State Space Model with Partially Opened Valve Considerations .....	217
6.9	Comparison of the Design Plant Models.....	218
7	CONTROLLER DESIGN AND PERFORMANCE TESTS.....	219
7.1	Controller Structure .....	219
7.2	Position Feedback Controller Design.....	221
7.3	Integrator Anti-Windup Strategy.....	226

7.4	Reference Feedforward Controller Design.....	230
7.5	Pre-Filter Equivalent of the Reference Feedforward Controller .....	233
7.6	Disturbance Feedforward Controller Design.....	235
7.7	Reference Trajectory Generation .....	238
7.8	Supervisory Controller .....	239
7.9	Performance Evaluation and Experimental Tests.....	240
7.10	Positioning Performance.....	241
7.11	Set Point Tracking Performance .....	245
7.12	Disturbance Rejection Performance .....	247
7.13	Conclusion .....	253
8	SUMMARY, CONCLUSIONS AND RECOMMENDATIONS.....	255
8.1	Summary and Conclusions .....	255
8.2	Future Recommendations.....	262
	REFERENCES .....	265
	CURRICULUM VITAE .....	273

## LIST OF TABLES

### TABLES

Table 2-1 Comparison of pump controlled and valve controlled systems.....	16
Table 3-1 Parameters of the hydraulic actuator .....	47
Table 3-2 Parameters of the hydraulic pump .....	50
Table 3-3 Parameters of the shuttle valve .....	55
Table 3-4 Parameters of the servo motor .....	59
Table 3-5 Parameters of the hydraulic accumulator.....	77
Table 3-6 Loading limits of the load simulator set-up .....	83
Table 3-7 EHA control system hardware .....	84
Table 3-8 EHA test system components .....	86
Table 5-1 Parameters of the kinematic EHA model .....	136
Table 5-2 Underlapped shuttle valve parameters .....	136
Table 5-3 Simulation test points and corresponding simulation inputs $\omega_M$ and $F_L$ .	154
Table 5-4 Shuttle valve parameter, with asymmetric spool .....	161
Table 5-5 Simulation test points and corresponding simulation inputs $\omega_M$ and $F_L$ .	163
Table 5-6 System parameters used in dynamic modeling.....	181
Table 7-1 Specifications of the closed loop system .....	224
Table 7-2 PI controller .....	226

## LIST OF FIGURES

### FIGURES

Figure 1-1 Schematic representation of general hydraulic drive systems.....	2
Figure 1-2 Industrial products offered by, Moog and Parker Corp.....	5
Figure 1-3 Pump controlled circuit concept for an asymmetric actuator.....	7
Figure 2-1 Classification of pump controlled hydraulic systems.....	13
Figure 2-2 Basic pump controlled systems, (a) open circuit, (b) closed circuit.....	14
Figure 2-3 A hydrostatic drive using a variable-displacement pump .....	18
Figure 2-4 Alternative forms of hydrostatic circuits.....	19
Figure 2-5 Shuttle valve structures (a) prior art closed center, (b) Sauer Danfos, 2001 (c) Parker Hannifin, 2004.....	20
Figure 2-6 Boeing, electro-hydraulic actuator, patented in 1986.....	21
Figure 2-7 Parker electro-hydraulic actuator, patented in 1994.....	22
Figure 2-8 Injection molding machine proposed by Mannesman in 1992.....	23
Figure 2-9 Hydrostatic circuit with symmetrical single rod actuator .....	24
Figure 2-10 Digital displacement pump, e-dyn 96, proposed by Artemis .....	25
Figure 2-11 Possible circuit configurations for two pumps control.....	26
Figure 2-12 Two pump solutions (a) Helduser, (b) Plummer .....	27
Figure 2-13 Working principle of IHT, comparison with directional flow control, ..	28
Figure 2-14 The 3-port pump and asymmetric pump solutions.....	29
Figure 2-15 Use of pilot operated check valve for differential flow compensation ..	30
Figure 2-16 Hydraulic circuit flow control, hewet patented in 1994 .....	31
Figure 2-17 Pilot Operated Check Valves Solution, Rahmfeld .....	31
Figure 2-18 Four quadrant operation of differential cylinder .....	32

Figure 2-19 Alternative circuit solutions proposed by Rahmfeld .....	33
Figure 2-20 EHA circuit scheme patented by Parker in 2011 .....	34
Figure 2-21 Measured pump mode oscillations reported by Williamson .....	35
Figure 2-22 Working region of hydrostatic circuit (a) desired (b) P.O.C.V .....	36
Figure 2-23 The proposed hydraulic circuit configuration by Wang and Book .....	37
Figure 3-1 Proposed hydraulic system .....	39
Figure 3-2 Cartridge type shuttle valve and its components .....	40
Figure 3-3 Schematic cross-section view of a shuttle valve .....	41
Figure 3-4 Four quadrant operation of the proposed hydraulic circuit .....	42
Figure 3-5 Free body representation of the EHA components.....	44
Figure 3-6 Hydraulic actuator model .....	45
Figure 3-7 4-quadrant operation of the hydraulic internal gear unit, pump .....	48
Figure 3-8 Internal and external leakage losses of the hydraulic pump .....	49
Figure 3-9 Shuttle valve model .....	51
Figure 3-10 Shuttle valve orifice area .....	53
Figure 3-11 MATLAB <sup>®</sup> /Simulink <sup>®</sup> , non-linear model of the shuttle valve .....	56
Figure 3-12 PMSM model developed in MATLAB <sup>®</sup> /Simulink <sup>®</sup> environment .....	59
Figure 3-13 Speed and current controller of the PMSM .....	60
Figure 3-14 Integral reset model used in the speed and current controller .....	60
Figure 3-15 Simulink <sup>®</sup> model verification file.....	61
Figure 3-16 Comparison of measured and model output velocity response .....	62
Figure 3-17 Comparison of measured and model output d-q axis currents .....	63
Figure 3-18 Heat transfer across the hydraulic accumulator wall.....	68
Figure 3-19 MATLAB <sup>®</sup> /Simulink <sup>®</sup> , non-linear hydraulic accumulator model, 1 .....	69
Figure 3-20 MATLAB <sup>®</sup> /Simulink <sup>®</sup> , non-linear hydraulic accumulator model, 2 .....	70

Figure 3-21 MATLAB <sup>®</sup> /Simulink <sup>®</sup> , non-linear hydraulic accumulator model, 3.....	71
Figure 3-22 Linear graph of hydraulic accumulator .....	74
Figure 3-23 MATLAB <sup>®</sup> /Simulink <sup>®</sup> , linearized model of the hydraulic accumulator	75
Figure 3-24 Normalized P-V diagram for 0.01Hz and 0.5Hz excitation frequency ..	78
Figure 3-25 MATLAB <sup>®</sup> /Sim-Hydraulics <sup>®</sup> , non-linear model of the EHA.....	79
Figure 3-26 MATLAB <sup>®</sup> /Sim-Hydraulics <sup>®</sup> , shuttle valve model .....	80
Figure 3-27 MATLAB <sup>®</sup> /Sim-Hydraulics <sup>®</sup> , pump model .....	81
Figure 3-28 Schematic view of the experimental test set up .....	81
Figure 3-29 Operation region of the load simulator, [95].....	82
Figure 3-30 Experimental test set up .....	85
Figure 3-31 The EHA in compact form, demonstrated in HPKON 2014.....	87
Figure 3-32 Pressure response comparison for fully opened shuttle valve.....	88
Figure 3-33 Pressure response comparison with transient considerations.....	89
Figure 3-34 Position response comparison with transient considerations .....	90
Figure 4-1 Critical load pressure region and circuit configurations .....	96
Figure 4-2 Possible circuit configurations for partially opened valve positions.....	103
Figure 4-3 Critical speed.....	105
Figure 4-4 Possible valve positions and asymptotic stability limit in the critical load pressure region .....	107
Figure 4-5 Simulation model responses: asymptotically stable operation range of underlapped shuttle valve.....	109
Figure 4-6 Simulation model repose and experimental test results comparison.....	111
Figure 4-7 Open loop pressure responses to external load and pump speed inputs with an overlapped shuttle valve.....	113
Figure 4-8 Open loop pressure responses to external load and pump speed inputs with an underlapped shuttle valve.....	115

Figure 5-1 Representation of the circulating leakage flow rate .....	125
Figure 5-2 Orifice openings vs pilot pressure of an arbitrary shuttle valve with spool underlap.....	129
Figure 5-3 Orifice openings vs pilot pressure of an arbitrary shuttle valve with spool overlap.....	132
Figure 5-4 Transformer ratio in load pressure versus actuator velocity plane.....	134
Figure 5-5 Actuator velocity vs. load pressure, with pilot pressure 0.2 MPa .....	137
Figure 5-6 Actuator velocity vs. load pressure, with pilot pressure -0.2 MPa.....	138
Figure 5-7 Transformer ratio versus load pressure .....	140
Figure 5-8 Transformer ratio versus pilot pressure .....	141
Figure 5-9 Circulating leakage flow region on $\Delta P_L - v_A$ plane.....	143
Figure 5-10 Dead pump speeds formed inside the critical load pressure region .....	145
Figure 5-11 Relation between $\Delta P_b$ and $v_A$ for constant pilot pressure .....	147
Figure 5-12 Actuator velocity vs. chamber pressure for different pilot pressures...	150
Figure 5-13 Actuator velocity vs pilot pressure $\Delta P_{ab}$ for different load pressures..	151
Figure 5-14 Underlapped shuttle valve orifice openings and test points .....	153
Figure 5-15 Open loop response, where inverse kinematic model is off-line.....	154
Figure 5-16 OL model response, where inverse kinematic model is activate.....	155
Figure 5-17 OL $\omega_M$ and $\Delta P_L$ responses, where inverse kinematic model is on-line	156
Figure 5-18 Pilot pressure vs. actuator velocity for a load pressure of 0.54 MPa ...	157
Figure 5-19 Asymmetric shuttle valve solution, orifice opening vs. pilot pressure.	160
Figure 5-20 Actuator velocity vs pilot pressure $\Delta P_{ab}$ for different values of $\Delta P_L$ ...	161
Figure 5-21 OL model responses, where the inverse kinematic model is off-line...	163
Figure 5-22 OL model responses, where the inverse kinematic model is on-line ...	164
Figure 5-23 Structure of the numerical stability analysis program.....	180
Figure 5-24 Stability of the underlapped shuttle valve on $\Delta P_{ab} - v_A$ plane.....	182

Figure 5-25 Stability of the underlapped shuttle valve on $\Delta P_L - v_A$ plane.....	183
Figure 5-26 Stability of the asymmetric shuttle valve on $\Delta P_{ab} - v_A$ plane.....	184
Figure 5-27 Stability of the asymmetric shuttle valve on $\Delta P_L - v_A$ plane.....	185
Figure 5-28 Shuttle Valve without spring pre load, and effect of time constant .....	189
Figure 5-29 Stability relations of orifice opening, flow coefficient and pilot area..	190
Figure 5-30 Proposed shuttle valve solution, the spring pre-loading is removed, and the stiffness is increased.....	191
Figure 5-31 Proposed shuttle vave spool structures, a-) AC port underlapped, BC port closed, b-) spring pre-load removed, AC and BC ports are underlapped.....	192
Figure 5-32 Proposed hydraulic circuit solution .....	193
Figure 6-1 The physical systems that constitute the EHA and their interactions ....	197
Figure 6-2 Block diagram representation of the linearized servo motor model .....	199
Figure 6-3 Block diagram representation of the translational mechanical system ..	200
Figure 6-4 Block diagram representation of the hydraulic system .....	203
Figure 6-5 Shuttle valve model with linearized flow gains .....	204
Figure 6-6 Linearized whole system model in MATLAB <sup>®</sup> /Simulink <sup>®</sup> .....	209
Figure 6-7 Velocity response comparision of linearized and non-linear models.....	210
Figure 6-8 Root locations during the asymmetric spool switching .....	213
Figure 6-9 Root locations, of the shuttle valve proposed in Section 5.8. ....	214
Figure 6-10 Block diagram representation of the plant .....	214
Figure 6-11 Step response comparison of the design plant models.....	218
Figure 7-1 Control structure of the EHA .....	220
Figure 7-2 Block diagram representation of the simplified design plant model.....	220
Figure 7-3 Frequency response of the servo motor speed loop .....	222
Figure 7-4 Root locus of the plant transfer function .....	223
Figure 7-5 Open loop Bode diagram of compensated and uncompensated systems	224

Figure 7-6 Frequency response of the compliance.....	225
Figure 7-7 Step response of the close loop system .....	227
Figure 7-8 Feedback position controller and integral anti wind up strategy.....	228
Figure 7-9 Close loop linear syste model and theeffects of integrator anti-wind up	229
Figure 7-10 Step response with/without saturation and integrator anti windup .....	229
Figure 7-11 Block diagram representation of the reference feedforward .....	230
Figure 7-12 Bode diagram of the CL system and effects reference feedforward ....	233
Figure 7-13 The equivalent pre-filter of reference feedforward .....	233
Figure 7-14 Block diagram representation of the disturbance feedforward.....	235
Figure 7-15 Compliance of the CL system, the effect of disturbance feedforward.	237
Figure 7-16 Fourth order reference trajectory generator model.....	238
Figure 7-17 Reference trajectory generator output .....	239
Figure 7-18 Finite state machine of the supervisory control.....	240
Figure 7-19 The MATLAB <sup>®</sup> /Simulink <sup>®</sup> model of the real time EHA controller ....	241
Figure 7-20 Applied external load and the chamber pressures in positioning tests.	242
Figure 7-21 Position response for fully opened shuttle valve spool .....	242
Figure 7-22 Position reponse effects of the feed forward compensators .....	243
Figure 7-23 Critical external load and pressure responses in positioning tests .....	243
Figure 7-24 Position response under critical external load of 0.6 kN.....	244
Figure 7-25 Position and pressure response under critical external load of 2 kN....	244
Figure 7-26 External load and pressure responses in set point tracking tests .....	245
Figure 7-27 Set point tracking performance for fully opened shuttle valve .....	246
Figure 7-28 Set point tracking performance with feedback compensator only .....	246
Figure 7-29 Applied critical external load and pressure responses in tracking performance tests.....	247
Figure 7-30 Set point tracking performance under critical load of 0.7 kN .....	247

Figure 7-31 External load step input and pressure responses .....	248
Figure 7-32 Position and velocity response to external load step input.....	248
Figure 7-33 Critical external load step input and pressure responses.....	249
Figure 7-34 Position and velocity response to critical external load step input.....	250
Figure 7-35 Sinusoidal external load input,10 Hz, and pressure responses.....	250
Figure 7-36 Position and velocity response to sinusoidal external load, 10 Hz .....	251
Figure 7-37 Sinusoidal external load input, 5Hz, and pressure responses.....	251
Figure 7-38 Position and velocity response under sinusoidal external load,5 Hz ...	252
Figure 7-39 Sinusoidal critical external load input and pressure responses .....	252
Figure 7-40 Position and velocity response under sinusoidal critical external load	253

## LIST OF SYMBOLS

- $\alpha$  = area ratio of the hydraulic actuator  
 $\delta$  = small change  
 $\lambda_d, \lambda_q$  = d and q axis flux linkages, in  $Wb$   
 $\lambda_m$  = mutual flux linkages, in  $Wb$   
 $\rho$  = fluid density, in  $kg \cdot 10^{-3}/mm^3$   
 $\omega_p$  = angular velocity of the pump, in  $rad/s$   
 $\omega_r$  = electrical speed of the rotor, in  $rad/s$   
 $\omega_M$  = angular speed of the electric motor, in  $rad/s$   
 $\Sigma$  = sum  
 $\Delta$  = difference  
 $b$  = viscous friction coefficient of the hydraulic actuator, in  $Ns/mm$   
 $b_M$  = equivalent friction coefficient of the rotor bearings, in  $Nm \cdot s/rad$   
 $b_s$  = damping constant of the valve, in  $Ns/mm$   
 $b_p$  = viscous friction coefficient, in  $Nm/s$   
 $c_H$  = actuator friction force transition coefficient, in  $s/mm$   
 $c_{HP}$  = pump friction force transition coefficient, in  $s/rad$   
 $c_p$  = specific heat at constant pressure, in  $J/kgK$   
 $c_v$  = specific heat at constant volume, in  $J/kgK$   
 $u_d, u_q$  = d, q axis voltage, in  $V$   
 $h_{ci}, h_{co}$  = inner and outer convection coefficients, in  $W/m^2K$   
 $i_d, i_q$  = d and q axis currents, in  $A$   
 $k$  = specific heat ratio  
 $k_T$  = electric motor torque constant,  $Nm/A$   
 $k_s$  = stiffness of the valve spool centering spring, in  $N/mm$   
 $k_w$  = thermal conductivity of accumulator wall, in  $W/mK$   
 $m$  = combined mass of the piston and rod of the actuator, in  $kg \cdot 10^{-3}$   
 $m_g$  = mass of the gas, in  $kg$   
 $m_s$  = mass of the valve spool, in  $kg \cdot 10^{-3}$

- $n$  = polytropic exponent  
 $n_p$  = number of pole pairs  
 $r_{ci}, r_{co}$  = inner and outer radius of the accumulator, in  $m$   
 $r_h$  = hole radius on shuttle valve sleeve, in  $mm$   
 $s_g$  = specific entropy, in  $J/kgK$   
 $u_v$  = shuttle valve orifice opening, in  $mm$   
 $u_{v1}$  = orifice opening at shuttle valve port 1, in  $mm$   
 $u_{v2}$  = orifice opening at shuttle valve port 2, in  $mm$   
 $u_{v10}$  = orifice pre-opening at shuttle valve port 1, in  $mm$   
 $u_{v20}$  = orifice pre-opening at shuttle valve port 2, in  $mm$   
 $u_{vMax}$  = maximum orifice opening of the shuttle valve, in  $mm$   
 $y_A$  = hydraulic actuator position, in  $mm$   
 $y_s$  = shuttle valve spool position, in  $mm$   
 $y_{sMin}, y_{sMax}$  = minimum and maximum shuttle valve spool position, in  $mm$   
 $v_A$  = hydraulic actuator velocity, in  $mm/s$   
 $v_g$  = specific volume, in  $m^3/kg$   
 $A$  = effective piston area of the cap side chamber, in  $mm^2$   
 $A_c$  = surface area of the accumulator, in  $m^2$   
 $A_s$  = pressure-sensitive area of the shuttle valve spool, in  $mm^2$   
 $A_v$  = orifice area of the shuttle valve, in  $mm^2$   
 $A_{v0}$  = orifice area provided by pre-opening, in  $mm^2$   
 $A_{vMax}$  = maximum orifice area of the shuttle valve, in  $mm^2$   
 $C_a$  = hydraulic capacitance of the cap side chamber, in  $mm^3/MPa$   
 $C_b$  = hydraulic capacitance of the cap side chamber, in  $mm^3/MPa$   
 $C_d$  = shuttle valve discharge coefficient  
 $C_t$  = Accumulator capacitance in thermal domain, in  $J/K^2$   
 $C_f$  = Accumulator capacitance in fluid domain, in  $m^3/Pa$   
 $C_{s1}, C_{s2}$  = individual hydraulic capacitance of spool chambers, in  $mm^3/MPa$   
 $C_s$  = hydraulic capacitance of spool chambers, in  $mm^3/MPa$   
 $D_p$  = pump displacement, in  $mm^3/rad$   
 $E$  = bulk modulus of the hydraulic oil, in  $MPa$   
 $F_C$  = Coulomb friction, in  $N$   
 $F_H$  = break away friction, in  $N$

$F_f$  = friction force acting on the hydraulic actuator, in  $N$   
 $F_L$  = external load acting on the hydraulic actuator, in  $N$   
 $F_{Lcr}$  = critical load, in  $N$   
 $F_{L1}$  = critical load region lower limit, in  $N$   
 $F_{L2}$  = critical load region upper limit, in  $N$   
 $H_e$  = pump external leakage coefficient, in  $mm^3/s \cdot MPa$   
 $H_i$  = pump internal leakage coefficient, in  $mm^3/s \cdot MPa$   
 $J_M$  = inertia of the electrical machine rotor, in  $kg \cdot m^2$   
 $J_P$  = inertia of the hydraulic pump rotor, in  $kg \cdot m^2$   
 $L$  = stroke of the hydraulic actuator, in  $mm$   
 $L_d, L_q$  = d and q axis inductance, in  $H$   
 $P_a$  = cap-side chamber pressure, in  $MPa$   
 $P_b$  = rod-side chamber pressure, in  $MPa$   
 $P_c$  = accumulator pressure, equal to gas pressure  $P_g$ , in  $MPa$   
 $P_C$  = Coulomb friction pressure equivalent, in  $MPa$   
 $P_H$  = stiction pressure equivalent, in  $MPa$   
 $P_g$  = absolute gas pressure, in  $Pa$   
 $P_L$  = load pressure, in  $MPa$   
 $P_{Lcr}$  = critical load pressure, in  $MPa$   
 $P_1$  = line pressure of the cap-side, in  $MPa$   
 $P_2$  = line pressure of the rod-side, in  $MPa$   
 $P_{s1}$  = valve pilot pressure of the cap-side, in  $MPa$   
 $P_{s2}$  = valve pilot pressure of the rod-side, in  $MPa$   
 $P_{sc}$  = shuttle valve cracking pressure, in  $MPa$   
 $P_{op}$  = shuttle valve opening pressure, in  $MPa$   
 $R_c$  = equivalent resistance of the accumulator wall, in  $K/W$   
 $R'_c$  = equivalent resistance to entropy flow, in  $K^2/W$   
 $R_g$  = gas constant, in  $J/kg \cdot K$   
 $R_{sv}$  = resistance of the inner valve conduit, in  $MPa \cdot s/mm^3$   
 $R_s$  = electric motor stator resistance, in  $\Omega$   
 $Q_a$  = flow of actuator port A, in  $mm^3/s$   
 $Q_b$  = flow of actuator port B, in  $mm^3/s$   
 $Q_c$  = flow of through the hydraulic accumulator, in  $mm^3/s$

$Q_l$  = leakage flow between actuator chambers, in  $mm^3/s$   
 $Q_{v1}$  = flow rate through shuttle valve orifice 1, in  $mm^3/s$   
 $Q_{v2}$  = flow rate through shuttle valve orifice 2, in  $mm^3/s$   
 $Q_{sv}$  = simplified shuttle valve flow rate, in  $mm^3/s$   
 $Q_{s1}$  = flow rate through shuttle valve port 1, in  $mm^3/s$   
 $Q_{s2}$  = flow rate through shuttle valve port 2, in  $mm^3/s$   
 $S_g$  = entropy of the gas, in  $J/kgK$   
 $T_e$  = Electrical torque, in  $K$   
 $T_{eg}$  = environment temperature, in  $K$   
 $T_g$  = absolute gas temperature, in  $K$   
 $T_{sv}$  = shuttle valve spool time constant, in  $s$   
 $T_p$  = load torque of the pump shaft, in  $Nm$   
 $TF$  = hydraulic accumulo transformer ratio, in  $Pa/K$   
 $TR$  = transformer ratio between the pump and actuator speed, in  $mm/rad$   
 $V_{a0}$  = cap-side chamber dead volume, in  $mm^3$   
 $V_{b0}$  = rod-side chamber dead volume, in  $mm^3$   
 $V_g$  = gas volume, in  $m^3$



## CHAPTER 1

### INTRODUCTION

Fluid power control is the transmission and control of energy by means of pressurized fluid. With hydraulics, the fluid is a liquid, which is usually an oil, whereas with pneumatics a gas, which is usually compressed air, is used to transmit power from one location to another.

History of fluid power dates back to the 17<sup>th</sup> century, where Blaise Pascal formulated his law as: “Pressure exerted anywhere in a confined incompressible fluid is transmitted equally in all directions throughout the fluid.” Bramah is the first to exploit this law, in 1795 he was granted for a hydraulic press to transmit and amplify force by using a hand pump [1]. During the late 1800’s high pressure hydraulic systems for power distribution are used in England, which lead to the invention of variable stroke hydraulic pump and accumulator. Up through the start of the 20<sup>th</sup> century the control of fluid power systems was limited by mechanical and hydro-mechanical feedback devices. Burrows gives an overview of the early development of fluid power in [2].

Electrohydraulic systems commonly refer to the electric actuated valve controlled oil-hydraulic systems. The very first electrohydraulic systems are seen in 1920’s where the valve spool is actuated by a direct acting motor, usually a DC solenoid. The achievements of electrohydraulic systems are boosted in 1940’s, by the demand for automatic fire control and aircraft control systems [3]. The post war researches on fluid power systems concentrated on the electrohydraulic servomechanisms in military applications. Maskrey refers the history of electrohydraulic in this period, as the history of servo valve, which is the key element of the servomechanisms [4]. The servo valve enables high power gains, which makes it be a very effective forward loop amplifier as well as an electrical to hydraulic transducer. The achievements in

the military and flight control applications are also utilized in the industry such as, NC controlled machines, presses, flight simulators, robotics etc. Furthermore, a brief history of electrohydraulic servomechanisms is given by Maskrey et. al. in [4].

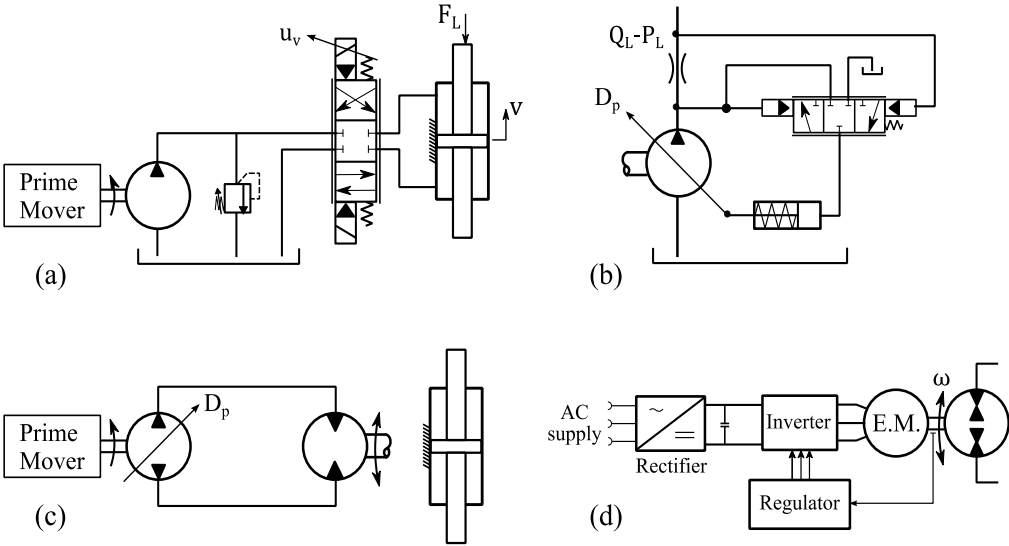


**Figure 1-1 Schematic representation of general hydraulic drive systems**

A conventional valve controlled electrohydraulic system is shown schematically in Figure 1-1 (a). It has an open-circuit structure, the servo valve (or proportional valve) is supplied by a constant pressure hydraulic power, regulates the flow rate, thus the power, through the hydraulic actuator and the load. The servo valve amplifies the electrical control signal to hydraulic power with a remarkable gain in the order of  $10^4$  to  $10^6$ . This high gain in the forward loop enables the electrohydraulic system to achieve a high bandwidth, and makes it be robust to external load disturbances. Furthermore, since the hydraulic actuator has a considerably high stiffness, the load can be considered as pure integrator with gain determined by actuator area. The electrohydraulic systems achieve these superiorities at the expense of quite poor energy efficiency. Valve controlled electrohydraulic systems are inherently inefficient, since the power flow to an actuator is regulated by dissipating readily generated hydraulic power. Theoretically, the maximum power that can be transferred to the load is only 38.5% of the total input power. The 42.5% of the loss is due to the generation of constant pressure hydraulic power which is lost on the relief valve, and remaining is due to the throttling losses of the valve. With the use of a load sensing pump as shown in Figure 1-1(b), the maximum power transfer to the

load can be increased to 67%, since the hydraulic power generation is regulated by the flow demand feedback of the actuator [5]. It should be noted that, the given percentages are calculated at the most efficient operation point. However, considering the whole operation region of an actuator, the overall efficiency will be much lower than these values. NFPA reports that the average efficiency of fluid power systems in USA is 22% [6].

By using electric analogy, the valve controlled electro hydraulic systems are generally named as “*resistance control*”, since the flow (current) through the actuator (load) is regulated by varying the orifice opening (resistance) of the valve spool.

Hydrostatic transmission, eliminates the throttling losses of the valve controlled systems, and offer high energy efficiency for power transmission. Hydrostatic transmission systems have a close-circuit structure as shown in Figure 1-1(c). A pump connected to a prime mover, usually internal combustion engine, controls the fluid flow through the hydraulic actuator, which is usually a hydraulic motor or double-rod actuator, by adjusting, its displacement. Since the pump is directly connected to the two ports of the actuator and the flow is regulated by displacement, this type of control is commonly referred as “*displacement control*” or “*valve-less control*”, furthermore, in the market “*direct pump control*” is also used to accentuate for the pump being the primary control element. Since the hydrostatic systems are highly efficient in comparison to valve controlled systems, they provide the control of high power levels, well above that achieved by the servo valves, but at some sacrifice with performance. The dynamic response of a servo pump is not comparable with a servo valve, furthermore, compliance of the entrapped fluid between the pump and actuator degrades the overall system response.

The conventional hydrostatic systems utilize a variable displacement pump driven by a constant speed primary mover. The displaced volume of the pistons is adjusted via a swash plate whose angle is regulated by a servo valve controlled actuator. Besides the frictional and the volumetric losses, the efficiency of the displacement controlled pump suffers from the resistance control of the swash plate actuator. Together with the throttling losses of the servo valve, the generation of the valve supply pressure further induces power losses. Moreover, fast response of the swash plate, require

higher supply pressure levels. One further and essential drawback of the conventional hydrostatic systems is the energy consumption of the constant speed primary mover during idling. Especially in low-duty-cycle applications, like injection molding machines that only require the system to move and/or apply pressure for a matter of seconds, considerable amount of power is wasted, since no power is transmitted to the load during the idling period, but it is consumed by the primary mover.

The idling losses can be eliminated by using a variable speed electric machine, which is shown in Figure 1-1(d). The hydraulic pump is driven by a speed controlled electric machine, usually a servo motor or an induction machine with vector or frequency control. The pump is directly connected to the two ports of the actuator, and the flow is regulated by adjusting the drive speed of the fixed displacement pump. In drive speed control applications, besides the throttling losses, idling losses are also completely eliminated and no additional power is required for the control of the pump displacement. Therefore, the input power is well adjusted to the required power at the hydraulic actuator. Furthermore, the dynamic response of a servo motor is sufficient for many applications and is comparable with a proportional valve. Variable speed pump drives receive an increasing interest, especially in aerospace and stationary industrial applications, where an electrical power net is available, like injection molding machines, press brakes, etc. [7]. Next to the energy efficiency features, the electro hydrostatic actuators have application areas in aircraft flight control systems for decentralized control purposes named as power-by-wire concept [8], [9].

The conventional valve controlled hydraulic servo-actuation systems used in the flight control systems have limitations, foremost of which is the need for a central hydraulic supply system [10]. These systems require a hydraulic pump, together with a prime mover, a reservoir, an accumulator and transmission lines to each remotely located servo-actuator. The main drawbacks are the investment cost, installation expense, energy losses at the pump, undesirable noise, considerable weight, bulk of hardware and potential maintenance problems due to the piping leakage. Therefore, there is a trend to “more electric aircraft”, usually named as “power-by wire” concept, which aims to eliminate the centralized hydraulic power network, reduce the

overall weight and increase the safety by utilizing de-centralized (local) control for each actuator. The first solution is to use electro mechanical actuators (EMA), where the rotational motion of the electric motor is converted to translational motion by means of screws, gears and clutches [11]. However, the EMA's cannot replace hydraulic servo-actuator, in many applications. The necessary gearing between electric motor and the load is reported to be the weakest link [10], [12]. The main drawbacks of the mechanical transmission are backlash, friction, fatigue and high inertia. Additionally, if a failure occurs, the EMA will typically jam in the failed position, resulting in catastrophic failure of the system because of consequent loss of control authority [13]. On the other hand, a hydraulic actuator easily provides redundant and advanced fail save systems. It does not lock in a particular position, but returns to a neutral position, which may also be passively damped. Together with these inherent superiorities, the electro hydrostatic system, which consists of a dc motor and a pump directly connected to a double rod symmetric actuator, can meet the stationary and dynamic requirements encountered on civil transport aircraft [14].



**Figure 1-2 Industrial products offered by, Moog and Parker Corp.**

The electro hydrostatic actuator (EHA) systems combine the benefits of electrical and hydraulic systems and have an increasing interest. Figure 1-2, shows the products developed by Boeing and Parker. These products are highly specialized to aerospace applications, advanced with fail safe functions. On the other hand there are also industrial solutions, like the REXA Electraulic<sup>TM</sup> actuators. However, the EHA products on the market are generally developed for double rod actuators.

The single-rod actuator is a challenge for the hydrostatic systems due to its asymmetric structure. Whether, displacement or speed controlled, the conventional closed-circuit configurations of the hydrostatic systems utilize a symmetric actuator

like a hydraulic motor or double rod actuator. Assuming that the actuator is leak-free, the incoming and outgoing flow rates of the actuator are the same, meaning that a constant volume of hydraulic oil is circulating between the pump and the actuator. The single rod actuator on the other hand contradicts with the conventional hydrostatic circuit structure. Since the single-rod actuator has an asymmetric structure, there exist unequal flow rates at the two ports of the actuator. Either a deficient or an excess flow rate is always formed in the closed circuit, corresponding to the difference between the swept fluid volumes by piston areas of the cap and rod sides. The unequal flow rate is named as “differential flow” and can be formulated as follows.

$$\Delta q = (1 - \alpha)Av_A \quad (1-1)$$

Here,  $v_A$  is the actuator speed,  $\alpha \in (0,1)$  is the ratio of piston areas of the rod side and the cap side of the actuator, and  $A$  is the piston area of the cap side. Therefore,  $(1 - \alpha)A$  represents the area of the rod cross-section and  $(1 - \alpha)Av_A$  can be considered as the swept volume difference per unit time between retraction and extension phases.

$$\alpha = \frac{A_{rod-side}}{A_{cap-side}} \quad (1-2)$$

If the differential flow compensation problem is restricted with single pump usage, excluding the usage of a (active controlled) secondary pump, the possible hydraulic circuit solution necessitates an external hydraulic source/sink at an elevated pressure, and some connection components enabling a bi-directional flow between the closed circuit and this source/sink. The solution of the differential flow compensation problem is shown conceptually in Figure 1-3.

The conventional hydrostatic systems utilize a symmetric actuator and only compensate the leakages losses by a uni-directional flow. When compared with the convention system, in the possible circuit solution of the single rod actuator, there should be a bi-directional flow in between the hydraulic source/sink and the closed circuit. An excess flow should be returned to the hydraulic sink in the retraction

phase of the actuator ( $v_A < 0$ ), and a deficient amount of flow should be supplied back to the closed circuit in the extension phase ( $v_A > 0$ ).

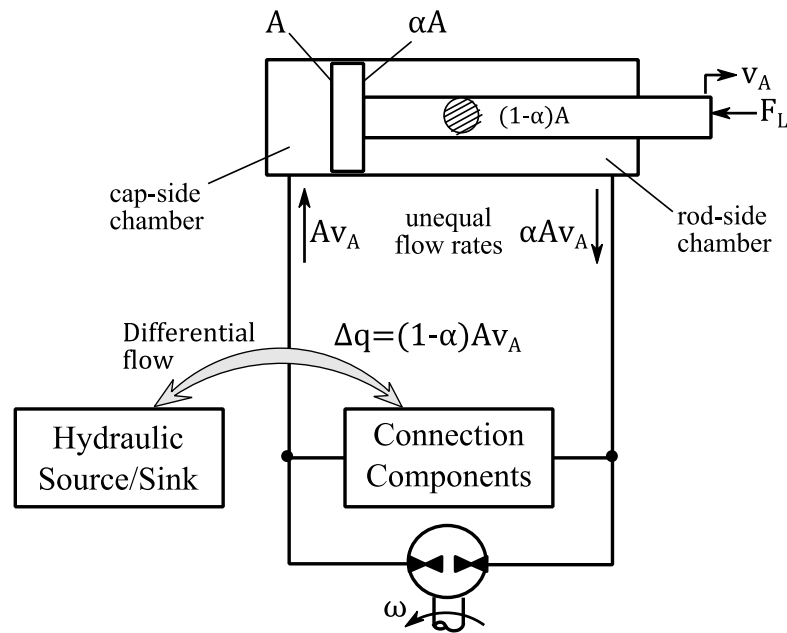


Figure 1-3 Pump controlled circuit concept for an asymmetric actuator

This thesis study addresses the development of a servo electro-hydrostatic actuator based on the concept given in Figure 1-3.

## 1.1 Research Motivations and Challenges

Today's engineering systems are forced to be energy efficient due to limited and high-priced energy resources together with increasing sensitivity to environmental issues. However, the fluid power systems are typically low in energy efficiency. A study conducted by Oak Ridge National Laboratory and NFPA, indicates that the efficiency of fluid power systems, is ranging from 6% to 40% depending upon the application, and across all industries in USA the average efficiency is 22% [6]. Despite the mobile hydraulic systems, where an electric power net is not available at high power levels, the hydraulic systems have to compete with electro-mechanical systems. Together with environmental concerns associated with noise and leakage, have led to fluid power systems replacement by electrical drives [1]. However, the

dynamic performance superiority of fluid power systems in large power drive systems, especially in linear motions, limits the replacement with electro-mechanical systems. Therefore, recent fluid power studies concentrate more on energy efficient drive systems and components. In order to compensate the future needs of customers and expand into new markets, NFPA announced six challenges for the industry, that are [15],

- increasing energy efficiency,
- improving reliability,
- building smart components and systems,
- reducing size and weight,
- reducing environmental impact,
- improving and applying energy storage and redeployment capabilities.

The variable speed pump driven electro hydrostatic actuator is inherently energy efficient, since it eliminates all the throttle losses; furthermore since it enables a direct coupling of the pump and the actuator, the transmission lines together with the hydraulic power pack related components are eliminated. Furthermore, since no bulky oil tanks are required for heat dissipation, the oil disposal and environmental impacts are reduced. Lastly, since it utilizes a hydraulic accumulator and a servo motor, hydraulic energy storage and electric energy regeneration are possible. As seen, the electro hydrostatic actuator (EHA) addresses all the challenges announced by the NFPA. Therefore, EHA can be considered as a significant product for the “future of hydraulics”, this constitutes the principal motivation of this thesis.

This research is further motivated by the need to improve a hydrostatic circuit configuration for single-rod actuators. In most of the hydraulic applications, single rod hydraulic actuators are utilized due to their compact design, low cost and ease of manufacture. When compared to a same size of double rod actuator, nearly a double stroke can be realized with a single rod actuator. On the contrary to its numerous advantages and general usage, the hydrostatic system solutions for single-rod actuators are limited in the market. Furthermore, considering the academic studies for the similar hydraulic circuit configurations, the offered solutions in the market are probable to suffer from stability problems [16], [17]. As reported in literature under

some working conditions the single-rod hydrostatic actuators suffer from undesirable pressure oscillations that occur due to the system switching between pumping and motoring modes. Investigating the instability problem and eliminating it by offering a physically realizable solution are the most challenging part of this thesis study.

This research is further motivated to gain an insight and challenge the potential problems of the electric driven hydrostatic systems. Due to the recent improvements of the electric drives, the usage of servo motors, frequency or vector controlled induction motors are continuously expanding in all fields of industrial applications. Next to the well-known, long established companies like Siemens, ABB, Fanuc, Mitsubishi, several new companies emerged in the market, which can provide sufficiently high power levels up to 100 kW. They are reliable with highly standardized safety regulations and offer cost effective solutions. Modern electric drives provide sufficient dynamics and superior energy efficiency characteristics. The speed loop of a standard industry use servo motor can achieve a bandwidth up to 100 Hz. Furthermore, regenerative power converters are available, which are able to recover the braking energy and feed it back to the power grid, instead of dissipating in the braking resistors. The marriage of the electrical drive systems with the hydraulics will bring a new market both for the electric and hydraulic industries. For example, nearly all of the press brakes produced in Turkey and Europe utilize valve controlled hydraulic drives. Only one company, SAFAN Darley E-brake, utilizes an electro-mechanical solution, which is limited up to 200-300 metric tons pressing capacity. However, with the use of high power electro hydraulic drives, it is possible to compete with the pressing capacity of the conventional valve controlled electro hydraulic systems, in the meantime offering energy efficiency over 50%. Currently Hoerbiger Company offers a servo motor controlled hydraulic drive solution, e-Prax, for the press brake manufacturers. Although not common, it is likely to spread in the industry. The press brakes use single rod actuators with a relatively small area down to 1/13 that necessitates a special hydraulic circuit structure. However, since the principles are the same, the results obtained through this research can easily be applied both in the press brakes and some other industrial presses.

## 1.2 Objective of the Thesis

The principle purpose of this thesis study is to develop a hydraulic circuit structure to be used for the motion control of a double acting single rod actuator. The study is based on variable speed pump drive concept, where an electric motor is utilized to regulate the speed of a constant displacement pump. The “single-rod actuator” refers to an asymmetric actuator that has different piston areas on the cap and rod side of the piston. The single-rod actuators considered in this thesis are assumed to have a moderate area ratio,  $\alpha \in (0.5,1)$ . An area ratio of  $\alpha = 0.5$ , physically means that the differential flow rate to be compensated is equal to the pump flow rate. Since higher differential flow rates will increase the size of connection components together with the hydraulic source and sink, practically the use of a second pump is reasonable for differential flow compensation of the single rod actuator with relatively big rod diameter,  $\alpha < 0.5$ .

The research targets to develop a servo electro hydrostatic single rod actuator, whose hydraulic circuit solution enables to compensate the differential flow rate without stability problems.

Some specific aims of the research can be classified as follows:

- to investigate the stability problems reported in the literature and provide a mathematical explanation,
- to develop a stable hydraulic circuit configuration utilizing a single pump for the motion control of a single-rod actuator,
- to develop a simple enough linear model of the hydrostatic system, to understand the system dynamics and to design a model based controller,
- to develop an industrial applicable control algorithm, with sufficient bandwidth and stiffness for general industrial applications,
- to validate the proposed hydraulic system solution, in terms of stability and performance.

### 1.3 Thesis Outline

In the first chapter the thesis subject is introduced

In the second chapter a review of pump controlled hydraulic systems are given. First the pump controlled systems are classified. Then, the EHA systems of the double rod actuators and the hydraulic circuit solutions proposed for single rod actuators are introduced.

In the third chapter, the general hydraulic circuit structure of the proposed system is introduced. The mathematical modelling is given and a non-linear numerical simulation model is developed, both in MATLAB<sup>®</sup>/Simulink<sup>®</sup> and SimHydraulics<sup>®</sup> environment. Furthermore, the experimental test set up constructed for the development of the EHA is explained.

In the fourth chapter, the reason of the instability problems reported in literature is investigated. A simplified linear model, which constitutes of load pressure and actuator velocity states, is derived. By using the simplified model, the critical operation region is introduced in the load pressure vs velocity plane. In this chapter, it is proposed that the main reason of the instability is the closed center shuttle valve. The propositions are supported with mathematical proofs. As a physical solution, use of an underlapped shuttle valve is proposed. Both theoretically and experimentally, it is shown that, with the use of underlapped shuttle valve, the undesired pressure oscillations can be eliminated.

In the fifth chapter the deficiencies of the underlapped shuttle valve solution, which is the circulating leakage flow rates formed during the centered valve spool position, are investigated. A kinematic model is developed in order to define the dead pump speeds together with the transformer ratio in between the pump drive speed and the hydraulic actuator speed. Then a novel asymmetric shuttle valve spool structure is proposed to eliminate the circulating leakage flow rates. In the proceedings section, both the underlapped valve and the asymmetric valve solution are evaluated in terms of stability. The linearized system model developed in chapter 4 is further extended to include the geometric non-linearity of the metering orifices which are formed by the circular holes on the valve sleeve. By using the extended linearized model a

numerical stability analysis is developed. The effects of shuttle valve parameters on stability are shown. At the end of the section, a second shuttle valve solution is proposed. This solution both modifies the shuttle valve spool structure and eliminates the pre-compression force of the spool centering springs.

In the sixth chapter, the linearized model of the whole system is derived to be used in the controller design. In previous chapters, the linearized models are derived for stability analysis purposes only, and they neglect the electric motor and pump dynamics together with the motor controller. In this chapter, the linearized model is derived considering all the physical components of the EHA. The full order system model is then simplified, by considering the root locations. All the linearized models are represented in state space form.

In the seventh chapter, the position control system developed. The proposed control structure is introduced. A combined feedback and feedforward control strategy is utilized. It is proposed that with the addition of torque feedforward, sufficiently high bandwidths can be achieved. The designed controller together with the proposed EHA system is tested experimentally. In the performance tests, the dynamic responses together with disturbance rejection capabilities are evaluated.

In the eighth chapter, discussions, conclusions and future recommendations are given.

## CHAPTER 2

### REVIEW OF PUMP CONTROLLED HYDRAULIC SYSTEMS

#### 2.1 Pump Controlled Systems

In literature there exists several researches conducted on the pump controlled hydraulic systems under various names. In order to prevent confusion and clarify the scope of the thesis, the pump controlled systems are classified as shown in Figure 2-1. The objective of this thesis is to develop a closed circuit (hydrostatic) system, for a single-rod (asymmetric) actuator, by utilizing a single speed controlled fix displacement pump.

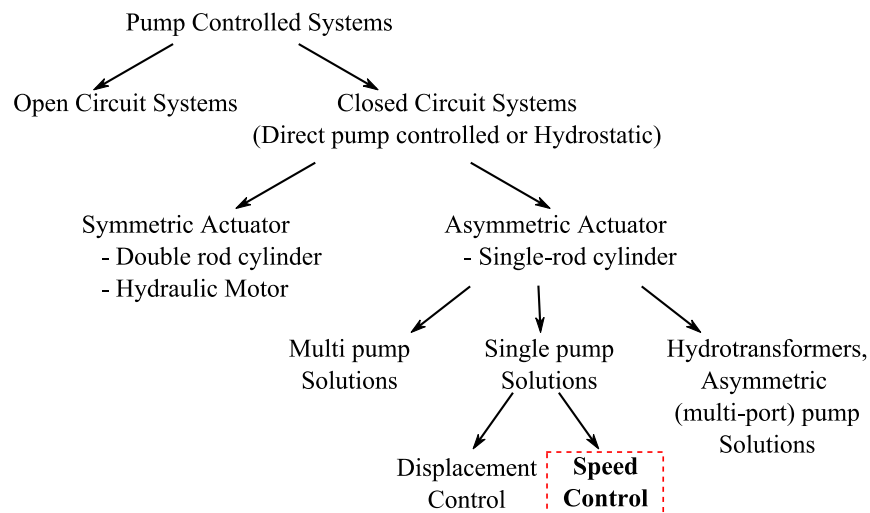


Figure 2-1 Classification of pump controlled hydraulic systems

For completeness first the difference between the closed and open circuit pump controlled systems is mentioned. Then, in the following section a historical comparison of hydrostatic system with the valve controlled system is given, which in fact describes the reason of increasing research on hydrostatic systems seen in recent years. Next, a brief review of the conventional hydrostatic system which utilizes a symmetrical actuator, i.e. hydraulic motor or double rod cylinder, is given. Then, the

hydrostatic solutions developed for single rod actuators are reviewed in two separate sections. First, the multi pump and hydro-transformer solutions are reviewed briefly, then single pump solutions, either displacement or speed controlled, are reviewed with respect to circuit configuration and stability.

**2.2 Closed and Open Circuit Pump Control**

Pump controlled systems can be classified mainly in two groups; open circuit and closed circuit systems. If the return fluid from the hydraulic motor is discharged back to the hydraulic reservoir, then it is named as open circuit, and is shown conceptually in Figure 2-2 (a). If the return fluid is ported back to the pump inlet, and recirculated, then it is named as closed circuit as shown in Figure 2-2 (b). In open circuit structure, the control valve still plays an important role. However, the valve is used to control the flow direction through the actuator chambers, rather than regulating the flow rate as in the conventional systems. The required flow rate is regulated by adjusting the pump drive speed or displacement. The pump is connected between a hydraulic reservoir and the actuator; therefore, only one port of the pump is pressurized.

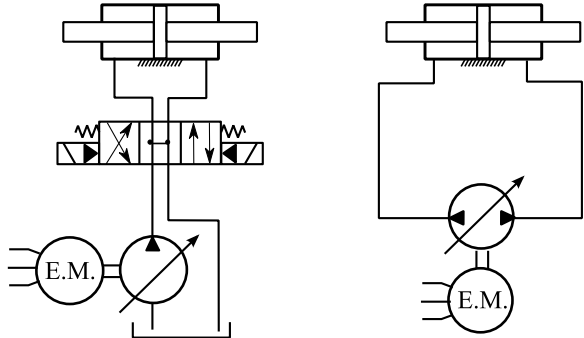


Figure 2-2 Basic pump controlled systems, (a) open circuit, (b) closed circuit

The open circuit structure provides an improved efficiency over the conventional valve controlled systems, since the resistance control is replaced with direction control. However, there still exist losses over the direction control valves determined by the valve efficiency. The valve losses may be reduced by selecting oversized valves, which will increase the cost in turn. One further drawback is the response times of the valves. Valve switching is not a problem for intermittent operations, like

an industrial press machine with a pre-defined work cycle. However in continuous operations, like a motion simulator requiring smooth position/speed changes, the open circuit system is not appropriate, since the opening/closing of the directional valve will require some time.

Direct pump controlled closed circuit or hydrostatic system on the other hand, eliminates all the throttling losses and provides continuous motion. The two ports of the pump are directly connected to the two ports of the actuator. The pump flow rate is regulated either by pump drive speed or displacement. The pump plays an important role in the closed circuit system. Since the two ports of the pump are directly connected to the actuator and there is no suction port, the pump should be able to pressurize one of the two ports according to the external load acting on the actuator. Furthermore, it should be bi-directional meaning that the pump should be able to change the direction of flow according to the direction of the speed of the actuator. Changing the location of the pressurized port, as well as the flow direction requires a closed operation region defined in the 4 quadrants of the pressure versus flow rate plane. Therefore, in the market these pumps are generally referred to as “4-quadrant pump”. Operation in 4-quadrant also implies that the pump is able to operate as a hydraulic motor, therefore instead of “pump” some manufacturers use “hydraulic unit”. The conventional pumps operate in one quadrant they are unidirectional and have a defined pressurized port location. Therefore, they are optimized for maximum volumetric efficiency and have a larger suction port. On the other hand, the 4-quadrant pumps are symmetric in structure, require a special bearing design, and may have less volumetric efficiency. When compared to an open circuit system, a direct pump controlled closed circuit system enables continuous operation, eliminates the valve losses completely, shortens the transmission lines, decreases the amount of hydraulic oil circulating in the system and reduces the space requirements, correspondingly requires a special 4-quadrant pump.

In the following sections, the closed circuit or hydrostatic pump controlled circuits will be reviewed.

### 2.3 History of Hydrostatic Systems with Valve Control

Hydrostatic system together with pump control principle is not a new concept. In 1960, Shearer mentions the pump displacement controlled servo motor drives which are employed in machine tool control systems, tension control systems, gun turrets drives, antenna drives and ship steering systems [3]. In 1967, Meritt compared the valve controlled and the pump controlled systems as shown in Table 2-1 [18]. Considering the 60's technology, since the variable speed electric drives were not common, only the variable displacement pump control is evaluated. Meritt mentioned that there is no cost advantage between the two systems due to replenishing arrangement and stroke servo for the pump. Furthermore, he mentioned that, applications which require large horse power for control purposes usually do not require fast response so that pump controlled systems are preferred because of its superior theoretical maximum operating efficiency of 100%, besides the 67% maximum theoretical efficiency of the valve controlled systems.

**Table 2-1 Comparison of pump controlled and valve controlled hydraulic systems, by Meritt, in 1967**

Pump Controlled	Valve Controlled
Slow response because pressures must built up, contained volumes are large, and the stroke is comparatively slow.	Fast response to valve and load inputs because contained volumes are small and supply pressure is constant
Much more efficient since both pressure and flow are closely matched to load requirements	Less efficient because supply pressure is constant regardless of load, and leakages are greater
Bulky power element size makes applications difficult if close coupled to actuator	Small and light power element but a bulky hydraulic power supply is required
Auxiliary pump and valving are required to provide oil for replenishing and cooling	Oil temperature builds up because of inefficiency which necessitates heat exchangers
An electrohydraulic servo valve is generally required to stroke the pump which increases system cost and complexity	Several valve-controlled systems can be fed from a single hydraulic power supply.

Today, due to recent improvement in the performance of electric motors and power electronics, the drawbacks of the pump controlled systems mentioned in Table 2-1, have mostly disappeared. Today, servo motors and frequency or vector controlled

induction motors are widely used in industrial applications, they provide sufficient dynamic responses with considerable power levels and are reliable with highly standardized safety regulations and cheaper. Consequently, besides the variable displacement pump with a servo stroke mechanism, a new area in pump controlled systems is opened, by coupling the variable speed electric motor with the fixed displacement pump opened.

Slow response is not a big problem as mentioned in the first row of Table 2-1, today a standard industry use servo motor can provide sufficiently high dynamic speed responses up to 100Hz bandwidths, which is comparable with a proportional valve. Next to the energy efficiency superiority mentioned in the second row, modern electric drives enable energy regeneration, with the use of matrix inverters. On the contrary to the third row, due to their compact design, an electric motor can be directly coupled to the hydraulic actuator, which will decrease the dead volumes as well as eliminating the transmission lines. The drawback mentioned in the fourth row still exists, however, using the cartridge type hydraulic valve technology the necessary valving can be integrated on the pump housing or into the manifold which is located between the pump and electric motor. Moreover, an external reservoir can be integrated on the actuator, due to developed manufacturing technology. Furthermore, the cost of a servo system is not a big problem as mentioned in the last row. Today there exist several electrical drive companies in the market which provide a power range up to 100kW's, and prices are compatible with the servo valves. Lastly, the single hydraulic power supply of the valve controlled systems is not seen as superiority but a drawback, since it requires lengthy transmission lines, together with leakage and maintenance problems. Today, there is a tendency to more-electric drive systems, which utilize electric power transmission instead of hydraulic, and prefer localized control instead of central control.

#### **2.4 Conventional Hydrostatic Circuit with Symmetric Actuator**

The earliest closed circuit, pump controlled systems consist of a displacement controlled pump and a hydraulic motor. Their usage in high performance systems was limited due to slow response of the servo pump. They were generally preferred

in applications which require considerable power for control purposes, because of their operating efficiency which can approach 90% in practice [18]. The basic pump controlled motor, often called “hydrostatic transmission or hydraulic transmission” are used in mobile machinery, thus giving an effectively an infinite gear ratio in both directions of motor wheel rotation [19]. The hydraulic circuit of a typical hydrostatic drive is shown schematically in Figure 2-3. A variable displacement pump, driven by a constant speed prime mover usually an internal combustion engine or a constant speed electric motor, is directly connected to a hydraulic motor. The direction of rotation and the speed of the motor are controlled by adjusting the pump stroke.

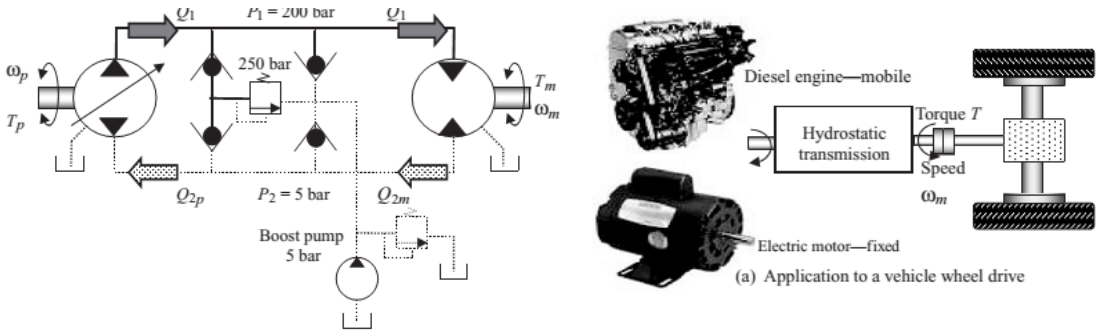


Figure 2-3 A hydrostatic drive using a variable-displacement pump

The flow deficiency of the closed circuit, due to leakage losses over the pump and motor drain as well as leakages from each line, is compensated by an auxiliary supply. A replenishing supply, often called “charge pump” or “boost pump”, delivers flow on a continuous bases, in order to replace the volumetric losses and to establish a minimum pressure level in each line. The auxiliary boost pump is a low capacity supply, since only leakage flows are compensated, and supply pressure is set to a low value to keep power losses at a minimum. The replenishing supply prevents cavitation and air entrainment since, it pressurizes each line, and helps to dissipate heat, since the cooler fluid replaces the leakage. The back to back connected two check valves, which are seen at the right most of the check valve bridge in Figure 2-3, ensure the minimum line pressure thus prevents the cavitation, while the remaining two together with the pressure relief valve ensures the maximum operating pressure.

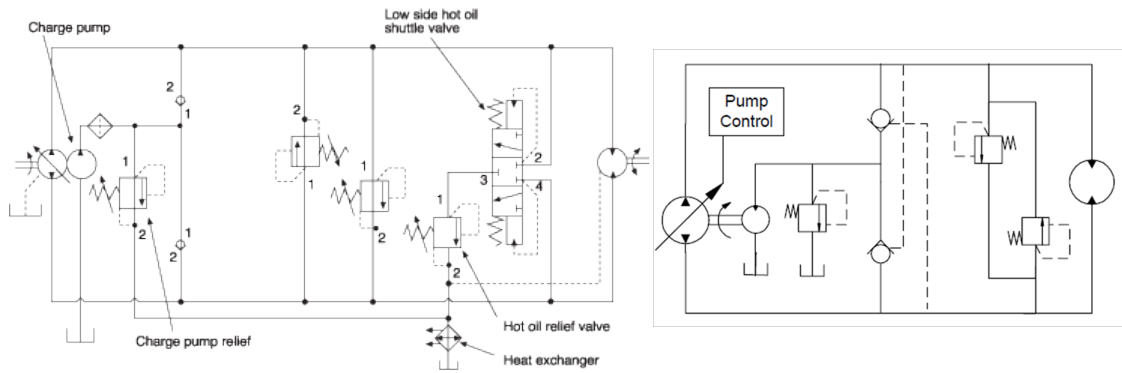


Figure 2-4 Alternative forms of hydrostatic circuits

In some applications considerable heat transfer from load to the hydraulic fluid occurs, this may be problematic, if the hot oil circulating in the closed circuit is not replaced with the cool oil. In order to replace the hot oil, besides compensating the leakage losses, the charge pump delivers an over excess flow to the closed circuit. Therefore, depending on the application the charge pump displacement is selected up to 15% of the main pump. The hydraulic circuit diagram of such a circuit is shown in Figure 2-4. The charge pump is tandem connected to the shaft of the main pump. Different from the main pump, which is variable displacement, the flow of the fixed displacement charge pump is one directional only. The charge pump delivers flow to the closed circuit on a continuous basis. The flow is filtered and then supplied to the lines, over two check valves. The charge pump supply pressure is limited by the charge pump relief valve, which also determines the minimum pressure of the circuit. The supply of the replenishing fluid of circuit scheme in Figure 2-4 is similar with the one given in Figure 2-3. The difference between these configurations is the extraction of the hot oil. This is generally handled with the use of pilot operated valves, whose pilot pressure is given by the opposite line, i.e., the pressurized line connects the unpressurized line to the hydraulic reservoir. In Figure 2-4 (a), an internal pilot operated 3/3 shuttle valve is utilized for that purpose. In the market, this shuttle valve is generally named as “hot-oil shuttle valve”, “tapping valve”, or “loop flushing valve”. In the conventional method, the valve is closed centered and has no opening to the hydraulic reservoir in neutral position, that is when the pressure difference of the two lines are lower than the valve cracking pressure. The hot oil is extracted from the circuit, only when the pressurized line overcomes the valve cracking pressure, together with the corresponding low pressure line.

The use of closed center shuttle valve is a known art in hydraulic industry, and may date back to 1977, which is a patent of Eaton for hydrostatic circuit [20]. On the other hand, in recent years, the shuttle valve structure used in the hydrostatic circuit has been changed. In 2001, Sauer-Danfoss patented a loop flushing circuit [21]. The patented circuit is principally the same with the circuit given Figure 2-4, but they replaced the closed center shuttle valve, with an open center one. By this way they ensured lubrication of all elements even in neutral position. In 2004 and later in 2008, Parker Hannifin Corporation patented two similar circuits [22], [23], which are again principally the same with the circuit given Figure 2-4. On the valve spool, they provided two orifice openings between the charge line and the two ports connected to the actuator chambers. The comparison of the proposed shuttle valve structures are given in Figure 2-5.

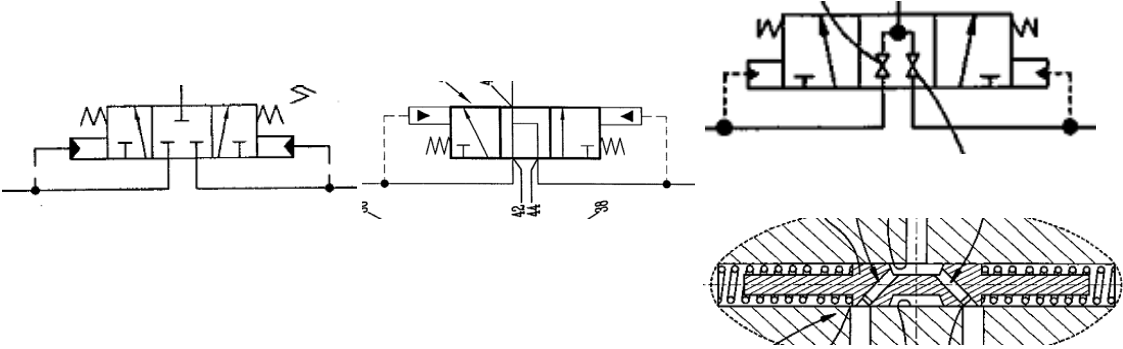


Figure 2-5 Shuttle valve structure, (a) prior art closed center, (b) Sauer Danfos, 2001 (c) Parker Hannifin, 2004

The limitations of the conventional hydrostatic system for dynamic applications are the slow response of the servo pump together with the loss of hydraulic stiffness which is due to the connection of the non-pressurized line to the hydraulic reservoir together with the lengthy transmission lines.

The aerospace industry was the first to focus on the performance improvement of the conventional hydrostatic circuit. Two main reasons of the research motivations were; to eliminate the bulky main supply of the conventional valve controlled drives, and to eliminate the possible failure of all actuators in case of the main supply inoperable [24]. The slow response problem of the variable displacement pump is eliminated, by replacing it with an electric motor driven fix displacement pump. The lengthy

transmission lines are eliminated by integrating the pump and electric motor on the actuator. Furthermore, the replenishment supply is eliminated by a hydraulic accumulator, which in fact increases the hydraulic stiffness together with the reduced transmission lines. In 1984, the Boeing Company applied for a patent utilizing the above mentioned principles, [25]. The hydrostatic circuit is designed for double rod symmetrical actuator which is shown in Figure 2-6. Different from the conventional circuit, the drain line of the pump (26) is connected to the accumulator (46) instead of external hydraulic tank and the two chambers of the hydraulic actuator are preloaded by the accumulator, which increases the stiffness of the system. The use of electric motor is further exploited by Liebherr Aero Technik [26]. In 1986, they applied for a patent of a hydrostatic circuit that controls a double rod actuator. They proposed a DC motor controlled swash plate for rapid response, together with the similar use of accumulator and check valves.

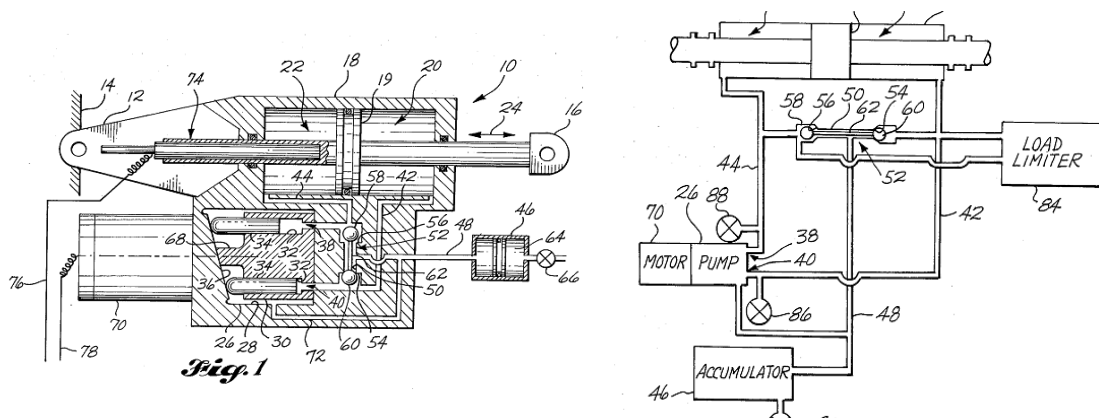


Figure 2-6 Boeing, electro-hydraulic actuator, patented in 1986, [25]

In 1989, Parker Hannifin Corp. made a patent application for a compact electro-hydraulic actuator as shown in Figure 2-7 (b) [10]. They utilized a fix displacement pump (23), which is driven by a DC motor (25) as shown in Figure 2-7 (a). Different from the others, they disposed the electric motor (25) and the pump in to the reservoir (17), which is pressurized by gas bellows (60), and similar to other solutions, they utilized check valves (71, 73) for the preloading the two chambers. This compact solution is proposed as an alternative to electro-mechanical drives, with the aim of local actuators replace major systems. Besides, eliminating the

clutches and gearing problems, it was proposed that the invention can provide a gear ratio 2000 to 1 between the motor and the load.

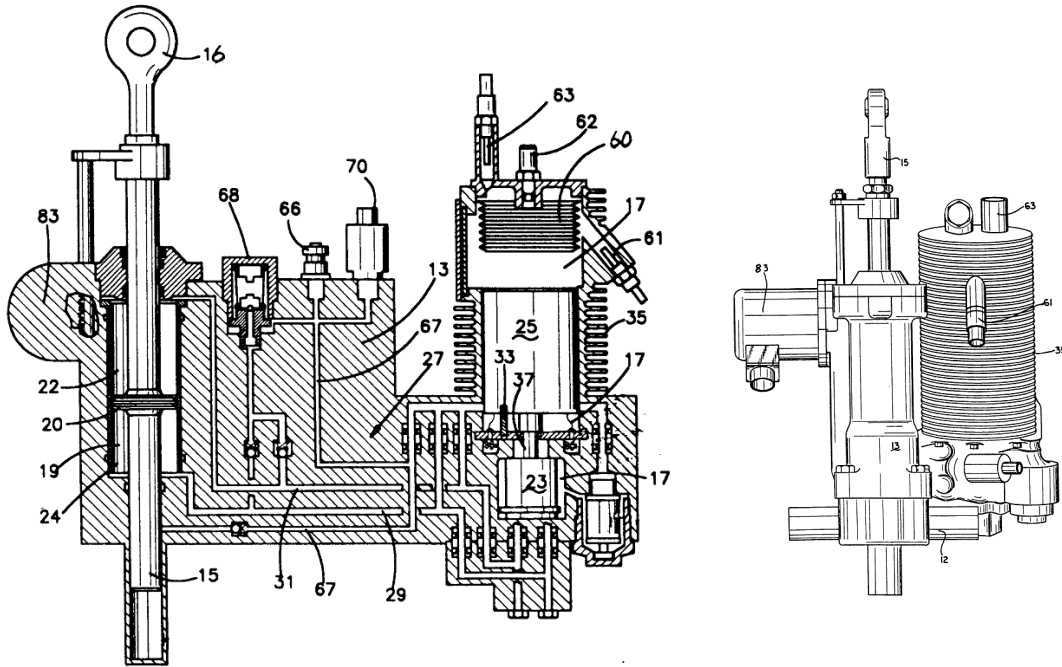


Figure 2-7 Parker electro-hydraulic actuator, patented in 1994, [10]

In 1997 NASA, tested the compact electro-hydrostatic actuator (EHA), by replacing it with a standard F-18 left aileron [9]. The tested EHA consists of a double rod actuator, fix displacement pump, and three phase permanent magnet, a hydraulic accumulator, and two back to back placed check valves similar to schematic given in Figure 2-6 (b). It was reported that the EHA performs as the standard actuator. The dynamics performances and the modeling and simulation of the symmetric double rod actuators, are further researched by [27], [28], [29], [30]. Moreover, Andersson studied on the heat generation problem of EHA's, which is a problem due to its compact structure without external reservoir. He compared the usage of fix displacement (FP) and variable displacement (VP) pumps, and concluded that FP has a better efficiency than VP [31].

In 1990, Mannesman applied a patent for injection molding machine utilizing hydrostatic drive, whose schematic is given in Figure 2-8, [32]. Similar to Parker, they utilized variable speed fixed displacement pump and utilized the hydraulic

accumulator for the preloading of the two chambers. In recent years, several studies aiming to improve the energy efficiency and the performance of a the conventional hydrostatic double rod actuator, by utilizing fix displacement pump and AC servo motor can be found in literature [33], [34].

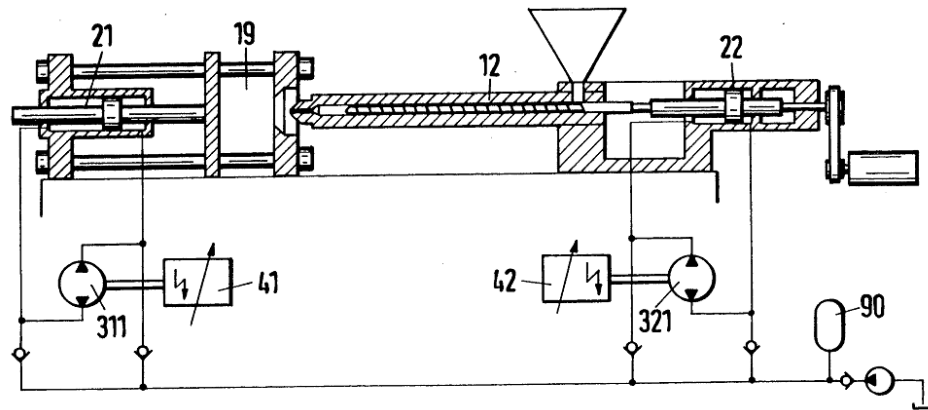


Figure 2-8 Injection molding machine proposed by Mannesman in 1992, [32]

Use of variable speed electric drive in the hydrostatic system, further improved the efficiency of the energy use. Variable displacement pump suffers from the resistance control of the swash plate actuator, furthermore, fast swash plate responses requires higher valve supply pressures. Fix displacement pump, however, does not need resistance control. On the other hand, the biggest portion of energy saving is due to well adjustment of the input electric power to the power required at the actuators, and eliminating the idling losses. A servo motor can adjust its speed according to the duty cycle of the machine. For example, during idling, it will stand by with zero speed, on the contrary to the constant speed motor of the variable displacement pump. Therefore, electric driven system offers a considerable reduction of the operating expenses by saving electric energy.

The use of electric motor for fast response and hydraulic accumulator for improved stiffness is further exploited by Habibi, in 1999 [35]. The schematic view of the electrohydraulic actuator (EHA), together with the unusual symmetrical actuator is shown in Figure 2-9. Habibi designed a novel single rod symmetrical actuator, by replacing the solid rod of the conventional piston with a hydraulic shaft. As shown in Figure 2-9 (b), he obtained two equal areas  $A_1$ , and  $A_2$ , by utilizing the hollow rod and opening the C3 chamber to atmosphere. He further showed that with the use of a

3 phase AC servo motor, it is possible to position a 20 kg moving mass with  $10 \mu\text{m}$  resolution within 0.6 s settling time and 0.2 s rise time.

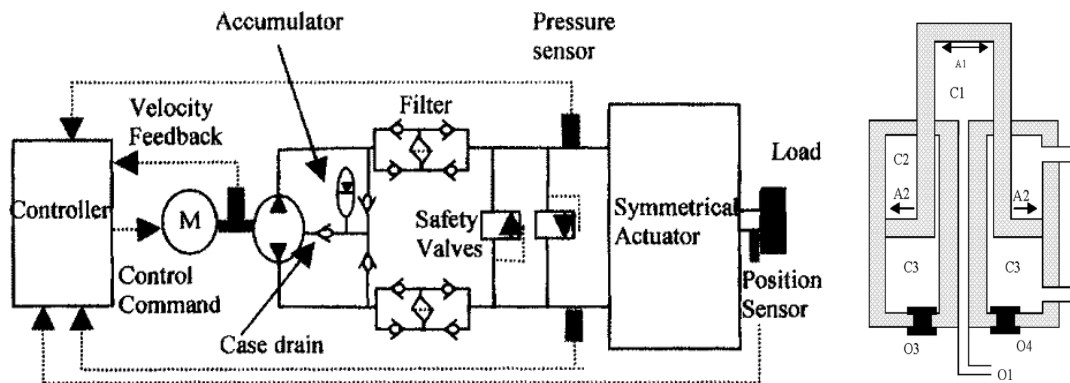
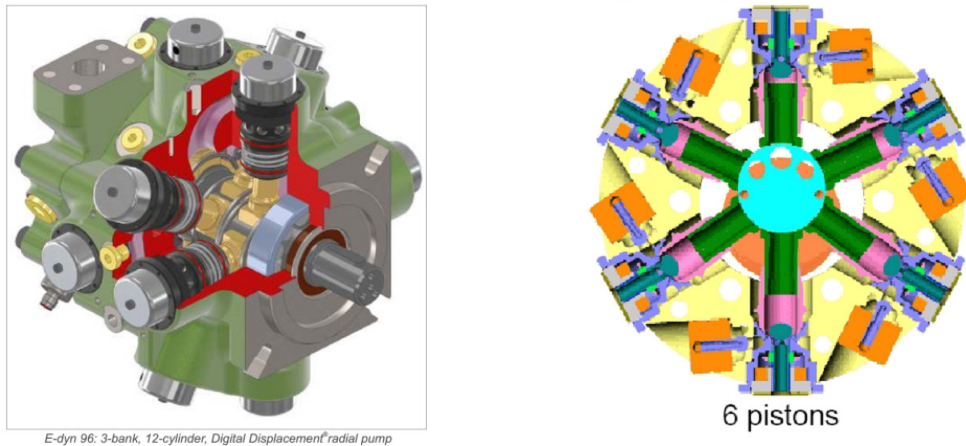


Figure 2-9 Hydrostatic circuit with symmetrical single rod actuator, [35]

He later improved the positioning performance of the EHA. In 2006, he reported that the 20 kg load can be moved with a precision of 100 nm and a stroke 12 mm and with rise time 0.3 s. He claimed that, this achieved precision level, raised the hydrostatic actuation concepts in competition with piezoelectric platforms, in terms of positioning accuracy [36].

The replacement of variable displacement pump with the variable speed fix displacement pump is appropriate for stationary industrial and aerospace applications where an electric net is available, but is not appropriate for mobile applications. Furthermore, for the relatively high power transmission for example wind turbines, the displacement controlled pump and motors are still a necessity. Therefore, several studies focused on to improve the dynamic performance of the variable displacement units [37]. Berg and Ivantysynova proposed a robust high-bandwidth controller [38]. They make tests on a displacement machine with maximum  $40 \text{ cm}^3/\text{mm}$ , utilized a standard 20 lpm-80 Hz servo valve with 140 bar supply pressure, the achieved bandwidth for the pump controller is reported as 80 Hz, for measured frequency response for 10% amplitude of the commanded swash plate angle. In further studies, Grabbel et al. showed the pump control achieves sufficient dynamics, to compete with valve controlled drives [39].



**Figure 2-10 Digital displacement pump, e-dyn 96, proposed by Artemis intelligent power ltd. [40]**

In recent years, one interesting solution came from Artemis Intelligent Power, which focus on the displacement control of the pumps used in hydrostatic transmission circuits. They realized the patent of Salter and Rampen [41], who are the co-founders of the company. Instead of varying the stroke of the pistons mechanically i.e. with an adjustable swash plate mechanisms, they proposed to control pump output by digitally enabling individual cylinders on a stroke by stroke bases. In their design they provided electronically controlled digital valves, having a fast response like a few milliseconds, for each cylinder of the pump cylinders. They named this new technology as “Digital Displacement”, and they showed 10% energy efficiency at full stroke, and 30% energy efficiency at 10% stroke, can be achieved. The digital displacement solution is applied by Mitsubishi to the hydrostatic transmission system of a 7MW wind turbine, the operation test were successful and the durability tests were on going [42]. Further research on digital pump can be found in Phd thesis [43] and proceedings, [44] and [45].

## **2.5 Single Rod (Asymmetric) Hydrostatic Actuators**

The challenge with the single-rod actuators in conventional hydrostatic systems is the unequal pistons area of the single rod actuator. Either a deficient or excess flow rate is always formed in the closed circuit, corresponding to the difference between the swept fluid volumes by piston areas of the cap and rod sides. The flow difference occurring between the inlet/outlet ports of the actuator is named as “differential

flow”. In literature, several solutions exist for the differential flow compensation. These solutions cover, the addition of secondary pump, utilizing hydraulic transformers, and providing a third port inside the pump. After the brief review of these solutions, the single pump solution which is the subject of this thesis will be discussed.

**2.5.1 Multiple Pumps and Transformers**

The simplest solution to compensate for the unequal flow rate requirement on the main pump is the addition of a flow adjustable pump as a second active element to the hydraulic circuit. Possible circuit schemes utilizing two pumps control is shown in Figure 2-11 [46]. The 1<sup>st</sup> and 3<sup>rd</sup> circuit solutions are much appropriate for displacement control since, the pumps are tandem connected. On the other hand, the 2<sup>nd</sup> and 4<sup>th</sup> circuits are appropriate for fixed displacement pumps with independent variable speed drives.

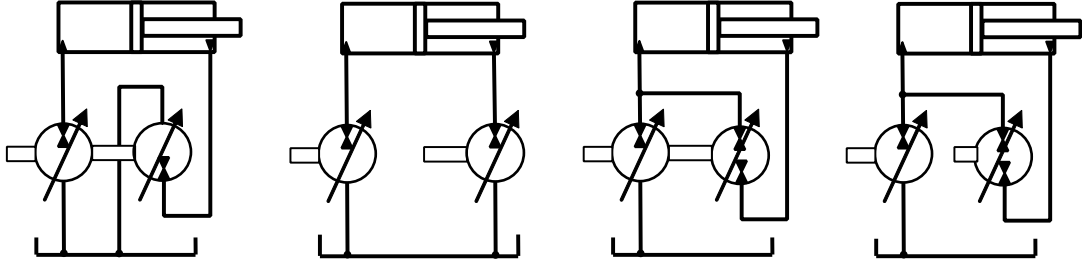


Figure 2-11 Possible circuit configurations for two pumps control

The first two circuit solutions, given in Figure 2-11, have an open circuit configuration. Therefore, for the motion control of the actuator, the pump flow rates should be adjusted synchronously with a ratio determined by the actuator piston side areas. On the other hand, in the last two hydrostatic circuit schemes only one pump, whose two ports are connected to the actuator, determines the motion control of the actuator, while the second pump is utilized to compensate the differential flow rate, as well as the leakage losses. Therefore, generally the 3<sup>rd</sup> scheme is utilized for the displacement control solutions [47], [48], [49], [50], [51], and the 4<sup>th</sup> scheme is utilized for the speed controlled solution [52], [53], [54].

The earliest two-pump solution dates back to 1970, which is proposed by Wetzel as a Patent application [47], however, the industrial realization is not that early. In 1999, Helduser applied the 4<sup>th</sup> circuit scheme on an injection molding machine [52]. He utilized two internal gear pumps with fix displacement and driven by two AC servo motor. The schematic view of the system is shown in Figure 2-12 (a). In his paper, Helduser showed the energy saving potential of the electric drives, elimination of idling losses, and regeneration of the braking energy. He further remarked the necessity of the pump that should operate under relatively small speed, below 300 rpm.

In 2008, the use of two pump solutions with variable speed pumps is further investigated by Plummer et al. [55]. They applied a hydraulic circuit similar to the 4<sup>th</sup> circuit scheme given in Figure 2-11. However, different from the conventional circuit, they utilized hydraulic accumulators for energy regeneration as shown in Figure 2-12 (b). The system is further realized by a flight simulator made by Tales [56].

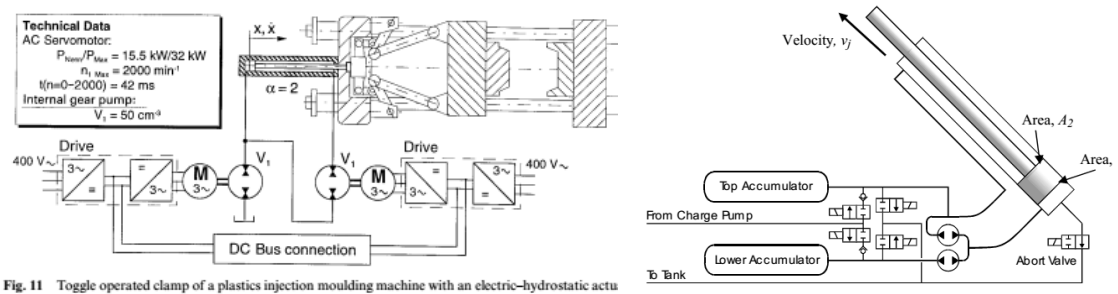


Figure 2-12 Two pump solutions (a) Helduser, [52] (b) Plummer, [55]

A theoretical and experimental analysis of the two pump solutions is also studied in the M.Sc. thesis of the author, further investigations can be found in [46]. Although, good dynamic responses that are comparable to a proportional valve controlled systems can be achieved [5], the application of two pump solution is limited, due to the increased cost and space requirements.

One further solution for differential flow compensation is the use of hydraulic transformers. In 1999, the company INNAS introduced an innovative transformer (IHT) for mobile applications. The principle of the IHT is based on a constant

displacement unit, like a bent axis axial piston unit. However, the IHT contains three ports instead of two and the valve plate can be rotated. The IHT combines the functions of a hydraulic pump and motor in one unit, therefore it is able to transform hydraulic power to hydraulic power [57]. In Figure 2-13, the working principle is illustrated with a comparison by conventional valve flow control. In 2003, floating cup principle is introduced by the same company [58]. By using this principle the number of pistons of the IHT is increased in order to reduce pressure pulsations, furthermore, the low speed behavior is improved [59]. In their further studies, hydraulic drive trains are prosed with the use of hydraulic transformers [60], [61].

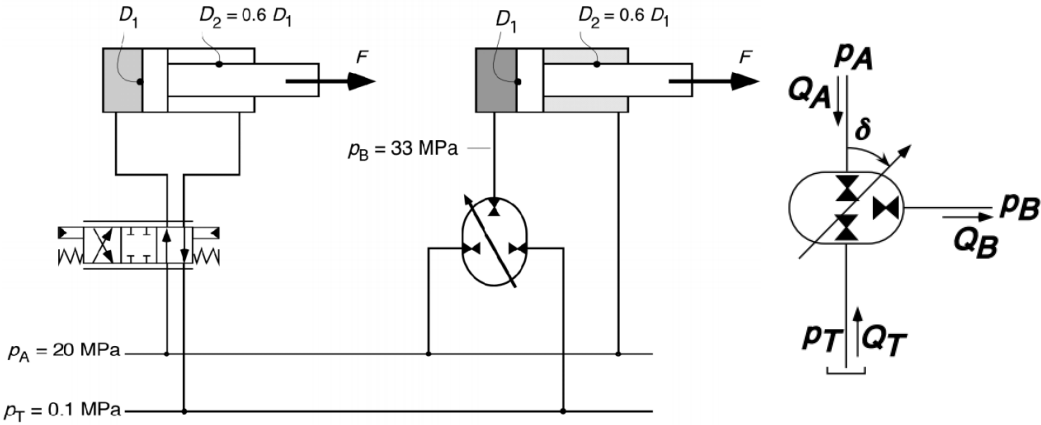


Figure 2-13 Working principle of IHT and comparison with directional flow control, [57]

Besides the two pump and hydro transformers, one further solution for differential flow compensation, is the use of three-port pump. In 1989, Parker Hannifin Corp. made a patent application for an embodiment utilizing a pump with 3 ports [10]. The circuit embodiment was proposed for the single rod actuator utilized in and electro hydrostatic circuit. They provided an asymmetrical port plate for the pump. A first port of this plate has a different radial extent from a second port which provides different sizes for the first and second ports. The mentioned dimensions are matched to the area ratio of the actuator piston. The hydraulic circuit diagram of the proposed system is Figure 2-14 (a). Two check valves (71, 73) are utilized to pressurize the transmission lines and to prevent cavitation, the differential flow is compensation by providing a third port (59) on the pump. Although published in 1990, no researches addressed the three-port pump concept. In 2008, Long presented the “asymmetric

pump” solution with 3-ports as shown in Figure 2-14 (b). He made simulation models and experimentally investigated the pressure, flow and noise characteristics [62]. In his further studies, he concentrated on the development of the fix displacement asymmetric axial piston pump (DAAPP) [63].

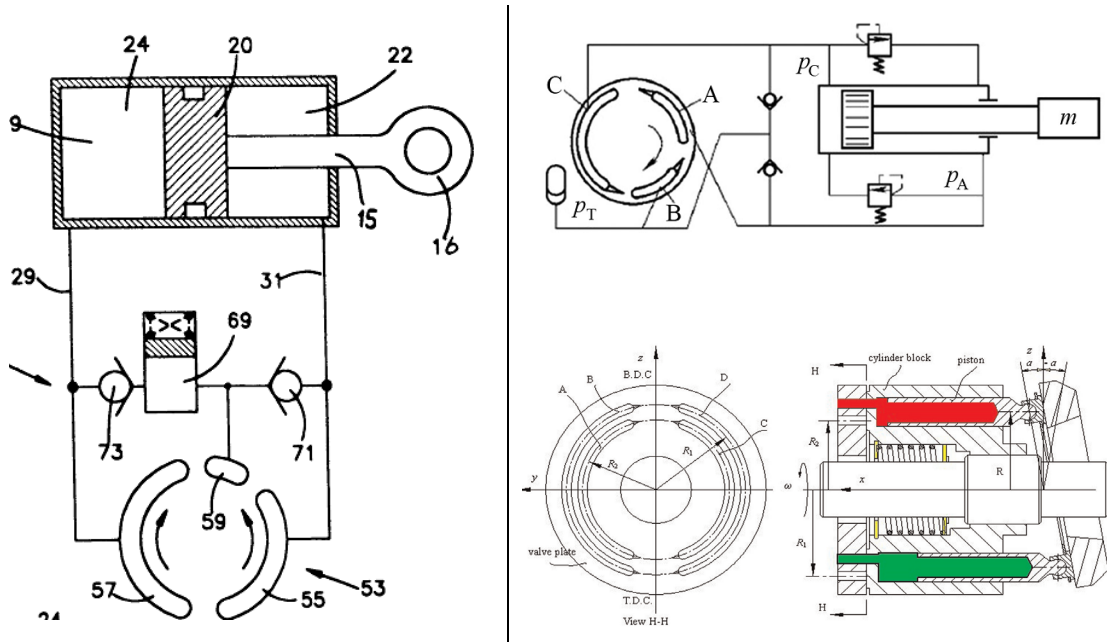


Figure 2-14 (a) 3-port pump solution, Parker Corp., [10], (b) Asymmetric pump solution, Long, Q., [62]

Since the number of control elements and efforts are not increased, the use of hydro-transformer or 3-port pump seems to be a reasonable solution when compared to the two-pump solutions. However, there also seems to be a need for the development of these recent hydraulic machine technologies. In the following section the solutions utilizing one “conventional pump”, either displacement or variable speed controlled, are reviewed. Further reviews, on the energy saving hydraulics can be found in [64], [65], [66].

### 2.5.2 Single Pump Solutions

If the differential flow compensation problem is restricted with the usage of a single conventional pump and if the usage of a multiple pumps or multiple port pumps are excluded, then the possible solution conceptually necessitates an external hydraulic source/sink and some connection components enabling flow in between the closed circuit and the hydraulic source/sink. This conceptual solution, shown in Figure 1-3, is similar to the conventional hydrostatic circuit, where an external supply replaces

leakage losses of the closed circuit over back to back connected check valves. However, beyond the one-directional flow of the check valves, here, the connection components should enable a bi-directional flow in between the hydraulic source/sink and the closed circuit. An excess flow should be returned to the hydraulic sink in the retraction phase of the actuator ( $v_A < 0$ ), and a deficient amount of flow should be supplied back to the closed circuit in the extension phase ( $v_A > 0$ ).

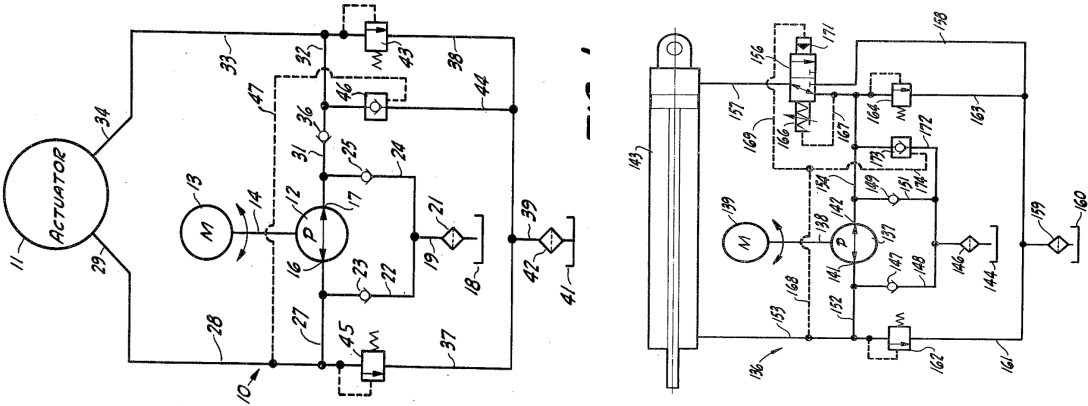


Figure 2-15 Use of pilot operated check valve for differential flow compensation, [67]

The differential flow compensation problem is not a new research topic. Early solutions dated back to 1949 and 1953, the use of check valve, [68], and suction shuttle valve, [69], were suggested, respectively. Both patents addressed the single rod actuator, and used a reversible pump. However, both the two do not provide continuous 4-quadrant operation. In 1975 Gellatly et al, utilized a pilot operated check valve shown in Figure 2-15, [67]. In the solution shown in Figure 2-15, a pilot operated check valve (a-46 or b-113) is connected in between the cap side chamber of the actuator and the reservoir. The pilot pressure of this valve is given by the rod side chamber. When raising a load (retraction), the pressurized rod side chamber opens the check valve (a-46 or b-113), and excess flow rate of the caps side chamber is extracted to the reservoir. When a lowering the load (extension), again the check valve is opened due to the pressurized rod side chamber, but this time deficient flow will be delivered from the reservoir to the cap-side chamber of the actuator.

In 1994, Hewet, from British Columbia University, patented a circuit solution utilizing a shuttle valve and a pressurized supply, [70]. His circuit solution is shown

in Figure 2-16. The differential flow rate of the single rod actuator is compensated over the “circulation valve” (42), which is a 2 way 3 position shuttle valve, located in between the “fluid supply” (50) and the actuator chambers. Furthermore, similar to conventional hydrostatic circuit, he utilized the back to back located check valves providing one direction flow, and preventing cavitation. In his patent, Hewet explained the required position of the circulation valve for each loading condition of the actuator. However, the actuation mechanism is not mentioned.

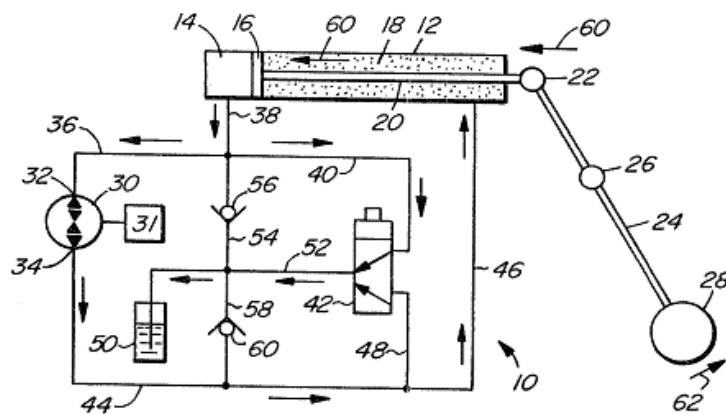


Figure 2-16 Hydraulic circuit flow control, Hewet patented in 1994, [70]

In 2000, Rahmfeld and Ivantysynova addressed the same problem [71], [72]. Similar to Hewet, they utilized a low pressure accumulator line and proposed the use of two pilot operated check valves in between the accumulator and closed circuit. The schematic view of the circuit is shown in Figure 2-17.

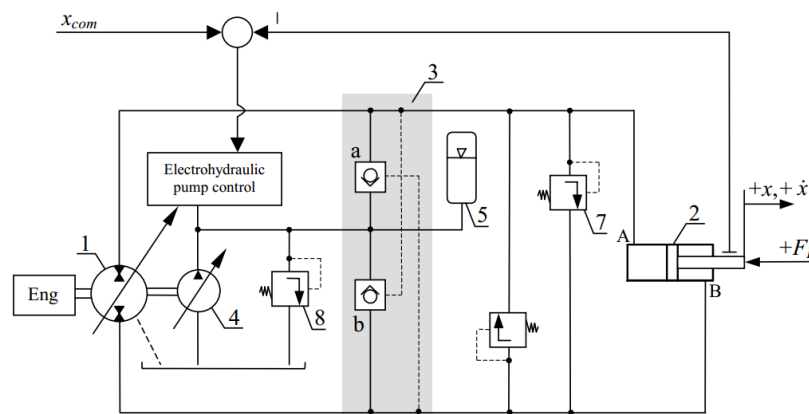


Figure 2-17 Pilot Operated Check Valves Solution, Rahmfeld, [71]

In the proposed solution given in Figure 2-17, a variable displacement pump is connected directly to a single rod actuator (2). A charge pump (4) together with an accumulator (5) and pressure relief valve (8) is used for the pressurization of low pressure line. Two pilot operated check valves (3) ensure that the low pressure side of the cylinder (2) is always connected to the accumulator line, which depends on the operating quadrant. In his thesis, by using the external load versus actuator velocity,  $F_L$ - $v$ , plane, Rahmfeld explained the four quadrant operation principle of this circuit [73].

In Figure 2-18,  $Q_{max}$  defines the maximum flow rate,  $A_K$  defines the caps side piston area, and  $\alpha$  defines the area ratio of the rod side piston area to the cap side piston area. Rahmfeld mentioned that different from the valve controlled systems, the high/low speeds of the actuator is defined by the load acting on the cylinder, not upon the moving direction. The distinction is determined by the “static switching force”,  $F_L^*$ , which is found by equating the chamber pressures,  $p_A, p_B$ , to the spring switching pressure,  $p_{sp}$ , namely,  $F_L^* = (1 - \alpha)A_K p_{sp}$ . When the load acting on the actuator is higher than the switching force,  $F_L > F_L^*$ , the pilot operated check valve (3-b) opens; if the actuator is extending ( $\dot{x} > 0$ ), flow is supplied from accumulator, to rod side chamber., else if it is retracting, then the flow is extracted to accumulator. Similarly, when the load is lower than the switching force  $F_L < F_L^*$ , pilot operated check valve (3-a) opens; if the actuator is extending ( $\dot{x} > 0$ ), flow is extracted from cap side chamber to accumulator, else if it is retracting, then the flow is supplied from accumulator to cap side chamber.

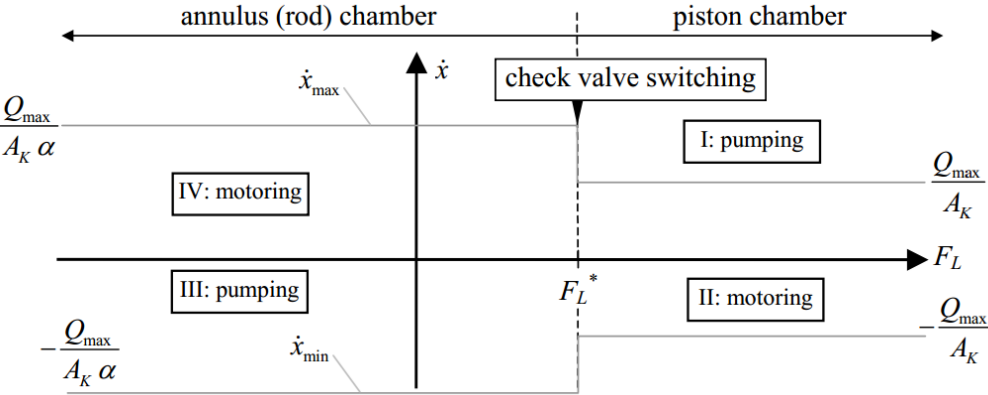
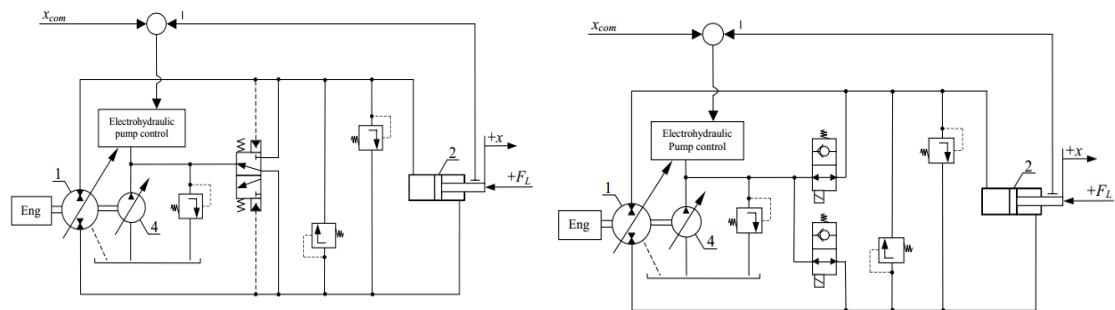


Figure 2-18 Four quadrant operation of differential cylinder in displacement control, [73]

In his thesis, Rahmfeld further suggested two more alternative hydraulic circuit schemes, which are shown in Figure 2-19. In the first circuit scheme, the two pilot operated check valves are replaced by a pilot operated 3/2-way switching (shuttle) valve. Similar to pilot operated check valves, this valve always connects the low pressure chamber to the accumulator line. As a second alternative, Rahmfeld proposed the replacement of two pilot operated check valves, by two switching or proportional 2/2-way valve. However, these alternative circuit solutions shown in Figure 2-19 are only explained conceptually and are not investigated. Only the pilot operated check valve circuit, given in Figure 2-17, is investigated and applied on several applications.



**Figure 2-19 Alternative circuit solutions proposed by Rahmfeld, [73]**

The pilot operated check valve circuit solution, given in Figure 2-17, is applied to wheel loader, where 15% fuel consumption is realized with respect to load sensing system [74]. The circuit is further evaluated for active vibration damping of off-road vehicles, [75]. Williamson applied the same circuit for the active vibration damping of skid steer loader, where the total vibration reduced up to 34% [76]. Later on Hippalgaonkar and Zimmermann applied the same circuit solution to mini excavator, [77], [78], and mentioned that 40% percent fuel saving is possible [79].

Besides mobile applications, the use of pilot operated check valve is also utilized in stationary applications. Ahn replaced the variable displacement pump with a fix displacement pump driven by an DC electric motor [80]. By using the same circuit, he worked on different force control techniques [81], [82], [83].

Although prosperous results are achieved in terms of energy efficiency, the challenge with the direct displacement pump control systems in mobile machinery applications is the space limitations and the cost. They have to fit more pumps in an already compact machine. On the other hand, by using electric drive and variable speed instead of variable displacement pump, Parker Hannifin realized the direct pump control circuit as an industrial product as shown in Figure 2-20 (a) [16]. In 2011, Parker Hannifin Corporation published a patent for an electro hydraulic actuator, with single rod cylinder [84]. The proposed EHA of the Parker, is designed for off road mobile applications, for example opening a door, and it works in an open loop manner. Since no feedback from the actuator position is utilized for the motor speed, problems named as “run-away” occurs. In their patent, they mentioned that in conditions when an external force (like gravity) is working in the same direction of the actuator movement, there is a potential that the load (like door) move faster than the maximum rate the actuator is capable of moving. In order to prevent this deficiency, they proposed to use of pressure compensated flow control (PTFC) valves (60) as shown in Figure 2-20. By integrating the PTFC valves, the hydrostatic circuit is able to maintain a minimum internal pressure sufficient to keep the pilot operated check valves operating correctly. Furthermore, they provide manual opening valves (62), as a backup, in case of power failure, and incorporate a filter (64) on the discharge of fluid to reservoir (16) as the rod either extends or retracts.

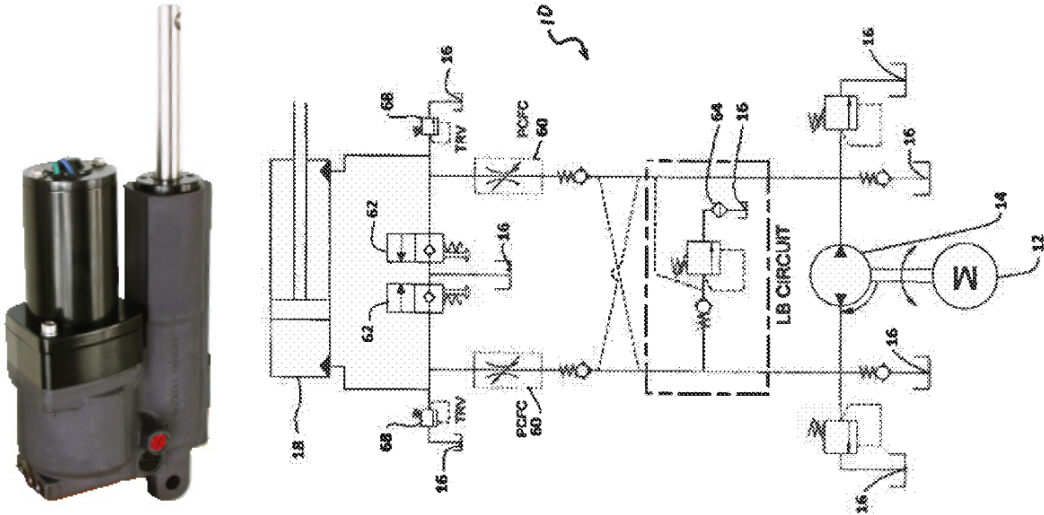


Figure 2-20 EHA circuit scheme patented by Parker in 2011, [84]

The problem with the pilot operated check valve circuit is first reported by Williamson and Ivantysynova [17]. They investigated the displacement controlled boom lift cylinders of a skid-steer loader, and reported that undesired pressure oscillations occur, while rapidly lowering small loads. The position and velocity response of the boom actuator together with chamber pressures are given in Figure 2-21. They mentioned that when the boom lowering speed increases to the point where the friction force on the cylinder is higher than the load, the check valves switch, the pump switches from motoring mode (4<sup>th</sup> quadrant) to pumping mode (3<sup>rd</sup> quadrant), and the cylinder velocity increase. Then, they commented that, due to flow resistance and pressure resonance in the cylinder and lines, cap side pressure may then rise above rod side pressure and the pump shifts back to 4<sup>th</sup> quadrant. Due to the switching between pumping and motoring modes, they named this problem as “pump mode oscillation”. For the solution of the problem, they proposed a predictive observer to provide sufficient lead time for feedforward control of actuator. They presented a discrete time observer, which predicts future system states by delaying the input signal, 40 ms or more.

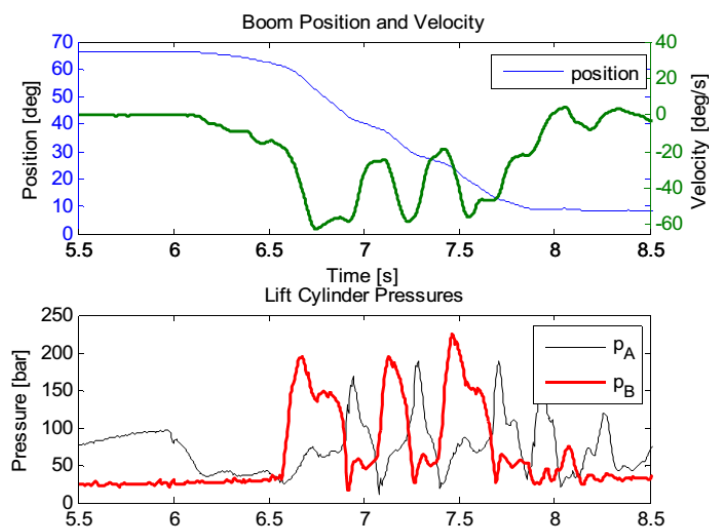


Figure 2-21 Measured pump mode oscillations reported by Williamson and Ivantysynova, [17]

The mode switching problem of the pilot operated check valve circuit solution is further investigated by Wang and Book [85], [86]. The undesired and uncontrolled pressure and velocity due to switching of the system, in between the pumping and the motoring modes, is named as the “internal instability” of the system, and the reason

of the problem is shown as pilot operated check valves. Wang defined the desired working region for problem-free operation of a hydrostatic circuit on a pressure plane, whose axes are defined by the cap-side ( $P_a$ ) and the rod-side ( $P_b$ ) chamber pressures of the actuator, as shown in Figure 2-22 (a). According to this working region, either the cap side  $P_a$  or rod-side chamber  $P_b$ , pressure should be equal to the accumulator line pressure  $P_0$ .

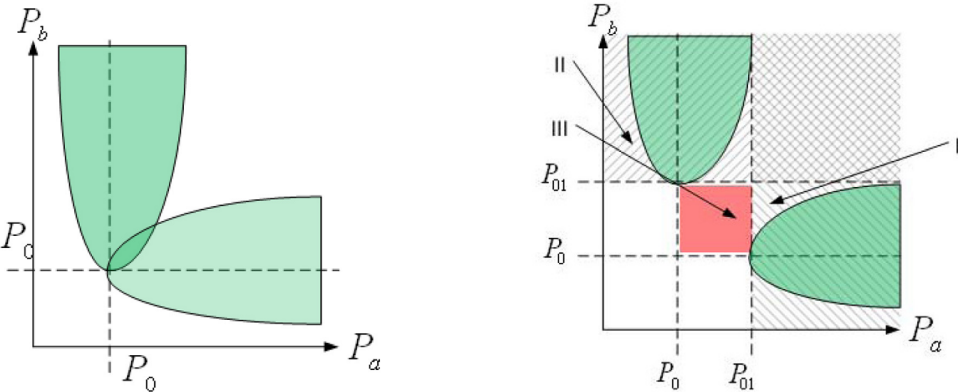


Figure 2-22 Working region of hydrostatic circuit (a) desired (b) P.O.C.V, [85]

Wang further draw the working region of the pilot operated check valve circuit solution, disclosed previously by Rahmfeld and Ivantsynova [71], as shown in Figure 2-22 (b). He further disclosed that, the instability occurs, since the two check valves (3 a,b in Figure 2-17) are closed in the operating region determined by the accumulator line pressure ( $P_0$ ) and pilot pressure ( $P_{01}$ ) as shown in Figure 2-22 (b).. In the same study, Wang et al. proposed a circuit configuration as shown in Figure 2-23. The circuit consists of a pair of check valves (3a, 3b), a pair of flow control valves (4a, 4b), a pair of relief valves (5a, 5b), a three-position three-way shuttle valve (6), two pressure sensors, and a controller. Besides the proposed circuit, the whole system includes a displacement controlled pump (1), a charge pump (2), and a single rod cylinder (7). The stability compensation is accomplished by using small controlled leakage over the flow control valves (4a, 4b), whose switching's are determined by an inner loop controller according to the chamber pressure feedback.

Although it was claimed that the proposed circuit meets the desired working region, shown in Figure 2-22, experiments revealed that, under some loading conditions, oscillations occur during the retraction of the actuator. In order to explain this

behavior, Wang and Book made a mathematical model of the whole system, [87]. In their study, the shuttle valve was considered as an “*ideal switching element*” and the system was modeled as a combination of two linear systems switching according to a critical load value. Wang and Book concluded that the primary reason for instability had been the switching between two system dynamics. Their proposal to resolve the instability problem was to employ either a physical leakage or virtual leakage compensation [15]. The application of physical leakage requires the use of some additional valve components (4a, 4b in Figure 2-23) and pressure sensors, whereas the virtual leakage solution is restricted by the natural frequency of the system and pumps.

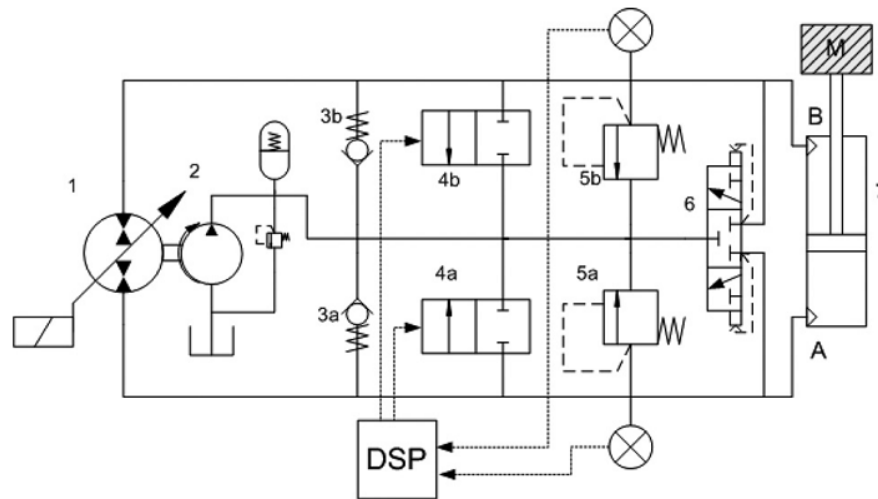


Figure 2-23 The proposed hydraulic circuit configuration by Wang and Book, [85]

In these two studies, Wang L. has neglected the shuttle valve dynamics and formed the mathematical model of the system by accepting the shuttle valve as an ideal switching component, either opened to the left or right. Actually, the closed center 3/3 shuttle valve (6 in Figure 2-23) that is used in his studies do not provide the required operating region on the actuator chamber pressure plane that he defined as shown in Figure 2-22-a. This is because the valve spool stays in the center position and does not switch until the difference between the actuator chamber pressures correspond to a force that would overcome the pre-compression of the spring that holds the shuttle valve in the center. Since the valve he uses is a closed centered one, when the pressure difference between the actuator chambers is less than the shuttle valve cracking pressure, both of the actuator chambers are closed to the accumulator

line, and thus an operating region similar to the use of pilot operated check valve (Figure 2-22-b) is formed.

## **2.6 Conclusion**

It is seen that the single pump hydraulic circuit solutions developed for single rod actuators mainly utilize pilot operated check valves or a shuttle valve for the compensation of the unequal flow rates. The common problem of these two circuit solutions is the undesirable pressure oscillations which are named as pump mode oscillation or system internal instability. In order to eliminate this problem, besides the controller related software solutions, addition of two on/off valve components together with sensor and actuator hardware is proposed as a physical solution. The stability problem is theoretically investigated only by Wang. However, in his mathematical model, he treated the shuttle valve as an ideal switching element.

In Chapter 4, the reason of system instability is investigated by including the shuttle valve parameters. Furthermore, different from the previous studies, a simple physical solution which is the use of an underlapped shuttle valve is proposed.

It should be ment

ioned that, in 2012, in the patent application [88], the author proposed the use of a shuttle valve for the flow compensation of single rod actuators. The proposed circuit is similar to Wang's solution in terms of the usage of an internal pilot operated shuttle valve. However, in the proposed system, the shuttle valve is not closed center and no additional valves are used for flow compensation. At last, it should be also noted that the Chapter 4 is mainly covered in the paper [89].

## CHAPTER 3

### MATHEMATICAL MODELING OF THE EHA

#### 3.1 Working Principle

In the scope of this thesis study, the very first proposed hydraulic circuit solution, [88], for a single-rod electro-hydrostatic actuator (EHA) is shown in Figure 3-1.

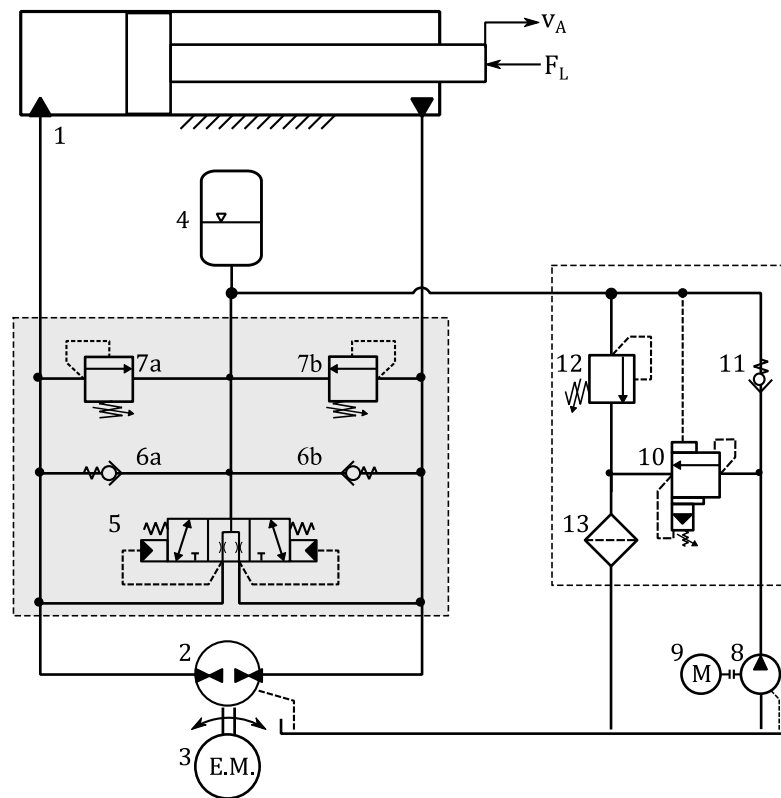


Figure 3-1 Proposed hydraulic system

A fixed displacement hydraulic internal gear unit, named as pump (2) is connected to two ports of a single rod actuator (1) in order to regulate the flow rate by changing its drive speed via an electric servo motor (3). A hydraulic accumulator (4) compensates the unequal flow rates for the retraction and extension of the actuator. The flow compensation is accomplished by a 3-position, 3-way shuttle valve (5), which is

spring-centered and has an internal pilot-operated spool. The shuttle valve connects the unpressurized chamber to the accumulator line by using the pressure of the pressurized chamber. A pair of, back to back connected, check valves (6a, 6b) ensures that the minimum line pressure is close to the accumulator pressure and prevent cavitation. Furthermore, they also compensate the deficient flow rate during actuator extension. A pair of pressure relief valves (7a, 7b) limits the maximum pressure of the closed system.

Besides these main components, the auxiliary accumulator charge circuit is seen in the right hand side of Figure 3-1. A fixed displacement pump (8), driven by an induction motor (9), delivers hydraulic fluid to the accumulator over the check valve (11). The accumulator charge pressure is limited by the pressure relief valve (12), whereas the pump pressure is limited by the unloading valve (10). When the accumulator pressure reaches the set level, unloading valve is opened and the pump flow rate is directed to the reservoir over the filter (13).

The accumulator charge circuit, shown inside the dashed-line square, is an auxiliary circuit which is only used to pressurize the hydraulic accumulator and can be any other type. The main valve components are shown inside a gray colored rectangular area. This part constitutes the connection between the hydraulic accumulator and the closed circuit of the pump/actuator coupling.



**Figure 3-2 Cartridge type shuttle valve and its components**

The hydraulic system has different circuit configurations determined by the shuttle valve position. Thus, the shuttle valve structure has to be mentioned first. The

structure of a standard cartridge type shuttle valve is shown in Figure 3-2. It consists of three main parts, valve spool, sleeve and head.

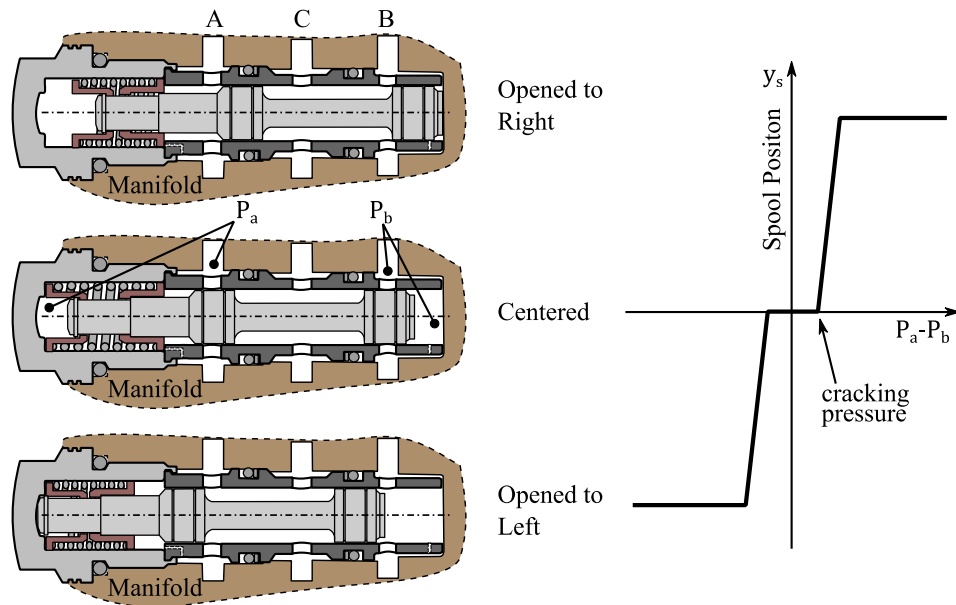


Figure 3-3 Schematic cross-section view of a shuttle valve mounted in hydraulic manifold

The representative view of a 3-way, 3-position shuttle valve is given in Figure 3-3. The two ports of the shuttle valve A and B are connected to the cap and the rod sides of the actuator, respectively, whereas the remaining port C is connected to the accumulator. Since the spool is centered by a pre-compressed spring, it is assumed to have 3-positions, namely: fully opened to the right or left or centered. The spool position is determined by the pilot pressures acting on the two sides of the spool. The spool starts to move when, the pilot pressure difference is greater than the valve cracking pressure, which corresponds to a force required to overcome the pre-compression force of the centering springs. Furthermore, each pilot pressure is determined by the related chamber pressure through the pilot conduit inside the valve. Therefore, the valve spool is positioned by the difference in chamber pressures resulting from the external load acting on the actuator. Heuristically, it can be concluded that the valve spool is saturated at the right end stroke when the external load  $F_L$ , is above some limit  $F_{L2}$ , and is saturated at the left end stroke when the external load  $F_L$  is below some limit,  $F_{L1}$ . Moreover, it can be further concluded that, if the external load is in between  $F_{L1}$  and  $F_{L2}$ , the valve spool is centered or partially opened to the right or left side.

Based on the above findings, the working principle of the system and possible circuit configurations are illustrated in 4-quadrants of the external force,  $F_L$ , versus actuator velocity,  $v_A$ , plane in Figure 3-4. In the 1<sup>st</sup> and 3<sup>rd</sup> quadrants, the system is working in the pumping mode, in which the power is delivered from the pump to the load, whereas in the 2<sup>nd</sup> and 4<sup>th</sup> quadrants, the pump is in the motoring mode, in which the power flow is from the load to the pump.

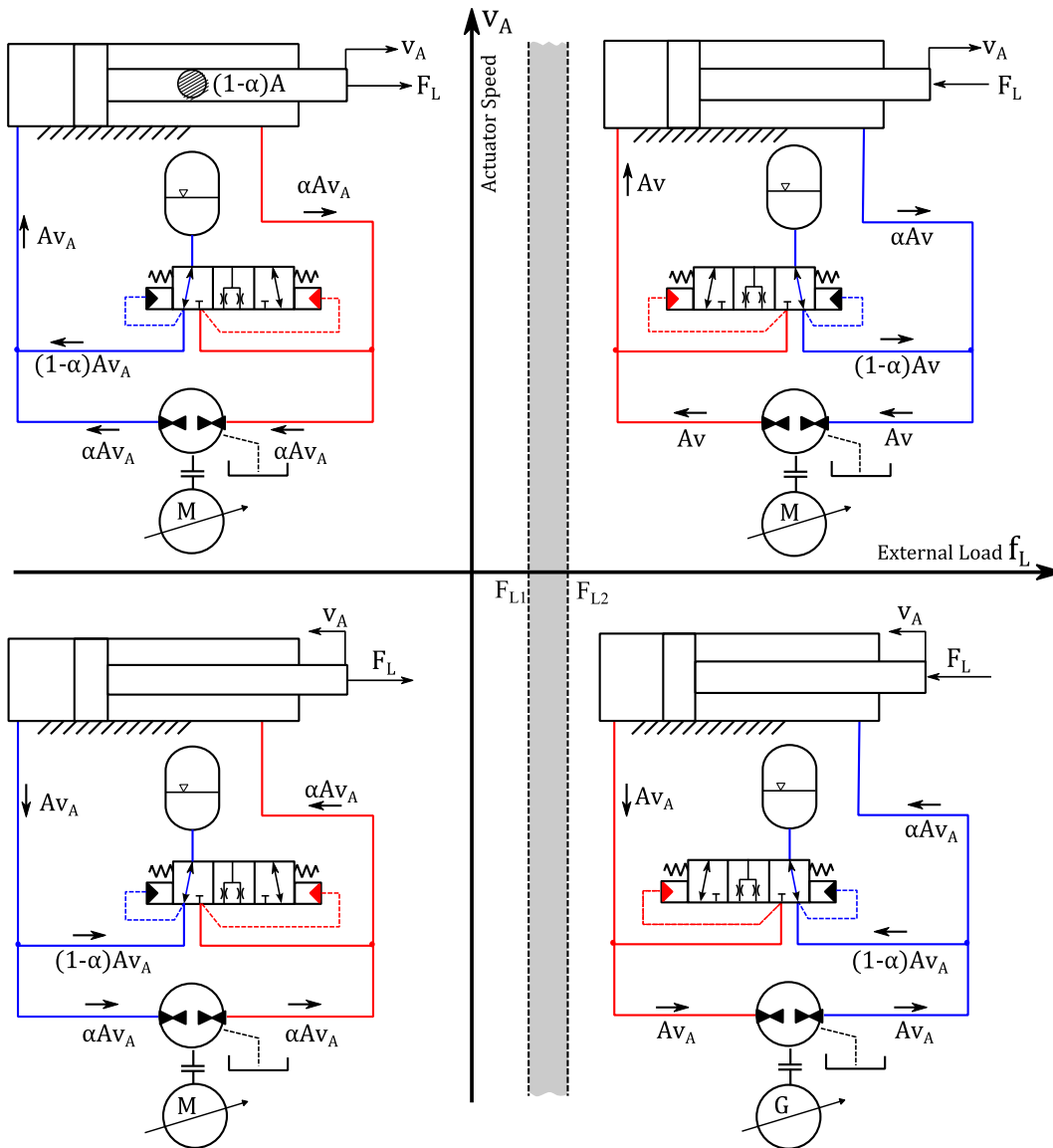


Figure 3-4 Four quadrant operation of the proposed hydraulic circuit

The circuit has mainly three possible configurations based on the spool position of the shuttle valve; namely, (i) the accumulator is connected to the chamber at the rod side of the actuator, (ii) it is connected to the chamber at the cap side of the actuator,

(iii) the spool is either centered or not centered (that is, partially opened to either both chambers or only one of the chambers). The spool of the internal pilot-operated shuttle valve is positioned according to the pressure difference between actuator chambers. This means that the circuit configuration is determined by the external load  $F_L$  acting on the actuator. The accumulator line is connected to the cap side when  $F_L < F_{L1}$  and to the rod side when  $F_L > F_{L2}$ . In these two regions, the shuttle valve is fully opened with a negligible resistance. Therefore, the accumulator and the actuator chamber connected to it can be assumed to have the same pressure. In the intermediate region in which  $F_L \in (F_{L1}, F_{L2})$  and pressures of two chambers are close to each other so that the spool of the shuttle valve is not fully opened but either centered or partially opened.

Next to the switching of circuit configurations, another important parameter is the flow direction of the accumulator, which is determined by the actuator motion. Neglecting all external leakages, the accumulator delivers a flow rate of  $(1 - \alpha)Av$  during the extension phase and stores the same flow rate during the retraction phase. Note that,  $\alpha \in (0,1)$  defined previously in Eq. (1-2), is the ratio of effective piston areas of the rod side and the cap side of the actuator, and  $A$  is the effective piston area of the cap side. Therefore,  $(1 - \alpha)A$  represents the area of the rod cross-section and  $(1 - \alpha)Av$  can be considered as the swept volume difference per unit time between retraction and extension phases.

### **3.2 Mathematical Modeling**

The EHA system consist of hydraulic actuator, hydraulic pump, transmission lines in between the pump and actuator, an electrical machine driving the pump, a shuttle valve and a hydraulic accumulator for differential flow compensation. The relations of these components together with the variables used in mathematical modeling are given in the free-body representation of the EHA given in Figure 3-5.

In this part of the thesis, the non-linear mathematical model of each component is derived. Based on the derived equation, a numerical simulation model developed in MATLAB<sup>®</sup>/Simulink<sup>®</sup> environment is constructed. Besides that model, a second numerical model consisting of the hydro-mechanical system is constructed in

MATLAB<sup>®</sup>/SimHydraulics<sup>®</sup> environment. The parameters used in the simulation models are either measured, or taken from the manufacturer catalogs.

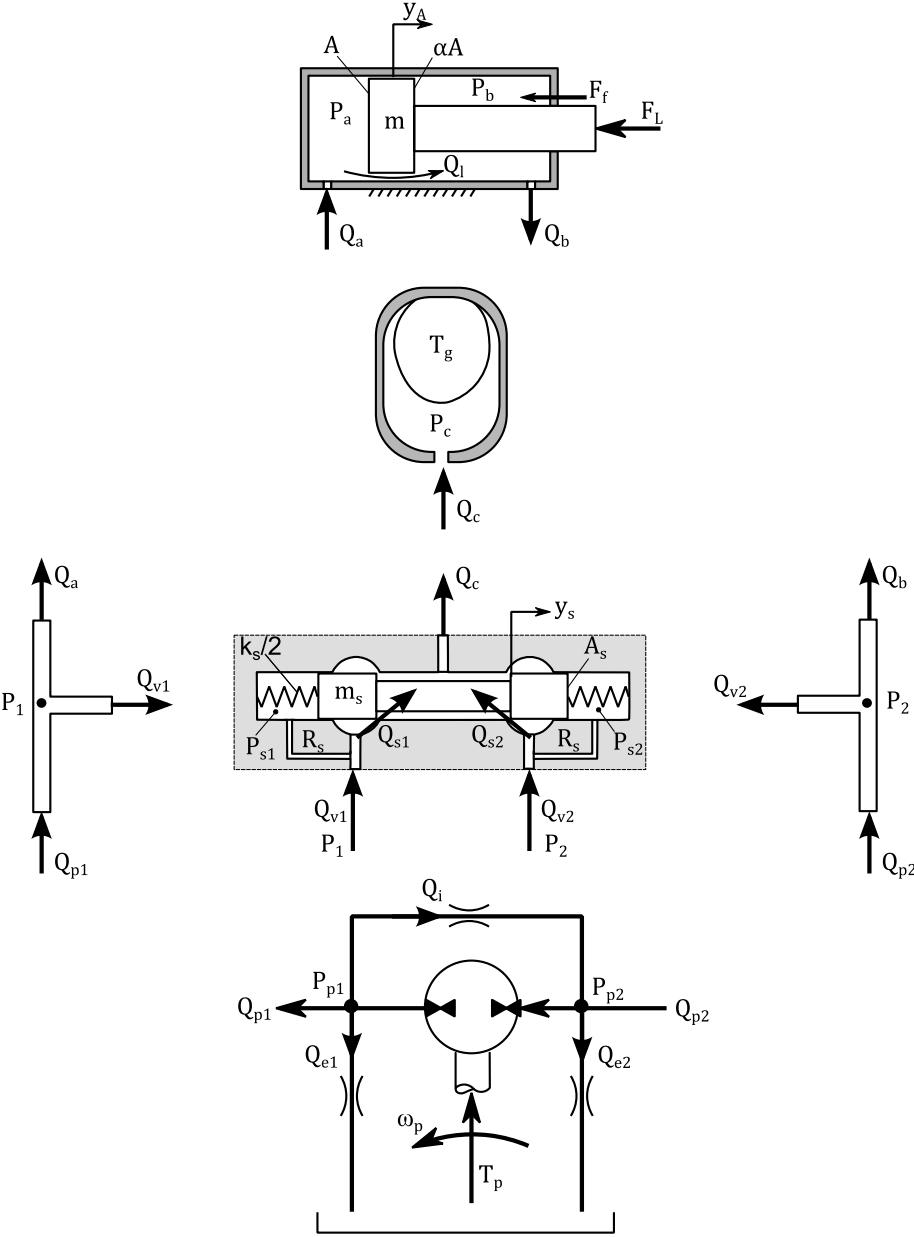


Figure 3-5 Free body representation of the EHA components

### 3.2.1 Hydraulic Actuator Model

The hydraulic actuator is a mechanic-hydraulic transducing element. It transforms the hydraulic energy to the mechanical energy or vice versa. In the mathematical modelling, only the cap-side piston surface area  $A$  is utilized. Instead of using a

different area parameter, the rod-side piston surface area is represented by using the area ratio defined in Eq. (1-2),  $A_{rod-side} = \alpha A$ .

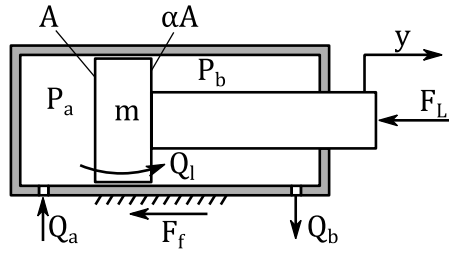


Figure 3-6 Hydraulic actuator model

The dynamics of the hydraulic actuator can be represented by one equation of motion and two flow continuity equations written for two actuator chambers. According to the direction definitions given in Figure 3-1, the equation of motion is written as

$$A(P_a - \alpha P_b) = m\ddot{y}_A + F_L + F_f \quad (3-1)$$

where,

$y_A$  = actuator position, in  $mm$

$P_a$  = cap-side chamber pressure, in  $MPa$

$P_b$  = rod-side chamber pressure, in  $MPa$

$A$  = cap side effective piston area, in  $mm^2$

$m$  = combined mass of the piston and rod of the actuator, in  $kg \cdot 10^{-3}$

$\alpha$  = is the rod-side to cap-side area ratio defined, previously

$F_L$  = total external force acting on the actuator, in  $N$

$F_f$  = friction force, in  $N$

The friction force,  $F_f$  is represented by Stribeck model given as

$$F_f = b\dot{y}_A + \text{sgn}(\dot{y}_A)(F_C + (F_H - F_C)e^{-c_H|\dot{y}_A|}) \quad (3-2)$$

where,

$b$  = viscous friction coefficient, in  $Ns/mm$

$F_C$  = Coulomb friction, in  $N$

$F_H$  = break away friction, in  $N$

$c_H$  = transition coefficient, in  $s/mm$

In this friction model, a constant Coulomb friction  $F_C$  and breakaway friction  $F_H$  are dominant when the actuator is changing its direction and the viscous friction becomes dominant with the coefficient  $b$  as the velocity of the actuator increases.

According to the direction definitions given in Figure 3-6, the flow continuity equations for two chambers of the actuator are written as follows.

$$Q_a = A\dot{y}_A - Q_l + C_a\dot{P}_a \quad (3-3)$$

$$Q_b = \alpha A\dot{y}_A + Q_l - C_b\dot{P}_b \quad (3-4)$$

where,

$Q_a$  = flow of actuator port A, in  $mm^3/s$

$Q_b$  = flow of actuator port B, in  $mm^3/s$

$Q_l$  = leakage flow between actuator chambers, in  $mm^3/s$

$C_a$  = hydraulic capacitance of the cap side chamber, in  $mm^3/MPa \cdot s$

$C_b$  = hydraulic capacitance of the rod side chamber, in  $mm^3/MPa \cdot s$

Capacitance values  $C_a$  and  $C_b$  of the actuator chamber in Eqs. (3-3) and (3-4) are determined according to the hydraulic actuator position  $y$  as follows.

$$C_a(y_A) = \frac{1}{E}(V_{a0} + Ay_A) \quad (3-5)$$

$$C_b(y_A) = \frac{1}{E}(V_{b0} + \alpha A(L - y_A)) \quad (3-6)$$

where,

$E$  = bulk modulus of the hydraulic oil, in  $MPa$

$V_{a0}$  = cap-side chamber dead volume, in  $mm^3$

$V_{b0}$  = rod-side chamber dead volume, in  $mm^3$

$L$  = stroke of the hydraulic actuator, in  $mm$

The leakage flow loss,  $Q_l$ , in between the hydraulic chambers is assumed to be laminar and proportional to difference of the chamber pressures and defined as follows.

$$Q_l = H_{iA} (P_a - P_b) \quad (3-7)$$

where, the  $H_{iA}$  is the leakage flow coefficient, in  $mm^3/s \cdot MPa$ .

The parameters used of the hydraulic actuator used in the simulation models are given in Table 3-1.

**Table 3-1 Parameters of the hydraulic actuator**

<b>Parameter</b>	<b>Description</b>	<b>Value</b>	<b>Unit</b>
$A$	cap side piston surface area	2827.4	$mm^2$
$\alpha$	area ratio	0.75	—
$m$	combined mass of the piston and rod	9.36	$kg$
$L$	stroke of the hydraulic actuator	200	$mm$
$b$	viscous friction coefficient	6300	$Ns/mm$
$F_C$	Coulomb friction	200	$N$
$F_H$	break away friction	300	$N$
$c_H$	transition coefficient,	500	$s/mm$
$V_{a0}, V_{b0}$	cap/rod side dead volume	0.2	$l$
$E$	bulk modulus of the hydraulic oil,	1100	$MPa$

### 3.2.2 Pump Model

The hydraulic pump is the heart of the EHA. A constant displacement internal gear pump is used in the developed EHA. The pump a symmetrical structure and is able to operate in 4-quadrant of the plane defined by the differential pressure versus flow rate axes. Operation in 4-quadrant means that the pump unit can both work as a hydraulic pump or a hydraulic motor that is both the high pressure port and the flow direction can change. Figure 3-7 represents on the pump how the high and low pressure ports and the flow direction changes in the 4-quadrant.

According to the positive direction definitions given in Figure 3-5, the flow continuity equations at the inlet and outlet ports of the pump are written as follows.

$$Q_{p1} = D_p \omega_p - H_i(P_{p1} - P_{p2}) - H_e P_{p1} \quad (3-8)$$

$$Q_{p2} = D_p \omega_p + H_i(P_{p1} - P_{p2}) - H_e P_{p1} \quad (3-9)$$

where,

$D_p$  = pump displacement, in  $mm^3/rad$

$\omega_p$  = angular velocity of the pump, in  $rad/s$

$P_{p1}$  = hydraulic pressure at delivery port, in  $MPa$

$P_{p2}$  = hydraulic pressure at suction port, in  $MPa$

$H_i$  = internal leakage coefficient, in  $mm^3/s \cdot MPa$

$H_e$  = external leakage coefficient, in  $mm^3/s \cdot MPa$

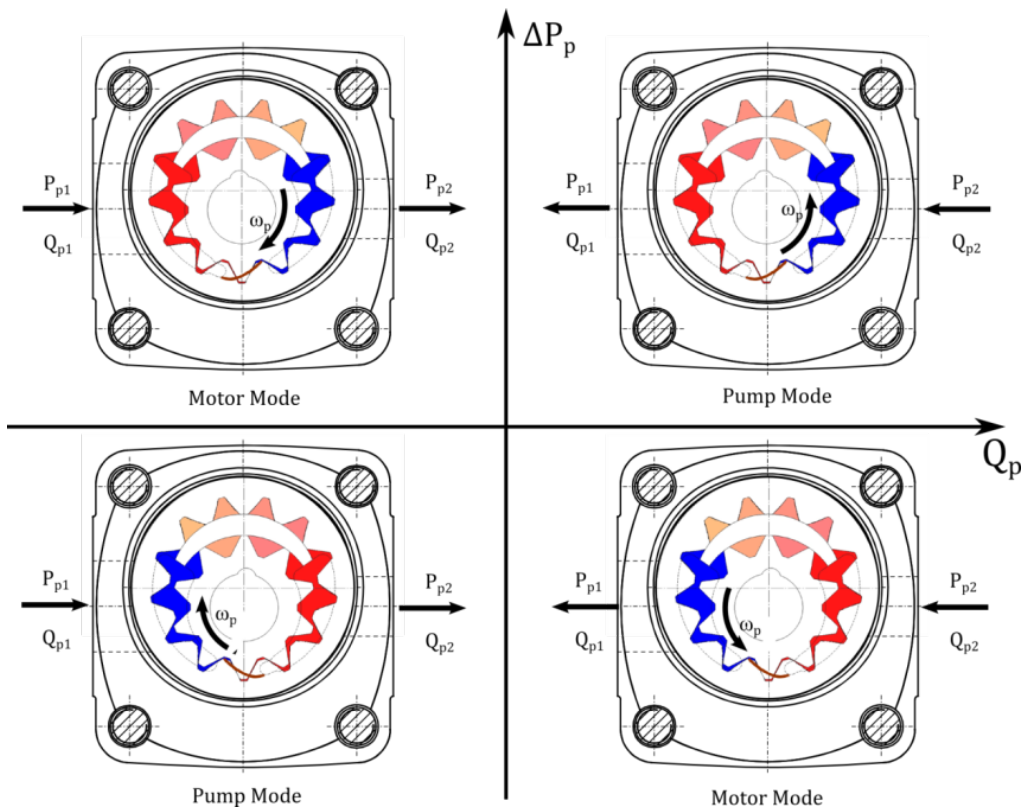


Figure 3-7 4-quadrant operation of the hydraulic internal gear unit, pump

In the pump flow continuity equations, the first term represents the theoretical flow rate, and the latter represents the internal and external leakage losses, respectively. There are many factors like temperature, pressure, drive speed etc. affecting the

leakage coefficients meaning that machine performance is almost impossible to define in general terms [90]. In this study, a 1D look up table is formed that determines the leakage coefficients based on the difference of the chamber pressures. The look up table is formed by the pressure versus leakage flow data received from the manufacturer data as shown in Figure 3-8.

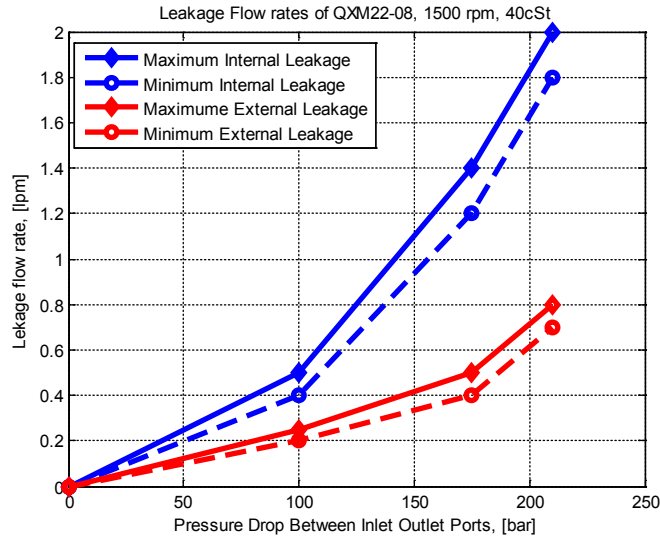


Figure 3-8 Internal and external leakage losses of the hydraulic internal gear pump

The torque community equation on the pump shaft is written as follows.

$$T_P = D_p(P_{p1} - P_{p2}) + T_f + J_P \ddot{\omega}_P \quad (3-10)$$

where, the first term represents the hydraulic torque while the second represents the losses.

$D_p$  = pump displacement, in  $mm^3/rad$

$P_{p1}$  = hydraulic pressure at delivery port, in  $MPa$

$P_{p2}$  = hydraulic pressure at suction port, in  $MPa$

The friction losses  $T_f$  is represented as follows.

$$T_f = b_p \omega_p + D_p |P_C + (P_H - P_C) e^{-c_{HP} |\omega_p|} | \text{sgn}(\omega_p) \quad (3-11)$$

where,

- $b_p$  = viscous friction coefficient, in  $Nm/s$   
 $P_C$  = Coulomb friction pressure equivalent, in  $MPa$   
 $P_H$  = stiction pressure equivalent, in  $MPa$   
 $c_{HP}$  = transition coefficient, in  $s/rad$

The parameters used of the hydraulic actuator used in the simulation models are given in Table 3-2.

**Table 3-2 Parameters of the hydraulic pump**

Parameter	Description	Value	Unit
$D_p$	displacement	8	$cm^3/rev$
$J_p$	mass inertia	1.9	$kgm^2 \cdot 10^{-4}$
$b_p$	viscous friction coefficient	0.035	$Nms/rad$
$P_C$	Coulomb friction pressure equivalent,	150	$Pa$
$P_H$	stiction pressure equivalent,	250	$Pa$
$c_{HP}$	transition coefficient	500	$s/rad$

### 3.2.3 Shuttle Valve Model

The 3-position, 3-way shuttle valve utilized in the hydraulic circuit is spring centered and internal pilot operated. A pre-compressed spring located at the head of the valve, as shown in the schematic cross-section view in Figure 3-3, centers the valve spool. However, for modeling purposes and to accentuate the symmetry, two parallel connected springs with stiffness  $k_s/2$  and located at the two ends of the spool are considered as shown in Figure 3-9.

The spool position is determined by the pilot pressures  $P_{s1}$  and  $P_{s2}$  acting on the two ends of the spool. The input port pressures  $P_1$  and  $P_2$  generate the pilot pressure, over an inner conduit with resistance  $R_{sv}$ . The pressure dynamics of the valve spool can be represented by two equations as follows.

$$\frac{P_1 - P_{s1}}{R_{sv}} - A_s \dot{y}_s = C_{s1} \dot{P}_{s1} \quad (3-12)$$

$$\frac{P_2 - P_{s2}}{R_{sv}} + A_s \dot{y}_s = C_{s2} \dot{P}_{s2} \quad (3-13)$$

where,

$R_{sv}$  = resistance of the inner conduit, in  $MPa \cdot s/mm^3$

$A_s$  = pressure-sensitive area of the shuttle valve spool, in  $mm^2$

$C_{s1}, C_{s2}$  = hydraulic capacitance of spool chambers, in  $mm^3/MPa$

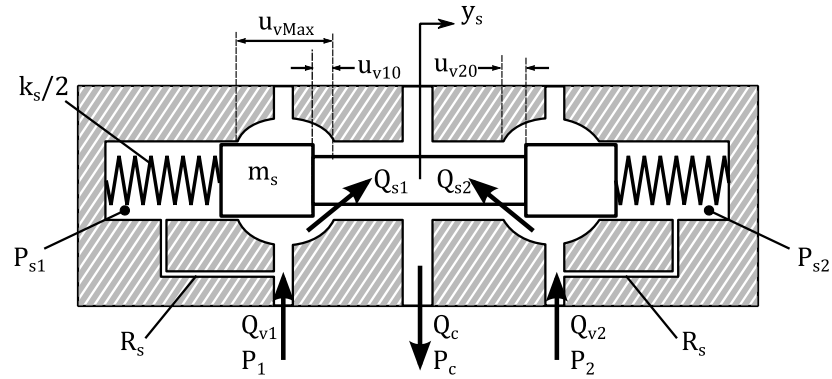


Figure 3-9 Shuttle valve model

The pressure dynamics can be well understood if it is represented with only one equation. The valve spool is symmetric and the pressure-sensitive areas at the two ends are equal, therefore, the pressure dynamics can be represented with only one equation by defining two new variables,  $\Sigma P_s$  and  $\Sigma P_{12}$ , which correspond to the summation of pilot and line pressures, respectively.

$$\Sigma P_s = P_{s1} + P_{s2} \quad (3-14)$$

$$\Sigma P_{12} = P_1 + P_2 \quad (3-15)$$

Summing Eq. (3-13) with Eq. (3-12), and assuming the spool chamber capacitances are equal  $C_{s1} = C_{s2} = C_s$ , the pressure dynamics in terms of sum pressures is defined as follows.

$$\frac{\Sigma P_{12} - \Sigma P_s}{R_{sv}} = C_s \Sigma \dot{P}_s \quad (3-16)$$

It should be noted that Eq. (3-16) states a first order low pass filter between the summation of the line and pilot pressures as given in Eq. (3-17). The valve spool motion can be isolated from the high frequency line pressure dynamics, by increasing the time constant, i.e., either increasing the line resistance  $R_s$  by utilizing a narrower conduit, or by increasing the chamber volume.

$$\Sigma P_s = \frac{1}{R_{sv}C_{sS} + 1} \Sigma P_{12} \quad (3-17)$$

Considering viscous type of friction between the spool and the bearings, and including the two parallel connected springs, the equation of motion of the valve spool is written as follows.

$$f_s(\Delta P_s)A_s = m_s \ddot{y}_s + b_s \dot{y}_s + k_s y_s \quad (3-18)$$

where,

$f_s(\Delta P_s)$  = net pressure acting on the spool, in *MPa*

$A_s$  = pressure-sensitive area of the shuttle valve spool, in *mm<sup>2</sup>*

$m_s$  = mass of the valve spool, in *kg · 10<sup>-3</sup>*

$b_s$  = damping constant of the valve, in *Ns/mm*

$k_s$  = valve spring stiffness, in *N/mm*

and  $\Delta P_s$  is the difference of the pilot pressures, in *MPa*

$$\Delta P_s = P_{s1} - P_{s2} \quad (3-19)$$

The net pressure acting on the spool is determined by the dead zone function  $f_s(\cdot)$  which calculates the effective net pressure difference acting on the valve spool as follows as follows.

$$f_s(\Delta P_s) = \begin{cases} 0 & |\Delta P_s| \leq P_{sc} \\ \Delta P_s - P_{sc} \cdot \text{sgn}(\Delta P_s) & |\Delta P_s| > P_{sc} \end{cases} \quad (3-20)$$

here,  $P_{sc}$  is the cracking pressure required to overcome the pre-compression force, of centering springs. The valve spool is centered,  $y_s = 0$ , for the pressure difference  $|p_{s1} - P_{s2}| \in [0, P_{sc}]$ .

According to the directions given in Figure 3-9, the orifice openings are related with the spool position  $y_s$  as follows.

$$u_{v1} = u_{v10} - y_s \quad (3-21)$$

$$u_{v2} = u_{v20} + y_s \quad (3-22)$$

where,  $u_{v10}$ , and  $u_{v20}$ , in  $mm$ , are the orifice pre-openings corresponding to port A and B, respectively. The value of  $u_{v10}$  or  $u_{v20}$  is negative if a closed centered shuttle valve is utilized, i.e. if there exists a spool overlap.

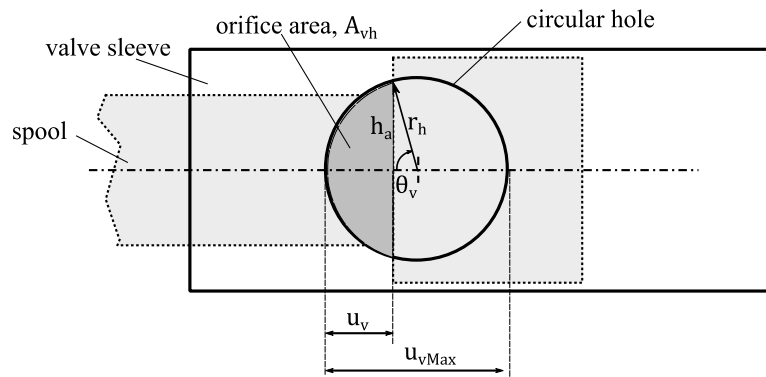


**Figure 3-10 Shuttle valve orifice area**

The spool position,  $y_s$ , is limited by the maximum orifice opening,  $u_{vMax}$ , and orifice pre-openings as follows.

$$y_{sMax} = u_{vMax} - u_{v10} \quad (3-23)$$

$$y_{sMin} = -(u_{vMax} - u_{v20}) \quad (3-24)$$

The shuttle valve utilized in the hydraulic system is a cartridge type and the orifice area is formed by the circular holes located on the valve sleeve. Therefore, the orifice area is not proportional to the valve spool position. Based on the given schematic in Figure 3-10, the orifice area corresponding to an orifice opening,  $u_v$ , is calculated as follows.

$$A_v(u_v) = \begin{cases} 0 & u_v < 0 \\ A_{vh}(u_v) & 0 < u_v < u_{vMax} \\ A_{vMax} & u_{vMax} < u_v \end{cases} \quad (3-25)$$

where, the function  $A_{vh}(\cdot)$  calculates opening area of each hole on the valve spool as follows.

$$\theta_v = \text{atan2} \left( \sqrt{r_h^2 - |r_h - u_v|^2}, (r_h - u_v) \right) \quad (3-26)$$

$$A_{vh} = n_h \frac{1}{2} r_h^2 (2\theta_v - \sin(2\theta_v)) \quad (3-27)$$

where,

$\theta_h$  = angle as defined in Figure 3-10, in *rad*

$r_h$  = hole radius, in *mm*

$n_h$  = number of holes on the valve sleeve

According to the direction definitions given in Figure 3-9, the flow rates,  $Q_{s1}$  and  $Q_{s2}$  through the orifices located at AC and BC ports, respectively, are defined by a quadratic relationship as follows.

$$Q_{s1} = A_v(u_{v1}) C_d \sqrt{\frac{2}{\rho} |P_1 - P_c| \text{sign}(P_1 - P_c)} \quad (3-28)$$

$$Q_{s2} = A_v(u_{v2}) C_d \sqrt{\frac{2}{\rho} |P_2 - P_c| \text{sign}(P_2 - P_c)} \quad (3-29)$$

where,

$A_v$  = area of each metering orifice defined in Eq.(3-25), in *mm*<sup>2</sup>

$C_d$  = discharge coefficient

$\rho$  = fluid density, in *kg · 10<sup>-3</sup>/mm<sup>3</sup>*

The accumulator flow rate is found by the flow continuity equation across the two metering orifices as follows.

$$Q_c = Q_{s1} + Q_{s2} \quad (3-30)$$

The valve inlet flow rates can be found by writing flow continuity equations at the input ports of the valve. According to direction definitions given in Figure 3-9, the flow continuity equations at each port are written as follows.

$$Q_{v1} = Q_{s1} + \frac{P_1 - P_{s1}}{R_s} \quad (3-31)$$

$$Q_{v2} = Q_{s2} + \frac{P_2 - P_{s2}}{R_s} \quad (3-32)$$

Note that, the accumulator flow rate can also be written in terms of valve inlet flows, by the summation of Eqs (3-31) and (3-32), and inserting (3-16) to the resulting equation, as follows.

$$Q_c = Q_{v1} + Q_{v2} - C_s \Sigma \dot{P}_s \quad (3-33)$$

where,  $C_s \Sigma \dot{P}_s$  is the total compressed flow inside valve spool chambers

In Table 3-3, the parameters of the closed center shuttle valve, which is from Bucher Company with code 400671602, are given.

**Table 3-3 Parameters of the shuttle valve**

Parameter	Description	Value	Unit
$k_s$	valve spring stiffness	4.62	$N/mm$
$C_d$	flow discharge coefficient	0.3	—
$A_{s1}, A_{s2}$	pressure-sensitive area of the shuttle valve spool	113.4	$mm^2$
$n_h$	number of holes on the sleeve	6	—
$r_h$	hole radius	2	$mm$
$m_s$	spool mass	35	$kg \cdot 10^{-3}$
$b_s$	damping constant of the valve	0.008	$Ns/mm$
$R_s$	resistance of the inner conduit	$6 \cdot 10^{-6}$	$MPa \cdot s/mm^3$
$C_{s1}, C_{s2}$	hydraulic capacitance of spool chambers	0.6	$mm^3/MPa$

Based on the above equations, the MATLAB<sup>®</sup>/Simulink<sup>®</sup> model of the shuttle valve is constituted as shown in Figure 3-11. The inputs of the model is the pressures at each port, namely,  $P_1$ ,  $P_2$ ,  $P_3$ , and the outputs are the flow rates  $Q_{v1}$ ,  $Q_{v2}$ ,  $Q_c$ . The uppermost part in Figure 3-11, represents the pressure dynamics, beneath that part represents the spool dynamics, beneath it represents the orifice area, and the undermost represents the flow rates at each port of the shuttle valve.

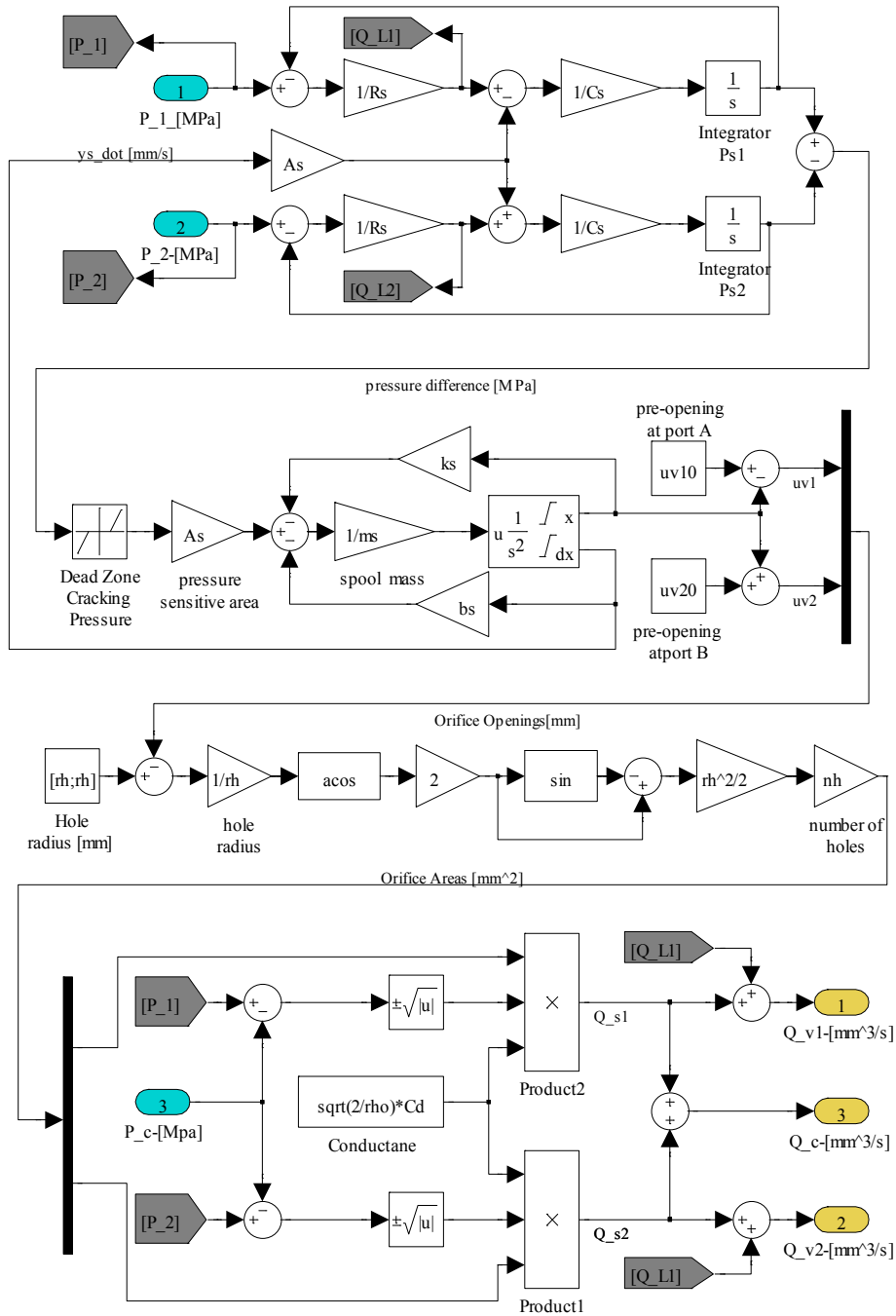


Figure 3-11 MATLAB<sup>®</sup>/Simulink<sup>®</sup>, non-linear simulation model of the shuttle valve

### 3.2.4 Electric Motor Model

The electric motor model is divided into two parts, the first part covers the modeling of the permanent magnet synchronous machine (PMSM) and the second part covers the motor controller. Note that in the scope of this thesis study, the converter is not modelled and assumed to be ideal. The motor controller model covers the speed and current regulators embedded in the motor driver.

#### 3.2.4.1 PMSM Model in d-q axis rotor reference frame

The servo motor utilized to drive the hydraulic pump is a 3-phase permanent magnet AC synchronous (PMSM). The synchronous machine equations are written in d, q rotor reference frame. The transformation of the synchronous machine equations from the a, b, c phase variables to the d, q variables forces all sinusoidal varying inductances in the a, b, c frame to become constant-in the d, q frame.

The d, q voltage equations are defined in rotor reference frame as follows [91].

$$u_d = R_s i_d + p(\lambda_d) - \omega_e \lambda_q \quad (3-34)$$

$$u_q = R_s i_q + p(\lambda_q) - \omega_e \lambda_d \quad (3-35)$$

where,  $p$  is the derivative operator, and

$\omega_r$  = electrical speed of the rotor, in  $rad/s$

$i_d, i_q$  = d and q axis currents, in  $A$

$u_d, u_q$  = d, q axis voltage, in  $V$

$R_s$  = stator resistance, in  $\Omega$

The electrical speed of the rotor is related with the mechanical rotor speed as follows.

$$\omega_e = n_p \omega_M \quad (3-36)$$

where  $\omega_M$  is the mechanical speed of the rotor, in  $rad/s$  and  $n_p$  is the number of pole pairs. The  $\lambda_d$  and  $\lambda_q$  terms are the d, q axis flux linkages, respectively, and are defined as follows.

$$\lambda_d = L_d i_d + \lambda_m \quad (3-37)$$

$$\lambda_q = L_q i_q \quad (3-38)$$

where,  $L_d, L_q$  are d, q, axis inductances, in  $H$  and  $\lambda_m$  is the mutual flux linkage of the permanent magnet, in  $Wb$ .

Inserting Eqs. (3-36), (3-37), (3-38) into the d,q axis equations (3-34), (3-35), the d and q axis stator currents are represented as follows.

$$L_d \frac{di_d}{dt} = u_d - R_s i_d + L_q n_q \omega_M i_q \quad (3-39)$$

$$L_q \frac{di_q}{dt} = u_q - R_s i_q - L_d n_p \omega_M i_d - \lambda_m n_p \omega_M \quad (3-40)$$

The electrical torque of a synchronous machine is defined as follows.

$$T_e = \frac{3}{2} n_p [\lambda_m i_q + (L_d - L_q) i_d i_q] \quad (3-41)$$

The electrical torque equation consists of two parts. The first part is the “mutual reaction torque”, and the second term corresponds to the “reluctance torque” which is due to the differences in d-axis and q-axis reluctance (or inductance). Note that for surface mounted permanent magnet motor,  $L_d = L_q$ , therefore, the reluctance torque term vanishes.

For constant flux operations when  $i_d$  equals zero, the electric torque  $T_e = 1.5 \lambda_m i_q = K_t i_q$ , where  $K_t$  is the motor torque constant. Note that the resulting torque equation of the PMSM resembles the dc machine.

The torque continuity equation on the rotor shaft is written as follows.

$$T_e = J_M \dot{\omega}_M + b_M \omega_M + T_P \quad (3-42)$$

where,

$J_M$  = inertia of the electrical machine rotor, in  $kg \cdot m^2$

$b_M$  = equivalent friction coefficient of the rotor bearings, in  $Nm \cdot s/rad$

$T_P$  = load torque of the pump shaft, in  $Nm$

By using the Eqs. (3-39)–(3-42), the PMSM is modelled in MATLAB<sup>®</sup>/Simulink<sup>®</sup> environment as shown in Figure 3-12. In this model the non-linearity due to current saturation are considered. The integrals of the  $i_d$  and  $i_q$  axis currents are limited. The saturation limit of  $i_q$  is taken to be the maximum current set point of the motor. On the other hand since no data is available for  $i_d$  current limit, therefore, it is also limited at the same value.

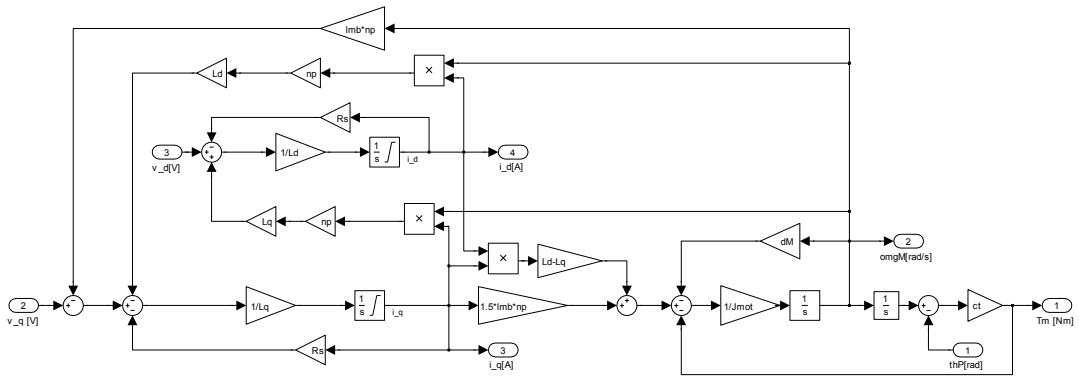


Figure 3-12 PMSM model developed in MATLAB<sup>®</sup>/Simulink<sup>®</sup> environment

The parameters of the electric motor, Siemens 1FK7083, used in the simulation model are given in Table 3-4.

Table 3-4 Parameters of the servo motor

Parameter	Description	Value	Unit
$J_M$	mass moment of inertia	27.3	$kg \cdot m^2 \cdot 10^{-4}$
$b_M$	viscous friction coefficient	$7 \cdot 10^{-3}$	$Nms/rad$
$L_d, L_q$	pressure-sensitive area of the shuttle valve spool	6.3	$mH$
$n_p$	number of pole pairs	4	—
$R_s$	mtator resistance	0.4	$\Omega$
$k_T$	torque constant	1.52	$Nm/A$
$k_V$	back emf constant	97	$V/10^3rpm$

### 3.2.4.2 Motor Driver and Controller

MATLAB<sup>®</sup>/Simulink<sup>®</sup> model of the motion control unit of Siemens CU320 is constituted. The Siemens controller uses cascade velocity and current controllers for the motion control of the electric motor. PI control action is utilized in both controllers. The controller model is shown in Figure 3-13. The velocity controller produces the torque set point as the control output. The torque set point is filtered by a second order discrete time filter and converted to current set point. In the current controller both q-axis and d-axis currents are controlled by PI regulator. Since the reaction torque is generated by the q-axis current only, its value is determined by the torque set point only. The d-axis current set point is zero, since d-axis current creates reluctance torque and decrease the generated motor torque.

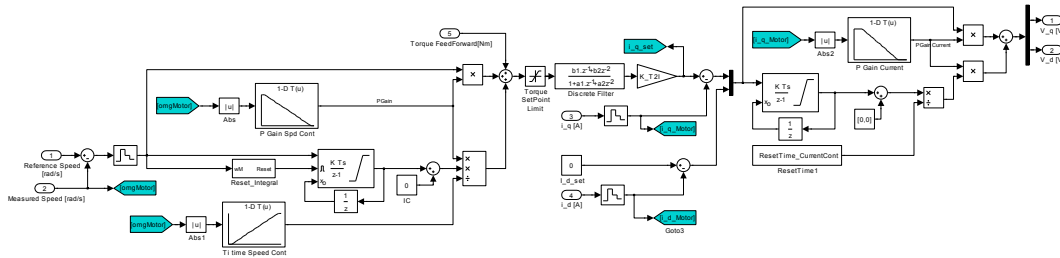


Figure 3-13 Speed and current controller of the PMSM, developed in MATLAB<sup>®</sup>/Simulink<sup>®</sup>

In Siemens motion controller, the proportional gain and the time constant of the velocity controller are scheduled according to the motor speed. Furthermore, the P gain of the current controller is reduced depending on the current. For that reason, a look up table is formed in Simulink. In order to prevent sharp changes soft adaptation is performed by using “*tanh*” function. The adaptation of the P gains and the integral time constant by look up tables is seen in Figure 3-13.

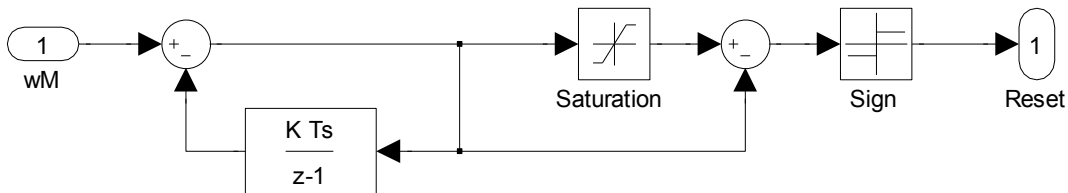


Figure 3-14 Integral reset model used in the speed and current controllers

The integral of the velocity controller is resettled at transient region, where the error change is considerably high. The integral reset model is shown in Figure 3-14. Note that no Siemens documentation can be found about the integrator wind up algorithm. However from the test results it is concluded that the integral is resettled at transient region. If the integral reset algorithm is disabled, then the overshoot of the model is considerably higher, (up to  $\approx 20\%$ ), than the real system response. Note also that the limit seen in the integral reset is found by trial and error and is set to the maximum torque set point.

### 3.2.4.3 Model Verification

The MATLAB<sup>®</sup>/Simulink<sup>®</sup> model responses of the motion controller and the PMSM model are compared with the real system responses. The model is constituted for comparison and it is shown in Figure 3-15. In the comparison and identification test, first a step input is given to the Siemens motion controller and data is collected with 4 ms sampling time by the Siemens SCOUT<sup>®</sup> software. The data taken from Siemens software are reference and actual velocity, q and d-axis currents and voltages. The test data is then converted to .xls file and finally converted to .mat file. The source blocks seen in the Figure 3-15 are the data collected by the Siemens software, i.e the real system response.

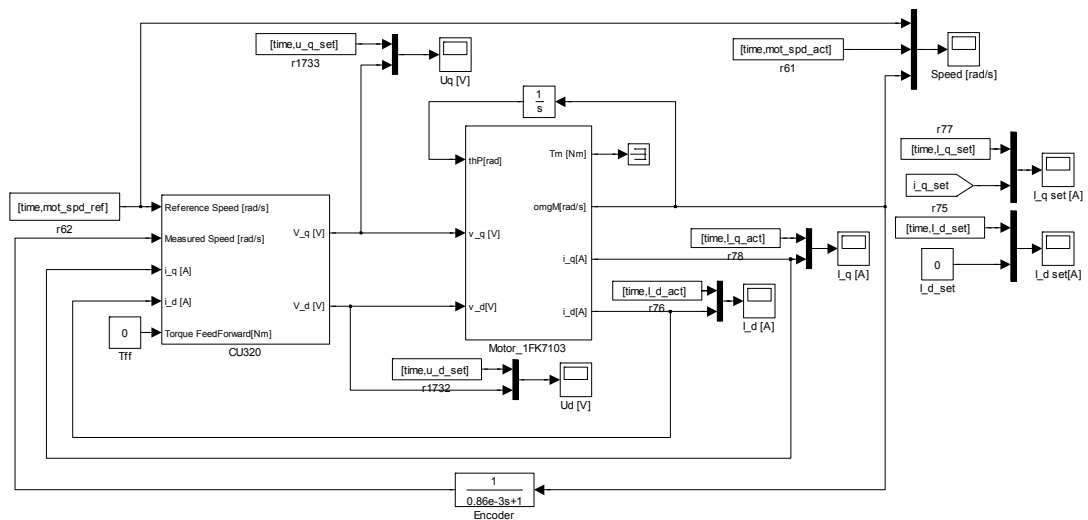


Figure 3-15 Simulink<sup>®</sup> model verification file

The comparison of the measured motor speed and d, q current responses with the MATLAB<sup>®</sup>/Simulink<sup>®</sup> model output are given in Figure 3-16 and Figure 3-17

respectively. In Figure 3-16 the rms error between the measured and model output velocity responses is 43.56 rpm. The maximum error is  $\approx 250\text{rpm}$ , but it occurs during the transition zone after the step input. On the other hand, the error between the maximum overshoots is  $\approx 50\text{rpm}$  and the error at steady state is zero.

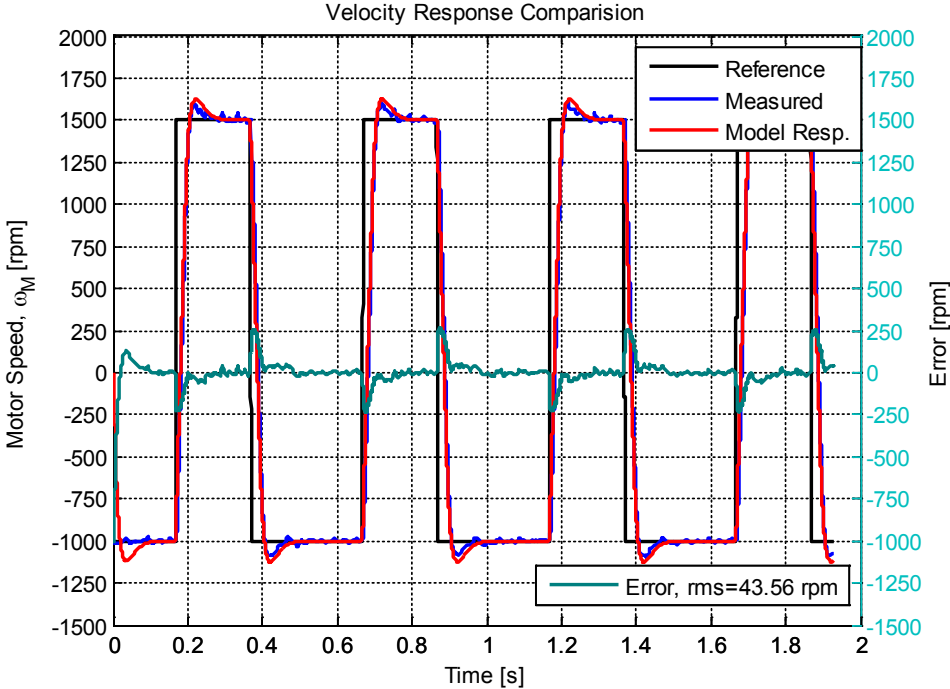


Figure 3-16 Comparison of measured and model output velocity response

In Figure 3-17, the d, q axis current response comparison is given. It is seen that the q-axis current responses of the model and measurement fits well. The rms of the error between the measured and model response data is 2.3 A. The highest error,  $\approx 40\text{ A}$ , occurs during the transition and is due to phase lag. On the other hand, at steady state the rms error is relatively low. For example between  $t = (0.55, 0.65)\text{s}$ , the rms of the error between the measurement and the model response is 0.25 A and the error between the mean of the measurement and model response is 0.025 A. The q-axis current is responsible for the reaction motor torque, therefore, the steady state current is mainly determined by the friction coefficient,  $b_M$ . The friction coefficient is not supplied by the manufacturer, its value,  $b_M = 0.7 \cdot 10^{-2}\text{ Nm} \cdot \text{s/rad}$  is found by fitting the model response to measurement data.

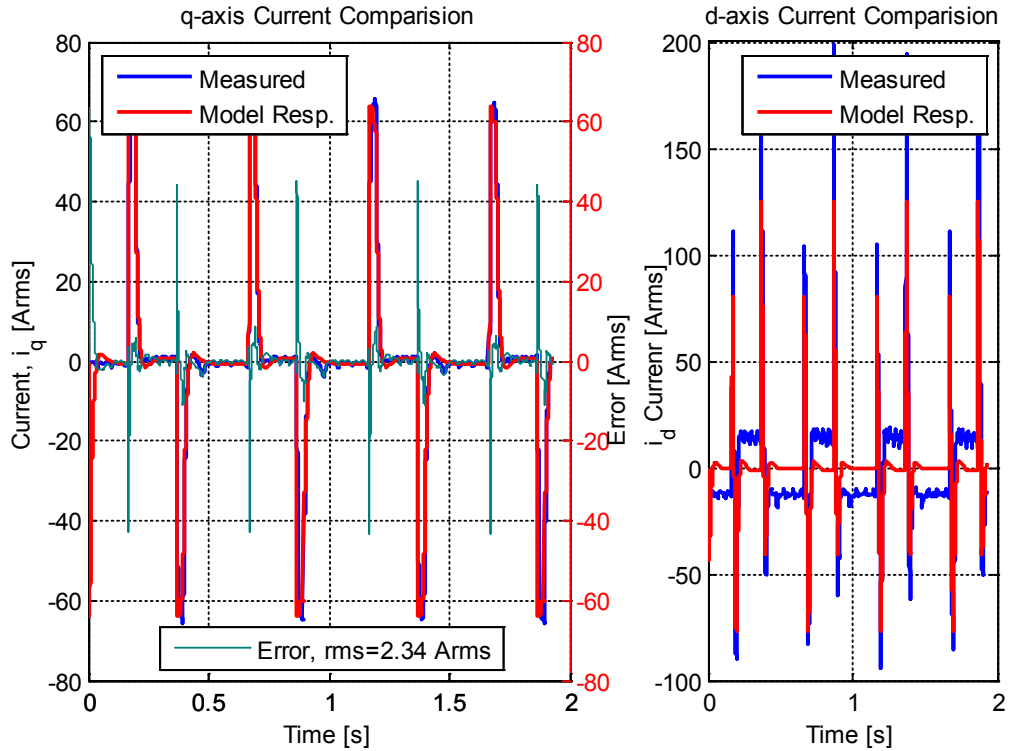


Figure 3-17 Comparison of measured and model output d-q axis currents

Unlike the q-axis current response, the d-axis current response does not fit the measurement response, there occurs steady state errors, and the peak values are not the same. The reference d-axis current is set to zero since it will create a reluctance torque. From the comparison results, it is seen that the d-axis current controller has to be modified. However, there is no information provided for that controller, the saturation limits and integrator windup algorithms are not provided by the manufacturer. As a conclusion, since the motor torque is related with q-axis current, and it fits well with the model response the motor model is considered as sufficient.

### 3.2.5 Hydraulic Accumulator

Hydraulic accumulator is a pressure vessel that can hold a relatively large volume of fluid under pressure. In fluid power applications it is generally used as an energy storage device, pulsation damper, surge compressor or emergency power source. On the other hand, in the proposed EHA system, the hydraulic accumulator is used as a pressurized source/sink for differential flow compensation. Therefore, its

mathematical model is obtained, in order to investigate the effects of hydraulic accumulator dynamics, on the EHA system.

In the EHA system, a bladder type gas charged hydraulic accumulator is preferred, because it is much more compact and lighter in weight when compared to weight or spring loaded accumulators. The gas charge accumulators utilize the compressibility of the gas (usually nitrogen) in order to store energy.

In literature the hydraulic accumulator is commonly modeled by assuming the gas undergoes a polytropic process, which is defined as follows.

$$P_g V_g^n = \text{Constant} \quad (3-43)$$

where,

$P_g$  = absolute gas pressure, in  $N/m^2$

$V_g$  = gas volume in  $m^3$

$n$  = polytropic exponent

The polytropic process as defined in Eq. (3-43) does not completely characterize the gas, it neglects the thermal losses. It is obvious that the gas temperature varies in response to mechanical work done on it. During the oil inflow through the accumulator, the charge-gas is heated by compression and begins to transfer heat to the walls. During the oil outflow the gas expands and the gas temperature falls below the surrounding temperature and heat flow occur in opposite direction. Although the heat flows in and out almost cancel each other, their dissipative effects do not cancel, since entropy is increased irrespective of flow direction. Therefore if the charge-gas pressure versus volume is plotted on a P-V plane, the thermal losses create a hysteresis loop [92]. On the other hand, polytropic process characterizes the gas dynamics with a single line on the P-V plane. Polytropic exponents cannot produce a hysteresis loop unless the value of  $n$  in Eq. (3-43) is varied in some way during the entire cycle. Neglecting thermal losses may be a reasonable assumption; however it will lead errors in low frequency, since there is time for heat transfer at low frequency excitations. Therefore in order to gain insight, investigate the effects of thermal losses and see the extent of polytropic process assumption a detailed model

is constructed and compared with the polytropic process model outputs. In this part of the thesis,

- first, in order to describe the thermo-mechanical transduction, i.e. the relation between the work done on the charge gas and the heat generated, the constitutive equations of the charge gas is derived
- second, in order to represent the entropy production, the heat transfer through the accumulator wall is modelled.

### 3.2.5.1 Constitutive Equations of the Charge-Gas

The constitutive equations of the charge-gas are derived by ideal gas assumption and energy balance equation. Many low density gases at low temperatures are modelled as ideal gases. The ideal gas is characterized by the following equation.

$$P_g V_g = m_g R_g T_g \quad (3-44)$$

where,

$P_g$  = gas pressure, in  $Pa$

$V_g$  = gas volume, in  $m^3$

$m_g$  = mass of the gas, in  $kg$

$R_g$  = gas constant, in  $J/kg K$

$T_g$  = absolute gas temperature, in  $K$

Thermal effect interaction can be modelled by writing energy balance equation. The first law of the thermodynamic states that,

$$dU = \delta Q - \delta W \quad (3-45)$$

where,

$dU$  = the net change in the internal energy of the system, in  $J$

$\delta Q$  = the heat added to the gas, in  $J$

$\delta W$  = the work done by the expansion of the gas, in  $J$

In the modelling process, in Eq. (3-45), the kinetic and potential energy change of the gas is neglected, only internal energy is considered. The work done by the expansion

of the gas is  $\delta W = P_g dV_g$ , and the heat added to the gas in terms of entropy is  $\delta Q = T_g ds_g$ . Furthermore, ideal gas assumption states that the internal energy of a gas is the function of temperature only.

$$dU = m_g c_v dT_g \quad (3-46)$$

where,

$c_v$  = specific heat at constant volume, in  $J/kgK$

Note that entropy and volume are extensive variables, that is their value vary with the amount (extent) of the substance, therefore the ideal gas and energy balance equation can be written in terms of specific entropy  $s_g$ , and specific volume  $v_g$ . In thermodynamics context “specific” means “per unit mass”, therefore, the relation between the extensive variables and their specific counterparts are,

$$s_g = S_g/m_g \quad (3-47)$$

$$v_g = V_g/m_g \quad (3-48)$$

where,

$s_g$  = specific entropy, in  $J/kgK$

$v_g$  = specific volume, in  $m^3/kg$

Writing the internal energy, heat transferred and work done,  $dU$ ,  $\delta Q$  and  $\delta W$  respectively, in terms of in terms of temperature, entropy, pressure and volume variables, the resulting energy balance equation per unit mass will be as follows.

$$c_v dT_g = T_g ds_g - P_g dv_g \quad (3-49)$$

Using the ideal gas assumption  $P_g v_g = R_g T_g$  and re-arranging the last term of into Eq.(3-49), the energy balance equation is re-written as follows.

$$c_v dT_g = T_g ds_g - \frac{R_g T_g}{v_g} dv_g \quad (3-50)$$

Rearranging Eq. (3-50) so that entropy and volume are on the input side

$$\frac{dT_g}{T_g} = \frac{ds_g}{c_v} - \frac{R_g}{c_v} \frac{dv_g}{v_g} \quad (3-51)$$

Integrating and then taking the exponential, the gas temperature is found in the form of  $T_g = T_g(s_g, v_g)$ .

$$\frac{T_g}{T_{g0}} = \left( \frac{v_g}{v_{g0}} \right)^{-\frac{R_g}{c_v}} e^{\left( \frac{s_g - s_{g0}}{c_v} \right)} \quad (3-52)$$

where,  $T_{g0}, v_{g0}, s_{g0}$  are the initial states. The pressure can also be written in terms of entropy and volume,  $P_g = P_g(s_g, v_g)$ .

$$\frac{P_g}{P_{g0}} = \left( \frac{v_g}{v_{g0}} \right)^{-\left( \frac{R_g}{c_v} + 1 \right)} e^{\left( \frac{s_g - s_{g0}}{c_v} \right)} \quad (3-53)$$

Equation (3-52) together with Eq. (3-53) defines the constitutive equations of the ideal gas. These two equations are derived from ideal gas assumption Eq. (3-44) and the energy balance equation Eq. (3-49). The pressure,  $P_g$ , and temperature,  $T_g$ , of the charged gas are the across variables, and the specific entropy  $s_g$  and the specific volume  $v_g$  are the integrated flow variables.

### 3.2.5.2 Heat transfer across the accumulator wall

In the modelling of the heat transfer through the accumulator wall, in order to not to complicate the model, standard methods given under steady state conditions with no heat generation is used. It is assumed that the heat flux through the gas is proportional to the temperature difference between the temperature of the environment and the gas. According to the direction definition given in Figure 3-18, the heat flux is modelled as follows [93].

$$\dot{Q} = T_g \dot{S}_g = \frac{T_{eg} - T_g}{R_c} \quad (3-54)$$

where,

$T_{eg}$  = environment temperature, in  $K$

$R_c$  = equivalent resistance of the accumulator wall, in  $K/W$

In order to find the accumulator resistance, it is assumed that the temperature gradients are in the radial direction only, therefore it is treated as one dimensional. Considering the convection of the inner and outer surface areas, and the conduction through the wall, the accumulator resistance is modelled as follows.

$$R_c = \left( \frac{A_c}{\frac{1}{h_{ci}} + \frac{r_{ci}}{k_w} \ln \left( \frac{r_{co}}{r_{ci}} \right) + \frac{1}{h_{co}}} \right)^{-1} \quad (3-55)$$

where,

$A_c$  = surface area of the accumulator, in  $m^2$

$r_{ci}, r_{co}$  = inner and outer radius of the accumulator, in  $m$

$h_{ci}, h_{co}$  = inner and outer convection coefficients, in  $W/m^2K$

$k_w$  = thermal conductivity of accumulator wall, in  $W/mK$

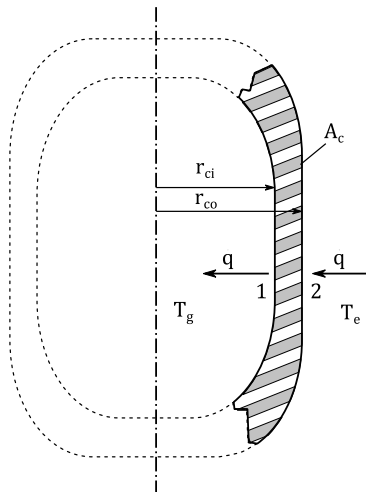


Figure 3-18 Heat transfer across the hydraulic accumulator wall

Note that entropy is produced irrespective of heat flux direction. According to the direction definition given in Figure 3-18, the net entropy generated is equal to  $\dot{S}_{net} = \dot{S}_{out} - \dot{S}_{in} = \dot{S}_1 - \dot{S}_2$ , which is always a positive quantity as given follows.

$$\dot{S}_1 - \dot{S}_2 = \frac{T_e - T_g}{T_g R_c} - \frac{T_e - T_g}{T_e R_c} = \frac{1}{R_c} \left( \frac{(T_e - T_g)^2}{T_e T_g} \right) \quad (3-56)$$

### 3.2.5.3 Non-Linear Simulation Model

The non-linear simulation model of the hydraulic accumulator is constructed in MATLAB<sup>®</sup>/Simulink<sup>®</sup> environment as shown in Figure 3-19. The input of the model is the shuttle valve flow rate,  $Q_c$  integrating this value give the volume change of the charge-gas ( $-dV_g$ ). The uppermost part in Figure 3-21, represents the gas temperature based on Eq. (3-52), and the undermost represents the gas pressure based the constitutive equation, Eq. (3-53). In between the two is the heat transfer and entropy generation process, which is defined by Eqs. (3-54) and (3-56).

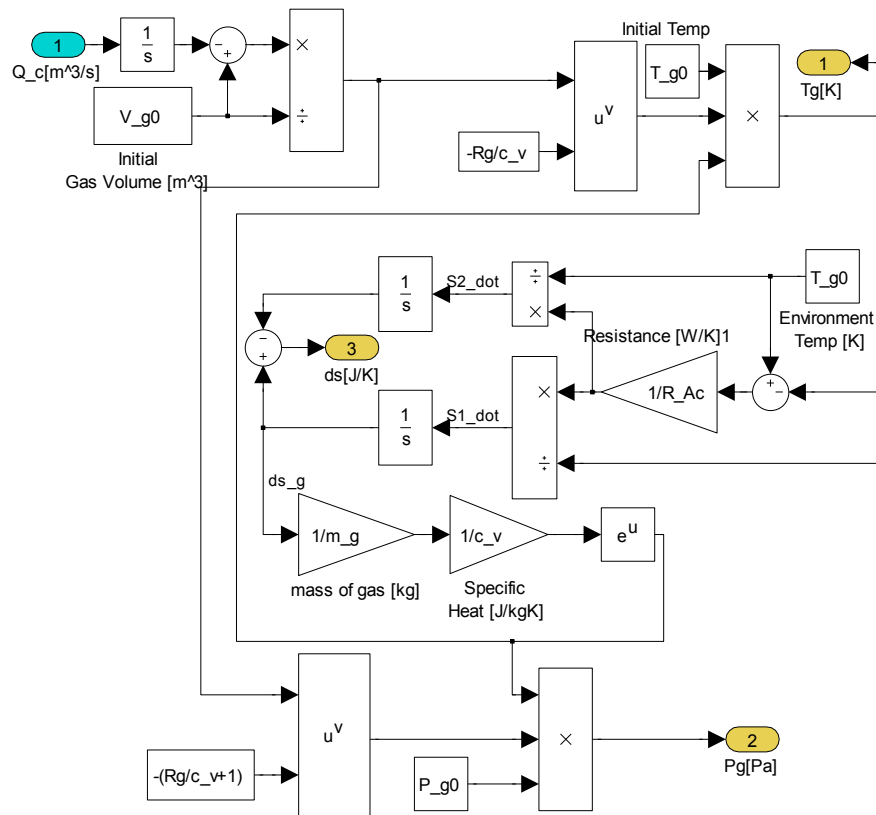


Figure 3-19 MATLAB<sup>®</sup>/Simulink<sup>®</sup>, non-linear hydraulic accumulator model, 1

Note that the energy balance equation (3-50) or (3-51) cannot be used in the simulation model directly, since  $T_g ds_g$  term creates an algebraic loop. Therefore, the energy balance equation is written in the form as follows.

$$c_v \frac{dT_g}{dt} = T_g \frac{ds_g}{dt} - \frac{R_g T_g}{v_g} \frac{dv_g}{dt} \quad (3-57)$$

Alternatively, the second term of Eq. (3-54), which describes the heat transfer rate through the charge-gas, can be replaced with Eq. (3-54) as follows.

$$c_v \frac{dT_g}{dt} = \frac{T_e - T_g}{R_c} - \frac{R_g T_g}{v_g} \frac{dv_g}{dt} \quad (3-58)$$

In the simulation model given in Figure 3-20 the energy balance (3-57) is utilized, whereas in Figure 3-21 the energy balance equation (3-58), which eliminates the entropy term, is utilized. The three non-linear models given in Figure 3-19 to Figure 3-21 are the same and are all casual. Therefore, their outputs are exactly the same for the same accumulator flow rate input.

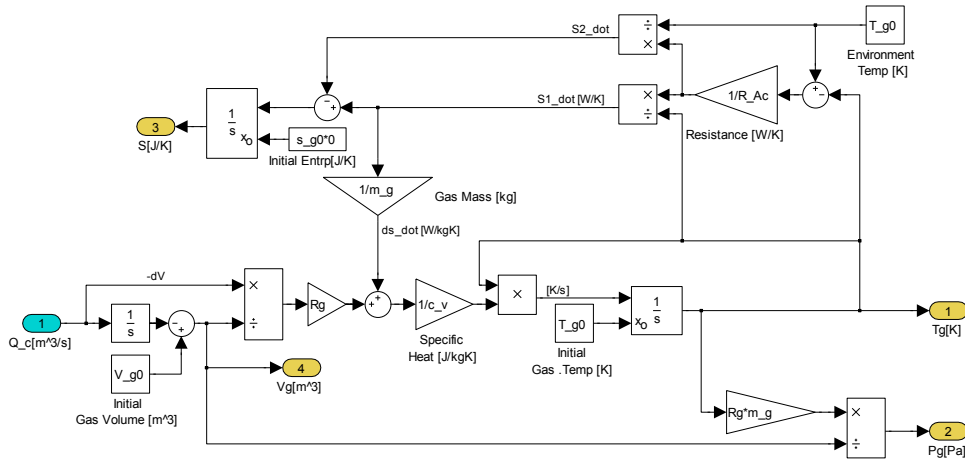


Figure 3-20 MATLAB<sup>®</sup>/Simulink<sup>®</sup>, non-linear hydraulic accumulator model, 2

### 3.2.5.4 Linearized Hydraulic Accumulator Model

The constitutive equations of the hydraulic accumulator Eq. (3-52) and Eq. (3-53) are linearized at operating points  $S_{g0}$  and  $V_{g0}$  by using the Taylor series expansion. Note that in the linearized model, specific variables are left out.

$$\delta T_g = \delta S_g \cdot \left. \frac{\partial T_g}{\partial S_g} \right|_{\substack{V_g=V_{g0} \\ S_g=S_{g0}}} + \delta(-V_g) \cdot \left. \frac{\partial T_g}{\partial(-V_g)} \right|_{\substack{V_g=V_{g0} \\ S_g=S_{g0}}} \quad (3-59)$$

$$\delta P_g = \delta S_g \cdot \left. \frac{\partial P_g}{\partial S_g} \right|_{\substack{V_g=V_{g0} \\ S_g=S_{g0}}} + \delta(-V_g) \cdot \left. \frac{\partial P_g}{\partial(-V_g)} \right|_{\substack{V_g=V_{g0} \\ S_g=S_{g0}}} \quad (3-60)$$

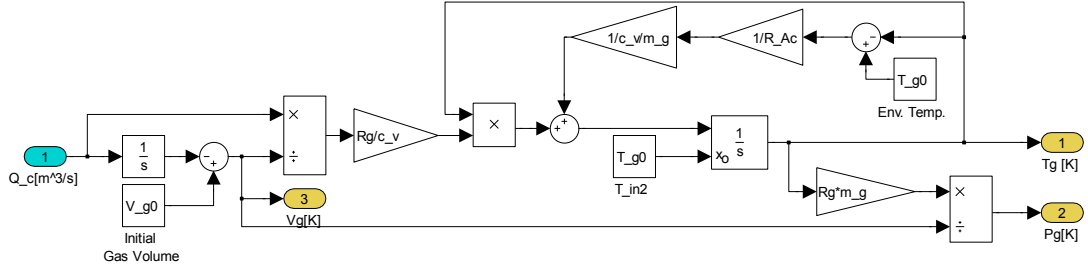


Figure 3-21 MATLAB®/Simulink®, non-linear hydraulic accumulator model, 3

The gains of the linearized temperature and pressure equations are as follows.

$$\left. \frac{\partial T_g}{\partial S_g} \right|_{\substack{V_g=V_{g0} \\ S_g=S_{g0}}} = \frac{T_{g0}}{m_g c_v} \quad (3-61)$$

$$\left. \frac{\partial T_g}{\partial(-V_g)} \right|_{\substack{V_g=V_{g0} \\ S_g=S_{g0}}} = \frac{T_{g0} R_g}{V_{g0} c_v} = \frac{P_{g0}}{m_g c_v} \quad (3-62)$$

$$\left. \frac{\partial P_g}{\partial S_g} \right|_{\substack{V_g=V_{g0} \\ S_g=S_{g0}}} = \frac{P_{g0}}{m_g c_v} \quad (3-63)$$

$$\left. \frac{\partial P_g}{\partial(-V_g)} \right|_{\substack{V_g=V_{g0} \\ S_g=S_{g0}}} = \frac{P_{g0}}{V_{g0}} \left( \frac{R_g}{c_v} + 1 \right) \quad (3-64)$$

The linearized constitutive equations are written in matrix form as follows.

$$\begin{bmatrix} \delta T_g \\ \delta P_g \end{bmatrix} = \begin{bmatrix} \frac{T_{g0}}{m_g c_v} & \frac{P_{g0}}{m_g c_v} \\ \frac{P_{g0}}{m_g c_v} & \frac{P_{g0}}{V_{g0}} \left( \frac{R_g}{c_v} + 1 \right) \end{bmatrix} \begin{bmatrix} \delta S_g \\ \delta(-V_g) \end{bmatrix} \quad (3-65)$$

where,

$$\delta S_g = S_g - S_{g0}, \text{ in } J/K$$

$$\delta V_g = V_g - V_{g0}, \text{ in } m^3$$

$$\delta T_g = T_g - T_{g0}(S_{g0}, V_{g0}), \text{ in } K.$$

$$\delta P_g = P_g - P_{g0}(S_{g0}, V_{g0}), \text{ in } K.$$

Note that the 2x2 matrix transforming the integrated through variables to across variables can be treated as the inverse of a two port capacitance. The determinant of the 2x2 matrix in Eq. (3-65) is positive and found as follows.

$$\det(\cdot) = \frac{P_{g0}}{m_g c_v} \left( \frac{T_{g0}}{V_{g0}} \left( \frac{R_g}{c_v} + 1 \right) - \frac{P_{g0}}{m_g c_v} \right) = \frac{P_{g0}}{m_g c_v} \frac{T_{g0}}{V_{g0}} \quad (3-66)$$

Then the resulting capacitance is written as follows.

$$C_g = \frac{1}{\det(\cdot)} = \begin{bmatrix} \frac{P_{g0}}{V_{g0}} \left( \frac{R_g}{c_v} + 1 \right) & -\frac{P_{g0}}{m_g c_v} \\ -\frac{P_{g0}}{m_g c_v} & \frac{T_{g0}}{m_g c_v} \end{bmatrix} = \begin{bmatrix} \frac{m_g c_v}{T_{g0}} \left( \frac{R_g}{c_v} + 1 \right) & -\frac{V_{g0}}{T_{g0}} \\ -\frac{V_{g0}}{T_{g0}} & \frac{V_{g0}}{P_{g0}} \end{bmatrix} \quad (3-67)$$

The energy stored in that two-port capacitor is defined as,

$$\begin{aligned} ES &= \int \left( \delta T_g \delta \dot{S}_g + \delta P_g \delta(-\dot{V}_g) \right) dt \\ &= \frac{1}{2} C_{g1} \delta T_g^2 + C_{g12} \delta T_g \delta P_g + \frac{1}{2} C_{g2} \delta P_g^2 \end{aligned} \quad (3-68)$$

where,

$$C_{g1} = \text{first diagonal element of the capacitance matrix, } C_g(1,1)$$

$$C_{g12} = \text{off-diagonal elements of the capacitance matrix, } C_g(1,2) = C_g(2,1)$$

$$C_{g2} = \text{second diagonal element of the capacitance matrix, } C_g(2,2)$$

Note that defining a new across variable  $\delta P'_g$  and capacitance term  $C'_{g1}$ , the two port capacitance given in Eq. (3-68) can be represented by an equivalent two one-port capacitance  $C'_{g1}$ ,  $C_{g2}$  and an ideal transformer with constant  $TF$ . The equivalent system must have the same energy given in Eq. (3-68).

$$ES = ES' = \frac{1}{2} C'_{g1} \delta T_g^2 + \frac{1}{2} C_{g2} \delta P_g'^2 \quad (3-69)$$

The conversion factor between a two-port inertance, and two one-port inertance together with a transformer is explained by Brown, for the analysis of real electrical transformers and rigid inertive floating disks [94]. Applying a similar conversion defined below, the two-port capacitance is converted to a two one-port capacitance and transformer.

$$TF = \frac{C_{g12}}{C_{g2}} \quad (3-70)$$

$$C'_{g1} = C_{g1} - (TF)^2 C_{g2} \quad (3-71)$$

$$\delta P'_g = \delta P_g + (TF) \delta T_g \quad (3-72)$$

Inserting the proposed conversions defined in Eqs. (3-70) - (3-72) into the energy equation (3-69) yields the same result with the energy equation (3-68). The equivalent linearized hydraulic accumulator system is modelled with two capacitances and one transformer, as shown in the bond graph in Figure 3-22.

The accumulator model consists of two domains namely: fluid and thermal, the capacitance in fluid domain is  $C_f = C_{g2}$  and the capacitance in thermal domain is  $C_t = C'_{g1}$ . The energy stored on the fluid side is converted to thermal energy by the transformer with ratio  $-P_{g0}/T_{g0}$ .

$$C_f = C_{g2} = \frac{V_{g0}}{P_{g0}} \quad (3-73)$$

$$C_t = C'_{g1} = \frac{m_g c_v}{T_{g0}} \quad (3-74)$$

$$TF = -\frac{P_{g0}}{T_{g0}} \quad (3-75)$$

where,

$TF$  = transformer ratio, in  $Pa/K$

$C_t$  = capacitance in thermal domain, in  $J/K^2$

$C_f$  = capacitance in fluid domain, in  $m^3/Pa$

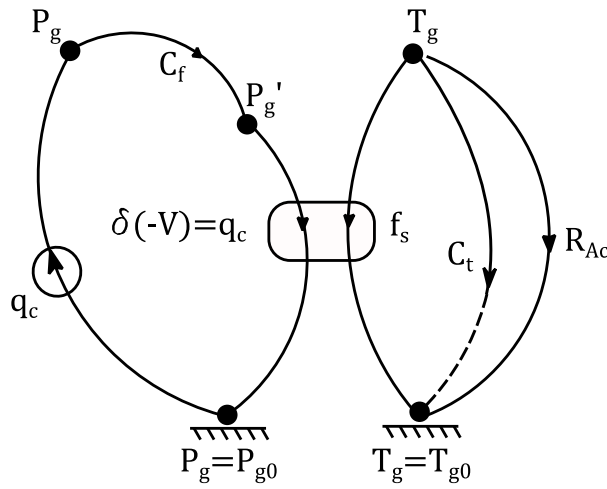


Figure 3-22 Linear graph of hydraulic accumulator

In Figure 3-22, besides the equivalent two port capacitance, the heat transfer is represented at the right most branch by the resistance  $R_c'$ . Note that this term is not the same with the accumulator resistance  $R_c$  given in Eq. (3-55). In the accumulator model, the through variable in the thermal domain is chosen to be entropy flow, therefore using the relation  $\dot{q} = T_g \dot{s}_g$ , the modified resistance is defined as follows.

$$R_c' = R_c T_{g0} \quad (3-76)$$

The constitutive equations of the hydraulic accumulator based on the linear graph given in Figure 3-22, are as follows.

$$Q_c = C_f(\dot{P}_g - \dot{P}'_g) \quad (3-77)$$

$$P'_g - P_{g0} = (-TF)(T_g - T_{g0}) \quad (3-78)$$

$$Q_c \cdot (TF) + C_t \dot{T}_g + \frac{T_g - T_{g0}}{R'_c} = 0 \quad (3-79)$$

Based on the above equations, the linearized MATLAB®/Simulink® model of the hydraulic accumulator is constructed as given in Figure 3-23.

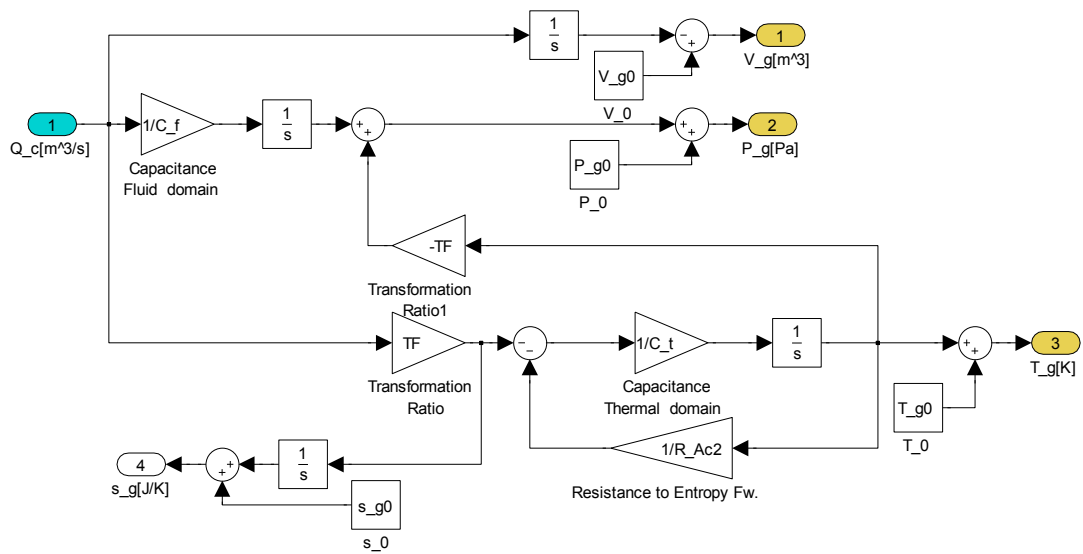


Figure 3-23 MATLAB®/Simulink®, linearized model of the hydraulic accumulator

### 3.2.5.5 Transfer functions

Inserting the values of  $(TF)$  and  $R'_c$  the Eq. (3-79) is written as follows.

$$\frac{m_g c_v}{T_{g0}} \dot{T}_g = -\frac{T_g - T_{g0}}{T_{g0} R_c} + \frac{P_{g0}}{T_{g0}} Q_c \quad (3-80)$$

Multiplying the equation with resistance  $R_c$ , and inserting,  $P_{g0} = \frac{m_g R T_{g0}}{V_{g0}} = \frac{m_g (c_p - c_v) T_{g0}}{V_{g0}} = \frac{m_g c_v (k-1) T_{g0}}{V_{g0}}$ , where  $k = c_p/c_v$ , and replacing  $m_g c_v R_c$  with a new variable  $\tau_g$ , named as thermal time constant, the temperature dynamics of the equation is defined as follows.

$$\frac{\tau_T}{T_{g0}} \dot{T}_g = -\frac{T_g - T_{g0}}{T_{g0}} + \frac{(k-1)\tau_g}{V_{g0}} Q_c \quad (3-81)$$

Defining a relative temperature variable,  $\Delta T_g = T_g - T_{g0}$ , the transfer function between the input flow rate and the output accumulator temperature is written as follows.

$$\frac{\Delta T_g(s)}{Q_c(s)} = \frac{T_{g0}}{V_{g0}} \cdot \frac{(k-1)\tau}{\tau_g s + 1} \quad (3-82)$$

In order to find the transfer function between the accumulator pressure; integrate Eq. (3-77), and insert Eq. (3-78) into the resulting equation. inserting  $C_f = \frac{V_{g0}}{P_{g0}}$ .

$$\frac{Q_c(s)}{C_f s} = P_g - \left( P_{g0} + \frac{P_{g0}}{T_{g0}} (T_g - T_{g0}) \right) \quad (3-83)$$

Since  $(T_g - T_{g0}) = \Delta T_g$ , inserting the transfer function defined in Eq. (3-82) further repacking the fluid capacitance,  $C_f = \frac{V_{g0}}{P_{g0}}$ , the transfer function is obtained as follows.

$$\frac{\Delta P_g(s)}{Q_c(s)} = \frac{P_{g0}}{V_{g0}} \cdot \frac{k\tau_g s + 1}{s(\tau_g s + 1)} \quad (3-84)$$

where,  $\Delta P_g$  is the relative pressure,  $\Delta P_g = P_g - P_{g0}$ .

### 3.2.5.6 Comparison of Accumulator Models

The non-linear and linear simulation models are compared with the polytropic process as defined in Eq. (3-43). The accumulator parameters that used in the simulation models are given in Table 3-5. The accumulator has 5 l volume, and is pre-charged at 25 bar in a 25 °C environment. In the Simulink model files a sinusoidal flow source is utilized to deliver 1.5 l hydraulic oil through the accumulator, with varying frequencies. Therefore, since the gas volume is changing in between 5l – 3.5 l, the operating points and initial accumulator pressure and temperature are calculated for the mid volume change.

**Table 3-5 Parameters of the hydraulic accumulator**

<b>Parameter</b>	<b>Description</b>	<b>Value</b>	<b>Unit</b>
$c_p$	specific heat at constant pressure, N <sub>2</sub> , @25°C	1042	J/kgK
$c_v$	specific heat at constant volume, N <sub>2</sub> , @25°C	745	J/kgK
$R_g$	Gas Constant, N <sub>2</sub> , @25°C	296.8	J/kgK
$T_{g_{chr}}$	accumulator charge temperature, no oil	298.5	K
$P_{g_{chr}}$	accumulator charge pressure, no oil	25.0 <sup>5</sup>	Pa
$V_{g_{chr}}$	accumulator volume, no, oil	5	liter
$r_{ci}, r_{co}$	inner outer accumulator radius	125/150	mm
$h_{ci}, h_{co}$	convection coefficients	70	W/m <sup>2</sup> K
$A_c$	accumulator surface area	0.471	m <sup>2</sup>
$k_w$	thermal conductivity, (AISI 302@300K)	15.1	W/mK
<b>Calculated Parameters</b>			
$m_g$	mass of the charge gas, N <sub>2</sub>	0.14	kg
$C_f$	fluid capacitance	1.44 · 10 <sup>-9</sup>	m <sup>3</sup> /Pa
$C_t$	thermal capacitance	0.35	J/K <sup>2</sup>
$TF$	transformer ratio	9853.2	N/m <sup>2</sup> K
$R_c$	resistance of accumulator wall	0.064	K/W
$R'_c$	resistance to entropy flow	19.05	K <sup>2</sup> /W
$k$	specific heat ratio	1.4	–
$\tau_g$	thermal time constant	6.71	s
$T_{g0}$	initial charge gas temperature,	298.5	K
$P_{g0}$	initial charge gas pressure,	29.4 · 10 <sup>5</sup>	Pa
$V_{g0}$	initial charge gas volume,	4.25	liter

The linearized and non-linear system responses are compared on gas pressure versus volume plane. Besides these two, the responses of the isothermal and adiabatic polytropic processes with polytropic exponents  $n = 1$  and  $n = 1.4$  are also provided on the same plot.

The gas pressure and volume responses for 0.01 Hz, and 0.5 Hz excitation frequencies are given in Figure 3-24. Note that the gas pressure and volume are normalized with respect to operating points  $V_{g0}$  and  $P_{g0}$ . From the figure it is seen that for 0.01 Hz excitation frequency, the linearized model response is compatible

with the non-linear model response up to  $\pm 5\%$  volume variation. Over that value, the linearized model responses begin to deviate from the non-linear model. However, the difference between the two is only  $\approx 15\%$  percent which occurs at the maximum displaced gas volume variation.

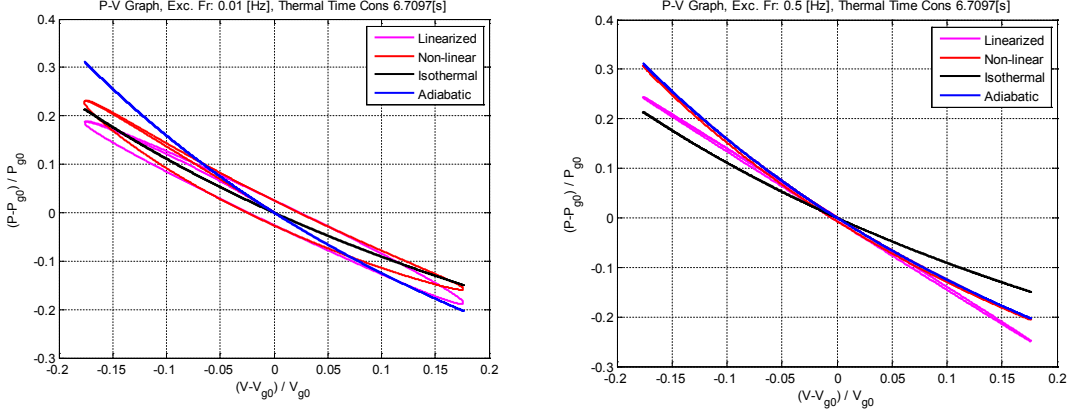


**Figure 3-24 Normalized P-V diagram for 0.01Hz and 0.5Hz excitation frequency**

In Figure 3-24, the hysteresis loop that is area formed by the closed curve of the  $p - v$  response corresponds to the heat losses. Note that when the excitation frequency is increase up to 0.5 Hz frequency the area of the hysteresis loop is decreased. This is an expected result since increasing the excitation frequency decreases the time required for heat transfer. It is seen that the deviation of the linearized model response from the non-linear model response is increase. More importantly, it is seen that the non-linear model response converge to adiabatic polytropic process response. It should be noted that increasing the excitation frequency will decrease the hysteresis loop more, and make the non-linear model response similar to adiabatic process response. Therefore, since the 0.01 Hz and 0.5 Hz excitation frequencies are very slow with respect to the electro hydrostatic actuators operation, it can be concluded that the accumulator dynamics together with thermal losses and thermal damping effects can be neglected in the dynamic analysis of the EHA.

### 3.3 Simulation Model

Two different non-linear simulation models are constructed. The first simulation model is the combination of the sub-system models given in section 3.2, and is constructed in MATLAB®/Simulink® environment. This model utilizes the mathematical formulation given in the previous sections. The second simulation model on the other hand is constructed on the MATLAB®/Sim-Hydraulics® environment and utilizes the readily available MATLAB®/SimScape® library.

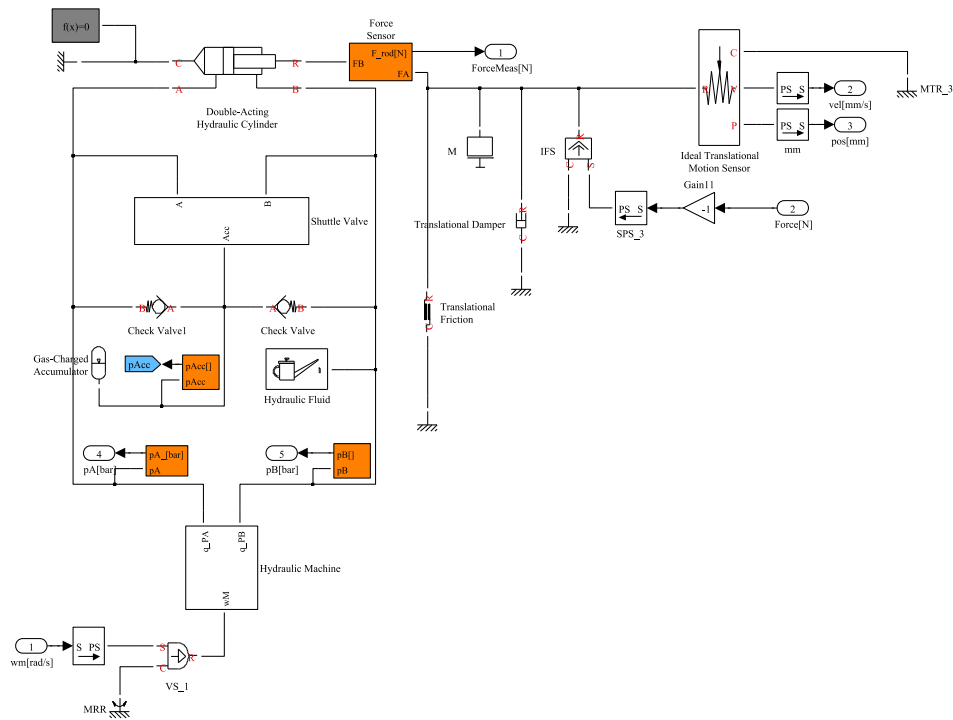


Figure 3-25 MATLAB®/Sim-Hydraulics®, non-linear model of the EHA

The non-linear simulation model of the EHA is shown in Figure 3-25. The model consists of hydraulic pump unit, shuttle and check valves, hydraulic accumulator, and hydraulic actuator together with the mass and frictional elements. The input of the simulation model is the pump drive speed and external force acting on the actuator. Note that this model represents only the hydro-mechanical system and is used in the stability analysis of the EHA. For the controller design purposes, the electric motor model together with its controller, which is discussed in section 3.2.4, is integrated into this model.

In the simulation model, mainly the Sim-Hydraulics<sup>®</sup> library elements are used. However the shuttle valve and the pump are constructed by using the basic elements, since no similar model exists in the Sim-Hydraulics<sup>®</sup> library.

The shuttle valve model is given in Figure 3-26. There exist two valve actuators and two variable orifices. The flow characteristics of the variable orifices are defined by orifice area vs. opening table. This table is constructed by considering the circular orifice geometry mentioned in Section 3.2.3. The double acting valve actuator block is based on static force equilibrium and utilizes the pressures of the chamber pressures in order to determine the spool position. The non-linearities such as preload force of the centering spring and stroke limits are all implemented in that block. The dynamics of the spool movement is considered in the valve actuator block which is simply a linear transfer function.

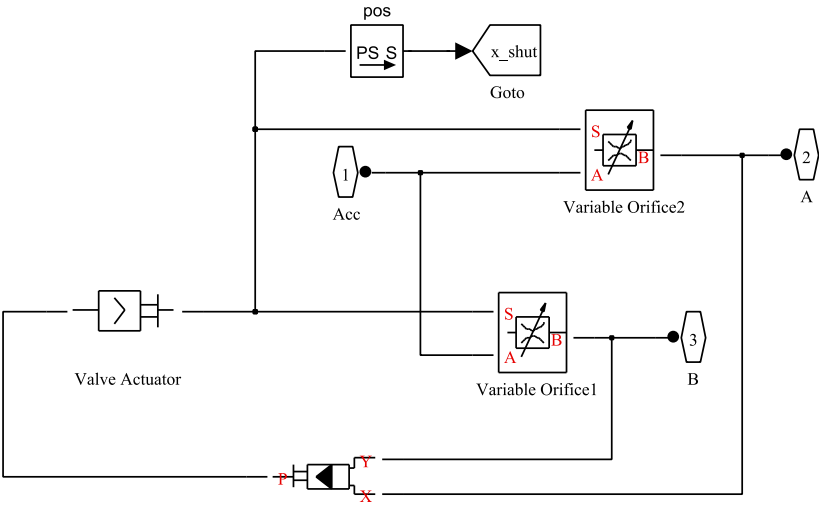


Figure 3-26 MATLAB<sup>®</sup>/Sim-Hydraulics<sup>®</sup>, shuttle valve model

The pump model is shown in Figure 3-27. Two hydro mechanical converters are used to generate flow rate by the input pump speed. Speed input instead of torque is used, since the inertia and friction characteristics of the pump are lumped into the motor dynamics. The leakage flow losses are modelled by look up tables whose data is taken from the manufacturer.

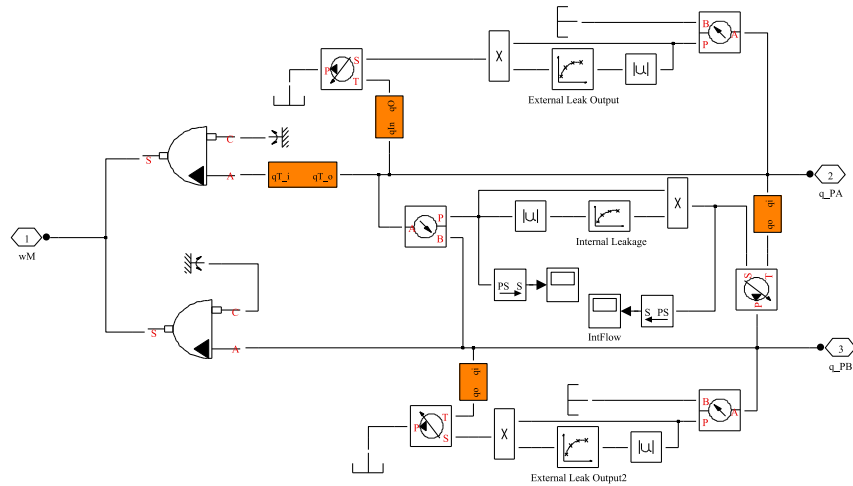


Figure 3-27 MATLAB®/Sim-Hydraulics®, pump model

### 3.4 Experimental Test Set Up

An experimental test set up is constructed for the design and development of the EHA system. The schematic view of the test set up is shown in Figure 3-28. It mainly consists of two parts. The first part (left side) is the pump speed controlled EHA system under development, and the second part (right side) is the valve controlled load simulator. The load simulator is constructed to facilitate the application of controlled external loads on the EHA and is the subject of M.Sc. thesis completed by Akova [16].

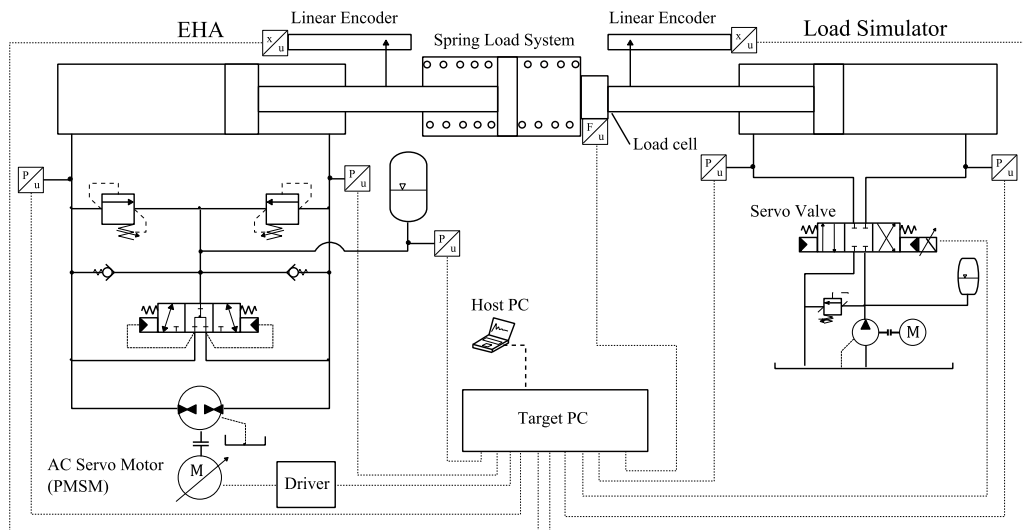


Figure 3-28 Schematic view of the experimental test set up

The two actuators shown in Figure 3-28 are connected to each other through a compliant spring arrangement (spring load system) and a force transducer. The force transducer provides a feedback signal for the closed-loop control of the load simulator. In order to track the EHA motion the close loop force control algorithm of the load simulator is continuously active. The load simulator is able to apply dynamic loads up to  $\pm 15 \text{ kN}$  with a  $200 \text{ N}$  precision and is driven by a Parker DF-Plus valve (D1FPE50HB9NB5) with  $120 \text{ bar}$  supply pressure. The allowable test region for the EHA together with the load loci of the load simulator is shown on the force versus velocity ( $F - v$ ) plane, in Figure 3-29. The load simulator is designed for a  $100 \text{ mm/s}$  EHA velocity under test. At that speed, the load simulator is able to apply a sinusoidal force of  $7.5 \text{ kN}$ , with  $4 \text{ Hz}$  frequency. Furthermore, for zero EHA speed, the load simulator can apply  $15 \text{ kN}$  force with  $2 \text{ Hz}$  frequency or  $1 \text{ kN}$  force with  $10 \text{ Hz}$  frequency. Further loading limits for the zero and maximum allowable speed of the EHA are given in Table 3-6.

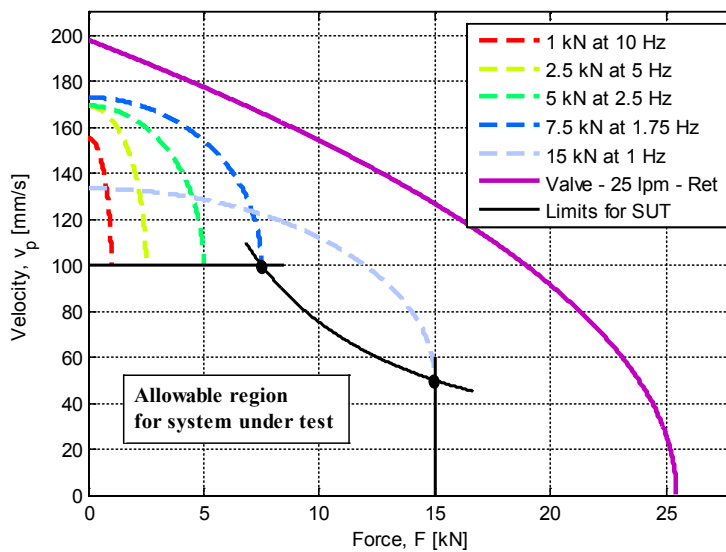


Figure 3-29 Operation region of the load simulator, [95]

A detailed information about the design, construction and control of the load simulator is given in the M.Sc. thesis study [95]. The description of the hardware components related with the load simulator can be found in that study. Therefore, in the below part only the hardware components that are related with the EHA test system are described.

Table 3-6 Loading limits of the load simulator set-up

<b>Limits of the Load Simulator for 100 mm/s EHA speed</b>				
Magnitude [kN]	1	2.5	5	7.5
Frequency [Hz]	10	10	6	4
<b>Limits of the Load Simulator for zero EHA speed</b>				
Magnitude [kN]	1	5	10	15
Frequency [Hz]	10	6	3	2

### 3.4.1 Control System Hardware Components

Control system hardware, related with the EHA test system, consists of real-time control computer, data acquisition cards, servo motor control unit together with its terminal module and a number of feedback devices. The interactions of all these components are given in Figure 3-28. The properties of these components are given in Table 3-7.

A Speedgoat modular real time target machine with various IO modules is utilized as the data acquisition system and control computer. This system is named as target PC in Figure 3-28. MathWorks® xPC Target™ real time kernel is running on the target PC, and it realizes the real time control of the two systems. The control algorithms are designed in a standard personal computer, which is named as host PC. The MATLAB® R2011a software, together with Simulink®, Real-Time Workshop®, xPC Target™ and necessary SpeedGoat IO drives are installed on the host PC. The designed controller in MATLAB®/Simulink® environment is compiled by a VisualC compiler in the host PC and downloaded to the real-time target machine via an Ethernet communication. The solver of the control algorithm is selected as 4<sup>th</sup> order Runge-Kutta (ode4) with 1 ms fixed step.

The SpeedGoat real time target PC is equipped by IO105 analog input and IO111 analog output modules. The servo motor speed and torque, pressures of the two chambers of the EHA and accumulator, and the actuator position are measured simultaneously, with a 1 kHz sampling frequency. The pressure transducers are made by Trafag and rated up to 250 bar with 0-10 V output. They are mounted on the hydraulic manifold. The position transducer is installed inside the EHA, it is made by Novotechnik and has 0-10 V output.

**Table 3-7 EHA control system hardware**

<b>DAQ system and control computer, Speedgoat</b>		
Control computer	Modular real time target machine	Intel Pentium-M 1.8GHz CPU, 1024MB RAM, 13 cPCI I/O module slots,
Analog input module	IO105	32 differential input channel, 16 bit
Analog output module,	IO111	16 output channels, 16 bit resolution
Encoder module,	IO401	6 counters, TTL/SSI, 32 bit resolution
Digital IO module,	IO203	
CAN bus module	--	
<b>Feedback Devices</b>		
Linear Encoder	ATEK, MLS-4	TTL output, Quadrature, 20 $\mu$ m resolution, 270 mm
Position transducer	NovoTechnik,	0-10 V analog output, 300 mm
Pressure transducer	Trafag, 8472	0-10 V analog output, 250 bar
<b>Servo motor control related components</b>		
Motor Controller	Siemens CU320	6SL3040-1MA00, Profibus interface
Terminal module	Siemens, TM31	2AI, 2AO channels, sampled at 1ms
CAN bus module	Siemens, CB10	

Besides the analog position transducer, the EHA position is also measured by a linear encoder made by ATEK. The encoder is connected to the rod of the EHA, it has 20 $\mu$ m grid spacing and enables 5 $\mu$ m resolution at 4X decoding. The speed and torque of the servo motor are controlled by a Siemens CU320 control unit. Siemens TM31 terminal module is used to establish an analog communication interface between the real time target PC and CU320. TM31 samples the servo motor set speed and torque commands, as well as, sending the calculated servo motor speed and torques with 1 ms interval. Furthermore, there exists a CAN-bus communication between the CU320 and target PC. The supervisory controller utilizes this interface, the digital commands like, motor enable, controller enable, set point switch, safe torque on, emergency stop etc. are sent to CU320 through that interface.

### 3.4.2 EHA Test System Components.

A photo of the test set up is shown in Figure 3-30. The pump controlled system (EHA) under test is shown at left, whereas the load simulator is shown at right. The two systems are coupled to each other via a spring load system, as mentioned previously. The EHA system consists of a Siemens 1FK7083 series servo motor, a Bucher Hydraulics QXM22 series  $8\text{ cm}^3/\text{rev}$  constant displacement pump, a Hanchen single rod actuator with a  $200\text{ mm}$  stroke length,  $\phi 60/\phi 30\text{ mm}$  piston and rod diameters, respectively. A  $5\text{ l}$  accumulator with a  $25\text{ bar}$  gas charge pressure is used for flow compensation. At the beginning of each test, an external pump/motor unit charges the hydraulic accumulator up to a desired pressure level. Two ports of the pump and the actuator, together with the accumulator and tank lines are connected to the hydraulic manifold through hydraulic hoses as shown in Figure 3-30. The hydraulic circuit shown in Figure 3-1 is implemented inside the hydraulic manifold. The hydraulic valve components are all cartridge type and mounted inside the manifold: one shuttle valve, two pressure relief valves, and two check valves.

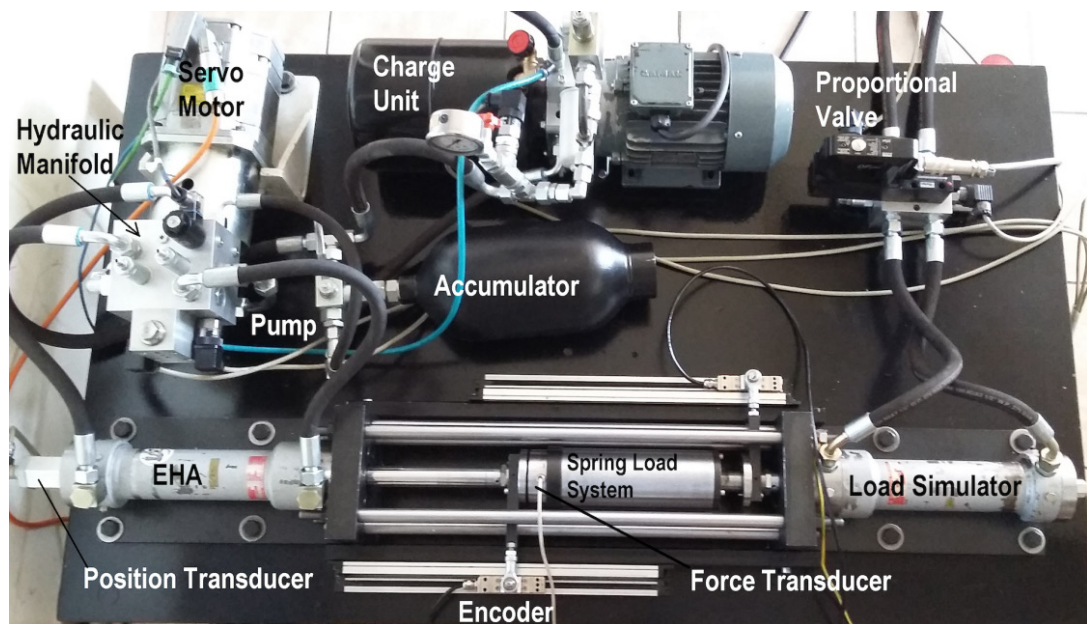


Figure 3-30 Experimental test set up

The components of the EHA test system are listed in Table 3-8. The components are mainly classified in three groups; hydraulic, electric and mechanical. Unlike the pump, motor and the actuator, the shuttle valve used in the thesis study is not unique.

Therefore, several different valve types utilized in the thesis are given in the table. The shuttle valves are from Parker Company and Bucher Company and have similar hydraulic conductance values. Throughout the thesis study, the closed center shuttle valves of the Bucher Company are further modified, by changing its orifice openings or spring loading which will be mentioned in the subsequent sections.

**Table 3-8 EHA test system components**

<b>Hydraulic Components</b>		
Pump	Bucher, QXM	$8\text{cm}^3/\text{rev}$ , max 210 bar
3/3 Shuttle valve, (internal pilot operated and spring centered)	Parker, K04C3	closed center, 5 bar switching, 55lpm-7bar
	Parker, K04F3	semi-open center (underlapped), 5 bar switching, 55lpm-7bar
	Parker,	open center, 5 bar switching, 55lpm-7bar
	Bucher, 400671602	closed center, 5 bar switching, 45lpm-5bar
	Bucher, 400671602	the spool is modified in OSTIM
Accumulator	SAIP	5 liter + 20 liter nitrogen tank
Charge circuit	OSTIM	25-50 bar, 1.5 kW, 3.5 lpm capacity
<b>Electrical System Components</b>		
Servo motor	1FK7083	3.3 kW, 10.5 Nm rated torque
Motor module	6SL3120-1TE21	In: 600V DC, Out :400V AC, 9A
Line module	6SL3130-6TE21-	In: 3AC 380-480 V, Out:600 VDC, 27A
<b>Mechanical System Components</b>		
Actuator	Hanchen	200 mm stroke, $\phi 60/\phi 30$ mm diameter
Pump-Motor Coupling	KTR	Rotex GS

### 3.4.3 Prototype EHA

In the experimental test set up, the electro hydrostatic actuator is not in a compact form. The hydraulic pump, hydraulic manifold, hydraulic accumulator and the hydraulic actuator are connected to each other through hydraulic hoses. This sparse structure is a desired property, since the components have to be assembled and disassembled during the development and testing period. On the other hand, in order to demonstrate that the proposed electro hydrostatic system can be manufactured in a compact form, a prototype EHA is constructed as shown in Figure 3-31. This

prototype EHA is demonstrated in the exhibition of the 7<sup>th</sup> national fluid power conference, HPKON 2014.

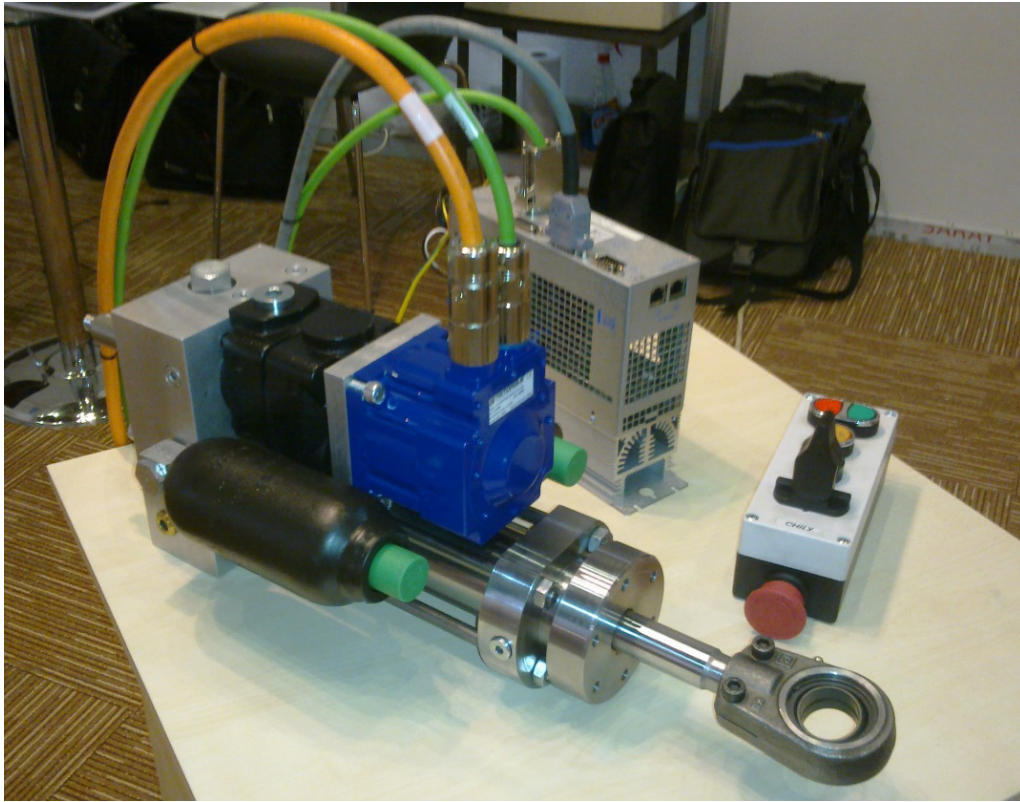


**Figure 3-31 The EHA in compact form, demonstrated in National Fluid Power Conference, HPKON 2014**

In the prototype shown in Figure 3-31, an internal coupling servo motor, ICM 09N, from HDD Company is utilized. The rotor has a hollow structure and is coupled to the pump shaft inside the motor. The allowable motor torque for continuous operation, (100% duty cycle), is  $5 - 3 \text{ Nm}$  up to  $3000 \text{ rpm}$ , and for intermittent operations (25% duty cycle), it is in between  $10 - 8 \text{ Nm}$ . The pump is from Bucher Company, QXM series with  $5 \text{ cm}^3/\text{rev}$  displacement. The pump casing is modified to assemble with the hydraulic manifold. The hydraulic manifold connects the pump-motor assembly with the hydraulic actuator; furthermore the hydraulic circuit for flow compensation is realized inside the manifold. The hydraulic actuator has  $200 \text{ mm}$  stroke,  $50 \text{ mm}$  diameter piston and  $25 \text{ mm}$  diameter rod. The  $1 \text{ l}$  hydraulic accumulators are further integrated on the hydraulic manifold. The prototype EHA can apply a maximum load of  $2.5 \text{ kN}$  for intermittent operations, and a load of  $1.3 \text{ kN}$  for continuous operations, and the maximum speed is  $170 \text{ mm/s}$ .

### 3.5 Simulation Model Validation

The Sim-Hydraulics model is verified by the measurement data from the test system. The non-linear model of the electric motor together with the control unit is validated with the measurement in Section 3.2.4.3. Note that the Sim-Hydraulics<sup>®</sup> model utilized in this section contains only the hydro-mechanical part and does not include the electrical part. Therefore, the simulation model is validated by considering the measured motor speed is the input pump drive speed model. Furthermore the force measurement is entered in the model as a disturbance input.

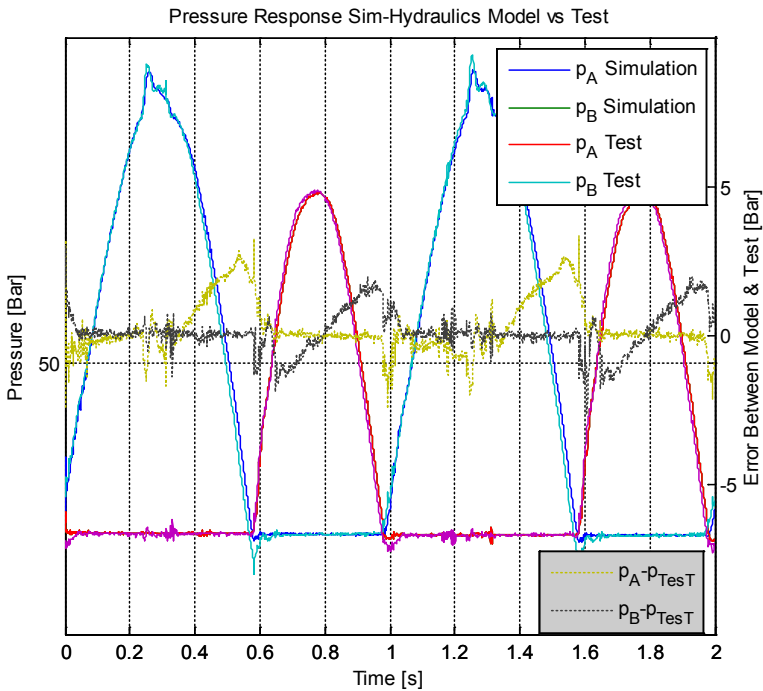
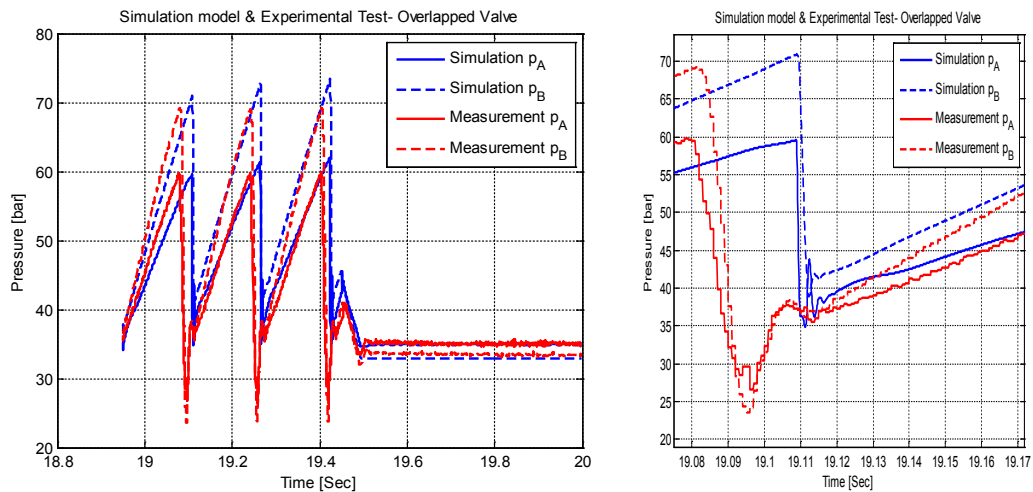


Figure 3-32 Pressure response comparison for fully opened shuttle valve

In order to show the qualification of the simulation model, first the pressure response that corresponds to fully opened shuttle valve positions are given. The sample pressure response comparison of the simulation model and the real system is given in Figure 3-32. It seems the model response fits to the real system response, however at the switching times of the shuttle valve, where one of the chambers is connected to the accumulator, pressure dynamics differs with the test case. This is due to the check valve crack pressure settings.

The simulation model is extensively used in the stability analysis that will be investigated in the subsequent sections in detail. In order to show the qualification of the simulation model, the pressure responses are compared with the measurements acquired during an unstable operation condition. Note that a closed centered shuttle valve is utilized both in the simulation model and the experimental test set up. The pressure response comparison is given Figure 3-33. As seen from the figure, the behaviors of the pressure responses are qualitatively compatible. Both chamber pressures increase up to certain level, then when the shuttle valve is opened both decreases abruptly. This switching phenomenon causes rapid speed changes, and its position result is shown in Figure 3-34.



**Figure 3-33 Pressure response comparison with transient considerations**

It should be noted that the pressure and position responses of the simulation model are comparable qualitatively with the measured test results. It is seen that quantitatively measurements and model responses are different. For example there exists an offset between the sudden pressure falling in Figure 3-33. However, this is an expected result, since nominal parameters are used in the simulation model and they are not tuned to fit the measurements.

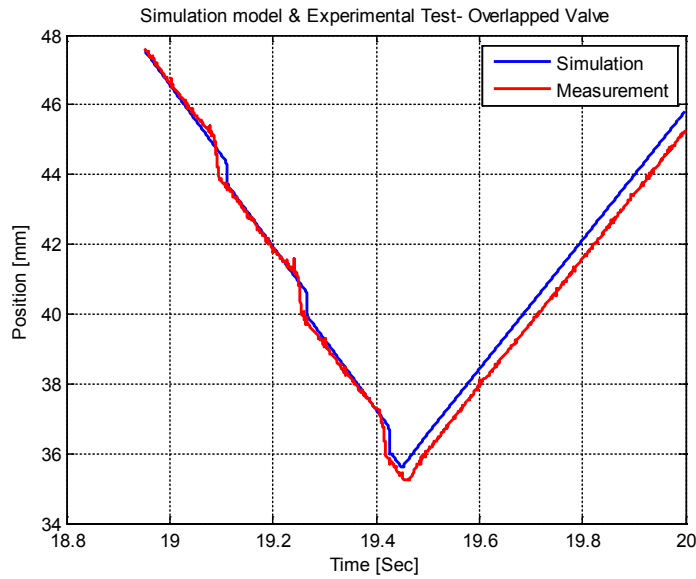


**Figure 3-34 Position response comparison with transient considerations**

The non-linear simulation model is concluded to be sufficient to investigate the stability of the system. It is concluded that with the use of nominal parameters either obtained from the manufacturer or simple dimensional measurements are sufficient to construct a non-linear simulation model that represents the switching behavior of the system. Therefore, in the scope of this thesis study there is no need to make parameter estimations to obtain a quantitative agreement between the measurement data.

## CHAPTER 4

### STABILITY ANALYSIS OF THE EHA

The EHA system consists of a hydraulic pump which is driven by a servo motor, a single rod cylinder, a shuttle valve, a hydraulic accumulator, and some transmission lines. Throughout the experimental studies, it is observed that some undesired pressure oscillations occur under certain operating conditions although the pump is driven at a constant speed. Since the focus of this chapter is to investigate this so-called instability problem rather than constructing a full simulation model, the dynamics of the servo motor together with the pump is neglected. The pump is considered as a flow source driven by a constant velocity source. In most pump control applications a common hydraulic accumulator source named as low pressure line is used and a constant pressure is maintained via a charge pump. In this study, a relatively large accumulator is utilized. Since the maximum possible displaced volume, which is equal to the rod volume inside the hydraulic actuator, is very small (0.14 l) with respect to the accumulator gas volume (5 l), the accumulator is considered as an infinite capacitance. Furthermore, the transmission lines are assumed to be lossless and their volumes are lumped into the actuator dynamics. The resulting hydraulic system model, simplified for stability analysis, includes

- the shuttle valve,
- the actuator with its two chambers,
- the pump as flow source.

#### 4.1 Simplified Shuttle Valve Model and Flow Continuity Equations

The simplifying assumptions made for the shuttle valve is as follows.

- the valve spool dynamics is neglected,

- the pilot pressure line lossless are neglected,
- the valve spool is assumed to be symmetric,
- the orifice area is proportional to the valve spool position,
- the discharge coefficient is constant for all spool positions,

According the above simplifying assumptions, since all the line losses are neglected, the pilot pressures are equal to the actuator chamber pressure  $P_{s1} = P_a$  and  $P_{s2} = P_b$ . Furthermore, since the valve dynamics is neglected, the previously defined equation of motion of the valve spool, Eq. (3-18), is modified and a static relationship between the spool position and chamber pressures is formed as follows.

$$y_s = \frac{A_s}{k_s} (P_a - P_b - P_{sc} \text{sign}(P_a - P_b)) \quad (4-1)$$

Furthermore, since the orifice area,  $A_v$ , is assumed to be proportional with the orifice opening,  $u_v$ , the orifice area function  $A_v(\cdot)$  that is defined in Eq. (3-25) is re-defined as follows.

$$A_v(u_v) = \begin{cases} 0 & u_v < 0 \\ A_{vMax} \frac{u_v}{u_{vMax}} & 0 < u_v < u_{vMax} \\ A_{vMax} & u_{vMax} < u_v \end{cases} \quad (4-2)$$

where  $u_v$  represents the orifice opening  $|y_s + u_{v0}|$ , and parameters  $u_{vMax}$  and  $A_{vMax}$  are the maximum orifice opening and maximum orifice area, respectively.

The valve spool is assumed to be symmetric, it has equal valve spool overlap or underlap at each port,  $u_{v10} = u_{v20} = u_{v0}$ . Therefore shuttle valve flow equations previously defined in Eq. (3-28) and Eq. (3-29) are re-written as follows.

$$Q_{a \rightarrow c} = C_d A_v(u_{v0} - y_s) \sqrt{\frac{2}{\rho} |P_a - P_c| \text{sgn}(P_a - P_c)} \quad (4-3)$$

$$Q_{b \rightarrow c} = C_d A_v (u_{v0} + y_s) \sqrt{\frac{2}{\rho} |P_b - P_c| \text{sgn}(P_b - P_c)} \quad (4-4)$$

where,  $C_d$  is the discharge coefficient,  $\rho$  is the mass density of hydraulic fluid. The parameter  $u_{v0}$  corresponds to the spool underlap or initial opening and its value is negative if a closed center valve is utilized.

For the partially opened valve position,  $u_v \in [0, u_{vMax}]$ , since the orifice area  $A_v$  is assumed to be proportional with the orifice opening  $u_v$ , the flow equations (4-3) and (4-4) can be re-written as a direct relationship with the chamber pressures as follows.

$$Q_s = K_V (|P_a - P_b| - P_{op}) \sqrt{\Delta P} \text{sgn}(\Delta P) \quad (4-5)$$

Here,  $P_{op}$  is the pressure when only one port of the valve is opened and it is defined as follows.

$$P_{op} = P_{sc} - \frac{u_{v0} k_s}{A_s} \quad (4-6)$$

Note that  $P_{op}$  would be higher than the cracking pressure  $P_{sc}$ , if a closed center valve were used. The gain  $K_V$  in Eq. (4-5) is given as

$$K_V = C_d A_{vMax} \frac{1}{u_{vMax}} \frac{A_s}{k_s} \sqrt{\frac{2}{\rho}} \quad (4-7)$$

Assuming that leakage flows of the pump are proportional to corresponding pressure differences, the flow continuity equations for two chambers of the actuator are written as

$$D_p \omega - A v_A - H_e P_a - H_i (P_a - P_b) - Q_{a \rightarrow c} = C_a \dot{P}_a \quad (4-8)$$

$$\alpha A v_A - D_p \omega - H_e P_b + H_i (P_a - P_b) - Q_{b \rightarrow c} = C_b \dot{P}_b \quad (4-9)$$

where  $D_p$  is the pump displacement,  $H_e$  and  $H_i$  are external and internal leakage coefficients of the pump, and  $\omega$  is the pump drive speed, and  $C_A$ ,  $C_B$  are the hydraulic capacitances of the actuator chambers.

## 4.2 Linear Model

The system dynamics of the EHA is defined by four states; namely, the valve spool position  $y_s$ , the velocity  $v$  of the actuator, and pressures  $P_a$  and  $P_b$  in each chamber. Note that for the fully centered valve position, the spool is stationary since the pilot pressures are not enough to overcome the pre-compression force of the centering springs. Furthermore, for the fully opened valve positions, the spool is saturated at the end stroke. Therefore, for these two cases, the system can be investigated without considering the valve dynamics. However, it effects the transition between two hydraulic circuit configurations. A fast switching occurs if a valve with a small time constant is used. This switching can be smoothed by increasing the pilot line resistance, which slows the dynamic response of the EHA, in turn. During the experimental studies, it is seen that some abrupt pressure drops due to valve position changes occur in 10 ms, while the frequency of undesired pressure oscillations are observed in the range of 6-12 Hz. Furthermore, after measuring the force displacement relation of the centering springs and calculating the spool mass from the nominal dimensions, it is found that the natural frequency of the spool spring assembly is roughly 60 Hz (for  $k_s = 4.6 \text{ N/mm}$  and  $m_s = 34 \text{ g}$ ). Therefore, only a static relationship is formed between the spool position and chamber pressures in the linearized model since the valve dynamics is relatively high with respect to the frequency of observed pressure oscillations.

When the shuttle valve is fully opened, it can be considered as a lossless line, since it has relatively low resistance value of  $6.5 \cdot 10^{-7} \text{ MPa.s/mm}^3$ . Therefore, the chamber connected to the accumulator has very slow pressure response due to a large accumulator capacitance. Hence, the pressure dynamics is governed by the other chamber which is closed to the accumulator line. Using this configuration, the order of the system can be reduced from three to two by neglecting the slow dynamics of the chamber connected to the accumulator.

At this stage of the formulation, it would be appropriate to use a single pressure state named as the load pressure which is defined as follows.

$$P_L = P_a - \alpha P_b \quad (4-10)$$

where,

$\alpha$  = area ratio

$P_a$  = cap-side chamber pressure, in MPa

$P_b$  = rod-side chamber pressure, in MPa

Through this reduced order representation of the dynamics of the system, a second order relationship between the external load input and the resulting hydraulic circuit configuration can be defined and the system behavior can be investigated in the  $P_L - v$  plane.

### 4.3 Critical Load Pressure Region

Simplified models of possible hydraulic circuit configurations in the  $P_L - v$  plane are shown in Figure 4-1. The plane is divided into 3 regions determined by the valve spool position. In the right and left regions, the shuttle valve is fully opened. Therefore, the related chamber pressure is equal to the accumulator pressure. The middle region is defined as the *critical load pressure region*. This region corresponds to centered or partially opened valve positions. The upper and lower critical load pressure ranges can be defined by considering the region  $P_L \notin (P_{L1}, P_{L2})$ . In these regions, the pressure of the chamber connected to the accumulator line is constant. Therefore, there is a one-to-one mapping between chamber pressures and the load pressure  $P_L$ .

The location of the critical load pressure region is determined by the accumulator pressure. In Figure 4-1, both chamber pressures are equal to the accumulator pressure when  $P_L = P_{L_{cr}}$ ; hence,  $P_{L_{cr}}$  is expressed as follows.

$$P_{L_{cr}} = P_a - \alpha P_b = (1 - \alpha)P_c \quad (4-11)$$

where,  $P_c$  is the accumulator pressure.

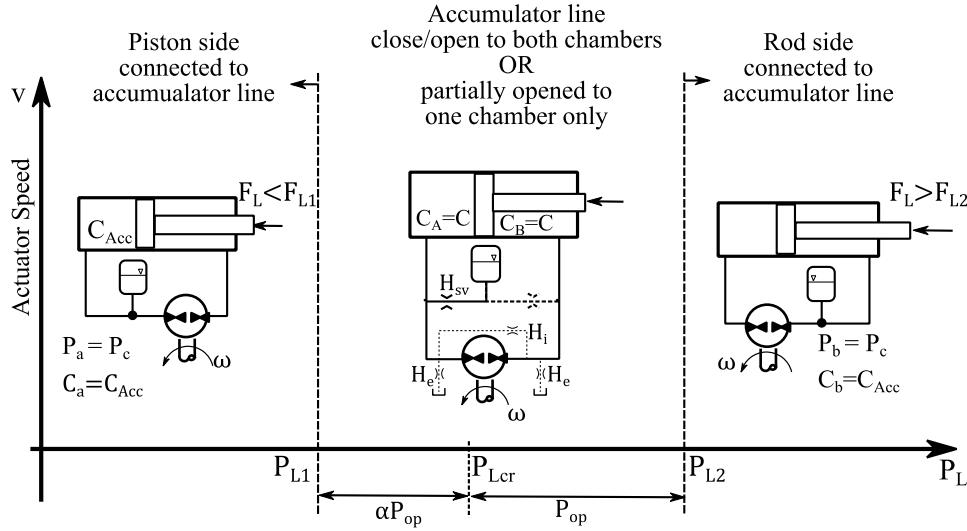


Figure 4-1 Critical load pressure region and circuit configurations

The size of the critical region is determined by the shuttle valve opening pressure. Considering the case where the rod side chamber is connected to the accumulator line, and thus  $P_a > P_b + P_{op}$  and  $P_b \approx P_c$ , the upper limit  $P_{L2}$  is defined as follows.

$$P_{L2} = P_a - \alpha P_b \approx (P_c + P_{op}) - \alpha P_c = P_{Lcr} + P_{op} \quad (4-12)$$

Similarly, considering the case where the cap side chamber is connected to the accumulator line, since  $P_b > P_a + P_{op}$  and  $P_a \approx P_c$ , the lower limit of the critical load pressure region  $P_{L1}$  is defined as follows.

$$P_{L1} \approx P_c - \alpha(P_c + P_{op}) = P_{Lcr} - \alpha P_{op} \quad (4-13)$$

Note that the location of the critical load region is constant if the accumulator pressure is constant, i.e., it has an infinite capacitance. However, if a small size accumulator were used instead, the critical load pressure location would change with the actuator position. The critical load pressure can be determined by using ideal gas assumption as follows.

$$P_{Lcr}|_{y=L} = P_{Lcr}|_{y=0} \left( \frac{V_{g0}}{V_{g0} - A(1 - \alpha)L} \right)^n \quad (4-14)$$

Here,  $L$  is the actuator stroke,  $n$  is the polytropic gas constant, and  $V_{g0}$  is the gas volume calculated for zero actuator position. The pressure drops during the extension the accumulator. At the end stroke of the actuator, the total displaced gas volume is equal to the actuator rod volume defined by the term  $A(1 - \alpha)L$ .

The accumulator line prevents any possible cavitation and air entrainment in addition to compensating the unequal flow rate of the actuator and the pump leakage losses. Therefore, the check valve and shuttle valve characteristics together with line losses should be considered while determining the level of the accumulator pressure,  $P_c$ . Its minimum level should be higher than the cracking pressures and the maximum pressure drops across the valves. Furthermore, actuator's hydraulic stiffness can be increased by increasing the accumulator pressure. However, a pressurized accumulator will increase the energy losses in turn since the accumulator pressure is adjusted via a relief valve. It should be noted that, the accumulator pressure can be considered as a static parameter determining the location of the critical load pressure region since the capacitance of the accumulator is much higher than the actuator chambers.

#### 4.4 Equivalent Flow continuity equations

In order to represent the pressure dynamics with a single load pressure state, the flow continuity equations (4-8) and (4-9) of two actuator chambers are modified by considering the state deviations. Since state deviations around an equilibrium point are considered, the chamber capacitance terms  $C_a(y_A)$  and  $C_b(y_A)$  are assumed to be constant to a value,  $C$ , calculated at a stroke where the two chamber volumes are equal.

When the rod side chamber is connected to the accumulator line as shown in the right region in Figure 4-1, the pressure dynamics is governed by the cap side chamber. Since  $P_b = P_c$ , the deviations in  $P_L$  and  $P_a$  are related as  $\delta P_L = \delta P_a$ . Furthermore, the cap side flow continuity equation (4-8), is re-written in terms of deviations in pump speed, actuator velocity, and load pressure.

$$D_p \delta \omega - A \delta v_A = C_a \delta \dot{P}_L + (H_e + H_i) \delta P_L \quad (4-15)$$

Similarly, when the cap side chamber is connected to the accumulator line, the pressure dynamics is governed by the rod side chamber; hence, the deviations in  $P_L$  and  $P_b$  are related as  $\delta P_L = -\alpha \delta P_b$ . Since, no flow exists between the accumulator and rod side chamber,  $Q_{b \rightarrow c}$  is zero. Then, the rod side flow continuity equation (4-9) is re-written in terms of deviations in pump speed, actuator velocity, and load pressure as follows.

$$\alpha D_p \delta \omega - \alpha^2 A \delta v_A = C_b \delta \dot{P}_L + (H_e + H_i) \delta P_L \quad (4-16)$$

For the centered shuttle valve case, in which  $|P_a - P_b| \in (0, P_{op})$ , none of the chamber pressures is governed by the accumulator dynamics. However, assuming zero internal leakage of the pump and then re-arranging the two flow continuity equations of the chambers, the load pressure state  $P_L$  can be obtained. Zero internal leakage is a reasonable assumption since the centered shuttle valve case occurs for  $|P_a - P_b| < P_{op} \approx 5$  bar, resulting in a relatively small pump leakage ( $< 0.05$  lpm).

Considering the use of an underlapped valve, both chambers are connected to the accumulator line through the initial opening  $u_{v0}$  of the shuttle valve. The shuttle valve can be modeled as a constant resistance with a flow coefficient of  $H_V$  defined as follows.

$$H_V = C_d A_{vMax} \frac{u_{v0}}{u_{vMax}} \frac{1}{\sqrt{2\rho \Delta p_{ss}}} \quad (4-17)$$

Then, shuttle valve flow rates  $Q_{a \rightarrow c}$  and  $Q_{b \rightarrow c}$  in Eqs. (4-8) and (4-9) are replaced by the linear flow terms  $H_V (P_a - P_c)$  and  $H_V (P_b - P_c)$ , respectively. Multiplying Eq. (4-9) by  $\alpha$ , and subtracting it from Eq. (4-8) the flow continuity equation is expressed in terms of deviations in pump speed, actuator velocity, and load pressure as follows.

$$(1 + \alpha) D_p \delta \omega - (1 + \alpha^2) A \delta v = (C_s + H_e + H_V) \delta P_L \quad (4-18)$$

#### 4.5 State Space Representation

The equation of motion has the same form for all possible circuit configurations considered in this study. Considering relatively high actuator speeds (100 mm /s) , the nonlinear terms of the friction force defined in Eq. (3-2) are ignored and only the viscous effects are considered. The resulting equation of motion in terms of deviations in state variables  $v$  and  $P_L$  is expressed as follows.

$$m\delta\dot{v}_A + b\delta v_A + \delta F_L = A\delta P_L \quad (4-19)$$

Using the equation of motion (4-19) and the flow continuity equations (4-15), (4-16), and (4-18) written for each possible circuit configuration, a common state space representation of the system can be written as follows.

$$\begin{bmatrix} \delta\dot{v}_A \\ \delta\dot{P}_L \end{bmatrix} = \begin{bmatrix} \frac{-b}{m} & \frac{A}{m} \\ -\Gamma_v \frac{A}{C} & -\frac{H}{C} \end{bmatrix} \begin{bmatrix} \delta v_A \\ \delta P_L \end{bmatrix} + \begin{bmatrix} -\frac{1}{m} & 0 \\ 0 & \Gamma_\omega \frac{D_p}{C} \end{bmatrix} \begin{bmatrix} \delta F_L \\ \delta \omega \end{bmatrix} \quad (4-20)$$

Here,  $\Gamma_\omega$  and  $\Gamma_v$  gains are expressed according to the load pressure variation as follows.

$$\Gamma_v = \begin{cases} \alpha^2 & \delta P_L < -\alpha P_{op} \\ 1 + \alpha^2 & -\alpha P_{op} < \delta P_L < P_{op} \\ 1 & P_{op} < \delta P_L \end{cases} \quad (4-21)$$

$$\Gamma_\omega = \begin{cases} \alpha & \delta P_L < -\alpha P_{op} \\ 1 + \alpha & -\alpha P_{op} < \delta P_L < P_{op} \\ 1 & P_{op} < \delta P_L \end{cases} \quad (4-22)$$

Furthermore, depending on whether an open or closed center shuttle valve is utilized, the leakage coefficient  $H$  is expressed as follows.

$$H = \begin{cases} H_e + H_i & \delta p_L \notin (-\alpha P_{op}, P_{op}) \\ H_e & \delta p_L \in (-\alpha P_{op}, P_{op}) \quad \text{Overlap} \\ H_e + H_v & \delta p_L \in (-\alpha P_{op}, P_{op}) \quad \text{Underlap} \end{cases} \quad (4-23)$$

## 4.6 Stability Analysis

All parameters written in the 2x2 system matrix of Eq. (4-23) are positive quantities. For all three circuit configurations, the system has a unique asymptotically stable equilibrium point for any given pump speed and load force inputs, since the determinant of the state matrix is positive  $bH + K_v A^2 > 0$  and its trace is negative  $-(b + H) < 0$ .

However, a special attention should be paid to the critical load pressure region. In Eq. (4-23), only the centered shuttle valve case is considered, and the intermediate stage, where the valve is partially opened to one of the chambers, is excluded. The centered shuttle valve case may result in some non-realizable equilibrium states depending on the valve type, pump speed, and external load input. A physical understanding of this situation can be illustrated by considering the closed center shuttle valve. Since both actuator chambers are closed to the accumulator line, the only way to compensate for the excess (or deficient) flow rate is the flow through the external pump leakage line, since it is the only port of the closed hydrostatic circuit. The mathematical expression for this situation can be defined by the addition of the flow continuity equations (4-8) and (4-9). At equilibrium ( $\dot{P}_a = \dot{P}_b = 0$ ), since the shuttle valve flow terms,  $Q_{a \rightarrow c}$  and  $Q_{b \rightarrow c}$ , are zero due to spool overlap, the actuator velocity is then written in terms of chamber pressures as follows.

$$v_{eq} = -\frac{H_e(P_{a_{eq}} + P_{b_{eq}})}{A(1 - \alpha)} \quad (4-24)$$

This equation verifies that if the shuttle valve is centered, i.e., no connection exists between actuator chambers and the accumulator line, the only way to compensate for the unequal flow rate developed by actuator velocity  $v_{eq}$  is the flow through the external leakage  $H_e$  of the pump.

Furthermore, Eq. (4-24) states that, during the extension of the actuator ( $v_{eq} > 0$ ), the sum of chamber pressures should be negative. That is, this sum must be lower than atmospheric pressure to create a leakage flow into the closed hydraulic circuit to compensate for the flow deficiency, which is not physically feasible. A physically realizable equilibrium point may exist during the retraction phase ( $v_A < 0$ ).

However, this is restricted with the actuator speed, since high speed movements require considerably high chamber pressures in order to compensate for an excess flow over the pump leakage line.

The solution is to increase the external leakage coefficient  $H_e$ . This can be accomplished by the addition of low resistance on/off valves and opening them in the critical load pressure region. In fact, this exactly corresponds to the solution of Wang and Book [86]. They connected two 2/2 flow control valves between actuator chambers and accumulator line. An inner loop controller determined the opening signal of the flow control valves by using the two pressure feedbacks of the actuator chambers. Through this application, the unequal flow was compensated through the accumulator line and possible pressure oscillations were inhibited. However, the addition of two valves will increase the hydraulic block size and the cost, and also necessitate additional control effort and elements.

The proposed novel solution in this study is to provide a valve spool underlap in order to compensate for the excess/deficient flow of the circuit for the centered shuttle valve case. In such a case, inserting the linearized shuttle valve flow terms  $Q_{a \rightarrow c} = H_V(P_a - P_c)$  and  $Q_{b \rightarrow c} = H_V(P_a - P_c)$  into the flow continuity equations (4-8) and (4-9), the equilibrium velocity is expressed as follows.

$$v_{eq} = - \frac{H_e (P_{aeq} + P_{beq}) + H_V(P_{aeq} + P_{beq} - 2P_c)}{A(1 - \alpha)} \quad (4-25)$$

This equation implies that the flow deficiency for  $v_{eq} > 0$  can be compensated if the sum of chamber pressures is much smaller than the accumulator pressure, and the excess flow is compensated if the sum of chamber pressures is much higher than the accumulator pressure. Neglecting the external leakage coefficient  $H_e$ , Eq. (4-25) implies that the chamber pressure sum is higher/lower than two times of the accumulator pressure during the retraction/extension of the actuator, respectively.

Based on these two findings, it can be concluded that in the critical load pressure region, the centered shuttle valve circuit configuration results in physically realizable

system states if and only if there exists a valve spool underlap, permitting a flow between accumulator and actuator chambers.

#### 4.7 Stability Analysis of Partially Opened Shuttle Valve Circuit

In the critical load pressure region, the asymptotic stability is guaranteed if the shuttle valve remains in center position. However, a closed center valve spool cannot maintain in its center position, but will open partially since the flow through the external leakage line of the pump is not enough to compensate for the unequal flow rate of the actuator. Furthermore, an underlapped valve spool can only remain in its center position up to some certain retraction speeds, over which the corresponding unequal flow rate cannot be compensated by the valve underlap. Therefore, the stability of an equilibrium point requiring a partially opened spool position is to be investigated.

In the critical load pressure region, possible circuit configurations for the partially opened shuttle valve position are shown in Figure 4. In that region, none of the chamber pressures is governed by the accumulator dynamics. The spool position resulting from the chamber pressures makes the valve either partially opened to the rod side or cap side of the actuator. Therefore, two possible circuit configurations are drawn both in upper and lower halves of the  $P_L - v$  plane as shown in Figure 4. Two different circuit configurations for the same region mean that an equilibrium point can exist for both circuit configurations. However, in the following proposition 1 and proposition 2, it is stated that an equilibrium point exists only for one circuit configuration during the extension or retraction of the actuator. The stability features of possible circuit configurations shown in Figures 4-b and 4-c are defined in propositions 3 and 4. The proofs of all propositions are given at the end of this chapter, pg. 118. In the proofs of propositions 1 and 2, an inequality is derived, describing whether an equilibrium point  $P_{Leq}$  satisfies  $P_L \in (P_{L1}, P_{L2})$ . Each inequality is derived by utilizing the shuttle valve flow equation (4-5), neglecting the actuator friction and pump leakage losses. On the other hand, in the proofs of propositions 3 and 4, the nonlinear characteristic flow equation (4-5) of the shuttle valve is linearized and state equations of the corresponding circuit configuration are

re-written. The stability is determined by Routh criterion after deriving the characteristic equation.

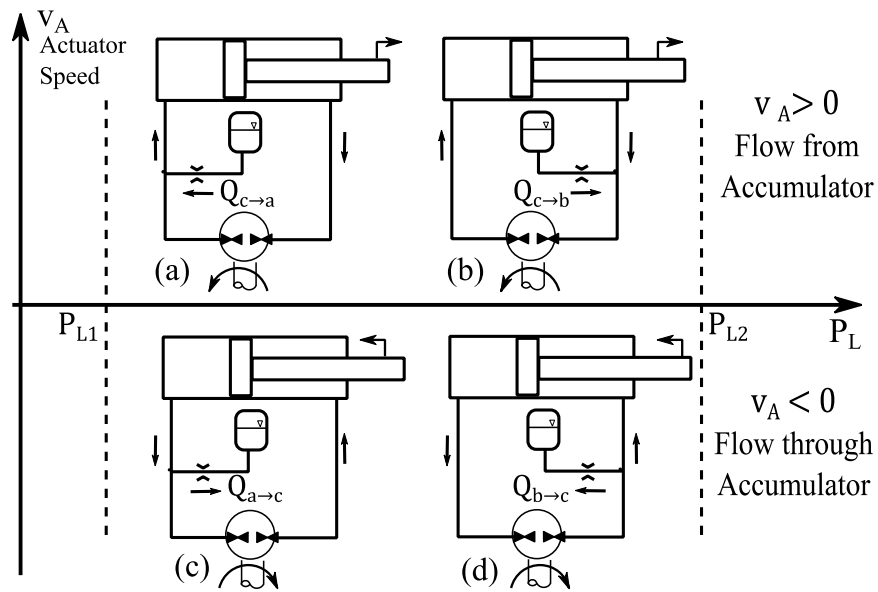


Figure 4-2 Possible circuit configurations for partially opened valve positions

#### 4.7.1 Proposition 1

During the extension of the actuator ( $v > 0$ ), no equilibrium point  $P_{Leq} \in (P_{L1}, P_{L2})$  exists for the circuit scheme connecting the accumulator line to the cap side of the actuator as shown in Figure 4-2-a.

#### 4.7.2 Proposition 2

During the retraction of the actuator ( $v < 0$ ), no equilibrium point  $P_{Leq} \in (P_{L1}, P_{L2})$  exists for the circuit scheme connecting the accumulator line to the rod side of the actuator as shown in Figure 4-2-d.

#### 4.7.3 Proposition 3

During the extension of the actuator, an equilibrium point requiring a partially opened spool position is asymptotically stable.

#### 4.7.4 Proposition 4

During the retraction of the actuator, an equilibrium point requiring a partially opened spool position is unstable, if the area ratio  $\alpha > 0.28$ . The asymptotic stability of such a point is not guaranteed if  $\alpha < 0.28$ .

An area ratio of  $\alpha = 0.28$  physically means that the actuator has a relatively large rod diameter. Therefore, the deficient flow rate shown as  $(1 - \alpha)Av_A$  in Figure 3-4 is two and half times higher than the pump flow rate shown as  $\alpha Av_A$ . However, the hydraulic circuit which is the subject of this study is not appropriate for that kind of actuators, since it will increase the shuttle valve and accumulator dimensions. Practically, the use of a second pump for flow compensation is reasonable for the motion control of the actuators with  $\alpha < 0.5$ . The unequal flow rate that should be supplied over the shuttle valve is rather equal to or smaller than the pump flow rate for actuators with  $\alpha \in (0.5,1)$ . Therefore, they are more appropriate for the investigated circuit.

#### 4.8 Determination of the Valve Underlap

In the bottom half of the critical load pressure region ( $v_A < 0$ ), any equilibrium point, requiring a partially opened valve position for the compensation of the unequal flow rate, is unstable. In order to avoid the instability, it is proposed to provide a valve underlap to compensate the unequal flow rate while maintaining the spool at centered position. By increasing the valve underlap, higher flow rates can be compensated. However, high underlap values increase the energy consumption of the circuit. A high underlap value, such as an open center valve with maximum orifice opening at center position, can be considered as a direct line connecting the two ports of the pump, which is similar to a short circuit by electrical analogy. In such a case, the actuator velocity will be zero whatever the pump speed is. Mathematically, the same conclusion can be reached by considering the equilibrium velocity in Eq. (4-25). Taking the flow coefficient  $H_V$  infinite makes the velocity independent of pump speed and the function of external force only.

The value of valve underlap should be determined in a way that the unequal flow rate of the actuator formed at its maximum retraction speed is lower than the flow rate that can be supplied by the shuttle valve at its center position. The critical retraction speed can be found by considering a special reference point as shown in Figure 4-3.

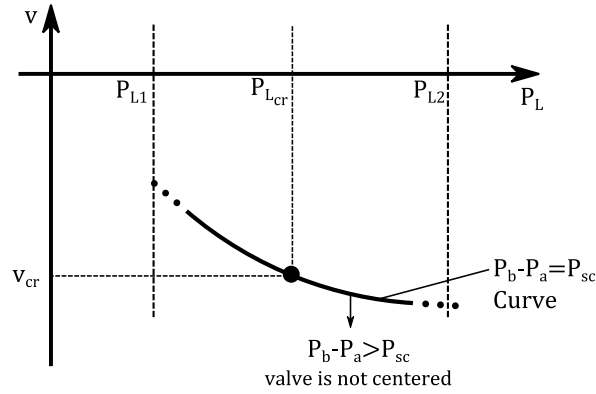


**Figure 4-3 Critical speed**

The critical retraction speed is found by intersecting the critical load pressure line,  $P_{L_{cr}} = (1 - \alpha)P_c$ , by the pressure difference curve defined by  $P_b - P_a = P_{sc}$  equality. This curve defines the maximum pressure difference to maintain the valve spool at center position, below that curve, the pressure difference is greater than the valve cracking pressure, therefore, the spool is partially opened to left and the system is unstable. The chamber pressures can be found by using the below relations written for the critical point shown in Figure 4-3.

$$P_a - \alpha P_b = P_{L_{cr}} = P_c(1 - \alpha) \quad (4-26)$$

$$P_a - P_b = P_{sc} \quad (4-27)$$

Solving the above two equations, the chamber pressures are found as follows.

$$P_a = P_c + \frac{\alpha P_{sc}}{1 - \alpha} \quad (4-28)$$

$$P_b = P_c + \frac{P_{sc}}{1 - \alpha} \quad (4-29)$$

Neglecting the pump leakage terms and summing the cap and rod side flow continuity equations (4-8) and (4-9) reveals that the unequal flow rate  $A(1 - \alpha)v_{cr}$  is to be compensated by shuttle valve flow rates  $Q_{a \rightarrow c}$  and  $Q_{b \rightarrow c}$  only. Inserting the pressure values of the chambers defined in Eqs.(4-28) and (4-29), into shuttle valve flow equations (4-8) and (4-9) the critical speed for the actuator retraction is found as follows.

$$v_{cr} = -\frac{1}{A(1 - \alpha)} C_d A_{vMax} \frac{u_{v0}}{u_{vMax}} \sqrt{\frac{2}{\rho} \frac{P_{sc}}{1 - \alpha}} (1 + \sqrt{\alpha}) \quad (4-30)$$

In Eq. (4-30), the required underlap value  $u_{v0}$  of a shuttle valve can be obtained by equating the critical velocity  $v_{cr}$  to the maximum retraction speed of the actuator. However, parameters like discharge coefficient  $C_d$ , maximum orifice opening  $u_{vMax}$ , and area  $A_{vMax}$  are not specified in valve manufacturer catalogs. Generally, shuttle valves in the market are specified or categorized according to their cracking pressure, and their hydraulic conductance is specified with a corresponding pressure drop versus flow diagram drawn for their fully opened position. Therefore,  $C_d A_{vMax} \sqrt{\frac{2}{\rho}}$  gain can be obtained from these pressure flow diagrams. Hence, the underlap ratio  $u_{v0}/u_{vMax}$  remains as the only unknown parameter in (4-30). If provided in the manufacturer's catalog, the underlap ratio can be obtained from the pressure flow relations given for the centered spool position. Otherwise it should be inquired from its manufacturer. In addition to the maximum retraction speed of the actuator, the maximum pump speed  $\Omega_{cr}$  can also be utilized for the selection of shuttle valve. In this case, Eq.(4-31), which is derived with a similar procedure as Eq. (4-30), is to be used.

$$\Omega_{cr} = -\frac{1}{D_p(1 - \alpha)} C_d A_{oMax} \frac{x_{s0}}{x_{oMax}} \sqrt{\frac{2}{\rho} \frac{p_{cr}}{1 - \alpha}} (1 + \sqrt{\alpha^3}) \quad (4-31)$$

Whether the maximum pump or actuator retraction speed is utilized, it is suggested to select a shuttle valve with an underlap ratio 2-3 times higher than the required value. This is because the above analysis is performed just for the critical load

pressure  $P_{Lcr}$  value, instead of the whole critical region. Besides increasing the spool underlap, Eqs. (4-30) and (4-31) reveals that high retraction speeds can also be achieved by increasing the valve cracking pressure  $P_{sc}$ . However, this will increase the size of the critical load pressure region, in turn.

An approximate stability region can be drawn in the  $P_L - v$  plane as shown in Figure 4-4. Inserting the critical pump speed  $\Omega_{cr}$  into the flow continuity equation (4-18) written for the centered valve scheme, the equation of line defining the critical load pressure region corresponding to asymptotically stable operations is expressed as follows.

$$(1 + \alpha)D_p\Omega_{cr} = (H_e + H_V)\delta P_L + (1 + \alpha^2)A\delta v \quad (4-32)$$

The solid oblique line in Figure 4-4 represents  $P_b - P_a = P_{sc}$  equality, since it is written for the centered valve case. Therefore, above that line, the chamber pressure difference, i.e. pilot pressure, is below the valve cracking pressure so that the shuttle valve is at centered position and equilibrium points are asymptotically stable. Below that line, the shuttle valve opens only partially, and thus any possible equilibrium point in that region is unstable.

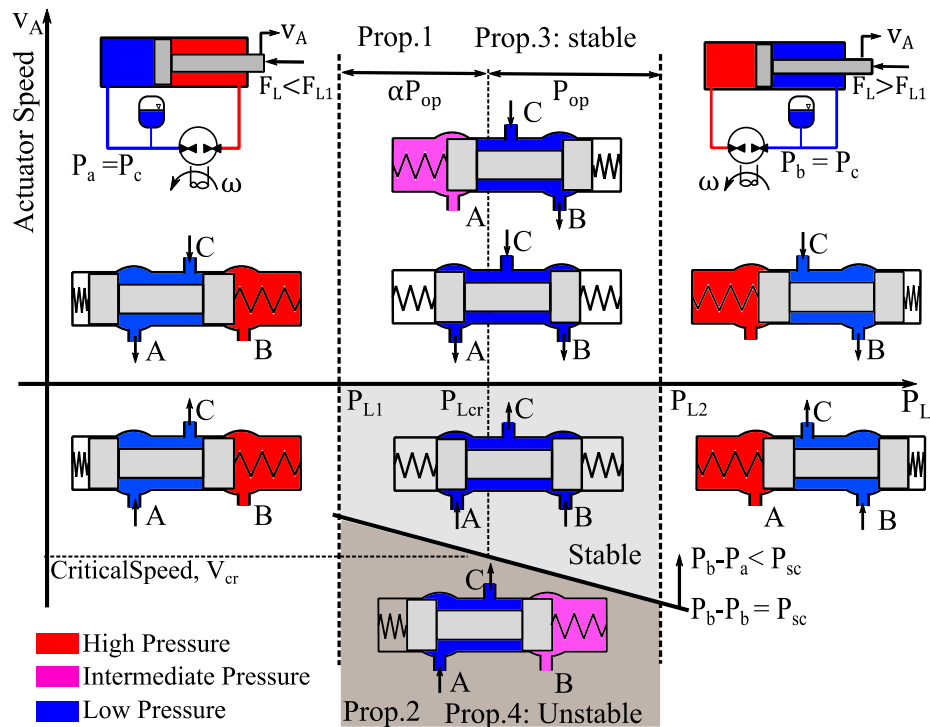


Figure 4-4 Possible valve positions and asymptotic stability limit in the critical load pressure region

## 4.9 Simulation Results

Numerical simulations are used to illustrate the critical load pressure region defined in this study and to verify the stability limit obtained by valve underlap. The simulation model given in section 3.3 is developed in MATLAB<sup>®</sup>/SimHydraulics<sup>®</sup> environment, and it includes the orifice flow, actuator friction, and chamber capacitance nonlinearities. Furthermore, the spool dynamics is modeled by a valve actuator with a time constant of 1 ms.

In the simulation model, an underlapped valve with 5 bar cracking pressure and accumulator line with 35 bar pressure are used. The resulting critical load pressure region is shown in Figure 4-5, with vertical lines  $P_{L_{cr}} = 8.75$  and  $P_L \in (4.5 - 14.3)$ . The trajectories of the state portrait are drawn by using the open loop actuator velocity  $v$  and load pressure  $P_L$  responses of the nonlinear simulation model to various pump speeds and external force step inputs whose values are given in the legend of the Figure 4-5. It is seen that the equilibrium points inside the critical load pressure region are stable, up to certain retraction speeds.

In Figure 4-5, all the trajectories are starting from  $[p_{L_{cr}}, 0]$ , since initially the velocity is set to zero and the chamber pressures are set to the accumulator pressure. The first trajectory, which is obtained for  $-2500 \text{ rpm}$  pump speed and  $2 \text{ kN}$  external load, converges to a stable equilibrium point outside the critical load pressure region. By increasing the external load to  $2.9 \text{ kN}$  and maintaining the same pump speed, the equilibrium point is shifted into critical load pressure region, as represented by the second trajectory. It is seen that the equilibrium velocity for the same pump speed input decreases from  $156 \text{ mm/s}$  to  $132 \text{ mm/s}$ , which is due to the lost flow rate over the valve underlap. The third trajectory is obtained by decreasing the pump speed down to  $-2750 \text{ rpm}$  while maintaining the external load constant at  $2 \text{ kN}$ . It is seen that the resulting equilibrium point is unstable. The actuator velocity is oscillating between  $145 \text{ mm/s}$  to  $255 \text{ mm/s}$ , while the load pressure is oscillating between  $3.7 \text{ bar}$  to  $7 \text{ bar}$ . The same situation happens for the 4<sup>th</sup> - 5<sup>th</sup> and the 6<sup>th</sup> - 7<sup>th</sup> trajectory pairs. In each of them, an unstable equilibrium point is obtained by increasing the pump speed by  $250 \text{ rpm}$  while maintaining the force constant. Up to certain velocities, the excess flow rate of the actuator is returned to the hydraulic

accumulator over the preopening of the shuttle valve. Since the spool is centered, the equilibrium points are stable. However, when the retraction speed is increased, the shuttle valve is forced to open partially, which results in an unstable equilibrium point as defined in Proposition 4.

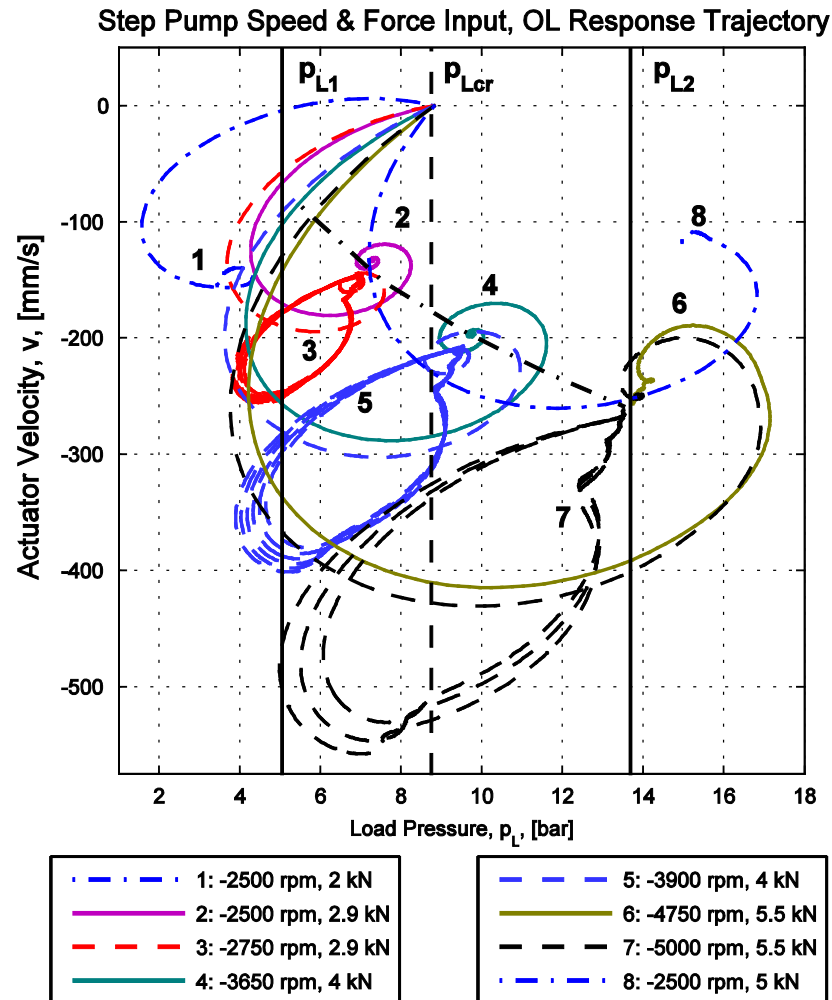


Figure 4-5 Simulation model responses: asymptotically stable operation range of underlapped shuttle valve

The 8<sup>th</sup> trajectory is drawn for  $-2500 \text{ rpm}$  pump speed and  $5 \text{ kN}$  external load. It is seen that the equilibrium point is stable with a retraction speed of  $-118 \text{ mm/s}$ . It is seen that the actuator velocity has decreased by  $\alpha = 0.75$  amount for the same pump speed with the 1<sup>st</sup> input. This is an expected result and can be understood by checking the circuit configurations given in Figure 4-4. At the left of the critical region, the cap side is connected to the accumulator line; therefore, the pump controls the flow through the rod side chamber with area piston  $\alpha A$ . However, at the

right of the critical region, the rod side is connected to the accumulator line and the pump controls the flow of cap side with piston area  $A$ .

The stable and unstable equilibrium points are separated by the black dot-solid curve in Figure 4-5. Note that the locus connecting the borderline between stable and unstable retraction speed points is not a straight line as shown in Figure 4-4. This is an expected result since the line equation (4-32) is derived by linearizing the shuttle valve flow equation containing a square root nonlinearity, while the curve is drawn by calculating the critical velocity defined in Eq. (4-30) at various load pressure values in the critical region.

The verification of the nonlinear simulation model is illustrated in Figure 4-6. The chamber pressure and actuator position response of the model are compared with the experimental test results obtained for open loop constant pump speed input. In order to illustrate the switching behavior, the spool position response  $y_s$ , of the simulation model is also provided. Furthermore, the actuator position response is offset by  $-50\text{ mm}$  for scaling purposes. For model verification, the parameters of a closed center valve, Bucher Hydraulics (400671602), are utilized instead of an underlapped valve. The shuttle valve has  $2.5\text{ mm}$  spool overlap and  $5\text{ bar}$  cracking pressure, the hydraulic conductance is similar to the previous one. The use of an overlapped valve is due to the experimental set up; since relatively high retraction speeds exceeding design limitation are required to demonstrate the instability of the underlapped valve. Note that, the instability is independent of valve type but related with the equilibrium point requiring a partially opened spool position as mentioned in proposition 4. As seen in Figure 4-6, the pressure and position responses of the simulation model are comparable qualitatively with the measured test results. The quantitative difference between model response and test results is an expected result, since nominal parameters are used in the simulation model and they are not tuned to fit the measurement data. At the beginning of Figure 4-6, the actuator is retracting with a constant velocity and the shuttle valve is centered with zero spool position. However, since not all of the excess flow is returned to accumulator line, the two chamber pressures increase up to certain level, where their difference is enough to move the shuttle valve spool. The valve is opened in negative direction, and returning the excess flow to the accumulator, the pressures decrease suddenly. The valve spool

cannot remain in a partially opened position as mentioned in proposition 4 and goes to center position, which again leads to the increase in chamber pressures. The result of these pressure oscillations is a sudden decrease in the actuator velocity, which can be understood from the abrupt decrease off the position response, during the valve switching time. In the second half of the Figure 4-6, the actuator is extending, no instability is observed as mentioned in proposition 3. The chamber pressures are stationary and the spool is centered. The deficient flow is compensated over the check valve connecting the rod side chamber to accumulator line.

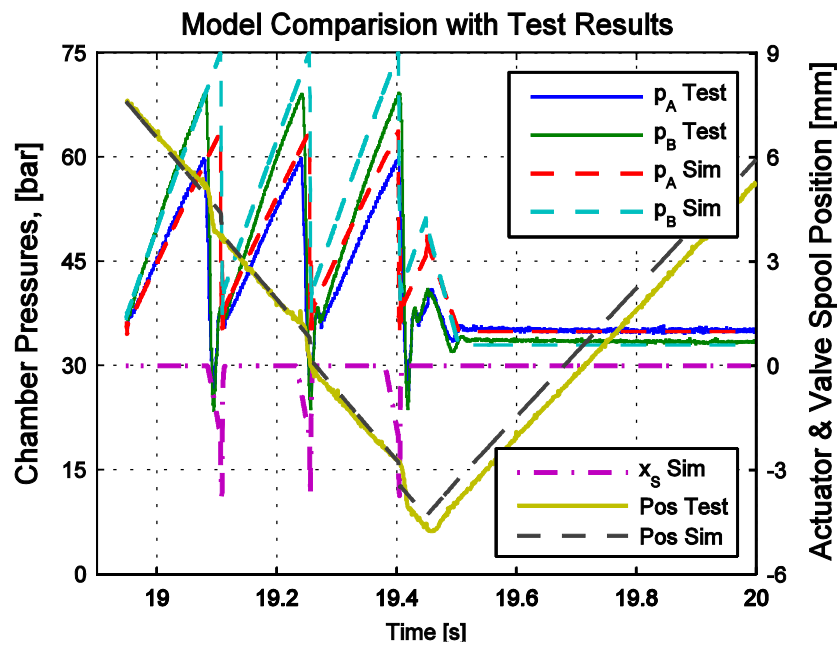


Figure 4-6 Simulation model repose and experimental test results comparison

#### 4.10 Experimental Tests

In order to illustrate the pressure oscillations problem and validate the proposed solution, two sets of experiments are conducted. The first experiment is conducted by a closed centered shuttle valve. It illustrates the existence of pressure oscillations in the critical load pressure region.

The second experiment utilizes an underlapped valve and aims to validate the proposed solution, i.e., removing pressure oscillations. Both experiments are conducted in an open loop manner. First, a constant external load is applied on the EHA by the load simulator. Then, the pump is driven by constant motor speed, both

for extension and retraction of the actuator. Measured pressure responses, pump speeds, and external load inputs are presented. Furthermore, the actuator velocity is displayed, which is estimated online by a kinematic Kalman filter.

#### 4.11 Experimental Results with Closed Center Valve

In the first experiment, a closed centered shuttle valve of Bucher Hydraulics (400671602) is utilized. The cracking pressure of the valve is 5 *bar*, the overlap value of the valve spool is measured as 2.5 *mm*. Furthermore, its maximum orifice opening is 4 *mm* corresponding to 75.4 *mm*<sup>2</sup> orifice area. According to the manufacturer data, the hydraulic conductance for fully opened valve position is 45 *lpm* for 5 *bar* pressure drop.

The accumulator is pressurized up to 35 *bar*, then a 20 *l* gas tank is connected to the accumulator in order to increase the gas capacity and prevent pressure fluctuation due to actuator motion. Using this accumulator pressure value in Eq. (4-11), the critical load region is found to be located at  $P_{L_{cr}} = 8.75 \text{ bar}$ , with a range of 4.4 – 14.6 *bar*. By using Eq. (4-19) and neglecting the frictional and inertial effects of the actuator, an approximate critical force region can be calculated as 1210 – 4100 *N*.

Figure 4-7 shows the EHA response for applied loads of 2.5 – 3 – 3.5 – 5 *kN*, respectively. Throughout each load, the servo motor speed is reversed between  $\pm 400 \text{ rpm}$ . In each sub-figure, responses of the accumulator and the actuator chamber pressures, the difference of chamber pressures  $P_b - P_a$ , pump speed  $\omega_m$ , actuator velocity, and external load  $F_L$  are displayed. The first three sub-figures correspond to the approximated critical force region. It is clearly seen that the pressure oscillations occur only for the negative pump speeds, i.e., during the retraction of the actuator, as proposed in Proposition 4. However, for positive pump speed inputs, i.e., during the extension of the actuator, no oscillations occur as proposed in Proposition 3. Note that, when the two chambers are closed to the accumulator line, the excess flow formed during the retraction of the actuator cannot be returned to the accumulator line, the two actuator chambers are pressurized, till

the opening pressure of the valve is reached. It is seen that the rod side pressure is higher than the cap side pressure, therefore as proposed in Proposition 2, the shuttle valve is opened to connect the cap side chamber to the accumulator line. Chamber pressures drop to the accumulator pressure level abruptly in 10 ms time, causing large sized velocity oscillations. Amplitudes of velocity oscillations are also qualitatively consistent with the simulation results as shown in Figure 4-5. They increase with the increasing load.

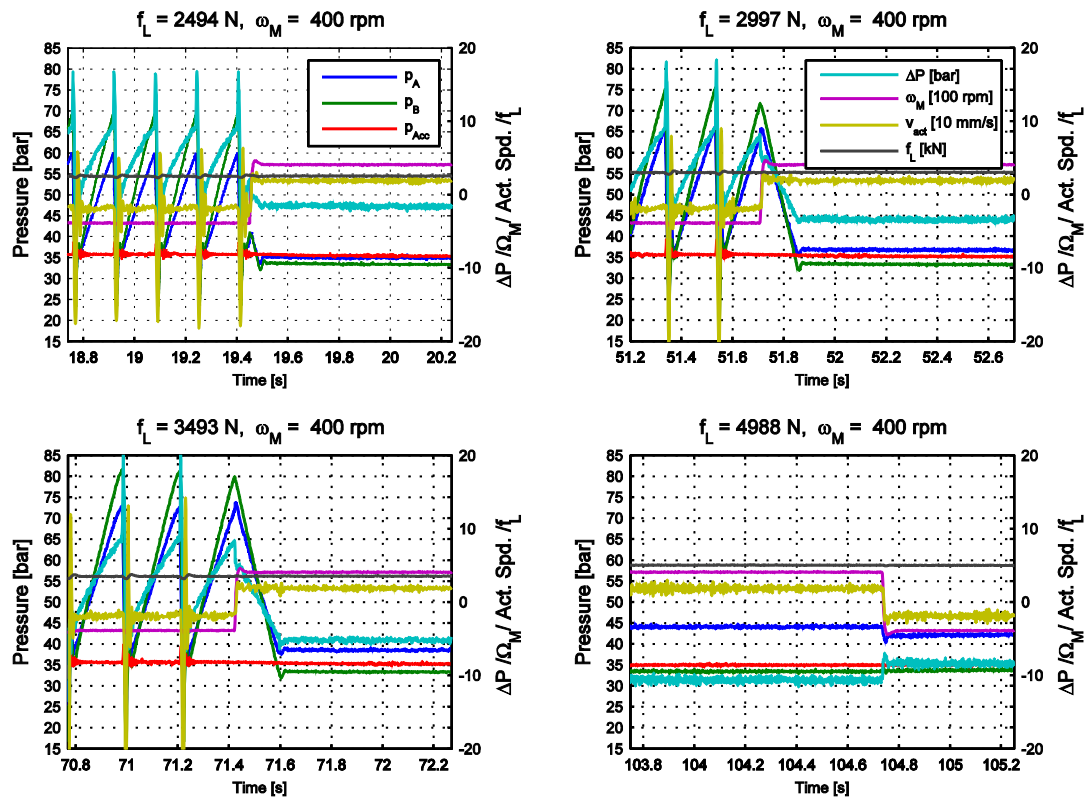


Figure 4-7 Open loop pressure responses to external load and pump speed inputs with an overlapped shuttle valve

For the extension of the actuator, i.e., positive pump speeds, although the pilot pressure ( $-2$  bar) is smaller than the valve cracking pressure, no pressure oscillations are observed. The pressure of the cap side chamber is higher than the rod side, and the valve tends to connect the rod side chamber to the accumulator line, as proposed in Proposition 1. The shuttle valve is either partially opened or centered. Note that during the extension, it is also possible to compensate the flow deficiency over the check valves. In the last sub-figure of Figure 4-7, the external load is

increased to 5 *kN*; it is seen that the pilot pressure is higher than valve cracking pressure, meaning that operation is outside the critical region. Therefore, no pressure oscillations occur. Note that, for loads higher than the critical load, the rod side chamber is connected to the accumulator line. In that region, the shuttle valve position is determined by the external load. The retraction and extension speeds are the same with  $\pm 19 \text{ mm/s}$ , for the pump speed input of  $\pm 400 \text{ rpm}$ .

#### 4.12 Experimental Results with Underlapped Valve

In the second experiment, an underlapped shuttle valve of Parker K04F3-5.0 is utilized. The cracking pressure of the valve is 5 *bar*. According to the data taken from the manufacturer, the maximum orifice area is  $64.4 \text{ mm}^2$  and the pre-opening area is  $3.02 \text{ mm}^2$  corresponding to a 0.15 *mm* spool underlap. The hydraulic conductance for fully opened valve position is given as 55 *lpm* for 7 *bar* pressure drop. Therefore, it is comparable with the closed center one.

A different hydraulic manifold is manufactured and mounted for the second test, since the port size of Parker's valve is different from the Bucher's valve. The accumulator is pressurized up to 31 *bar*, this time the gas tank is not connected to the 5 *l* accumulator. Therefore, it is observed that the accumulator gas pressure varies by an amount of 1.25 *bar* due to the displaced actuator rod volume. Using Eq. (4-11), the critical load region is calculated to be located at  $P_{L_{cr}} = 7.75 \text{ bar}$ , with range 5.9 – 10.2 *bar*. By using Eq. (4-19) and neglecting the frictional and inertial effects of the actuator an approximate critical force region can be calculated as 2.3 *kN* – 3.50 *kN*.

The same test procedure used for overlapped valve test is repeated for the underlapped valve test. Figure 4-8 shows the pressure and speed responses of the EHA system for external loads of 0.5 – 2 – 2.5 – 4 *kN*, respectively. Throughout each load, the servo motor speed is reversed between  $\pm 1500 \text{ rpm}$ . The use of axes and legends are coherent with Figure 4-7.

Second and third sub-figures of Figure 4-8 correspond to the critical load region, since the pilot pressure is below the valve cracking pressure 5 *bar*. When compared

with the closed center valve test, it is clearly seen that no pressure oscillations occur during the retraction of the actuator. The results show that a stable operation region in the critical load pressure range is obtained, by providing a valve underlap. Since the valve is at center position, during the retraction (extension) of the actuator, the excess (deficient) flow rate is returned (supplied) to (from) the hydraulic accumulator over the pre-openings of the valve spool at its two ports. It is seen that during the retraction (extension) of the actuator that is for negative (positive) pump speeds the rod (cap) side pressure is higher than the pressure of the cap (rod) side. Therefore, the shuttle valve tends to connect the cap (rod) side chamber to accumulator line as proposed by Proposition 2 (Proposition 1) and shown in Figure 4-4.

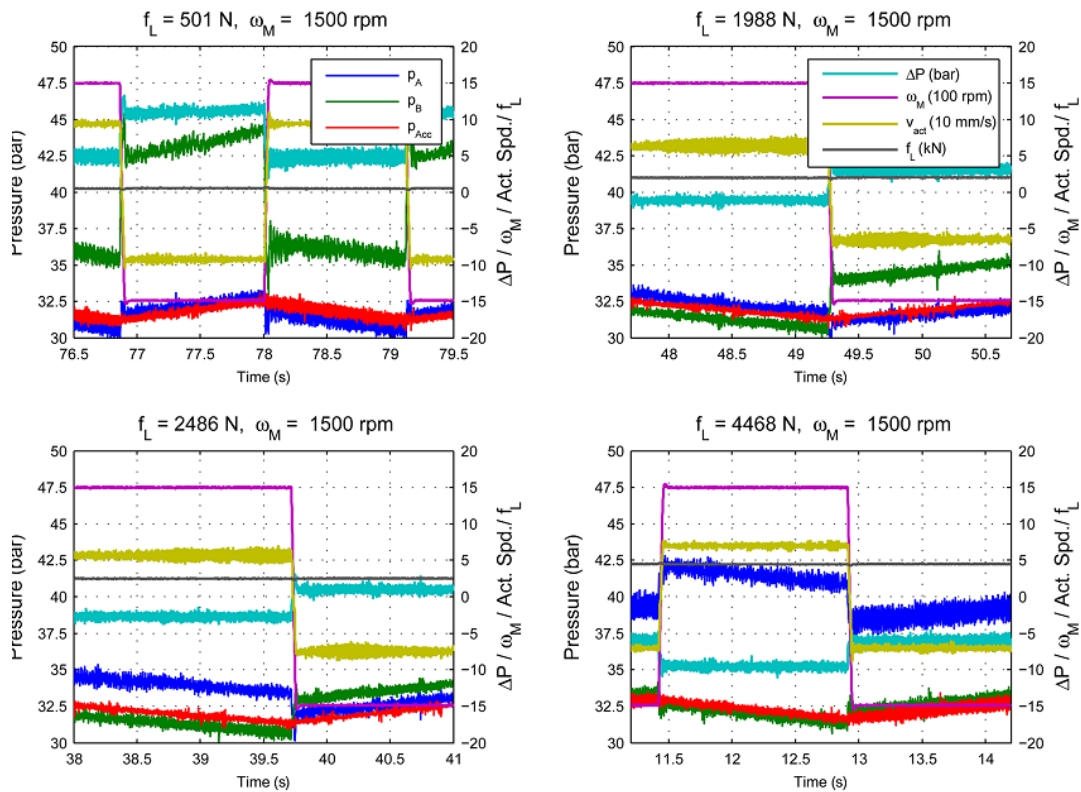


**Figure 4-8 Open loop pressure responses to external load and pump speed inputs with an underlapped shuttle valve**

The instability is avoided at the expense of flow losses which can be understood by checking the transformer ratio of the pump/actuator assembly. Assuming incompressible fluid and leak free system, the transformer ratio between the pump speed input and the actuator speed output is  $\frac{D_p}{A} = 0.6 \frac{mm}{rad}$ . Note that this ratio is not

constant and decreases by  $\alpha$  amount to 0.45 mm/rad when the rod side chamber is connected to the accumulator line. In the first sub-figure for  $F_L = 0.5 \text{ kN}$ , the cap side chamber, and in the last sub-figure for  $F_L = 4.5 \text{ kN}$  the rod side chamber is connected to the accumulator line. In these two figures, the speed of the actuator is constant  $\pm 94 \text{ mm/s}$ ,  $\pm 70 \text{ mm/s}$ , respectively and not changing with the pump speed direction. Remembering that the pump drive speed is 1500 rpm, the transformer ratios are nearly the same as the theoretical values. This means that a negligible amount of fluid is leaked over the pump leakage line. However, when the second sub-figure is observed, it is seen that the transformer ratios are decreasing to  $\approx 0.40 \text{ mm/rad}$  ( $0.48 \text{ mm/rad}$ ) during the extension (retraction) of the actuator. In the second sub-figure drawn for  $F_L = 2 \text{ kN}$ , during the extension of the actuator, the chamber pressure relations reveals that there exist a flow from the cap side chamber to the accumulator line, since  $P_a > P_c$ , whereas the flow returns to the rod side chamber, since  $P_c > P_b$ . Due to this short circuit like structure, the actuator speed is decreased to  $63 \text{ mm/s}$ . This corresponds to a transformer ratio of  $0.40 \text{ mm/rad}$ . The loss for the extension of the actuator is even higher in the third sub-figure for with a transformer ratio of  $0.36 \text{ mm/rad}$ . However, during the retraction of the actuator in the third sub-figure, it is seen that no circulating leakage flow forms. Since both chamber pressures are higher than the accumulator pressure, a flow occurs from two chambers to the accumulator, the resulting velocity is  $75 \text{ mm/s}$  with a corresponding transformer ratio of 0.48.

### 4.13 Conclusion

In the current study, a pump control circuit is analyzed, in which a spool type shuttle valve is utilized to compensate for the unequal flow rate of a single rod actuator. Although an electro-hydraulic actuator with a variable speed motor is considered, the approach given here can be extended to displacement controlled circuits. The system model is obtained in the load pressure versus velocity domain instead of using individual actuator chamber pressures as separate variables. A critical load pressure region is defined in the load pressure versus velocity plane. The location and size of this region are determined in terms of the accumulator pressure and the shuttle valve

opening pressure. In the critical load pressure region, the shuttle valve is whether centered or partially opened, and outside that region it is fully opened.

A common state space representation of the whole system is obtained for both centered and fully opened shuttle valve cases and it is shown that all the possible equilibrium points have stable nature. For the equilibrium points requiring a partially opened valve position, it is shown that a continuous oscillatory response occurs in the critical load pressure region during the retraction of the actuator, commonly termed as instability in earlier work. A mathematical proof of this instability is given by linearizing the flow equations for shuttle valve characteristics. In the critical load pressure region, a close center shuttle valve cannot remain in the centered position but likely to open partially since it has no pre-opening to compensate for the unequal flow rates of the actuator. Therefore, the use of an underlapped shuttle valve is proposed to avoid instability, which remains in the centered position up to a certain retraction speed. A relationship between the critical retraction speed limit and the amount of valve underlap is derived for a stable operation. This relationship can be used in selecting the shuttle valve to ensure a stable operation of the corresponding system as long as the speed of the actuator is below a critical limit.

The theoretical findings are validated by numerical simulations by using a model developed via MATLAB<sup>®</sup>/SimHydraulics<sup>®</sup> toolbox. Furthermore, the instability of the system with the use of a closed center shuttle valve is demonstrated with an experimental study. After replacing the shuttle valve with the underlapped one, the solution to avoid instability is also demonstrated on the same test set up via similar open loop tests. It is shown that in the critical load pressure region, an underlapped shuttle valve provides a stable operation region; however, it decreases the transformer ratio between pump speed input and the actuator speed output. Therefore, a significant emphasis should be given for the selection of the underlapped shuttle valve.

#### **4.14 Proofs of the propositions**

The proofs of the proposition given in section 4.7 are given as follows.

#### 4.14.1 Proof of Proposition 1

The case in which the accumulator line is connected to the cap side chamber is shown in Figure 4-2-a and Figure 4-2-c. The existence of an equilibrium point with this circuit scheme requires that  $P_{b_{eq}} > P_{a_{eq}} + P_{op}$ . By using this inequality, the following load pressure inequality is written.

$$P_{L_{eq}} = P_{a_{eq}} - \alpha P_{b_{eq}} < (1 - \alpha)P_{a_{eq}} - \alpha P_{op} \quad (4-33)$$

Modifying the cap side flow continuity given in Eq. (4-8) with the additional shuttle valve flow term defined in Eq. (4-5), the state equations at equilibrium ( $\dot{\mathbf{x}} = 0$ ) are re-written as follows.

$$0 = -F_L + AP_a - \alpha AP_b \quad (4-34)$$

$$D_p \omega - Av_A = K_V (P_b - P_a - P_{op}) \sqrt{P_a - P_c} \operatorname{sgn}(P_a - P_c) \quad (4-35)$$

$$0 = -D_p \omega + \alpha Av_A \quad (4-36)$$

From Eq. (4-36) the equilibrium velocity is found as

$$v_{eq} = \frac{D_p}{\alpha A} \omega \quad (4-37)$$

Inserting  $v_{eq}$  into Eq. (4-45) yields

$$-D_p \frac{(1 - \alpha)}{\alpha} \omega = K_V (p_B - p_A - p_{op}) \sqrt{p_A - p_S} \operatorname{sgn}(P_a - P_c) \quad (4-38)$$

During the extension of the actuator, that is for positive pump speeds  $\omega > 0$ , the sign function in the flow continuity equation (4-38) must be negative. Inserting  $P_a < P_c$  into previously defined load pressure relation Eq. (4-33) one gets,

$$p_{L_{eq}} < (1 - \alpha)p_S - \alpha p_{op} = p_{L1} \quad (4-39)$$

Since  $P_{Leq} = P_{aeq} - \alpha P_{beq} \notin (P_{L1}, P_{L2})$ , the inequality in Eq. (4-39) proves that no actual equilibrium point exists in the critical load pressure region for the circuit scheme in which the accumulator line is connected to the cap side of the actuator during the extension of the actuator.

#### 4.14.2 Proof of Proposition 2

The case in which the accumulator line is connected to the rod side chamber is shown in Figure 4-2-b and Figure 4-2-d. The existence of an equilibrium point with this circuit scheme requires that  $P_a > P_b + P_{op}$ . By using this inequality, the following load pressure inequality is written.

$$P_{Leq} > (1 - \alpha)P_{beq} + P_{op} \quad (4-40)$$

Modifying the rod side flow continuity given in Eq. (4-11) with the additional shuttle valve flow term defined in Eq. (4-5), the state equations at equilibrium ( $\dot{\mathbf{x}} = 0$ ) are written as follows.

$$0 = -F_L + AP_a - \alpha AP_b \quad (4-41)$$

$$0 = D_p \omega - Av_A \quad (4-42)$$

$$\alpha Av_A - D_p \omega = K_V (P_a - P_b - P_{op}) \sqrt{|P_b - P_c|} \text{sgn}(P_b - P_c) \quad (4-43)$$

From Eq. (4-42), the equilibrium velocity is found as

$$v_{eq} = \frac{D_p}{A} \omega \quad (4-44)$$

Inserting  $v_{eq}$  into Eq. (4-43) yields

$$-D_p(1 - \alpha)\omega = K_V (P_a - P_b - P_{op}) \sqrt{|P_b - P_c|} \text{sgn}(P_b - P_c) \quad (4-45)$$

During the retraction of the actuator, that is for negative pump speeds  $\omega < 0$ , the sign function  $sgn(P_b - P_c)$  in the flow continuity equation (4-45) must be positive. Inserting  $P_b > P_c$  into previously defined load pressure relation Eq. (4-40), one gets

$$p_{Leq} > (1 - \alpha)p_s + p_{op} = p_{L2} \quad (4-46)$$

Since  $P_{Leq} = P_{aeq} - \alpha P_{beq} \notin (P_{L1}, P_{L2})$ , the inequality in Eq. (4-46) proves that no actual equilibrium point exists in the critical load pressure region for the circuit scheme in which the accumulator line is connected to the rod side of the actuator during the retraction of the actuator.

#### 4.14.3 Proof of Proposition 3

During the extension of the actuator, the accumulator is connected to rod side chamber as shown in Figure 4-2-b. The shuttle valve position requires a cap side pressure as  $P_a > P_b + P_{op}$ . Furthermore, the deficient flow rate supplied by the accumulator, shown as  $Q_{c \rightarrow b}$  with a positive direction in Figure 4-2-, requires a rod side pressure as  $P_b < P_c$ . Therefore, the characteristic flow equation (4-5) is re-written as follows.

$$Q_{c \rightarrow b} = K_V (P_a - P_b - P_{op}) \sqrt{P_c - P_b} \quad (4-47)$$

The shuttle valve flow rate  $Q_{c \rightarrow b}$  is defined by linearizing the Eq. (4-47) around an equilibrium point  $(P_{aeq}, P_{beq})$  as follows.

$$Q_{c \rightarrow b} = Q_{c \rightarrow b_{SS}} + K_1 \delta P_a - K_2 \delta P_b \quad (4-48)$$

where,

$$K_1 = \left. \frac{\partial Q_{c \rightarrow b}}{\partial P_a} \right|_{\substack{P_a = P_{aeq} \\ P_b = P_{beq}}} = K_V \sqrt{P_c - P_{beq}} \quad (4-49)$$

$$K_2 = -\left. \frac{\partial Q_{c \rightarrow b}}{\partial P_b} \right|_{\substack{P_a = P_{a_{eq}} \\ P_b = P_{b_{eq}}}} = K_V \frac{P_{a_{eq}} - P_{op} + 2P_c - 3P_{b_{eq}}}{2\sqrt{P_c - P_{b_{eq}}}} \quad (4-50)$$

Here,  $K_1$  gain is positive since  $P_c > P_{b_{eq}}$ . Furthermore,  $K_2 > K_1$ , since the condition for spool opening  $P_{a_{eq}} > P_{b_{eq}} + P_{op}$  yields  $P_{a_{eq}} - P_{op} + 2P_c - 3P_{b_{eq}} > 2(P_c - P_{b_{eq}})$ .

Neglecting the pump leakage terms and the actuator friction and further modifying the rod side flow continuity equation (4-9) with the additional shuttle valve flow rate term  $Q_{b \rightarrow c} = -Q_{c \rightarrow b}$  defined in Eq. (4-48), the state equations in terms of deviations in state variables can be written as follows.

$$\delta F_L = -m\delta \dot{v}_A + A\delta P_a - \alpha A\delta P_b \quad (4-51)$$

$$C\delta \dot{P}_a = D_p\delta\omega - A\delta v_A \quad (4-52)$$

$$C\delta \dot{P}_b = \alpha A\delta v_A - D_p\delta\omega + (K_1\delta P_a - K_2\delta P_b) \quad (4-53)$$

The characteristic polynomial is derived as follows.

$$C^2m s^3 + CmK_2s^2 + A^2C(1 + \alpha^2)s + A^2(K_2 - \alpha K_1) \quad (4-54)$$

Since  $K_2 > K_1 > 0$  and  $\alpha \in (0,1)$ , all coefficients of characteristic equation are positive and  $(CmK_2)A^2C(1 + \alpha^2) > (C^2m)A^2(K_2 - \alpha K_1)$  or simply  $\alpha K_2 > -K_1$ . Therefore, the system is asymptotically stable according to Routh stability criterion.

#### 4.14.4 Proof of Proposition 4

During the retraction of the actuator, the accumulator is connected to cap side chamber as shown in Figure 4-2-c. The shuttle valve position requires a rod side pressure as  $P_b > P_a + P_{op}$ . Furthermore, the excess flow rate returning to the accumulator, shown as  $Q_{a \rightarrow c}$  with a positive direction in Figure 4-2-c, requires a cap

side pressure as  $P_a > P_c$ . Therefore, the characteristic flow equation (4-5) is re-written as follows.

$$Q_{a \rightarrow b} = K_V (P_b - P_a - P_{op}) \sqrt{P_a - P_c} \quad (4-55)$$

The shuttle valve flow rate  $Q_{a \rightarrow c}$  is defined by linearizing the characteristic flow equation (4-5) around an equilibrium point  $(P_{aeq}, P_{beq})$  as

$$Q_{a \rightarrow c} = Q_{a \rightarrow c_{SS}} - K_1 \delta P_a + K_2 \delta P_b \quad (4-56)$$

where

$$K_1 = - \left. \frac{\partial Q_{a \rightarrow c}}{\partial P_a} \right|_{\substack{P_a = P_{aeq} \\ P_b = P_{beq}}} = -K_V \frac{P_{beq} - P_{op} + 2P_c - 3P_{aeq}}{2 \sqrt{P_{aeq} - P_c}} \quad (4-57)$$

$$K_2 = \left. \frac{\partial Q_{a \rightarrow c}}{\partial P_b} \right|_{\substack{P_a = P_{aeq} \\ P_b = P_{beq}}} = K_V \sqrt{P_{aeq} - P_c} \quad (4-58)$$

Here,  $K_2$  gain in Eq. (4-58) is positive since  $P_{aeq} > P_c$ .

Neglecting the pump leakage terms and the actuator friction and further modifying the cap side flow continuity equation (4-8) with the additional shuttle valve flow rate term  $Q_{a \rightarrow c}$  defined in Eq. (4-56), the state equations in terms of deviations in state variables can be written as follows.

$$\delta F_L = -m \delta \dot{v}_A + A \delta P_a - \alpha A \delta P_b \quad (4-59)$$

$$C \delta \dot{P}_a = D_p \delta \omega - A \delta v_A - (-K_1 \delta P_a + K_2 \delta P_b) \quad (4-60)$$

$$C \delta \dot{P}_b = -D_p \delta \omega + \alpha A \delta v_A \quad (4-61)$$

The characteristic polynomial is derived as follows.

$$C^2m s^3 - CmK_1s^2 + A^2C(1 + \alpha^2)s + \alpha A^2(K_2 - \alpha K_1) \quad (4-62)$$

According to Routh criterion, the necessary and sufficient conditions for asymptotic stability are;  $-K_1 > 0, K_2 > \alpha K_1$  and  $(-CmK_1)A^2C(1 + \alpha^2) > (C^2m)\alpha A^2(K_2 - \alpha K_1)$  or simply  $-K_1 > \alpha K_2$ . The last condition covers the remaining two, since  $K_2 > 0$  and  $\alpha \in (0,1)$ . Therefore, the condition for asymptotic stability reduces to  $-K_1 > \alpha K_2$ .

Using  $K_1$  and  $K_2$  definitions given in Eqs. (3-17) and (3-18) the condition for asymptotic stability in terms of equilibrium pressures is written as follows.

$$(P_{beq} - P_{aeq}) - P_{op} > 2(\alpha + 1)(P_{aeq} - P_c) \quad (4-63)$$

According to Eqs. (4-12) and (4-13), an equilibrium point in the critical load pressure region is defined as  $p_{Leq} = P_{aeq} - \alpha P_{beq} = P_c(1 - \alpha) + \Delta P_L$  where  $\Delta P_L \in (-\alpha P_{op}, P_{op})$ . Furthermore, the partially open shuttle valve position requires a rod side chamber pressure as  $P_{beq} = P_{aeq} + P_{op}^*$  where  $P_{op}^* \in (P_{op}, p_{max})$ . Here,  $p_{max}$  corresponds to chamber pressures difference required for the maximum orifice opening. By using these two relations, the equilibrium pressures are written as follows.

$$P_{aeq} = P_c + \frac{\alpha P_{op}^* + \Delta p}{1 - \alpha} \quad (4-64)$$

$$P_{beq} = P_c + \frac{P_{op}^* + \Delta p}{1 - \alpha} \quad (4-65)$$

Inserting these equilibrium pressures into the asymptotic stability condition Eq (4-63) yields,

$$(1 - \alpha)(P_{op}^* - P_{op}) > 2(\alpha + 1)(\alpha P_{op}^* + \Delta p) \quad (4-66)$$

The left and right hand sides of this inequality is positive since  $\alpha \in (0,1)$ ,  $P_{op}^* \in (P_{op}, P_{max})$  and  $\Delta p \in (-\alpha P_{op}, P_{op})$ . One can conclude that if the asymptotic stability condition is not satisfied for an equilibrium point with minimum value of  $\Delta p$ , then all remaining points in the whole critical load pressure region are not asymptotically stable. Therefore, inserting  $\Delta p = -\alpha P_{op}$  into Eq. (4-66) yields,

$$(1 - \alpha) > 2(\alpha + 1)\alpha \tag{4-67}$$

$$(\alpha - 0.28)(\alpha + 1.78) < 0$$

The inequality in Eq. (4-67) proves that an equilibrium point in the critical load pressure region is unstable if the actuator area ratio is  $\alpha > 0.28$ . The asymptotic stability of such a point is not guaranteed if  $\alpha < 0.28$  but depends on the values of  $P_{op}^* - P_{op}$  and  $\Delta p$ .

## CHAPTER 5

### DEVELOPMENT OF HYDRAULIC CIRCUIT SOLUTIONS

In the previous chapter a critical load pressure region, whose location and size are determined by accumulator and valve cracking pressures respectively, is defined. It is shown that the main reason of instability, reported in literature, is the closed centered shuttle valve. Therefore, use of an underlapped shuttle valve is proposed in order to obtain a stable operation region. In the experimental results it is shown that undesired pressure oscillations are eliminated. However, it is observed that, inside the critical load pressure region, the transformer ratio between pump speed input and the actuator speed output decreases at certain pressure intervals.

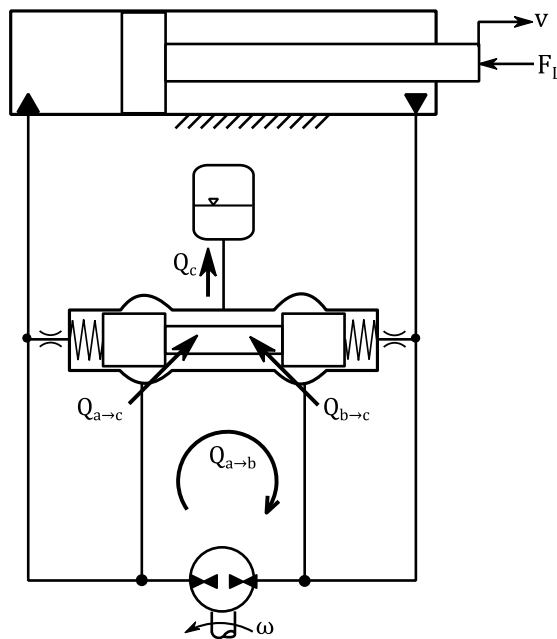


Figure 5-1 Representation of the circulating leakage flow rate

As shown in Figure 5-1, flow passage may occur between A-B ports, since both A-C and B-C conduits are open in an underlapped shuttle valve. The flow rate between A-B ports is named as “*circulating leakage flow*”. This undesired bypass flow, leads to

dead pump speeds, thus increases the loss of energy. Furthermore, it leads to a complicated control algorithm, since it is not possible to write a direct relationship between the pump drive speed and the actuator response. The mentioned leakage flow occurs only during the centered shuttle valve position. The centered spool corresponds to a pressure interval that is lower than the valve cracking pressure. Therefore, considering the whole operation region, the possible energy losses might not be seen as a problem.

In the previous chapter the critical load pressure region is investigated with regard to stability concerns and only a single point named as critical speed,  $v_{cr}$ , was considered in order to determine the minimum necessary spool underlap. However, in this part of the thesis the proposed underlapped shuttle valve solution is further analyzed in the whole critical load pressure region. The extent of dead pump speed and circulating leakage flow losses are investigated. Then a novel shuttle valve solution and circuit structure is proposed. It is aimed to eliminate the dead pump speed as well as increase the size of the stable operation region, (inside the critical load pressure region), achieved by the use of underlapped valve.

## 5.1 Simplified Kinematic Model

In this part of the thesis in order to investigate the effects of the shuttle valve spool structure on the system response, further simplifications are made. The inertial forces of the actuator mass and the compressibility of the hydraulic fluid is neglected in order to obtain a kinematic relation between pump speed and the actuator speed. The assumptions made at this part of the thesis are,

- the hydraulic fluid is incompressible,
- the actuator piston is massless,
- the pump, actuator and transmission lines are leak free,
- the actuator, pump, and transmission lines are frictionless,
- the pump is driven by an ideal velocity source,
- the hydraulic accumulator is an infinite capacitance,
- the shuttle valve spool is massless,

- the shuttle valve position is proportional to the difference of the chamber pressures,
- the shuttle valve discharge coefficient is constant for all spool positions,

By using the above first five assumptions, and using the direction definitions given in Figure 5-1, the previously defined , the equation of motion (3-1) and flow continuity equations (4-8) and (4-9) of the cap-side and rod-side chambers of the hydrostatic circuit, respectively, are re-written as follows.

$$F_L = (P_a - \alpha P_b)A \quad (5-1)$$

$$\omega D_p = Av_A + Q_{a \rightarrow c}(P_a, P_b, P_c) \quad (5-2)$$

$$\omega D_p = \alpha Av_A - Q_{b \rightarrow c}(P_a, P_b, P_c) \quad (5-3)$$

where,

$F_L$  = external load acting on the actuator, in  $N$

$P_a, P_b$  = cap-side and rod side chamber pressures, respectively, in  $MPa$

$A$  = cap-side piston area of the hydraulic actuator, in  $mm^2$

$\omega$  = pump drive speed, in  $rad/s$

$v_A$  = actuator velocity, in  $mm/s$

$D_p$  = pump displacement, in  $mm^3/rad$

$\alpha$  = ratio of piston areas of the rod side and the cap side of the actuator

$A$  = piston area of the cap-side actuator chamber

$Q_{a \rightarrow c}$  = flow through shuttle valve port A, in  $mm^3/s$

$Q_{b \rightarrow c}$  = flow through shuttle valve port B, in  $mm^3/s$

as defined previously.

The equations (5-1), (5-2), (5-3) constitutes the kinematic model of the EHA system. Physically the inputs of the system are the pump speed  $\omega$ , external load acting on the actuator,  $F_L$  and the accumulator pressure  $P_c$ . The outputs are the pressures of the each actuator chamber,  $P_a, P_b$ , together with the hydraulic actuator velocity,  $v_A$ . Consequently, the EHA system model has three input and three outputs, that can be solved with the above three equations.

Note that the accumulator is assumed to have infinite capacitance. Therefore, its pressure  $P_c$  can be considered as a constant parameter, instead of an input variable. The representation of the above three system equations are further simplified, if the accumulator pressure input  $P_c$ , is eliminated. For that reason, the chamber pressure values are defined relative to the accumulator pressure. Furthermore, instead of using the external load  $F_L$  as the input variable, the load pressure,  $P_L$ , previously defined in Eq. (4-10) is considered as the input of the system. The new relative pressure variables are defined as follows.

$$\Delta P_a = P_a - P_c \quad (5-4)$$

$$\Delta P_b = P_b - P_c \quad (5-5)$$

$$\Delta P_L = P_L - P_{Lcr} \quad (5-6)$$

where,  $P_{Lcr} = (1 - \alpha)P_c$ , is the critical load pressure previously defined in Eq. (4-11).

The system equations are re-written by utilizing the new state definitions. Furthermore, in order to eliminate  $\omega - v_A$  coupling, the Eq. (5-3) is subtracted from the Eq. (5-2) and actuator speed is represented in terms of shuttle valve flow rates only. Similarly, the Eq. (5-2) is multiplied by  $\alpha$  and subtracted from Eq. (5-3) in order to represent the pump speed as a function of valve flow rates only. The new system equations are as follows.

$$\Delta P_L = \Delta P_a - \alpha \Delta P_b \quad (5-7)$$

$$-(1 - \alpha)Av_A = Q_{a \rightarrow c}(\Delta P_{ab}, \Delta P_a) + Q_{b \rightarrow c}(\Delta P_{ab}, \Delta P_b) \quad (5-8)$$

$$-(1 - \alpha)D_p \omega = \alpha Q_{a \rightarrow c}(\Delta P_{ab}, \Delta P_a) + Q_{b \rightarrow c}(\Delta P_{ab}, \Delta P_b) \quad (5-9)$$

where,  $\Delta P_{ab} = P_a - P_b$  is the difference of the chamber pressures, i.e. is equal to the shuttle valve pilot pressure, and can also be represented as follows.

$$\Delta P_{ab} = \Delta P_{ac} - \Delta P_{bc} \quad (5-10)$$

In the new system representation the two inputs (knowns) are the pump speed  $\omega$  and relative load pressure  $\Delta P_L$ . The four outputs (unknowns) are the actuator speed  $v_A$ , chamber pressure variations w.r.t accumulator pressure  $\Delta P_{ac}$ ,  $\Delta P_{bc}$  and the pilot pressure  $\Delta P_{ab}$  as defined by Eq. (5-10).

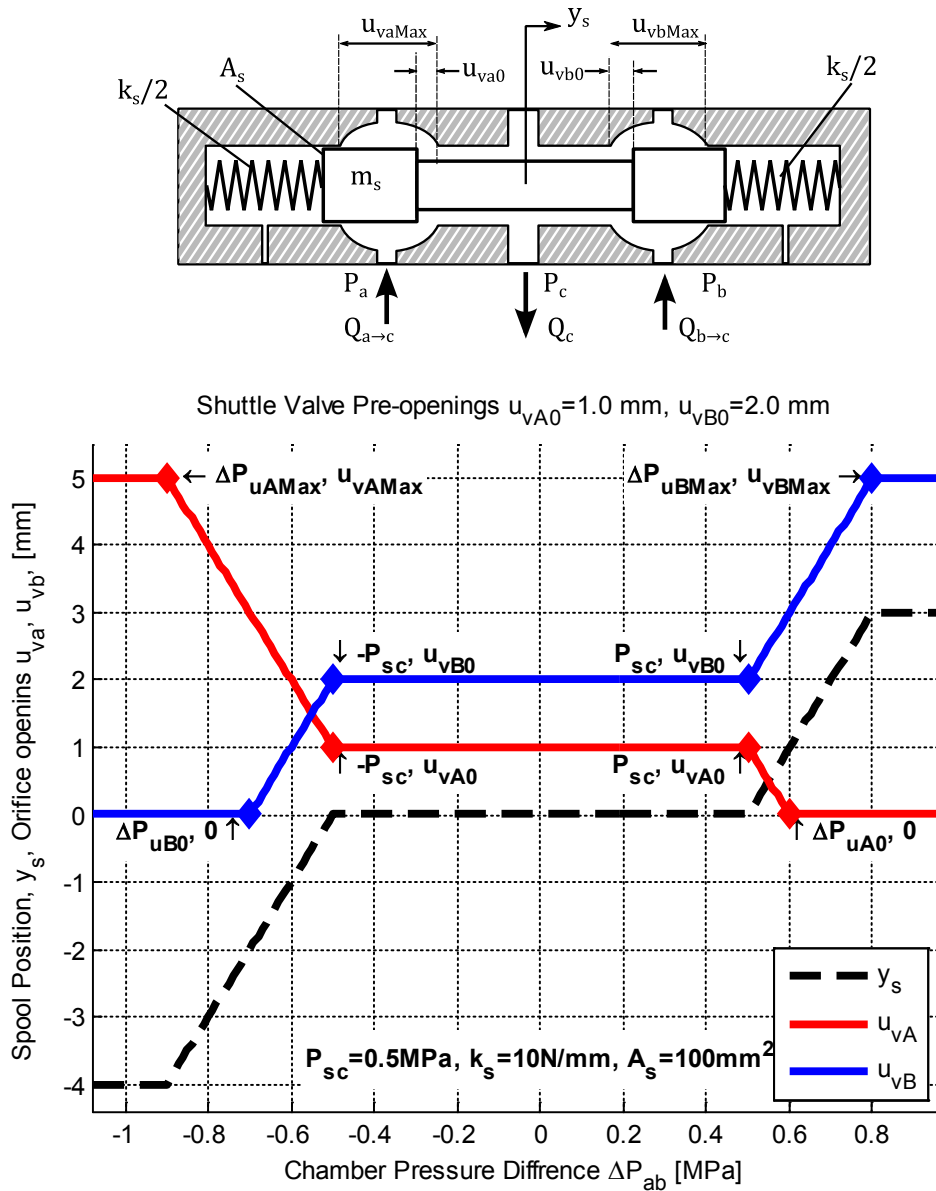


Figure 5-2 Orifice openings vs pilot pressure of an arbitrary shuttle valve with spool underlap

The shuttle valve flow rates  $Q_{a\rightarrow c}$  and  $Q_{b\rightarrow c}$ , are functions of  $\Delta P_a$  and  $\Delta P_b$ , respectively. Furthermore, since the orifice area is determined by the orifice opening, the flow rates are also functions of  $\Delta P_{ab}$ .

### 5.1.1 Calculation of Orifice Opening

The shuttle valve flow rates  $Q_{a \rightarrow c}$  and  $Q_{b \rightarrow c}$  are determined by the opening of each metering orifice,  $u_{va}$  and  $u_{vb}$ , which are functions of pilot pressure  $\Delta P_{ab}$ . The orifice openings are represented in Figure 5-2 for an arbitrary shuttle valve spool structure. Note that, the orifice opening values are constant and are not a function of  $\Delta P_{ab}$ , when the valve is centered or fully opened. Therefore, besides the shuttle valve cracking pressure  $P_{sc}$ , two more constants  $\Delta P_{uA_{Max}}$  and  $\Delta P_{uB_{Max}}$  are defined as shown in Figure 5-2.

According to the direction definitions, given in Figure 5-2, The constant  $\Delta P_{uA_{Max}}$  represents the pilot pressure  $\Delta P_{ab}$ , below which the orifice at port A is fully opened,  $u_{va} = u_{va_{Max}}$ . Similarly the constant  $\Delta P_{uB_{Max}}$  represents the pilot pressure  $\Delta P_{ab}$ , above which the orifice at port B is fully opened,  $u_{vb} = u_{vb_{Max}}$ . These two constants are defined as follows.

$$\Delta P_{uA_{Max}} = - \left( P_{sc} + (u_{vA_{Max}} - u_{vA_0}) \frac{k_s}{A_s} \right) \quad (5-11)$$

$$\Delta P_{uB_{Max}} = P_{sc} + (u_{vB_{Max}} - u_{vB_0}) \frac{k_s}{A_s} \quad (5-12)$$

where,

$A_s$  = pressure-sensitive area of the shuttle valve spool, in  $mm^2$

$k_s$  = valve spring stiffness, in  $N/mm$

According to the direction definitions, given in Figure 5-2, the constant  $\Delta P_{uA_0}$  represents the pilot pressure  $\Delta P_{ab}$ , above which the orifice opening at port A is zero,  $u_{va} = 0$ . Similarly the constant  $\Delta P_{uB_0}$  represents the pilot pressure, below which the orifice opening at port B is zero. These two constants are defined as follows.

$$\Delta P_{uA_0} = P_{sc} \cdot \text{sign}(u_{vA_0}) + u_{vA_0} \frac{k_s}{A_s} \quad (5-13)$$

$$\Delta P_{uB_0} = -P_{sc} \cdot \text{sign}(u_{vB_0}) - u_{vB_0} \frac{k_s}{A_s} \quad (5-14)$$

Note that the above four constants, defined by Eq. (5-11) though (5-14), are general and are valid for all possible valve spool structures.

The orifice openings are constant and are equal to either zero or their underlapped values, when the pressure difference is smaller than the cracking pressure. Furthermore, if the pressure difference is higher than its maximum value the orifice openings are again constant. These two conditions are defined as follows.

$$u_{va} = \begin{cases} u_{vA_0} h(u_{vA_0}) & |\Delta P_{ab}| \leq P_{sc} \\ u_{vA_{Max}} & \Delta P_{ab} \leq \Delta P_{uA_{Max}} \end{cases} \quad (5-15)$$

$$u_{vb} = \begin{cases} u_{vB_0} h(u_{vB_0}) & |\Delta P_{ab}| \leq P_{sc} \\ u_{vB_{Max}} & \Delta P_{ab} \geq \Delta P_{uB_{Max}} \end{cases} \quad (5-16)$$

where,  $h(\cdot)$  is the Heaviside step function meaning that  $u_v = 0$ , if the spool has negative pre-opening or overlap.

Outside the regions defined in Eq.(5-15) and (5-16), i.e. when  $\Delta P_{ab} \in (\Delta P_{uA_{Max}}, \Delta P_{uB_{Max}})$  and  $\Delta P_{ab} \notin (-P_{sc}, P_{sc})$ , the orifice openings  $u_{va}$  and  $u_{vb}$  are proportional to pilot pressure  $\Delta P_{ab}$ , and are defined as follows.

$$u_{va} = u_{vA_0} - (\Delta P_{ab} - P_{sc} \text{sgn}(\Delta P_{ab})) \frac{A_s}{k_s} \quad (5-17)$$

$$u_{vb} = u_{vB_0} + (\Delta P_{ab} - P_{sc} \text{sgn}(\Delta P_{ab})) \frac{A_s}{k_s} \quad (5-18)$$

If an underlapped valve with positive pre-opening  $u_{vB_0} > 0$ , is utilized, the Eq. (5-18) is valid inside the regions  $\Delta P_{ab} \in (P_{sc}, \Delta P_{uB_{Max}})$  and  $\Delta P_{ab} \in (\Delta P_{uB_0}, -P_{sc})$ . Note in Eq. (5-18) the sign of the  $P_{sc}$  term changes inside the region  $\Delta P_{ab} \in (\Delta P_{uB_0}, -P_{sc})$ , since  $\text{sgn}(\Delta P_{ab})$  is negative. On the other hand if there is an overlap meaning negative pre-opening,  $u_{vB_0} < 0$ , the equation is valid only inside the region  $\Delta P_{ab} \in (\Delta P_{uB_0}, \Delta P_{uB_{Max}})$ , where  $\Delta P_{uB_0} > P_{sc}$  since  $u_{vB_0}$  is negative. This region is shown in Figure 5 3. For overlapped spool case, there is no need to write  $\text{sgn}(\Delta P_{ab})$  since it is always positive for  $\Delta P_{ab} \in (\Delta P_{uB_0}, \Delta P_{uB_{Max}})$ .

The similar comments are valid for the port A. If an underlapped valve is utilized, the Eq. (5-17) is utilized inside the regions,  $\Delta P_{ab} \in (\Delta P_{uAMax}, -P_{sc})$  and  $\Delta P_{ab} \in (-P_{sc}, \Delta P_{uA0})$ . The sign of the  $P_{sc}$  term is positive for  $\Delta P_{ab} \in (\Delta P_{uAMax}, -P_{sc})$  and is negative for  $\Delta P_{ab} \in (-P_{sc}, \Delta P_{uA0})$ . On the other hand if there is a spool overlap, meaning  $u_{vA0} < 0$  the equation is valid only for  $\Delta P_{ab} \in (\Delta P_{uAMax}, \Delta P_{uA0})$ , as shown in Figure 5-3.

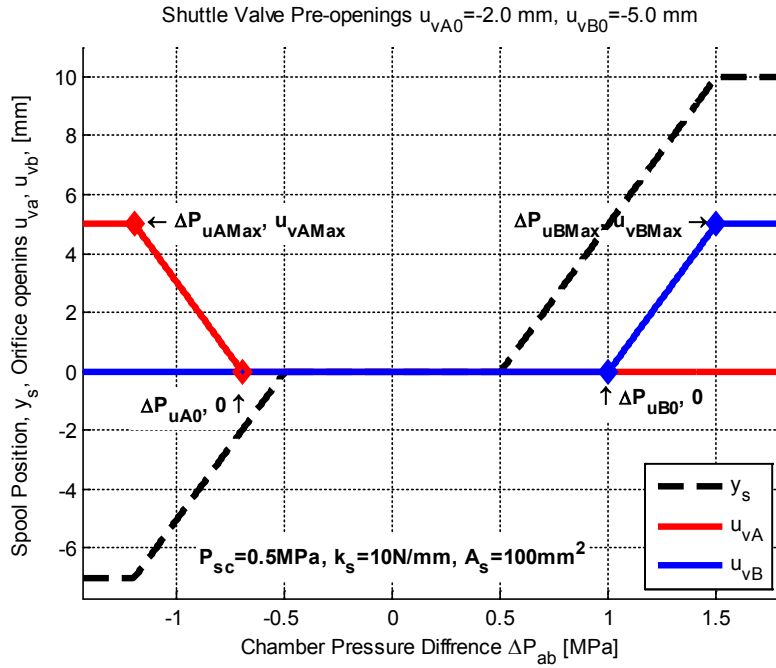


Figure 5-3 Orifice openings vs pilot pressure of an arbitrary shuttle valve with spool overlap

### 5.1.2 Calculation of Orifice Area

In the previous chapter, in order to simplify the equations and focus on stability, the orifice area and the orifice opening is assumed to be proportional. However, as mentioned in Section 3.2.3, the orifice area is created by a number of holes drilled on the valve sleeve, and has a non-linear relation between spool position. In this section this non-linear relation is considered in the kinematic model, and further in linearization. For completeness the orifice area equations (3-25) to (3-27) defined previously are re-written as follows.

$$A_v(u_v) = n_h \frac{1}{2} r_h^2 (2\theta_v - \sin(2\theta_v)) \quad (5-19)$$

where,

$$\theta_v = \text{atan2} \left( \sqrt{r_h^2 - |r_h - u_v|^2}, (r_h - u_v) \right) \quad (5-20)$$

and  $u_v$  is the orifice opening of the related port, either  $u_{va}$  or  $u_{vb}$ , the  $r_h$  and the  $n_h$  are the radius and number of holes on the related port respectively. The orifice area equation is valid for all orifice openings  $u_v \in [0, u_{vMax}]$  defined previously by Eqs. (5-15) to (5-18).

Knowing the orifice area, the shuttle valve flow rates can be calculated as follows.

$$Q_{a \rightarrow c} = G_{va}(\Delta P_{ab}) \sqrt{|\Delta P_a|} \text{sgn}(\Delta P_a) \quad (5-21)$$

$$Q_{b \rightarrow c} = G_{vb}(\Delta P_{ab}) \sqrt{|\Delta P_b|} \text{sgn}(\Delta P_b) \quad (5-22)$$

where, the hydraulic conductance  $G_{va}$  and  $G_{vb}$  are defined as follows.

$$G_{va}(\Delta P_{ab}) = C_d \sqrt{\frac{2}{\rho}} A_{va}(\Delta P_{ab}) \quad (5-23)$$

$$G_{vb}(\Delta P_{ab}) = C_d \sqrt{\frac{2}{\rho}} A_{vb}(\Delta P_{ab}) \quad (5-24)$$

## 5.2 Transformer Ratio and Dead Pump Speed

The term “*transformer ratio*” (TR) is a gain and is defined to construct a direct relationship between the hydraulic actuator and the pump drive speed. If all the flow losses in the hydraulic system are neglected, the TR corresponds to the dc gain or velocity constant of the forward transfer function between the hydraulic actuator and the pump drive speed. The TR of the EHA is the ratio of the actuator speed to pump drive speed as defined as in Eq. (5-25). Note that by using mechanical system analogy, the transformer ratio can also be considered as the inverse of the *gear ratio*.

$$TR = \frac{v_A}{\omega} \quad (5-25)$$

The mathematical representation of the transformer ratio, in terms of system parameters, can be found by taking the ratio of actuator speed equation as defined in Eq. (5-8) to pump drive speed equation as defined in Eq. (5-9). The resulting TR is find as follows.

$$TR = \frac{v_A}{\omega} = \frac{D_p}{A} \cdot \frac{Q_{a \rightarrow c} + Q_{b \rightarrow c}}{\alpha Q_{a \rightarrow c} + Q_{b \rightarrow c}} \quad (5-26)$$

Note that Eq. (5-26) is simplified, when one of the flow terms, either  $Q_{a \rightarrow c}$  or  $Q_{b \rightarrow c}$ , is zero, then the remaining is the function of pressure drop across the orifice only. This condition is satisfied for the fully opened cases.

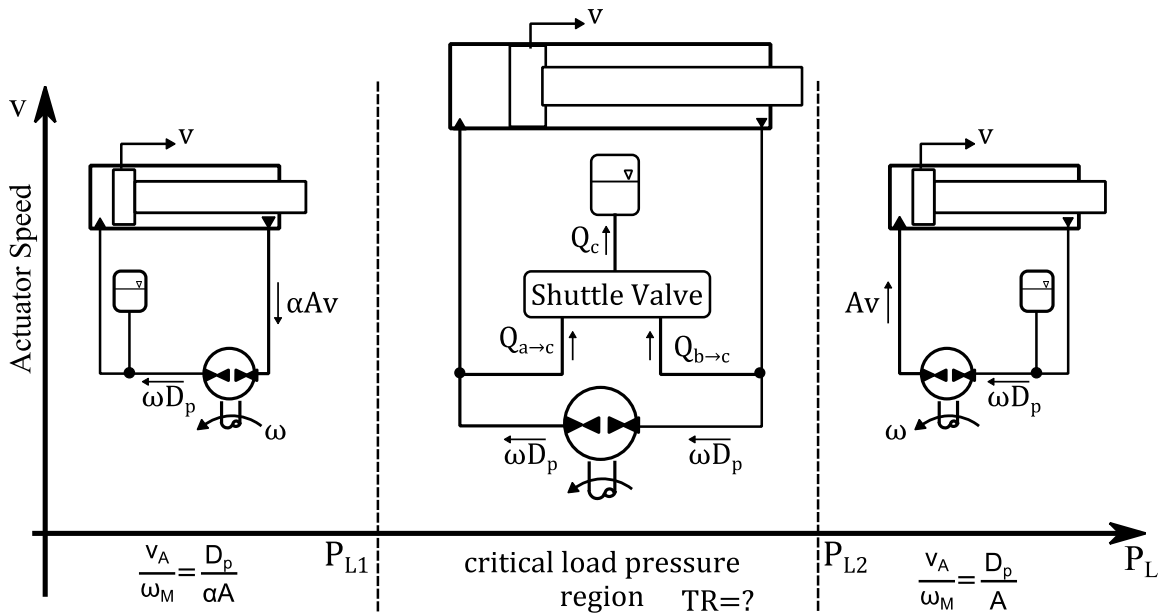


Figure 5-4 Transformer ratio in load pressure versus actuator velocity plane

In Figure 5-4, in the right most region of the  $P_L - v_A$  plane, the shuttle valve is fully opened to right, connecting the rod-side chamber to the accumulator line. The  $Q_{a \rightarrow c}$  term in Eq. (5-26) is zero. Furthermore, since the spool is saturated, the orifice area is at its maximum  $A_{vb} = A_{vb_{Max}}$  and the hydraulic conductance is constant. Therefore, the flow rate is the function of pressure drop only,  $Q_{b \rightarrow c} = G_{b_{Max}} \sqrt{\Delta P_b}$ .

Consequently, for the fully opened shuttle valve case,  $\Delta P_{ab} \geq \Delta P_{uB_{Max}}$  the transformer ratio is defined as follows.

$$TR|_{\substack{P_L > p_{L1} \\ \Delta P_{ab} \geq \Delta P_{uB_{Max}}} = \frac{D_p}{A} \quad (5-27)$$

Similarly, in the left most region of the  $P_L - v_A$  plane, the shuttle valve is fully opened to left. In Eq. (5-26) and the flow rate  $Q_{b \rightarrow c} = 0$ , and the flow rate  $Q_{a \rightarrow c} = G_{a_{Max}} \sqrt{\Delta P_a}$  with it maximum hydraulic conductance. Therefore, the transformer ratio for  $\Delta P_{ab} \leq \Delta P_{uA_{Max}}$  is defined as follows.

$$TR|_{\substack{P_L < p_{L1} \\ \Delta P_{ab} \leq \Delta P_{uA_{Max}}} = \frac{D_p}{\alpha A} \quad (5-28)$$

Inside the critical load pressure region,  $\Delta P_{ab} \in (\Delta P_{uA_{Max}}, \Delta P_{uB_{Max}})$ , the shuttle valve is not fully opened, i.e., either centered or partially opened. The orifice openings at the two ports of the valve provide a flow passage between the two chambers and the accumulator. Therefore, in Eq. (5-26) none of the flow terms,  $Q_{a \rightarrow c}$  and  $Q_{b \rightarrow c}$ , vanishes. Furthermore, the hydraulic conductance is also varying if the spool is not centered. Inside this region it is not possible to define the actuator speed by considering the piston area of only one chamber. However, Eq. (5-26) still reveals some conclusions.

In Eq. (5-26) since, the area ratio is smaller than unity  $\alpha \in (0,1)$ , it can be concluded that the transformer ratio TR, is in between its maximum and minimum values  $TR \in \left(\frac{D_p}{A}, \frac{D_p}{\alpha A}\right)$ , when both flow terms,  $Q_{a \rightarrow c}$  and  $Q_{b \rightarrow c}$ , have the same sign. However if the flow terms have different signs then the transformer ratio is higher/lower than its maximum/minimum values.

**Table 5-1 Parameters of the kinematic EHA model**

Actuator and pump parameters			
$A$	cap-side piston area of the actuator	2827.4	$mm^2$
$\alpha$	Area ratio	0.75	
$D_p$	Hydraulic pump displacement	$8e3/(2\pi)$	$mm^3/rad$
Calculated parameters			
$D_p/\alpha A$	Maximum transformer ratio	0.6	$mm/rad$
$D_p/A$	Minimum transformer ratio	0.45	$mm/rad$

The variation of transformer ratio inside the critical load pressure region is illustrated in Figure 5-5. An underlapped shuttle valve, Parker K04F3, is used to draw the actuator speed versus load pressure curve. the properties of the EHA are given in and the properties of the underlapped valve are given in Table 5-2. The shuttle valve spool has 0.3 mm underlap and 3.2 mm maximum opening. The orifice area at center position corresponds to 4.7% of the maximum orifice area.

**Table 5-2 Underlapped shuttle valve parameters**

Shuttle valve design parameters			
$u_{va_0}, u_{vb_0}$	Spool pre-openings	0.3, 0.3	$mm$
$P_{sc}$	Cracking pressure	0.5	$MPa$
$k_s$	Spring stiffness is	5	$N/mm$
$A_s$	Pilot area, in	100	$mm^2$
$n_h$	Number of holes on valve sleeve	8	
$r_h$	Hole radius	1.6	$mm$
$C_d$	Flow coefficient	0.325	
$\rho$	Hydraulic fluid density	850	$kg/m^3$
Calculated parameters			
$u_{vaMax}, u_{vbMax}$	Maximum opening,	3.2	$mm$
$A_{va_0}, A_{vb_0}$	Initial orifice area	3.04	$mm^2$
$A_{vaMax}, A_{vbMax}$	Maximum orifice area	64.34	$mm^2$
$G_{a0}, G_{b0}$	Hydraulic conductance at center	$4.8 \cdot 10^4$	$mm^3/\sqrt{MPa}$

The solid black line in Figure 5-5, is the actuator velocity corresponding to load pressures  $\Delta P_L \in (-\alpha P_{sc}, P_{sc})$ . The actuator velocity is calculated by using the

Eq.(5-8). Note that, the actuator velocity is drawn for an arbitrary pressure difference value  $\Delta P_{ab} = -0.2 \text{ MPa}$ . The corresponding actuator pressures are found by using the relations defined in Eqs. (5-4) to (5-6), and Eq. (5-10) as follows.

$$\Delta P_a = \frac{\Delta P_L - \alpha \Delta P_{ab}}{(1 - \alpha)} \quad (5-29)$$

$$\Delta P_b = \frac{\Delta P_L - \Delta P_{ab}}{(1 - \alpha)} \quad (5-30)$$

The dashed blue line, and dashed red lines shown in Figure 5-5, represents the ideal actuator velocities corresponding to maximum and minimum transformer ratios. First the pump speed  $\omega$  is calculated by Eq. (5-9), then by multiplying it with the maximum transformer ratio  $D_p/\alpha A$ , dashed red line is drawn, and by multiplying it with minimum transformer ratio  $D_p/A$  dashed blue line is drawn. The remaining dashed dotted straight lines represents the chamber pressures w.r.t accumulator pressure,  $\Delta P_a$  and  $\Delta P_b$  and is found through Eqs. (5-29) and (5-30).

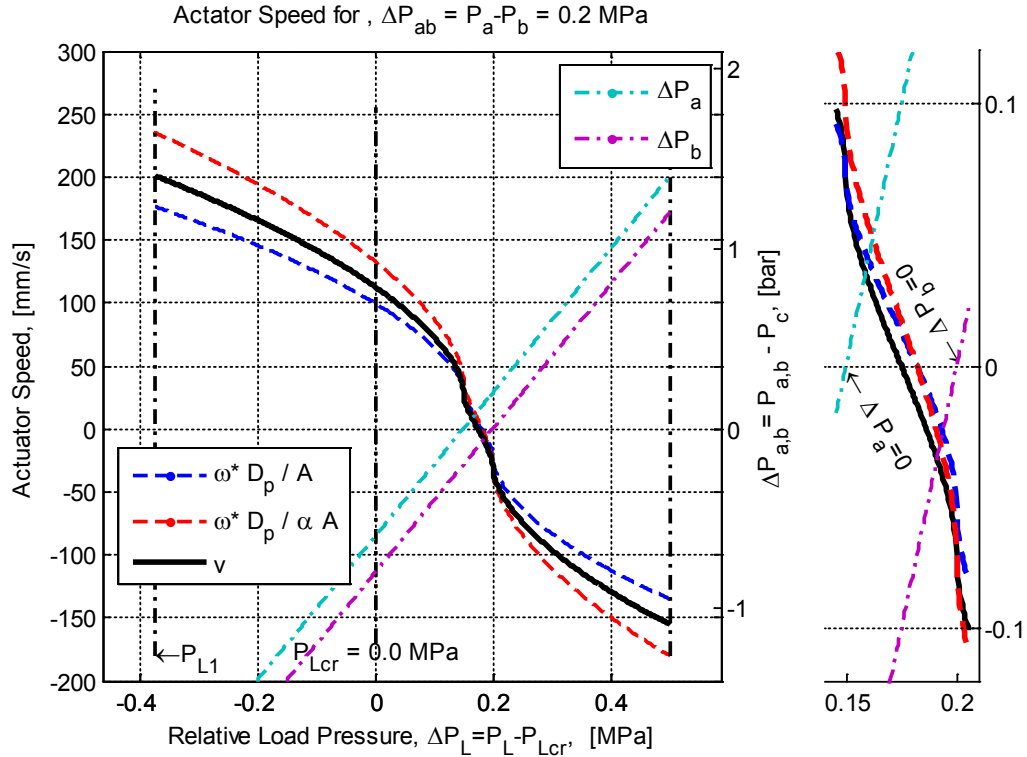


Figure 5-5 Actuator velocity vs. load pressure, with pilot pressure 0.2 MPa

In Figure 5-5, the y-axis at the right side is the relative chamber pressures  $\Delta P_a$  and  $\Delta P_b$ . The cap-side and rod-side chamber pressures are higher than accumulator pressure, if both  $\Delta P_a$  and  $\Delta P_b$  are positive. Similarly, the chamber pressures are smaller than accumulator pressure if  $\Delta P_a, \Delta P_b < 0$ . Note that the actuator velocity, solid black line, is in between the maximum and minimum ideal actuator speeds, which are  $\omega D_p / \alpha A$  and  $\omega D_p / A$  respectively, when the chamber pressures are both positive or both negative. However, it is smaller than the two ideal speeds, in between the two straight lines, which corresponds to the region  $\Delta P_a > 0$  and  $\Delta P_b < 0$ , as shown in the detail view located at the right side of the figure.

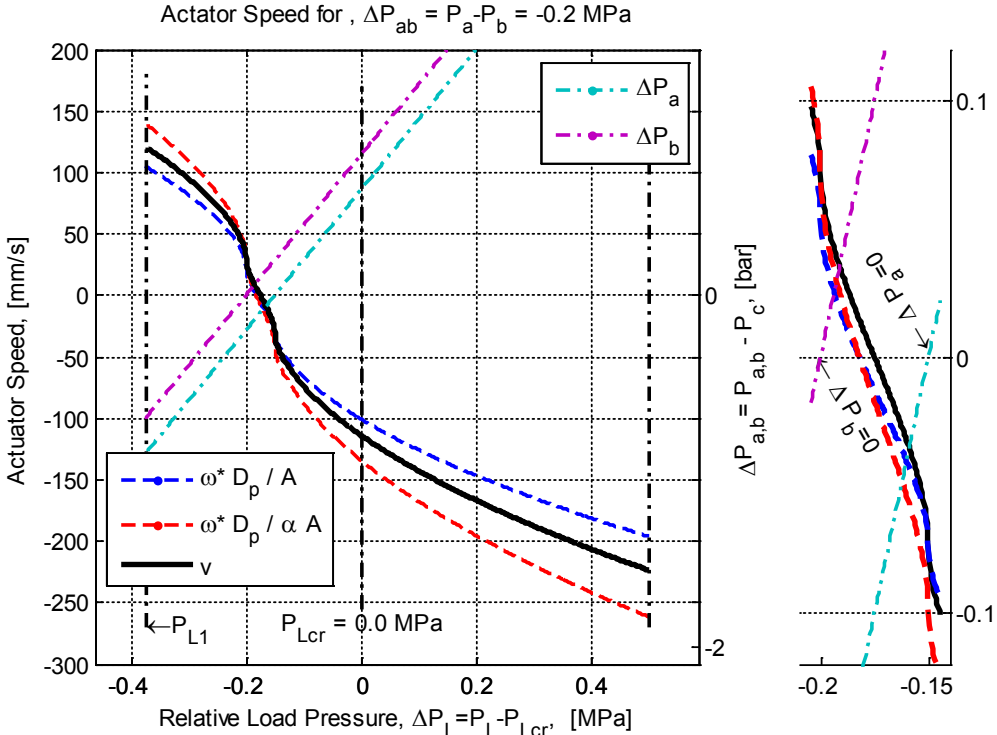


Figure 5-6 Actuator velocity vs. load pressure, with pilot pressure -0.2 MPa

A similar figure is obtained for negative pilot pressure. In Figure 5-6, the actuator velocity and pump speed is calculated for  $\Delta P_{ab} = -0.2 MPa$  and for  $\Delta P_L \in (-\alpha P_{sc}, P_{sc})$ . The actuator speed is in between the two ideal velocities, when both  $\Delta P_{ac}$  and  $\Delta P_{bc}$  have the same sign. On the other hand in between the two straight lines, relative rod side chamber pressure is positive,  $\Delta P_b > 0$ , while the cap-side is negative,  $\Delta P_a < 0$ . Different from, Figure 5-5, inside this region the actuator velocity is higher than the two ideal velocities,  $\omega D_p / \alpha A$  and  $\omega D_p / A$ .

The physical meaning of TR, defined for  $\Delta P_{ab} \in (\Delta P_{uA_{Max}}, \Delta P_{uB_{Max}})$ , can be easily understood if a closed volume around the shuttle valve is considered. The flow continuity requires that the input flow rate is equal to the output flow rate, which is defined as follows.

$$Q_{a \rightarrow c} + Q_{b \rightarrow c} = Q_c \quad (5-31)$$

According to the direction definitions given in Figure 5-1, the sign of the accumulator flow rate is the inverse of the actuator speed. During the actuator extension,  $v_A > 0$ , the deficient flow rate should be supplied by the accumulator,  $Q_c < 0$ , and during the retraction the excess flow rate should be returned to the actuator  $Q_c > 0$ . Furthermore, if the actuator is stationary  $v_A = 0$ , then there is no accumulator flow rate,  $Q_c = 0$ , since no differential flow rate is formed. However, zero actuator speed does not necessitates zero pump speed,  $\omega = 0$ . If the shuttle valve flow rates,  $Q_{a \rightarrow c}$  and  $Q_{b \rightarrow c}$ , have different signs. In such a case, the pump flow rate is defined as follows.

$$\omega_{dead} = \frac{Q_{a \rightarrow c}}{D_p} = -\frac{Q_{b \rightarrow c}}{D_p} \quad (5-32)$$

Equation, (5-32), is defined as the “*dead pump speed*”, although the actuator is stationary,  $v_A = 0$ , the pump rotates in order to compensate the circulating leakage flow rate. An open center shuttle valve with direct connection between A-B ports, can be considered as an extreme case, which is similar to a short circuit by electrical analogy. In this time, the actuator will be stationary whatever the pump speed is, therefore the transformer ratio, TR, will be infinite.

The transformer ratio  $v_A/\omega$  can be further illustrated on  $\Delta P_L$  vs TR plane, as given in Figure 5-7. Actuator speed, Eq. (5-8), and pump speed, Eq. (5-9), are calculated, for  $\Delta P_L \in [-1,1] MPa$  and for pilot pressure array  $\Delta P_{ab} = [-0.6, -0.5, -0.2, 0, 0.2, 0.4, 0.5]$ . Remembering that the cracking pressure of the shuttle valve is  $0.5 MPa$ , Figure 5-7, it is seen that for  $\Delta P_{ab} = \pm 0.6 MPa$ , the transformer ratio is constant irrespective of the  $\Delta P_L$  value. This is an expected result, since the shuttle valve is fully opened for  $|\Delta P_{ab}| > P_{sc} = 0.5 MPa$ . It is seen that the transformer

ratio is maximum,  $TR = D_p/\alpha A$ , thick solid blue line, for  $\Delta P_{ab} = -0.6 MPa$ , and is minimum  $TR = D_p/A$ , thick solid black line, for  $\Delta P_{ab} = 0.6 MPa$ . The transformer ratio is not constant for  $|\Delta P_{ab}| < 0.5 MPa$ , which corresponds to centered spool position. The TR's corresponding to that case are shown with dashed-line in the figure. It is seen that, the TR depends on the load pressure  $\Delta P_L$ . The TR is varying for some  $\Delta P_L$ , interval, which corresponds to critical  $\Delta P_L$  region. Inside the critical  $\Delta P_L$  region, the transformer ratio may go to zero or infinity. This is due to dead pump speed. In that region, since the chamber pressures w.r.t accumulator pressure have different signs, it is possible to have,  $Q_{a \rightarrow c} = -Q_{b \rightarrow c}$ , or  $\alpha Q_{a \rightarrow c} = -Q_{b \rightarrow c}$ , which makes Eq. (5-55) zero, or infinity respectively.

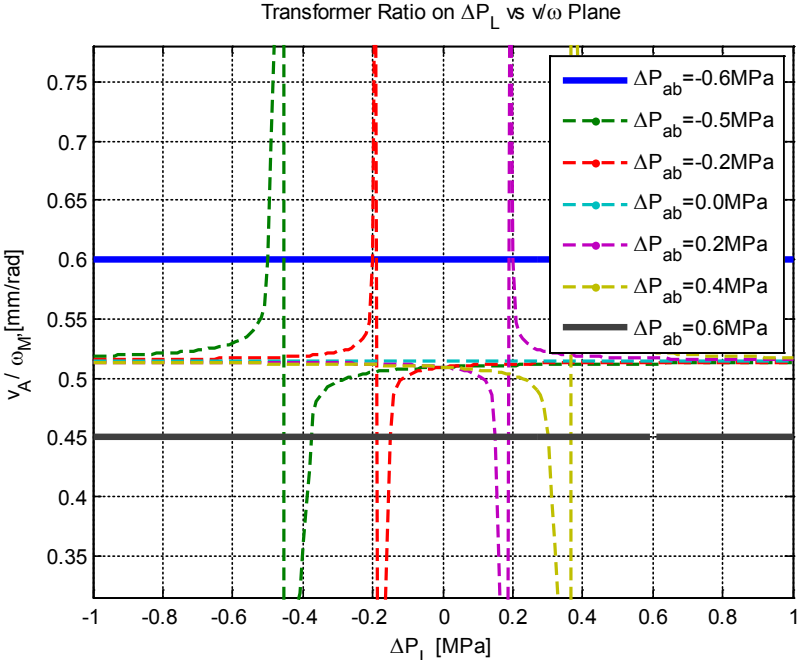


Figure 5-7 Transformer ratio versus load pressure

Although the TR vary between zero and infinity, its mean value converges to a constant ratio. This constant value corresponds to both negative and both positive relative chamber pressures,  $\Delta P_a$  and  $\Delta P_b$ . Since the shuttle valve flow rates,  $Q_{a \rightarrow c}$  and  $Q_{b \rightarrow c}$ , have the same sign, and the conductance of both metering orifices are equal, then the TR can be roughly found as follows.

$$TR \approx \frac{D_p}{A} \frac{2}{\alpha + 1} \quad (5-33)$$

The same conclusions can be made if the actuator speed, Eq. (5-8), and pump speed, Eq. (5-9), are calculated by varying  $\Delta P_{ab}$  for some constant  $\Delta P_L$ . This time the transformer ratio will be represented in  $\Delta P_{ab}$  vs TR plane as in Figure 5-8. It is seen that the TR is constant and independent of  $\Delta P_L$  above and below the cracking pressure of 0.5 MPa. When the shuttle valve is centered,  $|\Delta P_{ab}| < 0.5 \text{ MPa}$ , the mean value of TR is 0.515 mm/rad as defined by (5-33). The TR might go to infinity or zero only for  $|\Delta P_L| < 0.5 \text{ MPa}$ .

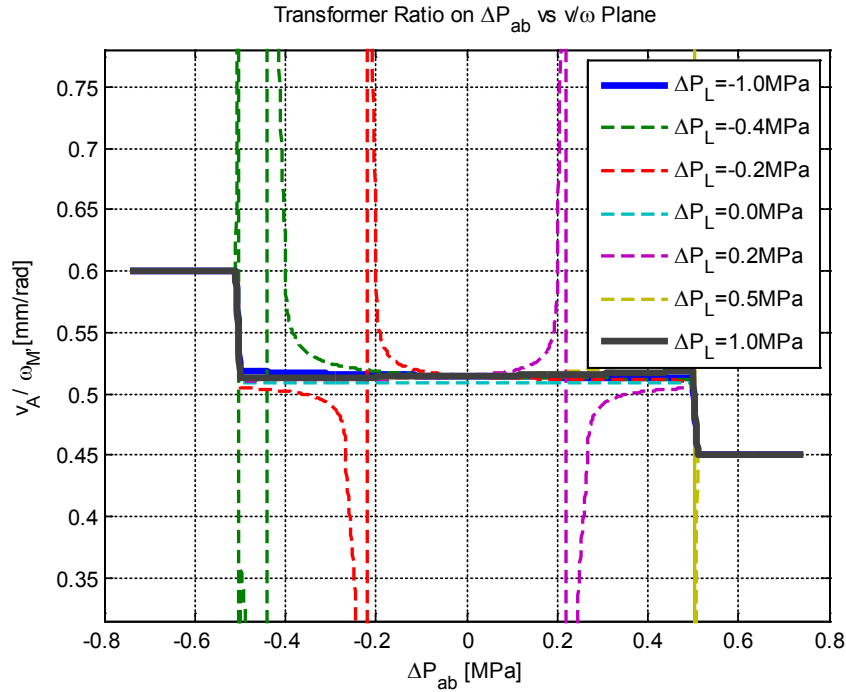


Figure 5-8 Transformer ratio versus pilot pressure

The variation of transformer ratio (TR) between zero and infinity may be problematic, in the closed loop control. It should be noted that if a shuttle valve with relatively big cracking pressure is selected, then the area of the critical load pressure region in  $P_L - v_A$  plane will increase. Since, a load loci is very probable to enter into this region, the dead pump speed has to be compensated in order to not to degrade the close loop performance, or this region have to be removed physically.

### 5.2.1 Circulating Leakage Flow Region

In this part the size of the shuttle valve leakage flow region is defined on the  $\Delta P_L - v_A$  plane. This region corresponds to the transformer ratio, lower than its minimum value or higher than its maximum value. Inside that region, circulating leakage flow rate occurs, i.e. pump rotates and creates a flow rate, but some of this flow rate circulates between the two chambers over the pre-openings of the underlapped valve as shown in Figure 5-1.

The circulating leakage flow rate in between the two chambers can only occur if the two metering orifices have some positive opening. There might be a conduit during the positioning of the spool from neutral position to end position. However, this pressure interval is relatively small when compared to the cracking pressure of the spool. For example, for the underlapped valve whose parameters are given in Table 5-2, the spool is centered for  $|\Delta P_{ab}| \leq 0.5 \text{ MPa}$ . This means that, throughout 1MPa pressure interval, there is a conduit in between the two actuator chambers through the valve pre-openings. On the other hand, during the positioning of the spool, from center to end position, the two chambers are connected to each other only for  $\Delta P_{ab} \in (-0.515, 0.5)$  and  $\Delta P_{ab} \in (0.5, 0.515)$ . Since the 0.03 MPa pressure interval is relatively small, w.r.t centered 1 MPa, it can be concluded that the size of the circulating leakage flow region is mainly determined by valve cracking pressure,  $P_{sc}$ . Therefore, the circulating leakage flow region is roughly defined by  $\Delta P_L \in (\alpha P_{sc}, P_{sc})$ .

If both  $\Delta P_a$  and  $\Delta P_b$  is greater/lower than zero, during the retraction/extension of the actuator, then no dead pump speed occurs. Dead pump speed occurs if one chamber pressure is greater than accumulator pressure while the other is lower. Therefore, the circulating leakage flow region can be drawn by considering zero relative chamber pressures.

In Figure 5-9, the circulating leakage flow region is shown on the  $\Delta P_L - v_A$  plane. This region is formed by drawing two actuator velocity curves that are calculated for  $\Delta P_a = 0 \text{ MPa}$  and for  $\Delta P_b = 0 \text{ MPa}$ . The shuttle valve and EHA parameters are taken from Table 5-1 and Table 5-2. The actuator velocities are calculated by using Eq.(5-8) for  $\Delta P_L \in (\alpha P_{sc}, P_{sc})$ . The solid red curve represents the actuator velocity

calculated for  $\Delta P_a = 0$ , the resulting rod side chamber pressure  $\Delta P_b = -\Delta P_L/\alpha$  is represented by dashed red line. Below the solid red curve, the cap side chamber pressure is higher  $\Delta P_a > 0$ , and above this curve it is lower  $\Delta P_a < 0$  than the accumulator pressure. Similarly, the solid blue curve is the actuator velocity calculated for  $\Delta P_b = 0$ , and the dashed blue line is the corresponding cap-side pressure variation  $\Delta P_a = \Delta P_L$ . Inside the region in between the solid curves, the relative chamber pressures have different signs, therefore, it is named as “*circulating leakage flow region*”. If the load loci of the EHA is passing through the critical load pressure region,  $\Delta P_L \in (\alpha P_{sc}, P_{sc})$ , then in between the velocity limits defined by the solid red and blue curves, the TR is lower and higher than its limits,  $TR > \frac{D_p}{\alpha A}$  or  $TR < \frac{D_p}{\alpha A}$ , i.e. the transformer ratio will vary between zero and infinity as shown in Figure 5-7 and Figure 5-8. However, if the actuator velocity is higher than these velocity limits, i.e. the load loci is not in between the two curves, then the transformer ratio will be close to the value  $TR \approx \frac{D_p}{A} \frac{2}{\alpha + 1}$  as defined by Eq. (5-33).

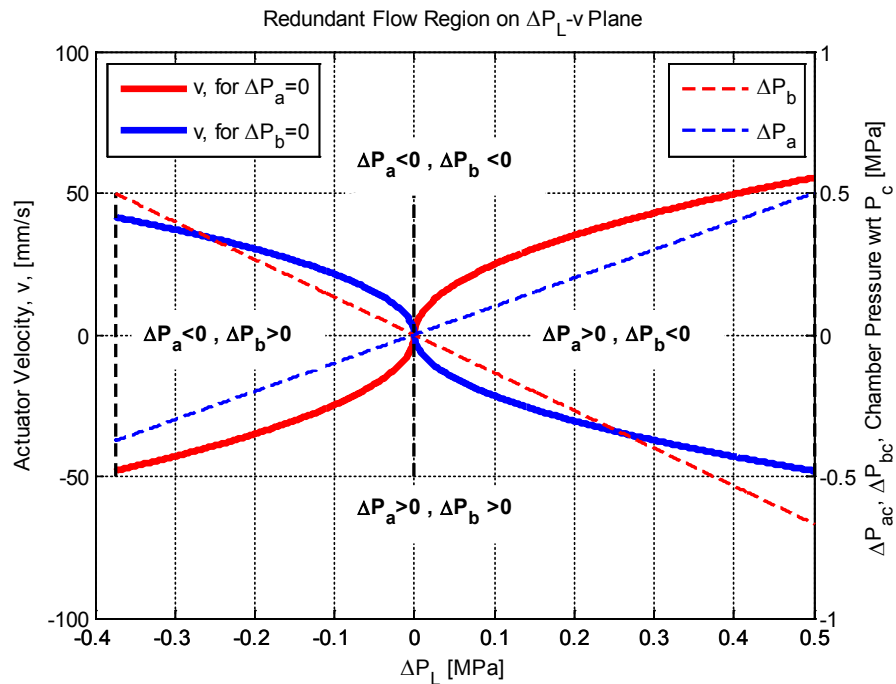


Figure 5-9 Circulating leakage flow region on  $\Delta P_L - v_A$  plane

Besides the valve cracking pressure which determines the size of the critical load pressure region  $\Delta P_L \in (\alpha P_{sc}, P_{sc})$ , the size of the circulating leakage flow region is closely related with the valve pre-openings, since it determines the hydraulic

conductance in Eq.(5-8). Increasing the hydraulic conductance,  $G_{va_0}$  and  $G_{vb_0}$ , increases the critical speed. The solid blue and red velocity curves are drawn for 0.3 mm spool underlapped as given in Table 5-2, and it is seen that inside the critical load pressure region, circulating leakage flows occurs up to  $\pm 50$  mm/s actuator velocity. This velocity limit will increase  $\pm 100$  mm/s if the spool underlapped is increased to 0.5 mm. Remembering from the previous chapter that, a stable operation region is achieved by providing spool underlap, there is a trade of between stability and circulating leakage flow rates. Therefore, the spool underlapped should be selected carefully.

### 5.2.2 Dead Pump Speed Required to Move the Actuator

The transformer ratio (TR), which is defined in Eq. (5-26), becomes zero when  $Q_{a \rightarrow c} = -Q_{b \rightarrow c}$ . Writing the shuttle valve flow equations,

$$G_{va} \sqrt{|\Delta P_a|} \text{sgn}(\Delta P_a) = -G_{vb} \sqrt{|\Delta P_b|} \text{sgn}(\Delta P_b) \quad (5-34)$$

The hydraulic conductance's  $G_{va} = G_{va_0}$  and  $G_{vb} = G_{vb_0}$ , are constant for the centered spool and determined by the pre-opening. Considering that the spool is symmetric and have equal pre-openings, the equality defined by Eq.(5-34) states that, dead pump speed occurs for  $\Delta P_{ac} = -\Delta P_{bc}$ .

Using the load pressure definition given, in Eq. (5-7), the chamber pressures w.r.t accumulator, are found as follows.

$$\Delta P_a = \frac{1}{1 + \alpha} \Delta P_L \quad (5-35)$$

$$\Delta P_b = -\frac{1}{1 + \alpha} \Delta P_L \quad (5-36)$$

The dead pump speed required to move the actuator inside the critical load pressure region can be found by calculating the shuttle valve flow rates as defined in the pump speed equation (5-9). The flow rates are calculated, for the centered shuttle valve

case, therefore the hydraulic conductance of each metering orifice is constant. Therefore, Eq. (5-9) reduces to the dead pump speed is defined as follows,

$$-(1 - \alpha)D_p\omega = \alpha G_{va_0}\sqrt{|\Delta P_a|}\text{sgn}(\Delta P_a) + G_{vb_0}\sqrt{|\Delta P_b|}\text{sgn}(\Delta P_b) \quad (5-37)$$

Considering the symmetric spool structure, therefore equal conductance  $G_{v_0} = G_{v_a} = G_{v_b}$ , and inserting the chamber pressures defined in Eqs. (5-35) and (5-36), the dead pump speed required to move the actuator for a given load pressure is found as follows.

$$\omega = \frac{G_{v_0}}{D_p} \sqrt{\left| \frac{1}{1 + \alpha} \Delta P_L \right|} \text{sgn}(\Delta P_L) \quad (5-38)$$

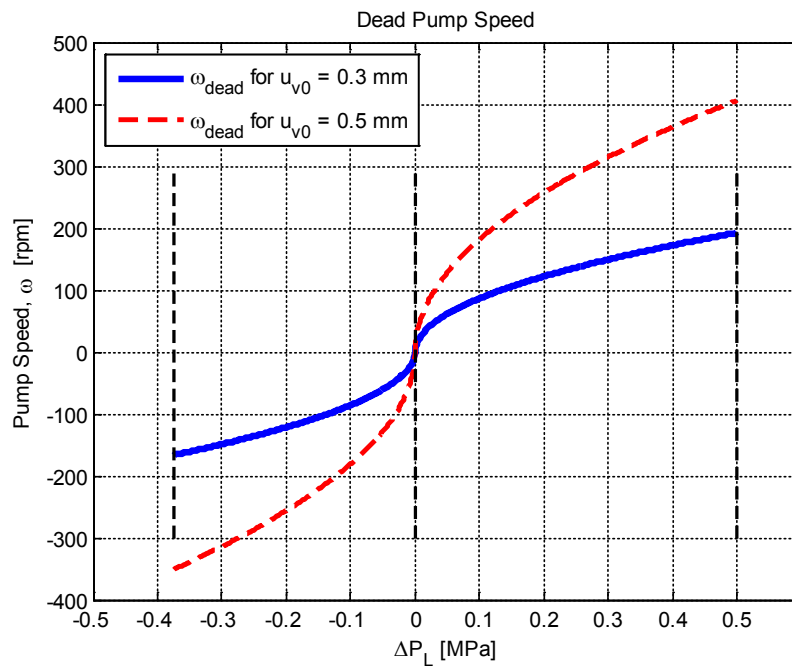


**Figure 5-10 Dead pump speeds formed inside the critical load pressure region**

The dead pump speed is illustrated in Figure 5-10, by using the EHA and shuttle valve parameters provided in Table 5-1 and Table 5-2 respectively. It is seen that, inside the critical load region, up to 200 rpm pump drive speed is necessary in order to hold the actuator at stationary position. The dead pump speed increases up to 400 rpm, if the spool underlapped is increased from 0.3 mm to 0.5 mm.

### 5.3 Inverse of the Kinematic Model

The kinematic model introduced in this chapter mainly consists of four equations. Two of these are the definitions of the relative load pressure,  $\Delta P_L$ , and pilot pressure,  $\Delta P_{ab}$ , variables, given in Eq. (5-7) and Eq. (5-10) respectively. The remaining two is the actuator speed  $v$ , and pump drive speed,  $\omega$ , equations, which are given in Eq.(5-8) and Eq.(5-9), respectively. The actuator and pump drive speeds are written in compact form, i.e. in terms of shuttle valve flow rates which are functions of relative chamber pressures  $\Delta P_a$ ,  $\Delta P_b$  and their difference  $\Delta P_{ab}$ .

In this part of the thesis it is aimed to calculate the pump drive speed  $\omega$ , for a desired actuator speed  $v_A$ . The pilot pressure  $\Delta P_{ab}$  is selected to be known input, since it is a measurable quantity with a differential pressure transducer. By this way the four unknown,  $\Delta P_a$ ,  $\Delta P_b$ ,  $\Delta P_L$ ,  $v_A$  can be solved by using the four equations.

Inserting, the shuttle valve flow terms  $Q_{a \rightarrow c}$  and  $Q_{b \rightarrow c}$ , defined in Eq. (5-21) and Eq. (5-22) respectively, into Eq. (5-8), the actuator velocity equation is re-written in explicit form as follows.

$$-(1 - \alpha)Av_A = G_{va}(\Delta P_{ab})\sqrt{|\Delta P_a|}sgn(\Delta P_a) + G_{vb}(\Delta P_{ab})\sqrt{|\Delta P_b|}sgn(\Delta P_b) \quad (5-39)$$

The hydraulic conductance's  $G_{va}$  and  $G_{vb}$ , in Eq.(5-39), are considered as the known parameters. Since the pilot pressure,  $\Delta P_{ab}$  is known, the related orifice openings,  $u_{va}$  and  $u_{vb}$  can be calculated by Eq.(5-17) and Eq. (5-18), then the corresponding orifice area can be calculated by Eq. (5-19), and finally the resulting conductance is found by Eq.(5-23) and Eq. (5-24). It should be noted that the hydraulic conductance calculation is made only for the partially opened valve case, i.e. for  $\Delta P_{ab} \in (\Delta P_{uA_{Max}}, \Delta P_{uB_{Max}})$  and  $\Delta P_{ab} \notin (-P_{sc}, P_{sc})$ . For the centered spool case,  $\Delta P_{ab} \in (-P_{sc}, P_{sc})$ , there is no-need to calculate the conductance since the spool is stationary  $G_{va} = G_{va_0}$  and  $G_{vb} = G_{vb_0}$ . Furthermore, for  $\Delta P_{ab} \leq \Delta P_{uA_{Max}}$  and  $\Delta P_{ab} \geq \Delta P_{uB_{Max}}$ , since the spool is fully opened there is no need to solve the velocity equation (5-39). The relation, between the pump speed and the actuator velocity is already defined by the transformer ratio equations (5-27) and (5-28).

Writing the cap-side chamber pressure in terms of relative rod-side pressure, i.e.  $\Delta P_a = \Delta P_{ab} + \Delta P_b$  the number of unknowns is reduced to one, which is rod-side relative chamber pressure  $\Delta P_b$ .

$$(-v_A) = K_{v1} \sqrt{|\Delta P_{ab} + \Delta P_b|} \text{sgn}(\Delta P_{ab} + \Delta P_b) + K_{v2} \sqrt{|\Delta P_b|} \text{sgn}(\Delta P_b) \quad (5-40)$$

where the coefficients  $K_{v1}$  and  $K_{v2}$  are treated as known parameters, since  $\Delta P_{ab}$  is known, and are defined as follows.

$$K_{v1} = \frac{G_{va}(\Delta P_{ab})}{(1 - \alpha)A} \quad (5-41)$$

$$K_{v2} = \frac{G_{vb}(\Delta P_{ab})}{(1 - \alpha)A} \quad (5-42)$$

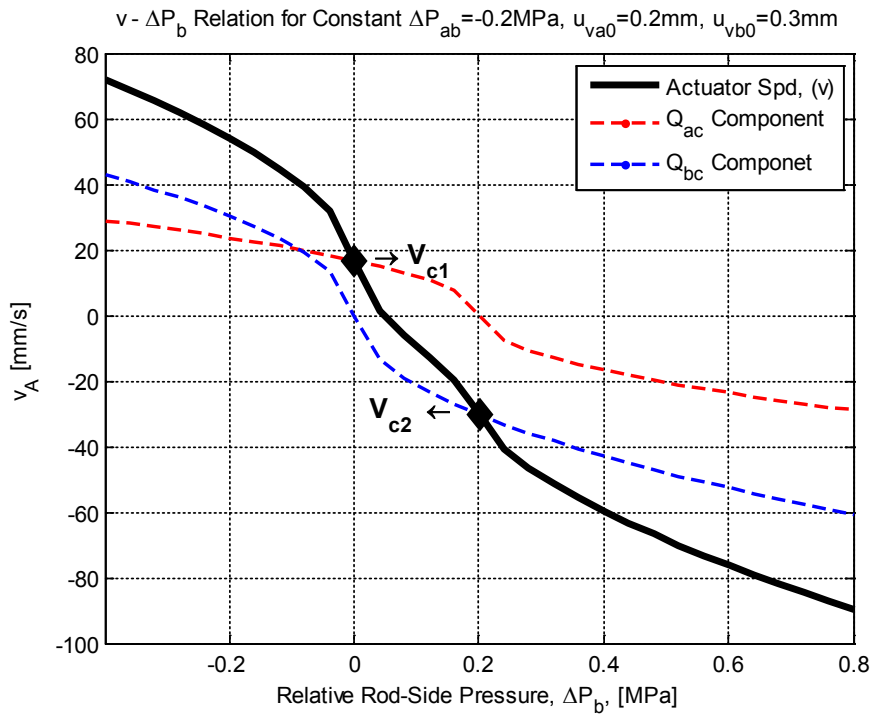


Figure 5-11 Relation between  $\Delta P_b$  and  $v_A$  for constant pilot pressure

The first term of Eq. (5-40) corresponds to  $Q_{a \rightarrow c}$  flow rate and the second term corresponds to  $Q_{b \rightarrow c}$  flow rate. Both the two flow rate terms are bijective, i.e. every single  $\Delta P_b$  defines a single unique  $v_A$ , and every single  $v_A$  corresponds a unique  $\Delta P_b$ . This condition is shown in Figure 5-11, where the dashed red and the dashed blues

corresponds to the first and second terms of the Eq. (5-40) respectively. The solid black curve is the sum of these two functions which corresponds to  $(-v_A)$ . Since the function between  $\Delta P_b$  and  $(-v_A)$  is bijective, its inverse exists to find  $\Delta P_b$  for the given  $v_A$ .

In order to handle the signs of the square root terms seen Eq. (5-40), two critical speed  $v_{c1} = v_A(\Delta P_b = 0)$  and  $v_{c2} = v_A(\Delta P_b = -\Delta P_{ab})$  are defined, above and below which the two sign terms becomes, positive and negative, respectively. As can be seen from the Figure 5-11, the critical velocity  $v_{c1}$  is calculated at  $\Delta P_b = 0$  MPa and corresponds to speed where the  $Q_{b \rightarrow c}$  term of Eq. (5-40) is zero. Similarly, the critical velocity  $v_{c2}$  is calculated for  $\Delta P_b = -\Delta P_{ab}$  which makes the  $Q_{a \rightarrow c}$  term of Eq. (5-40) is zero. Therefore, above and below these limits, the relative chamber pressures have the same signs, which is equal to  $sgn(-\Delta P_{ab})$  and  $sgn(\Delta P_{ab})$ , respectively. If the desired speed is in between these two limits,  $v_A \in (v_{c1}, v_{c2})$  then the signs of the relative chamber pressures  $\Delta P_a$  and  $\Delta P_b$  are equal to  $sgn(\Delta P_{ab})$  and  $sgn(-\Delta P_{ab})$  respectively. Then the resulting velocity equation is re-written as follows.

$$(-v_A) = K_{v1} \sqrt{\text{Cond}_A(\Delta P_{ab} + \Delta P_b)} \text{Cond}_A + K_{v2} \sqrt{\text{Cond}_B \Delta P_b} \text{Cond}_B \quad (5-43)$$

where, the sign conditions are defined as follows

$$\text{Cond}_B = \begin{cases} sgn(-v_A) & \text{for } v_A \notin (v_{c1}, v_{c2}) \\ -sgn(\Delta P_{ab}) & \text{for } v_A \in (v_{c1}, v_{c2}) \end{cases} \quad (5-44)$$

$$\text{Cond}_A = \begin{cases} sgn(-v_A) & \text{for } v_A \notin (v_{c1}, v_{c2}) \\ sgn(\Delta P_{ab}) & \text{for } v_A \in (v_{c1}, v_{c2}) \end{cases} \quad (5-45)$$

Taking the last term to left side and then taking the square root, Eq.(5-43) is solved for  $\Delta P_b$  as follows

$$\Delta P_b = \text{Cond}_B \left( \frac{-b - \sqrt{b^2 - 4ac}}{2a} \right)^2 \quad (5-46)$$

where

$$a = K_{v2}^2 - K_{v1}^2 \cdot \text{Cond}_A \cdot \text{Cond}_B$$

$$b = 2(v_A)K_{v2} \cdot \text{Cond}_A \quad (5-47)$$

$$c = (v_A)^2 - K_{v1}^2 \Delta P_{ab} \cdot \text{Cond}_A$$

After finding the relative rod-side chamber pressure, Eq. (5-46), the two unknowns  $\Delta P_a$  and  $\Delta P_L$ , that are the relative pressures of the cap-side chamber and the load can be found as follows.

$$\Delta P_a = \Delta P_b + \Delta P_{ab} \quad (5-48)$$

$$\Delta P_L = \Delta P_a - \alpha \Delta P_b \quad (5-49)$$

At last, the remaining unknown,  $\omega$ , that is the pump drive speed required for the desired actuator velocity can is found as follows.

$$\omega = \alpha K_{\omega1} \sqrt{|\Delta P_{ab} + \Delta P_b|} \text{sgn}(\Delta P_{ab} + \Delta P_b) + K_{\omega2} \sqrt{|\Delta P_b|} \text{sgn}(\Delta P_b) \quad (5-50)$$

where the coefficients  $K_{\omega1}$  and  $K_{\omega2}$  are,

$$K_{\omega1} = \frac{D_p}{A} K_{v1} = \frac{G_{va}(\Delta P_{ab})}{(1 - \alpha)D_p} \quad (5-51)$$

$$K_{\omega2} = \frac{D_p}{A} K_{v2} = \frac{G_{vb}(\Delta P_{ab})}{(1 - \alpha)D_p} \quad (5-52)$$

Considering the difference of the chamber pressures  $\Delta P_{ab}$  is known, then the function between the relative chamber pressures  $\Delta P_a$  or  $\Delta P_b$  and the actuator velocity  $v_A$ , defined by Eq. (5-40), is bijective as shown graphically in Figure 5-11. Therefore, for a given  $\Delta P_{ab}$  and actuator velocity  $v_A$  input set, a unique relative chamber pressure,  $\Delta P_a$  or  $\Delta P_b$ , can be calculated. However, the same conclusion is not true for the function between  $\Delta P_{ab}$  and  $v_A$ . The same actuator velocity  $v_A$  can be

reached for different  $\Delta P_{ab}$  values that corresponds a unique spool position. This case is illustrated in Figure 5-12.

The red line represents the  $\Delta P_b$  and  $v_A$  relation for a given  $\Delta P_{ab} = -0.505 \text{ MPa}$ , which corresponds to partially opened orifices at two ports. On the other hand, the blue line represent the  $\Delta P_b$  and  $v_A$  relation for a given  $\Delta P_{ab} = -0.727 \text{ MPa}$ , which corresponds to fully opened AC port and closed BC port. Note that, according to the Figure 5-12 an actuator velocity of  $v_A = 100 \text{ mm/s}$  can be achieved both for  $\Delta P_b = -0.165 \text{ MPa}$  and  $\Delta P_b = 0.7 \text{ MPa}$ , that corresponds to partially opened and fully opened spool positions respectively. Furthermore, since the corresponding relative cap-side chamber pressures are  $\Delta P_a = -0.67 \text{ MPa}$  and  $\Delta P_b = 0.005 \text{ MPa}$ , these two points corresponds to the same relative load pressure,  $\Delta P_L = \Delta P_a - \alpha \Delta P_b = -0.546 \text{ MPa}$ .

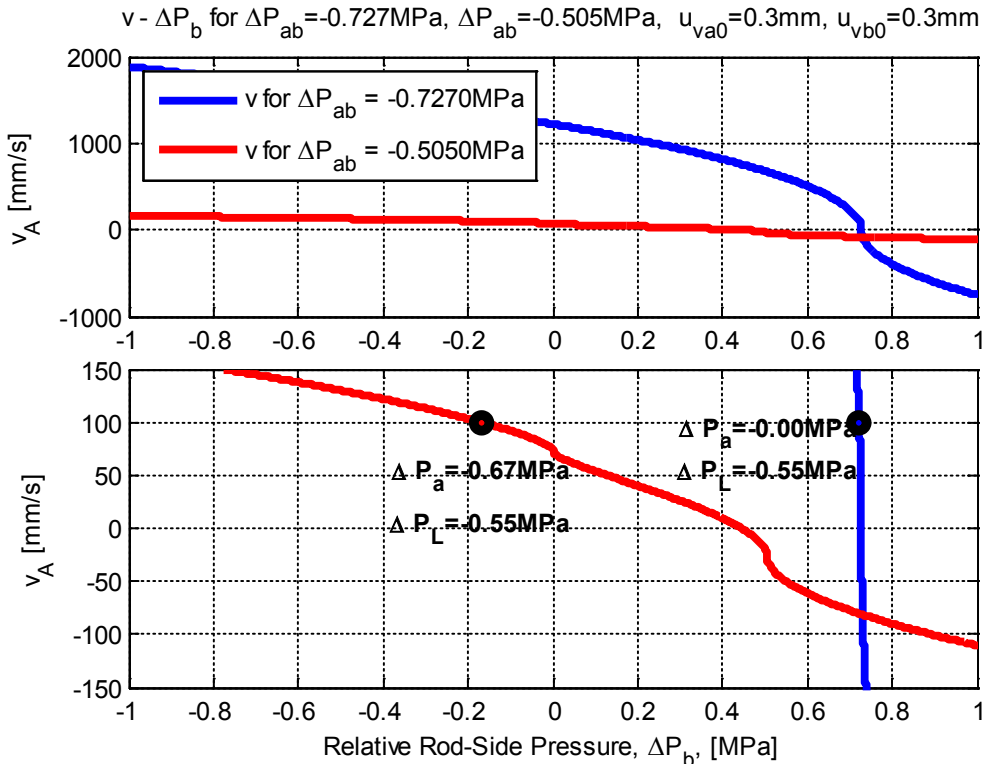


Figure 5-12 Actuator velocity vs. chamber pressure for different pilot pressures

The conclusion is interesting; an equilibrium point on  $\Delta P_L - v_A$  plane, which corresponds to a unique external load  $F_L = A \cdot \Delta P_L - b v_A$  and a desired actuator

speed  $v_A$ , can be achieved with different chamber pressure values,  $\Delta P_a$  and  $\Delta P_b$ , giving the same load pressure  $\Delta P_L$ , but having different pressure differences  $\Delta P_{ab}$  which corresponds to different orifice opening configurations or spool position.

The multiple spool positions corresponding to a single equilibrium point,  $v_A, \Delta P_L$ . This situation can be further illustrated, by drawing a  $\Delta P_{ab}$  versus  $v_A$  curves, for pre-defined  $\Delta P_L$  values. In order to draw a  $\Delta P_{ab} - v_A$  curve, first, the relative load pressure is taken as constant  $\Delta P_L = [-0.5, -0.2, 0.5] \text{ MPa}$ . Then, by varying the pilot pressure in the range of  $\Delta P_{ab} \in (-1.0, 0.6) \text{ MPa}$ , several relative chamber pressures  $\Delta P_a$  and  $\Delta P_b$  are calculated. The relative pressures are calculated based on Eqs. (5-35) and (5-36). Utilizing these relative chamber pressures, the actuator speed is calculated based on the Eq. (5-8). The resulting actuator velocity  $v_A$  is plotted on the  $\Delta P_{ab} - v_A$  plane as shown in Figure 5-13.

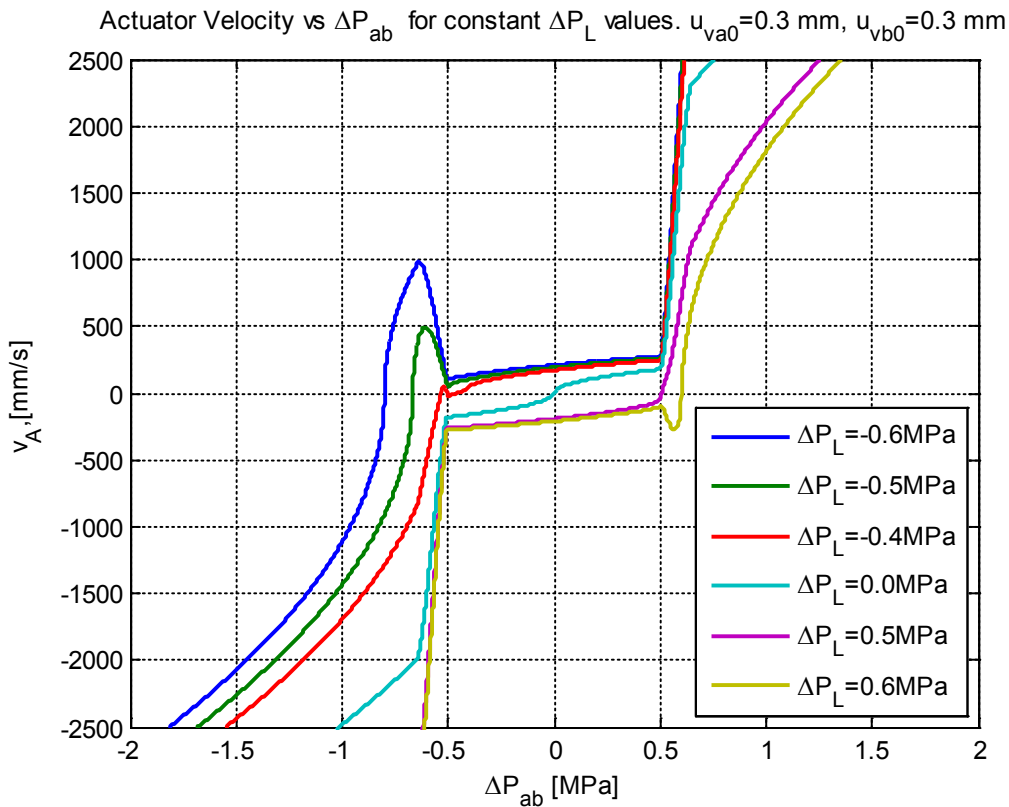


Figure 5-13 Actuator velocity vs pilot pressure  $\Delta P_{ab}$  for different load pressures

The right and left most region in Figure 5-13 corresponds to fully opened spool positions, i.e.  $\Delta P_{ab} < \Delta P_{uA_{Max}}$  and  $\Delta P_{ab} > \Delta P_{uB_{Max}}$ , respectively. In these regions,

since the valve is fully opened, the hydraulic conductance is relatively high. Therefore, relatively high actuator speeds are achieved with small variations of  $\Delta P_{ab}$ . On the contrary, in the intermediate region, which corresponds to centered or partially opened spool position, the achievable actuator velocity is limited, since the hydraulic conductance is relatively small. This Figure 5-13 shows that the function between the  $\Delta P_{ab}$  and the actuator velocity  $v_A$  is not bijective. That is, there is no one to one mapping between the actuator speed and the spool position. The non-bijectiveness depends on the load pressure  $\Delta P_L$ , which is determined by the external load acting on the actuator. Furthermore, it is seen that the non-bijective relation is valid for a range of  $\Delta P_{ab}$  region that corresponds to the spool position switching.

### 5.3.1 Numerical Simulations

The MATLAB<sup>®</sup>/Simhydraulics<sup>®</sup> numerical model introduced in Section 3.3 is used to verify the transformer ratio and inverse model formulation. The simulation model is modified; the pump leakages are neglected and only viscous type of friction is considered at the hydraulic actuator. The shuttle valve parameters used in the simulation model are given in Table 5-2. Furthermore, the shuttle valve spool position and orifice opening relations with pilot pressure input are shown in Figure 5-14.

The numerical simulation aims to verify the derived transformer ratio and inverse model formulation. For that purpose, test points are determined by defining  $\Delta P_{ab}$  and  $v_A$  values. The required pump drive speed  $\omega$  and the relative load pressure  $\Delta P_L$  is calculated, through the formulations given in the above sections 5.1.1 and 5.1.2. Then for the calculated, orifice openings and hydraulic conductance, the pump speed is determined. If the spool is saturated, the transformer ratios defined in Eqs. (5-27) and (5-28) are utilized, if it is not it is calculated through the inverse model formulation given by Eq. (5-46)-(5-52).

The simulation test points are given in Table 5-3. Furthermore, the orifice openings and spool position calculated for these desired test points are given in Figure 5-14. The calculated pump drive speeds together with the external loads are given at the end of Table 5-3. Note that the pump speed  $\omega$  and external load  $F_L$  are the inputs of

the simulation model. The accumulator pressure  $P_C$  is assumed to be constant at 3.0 MPa.

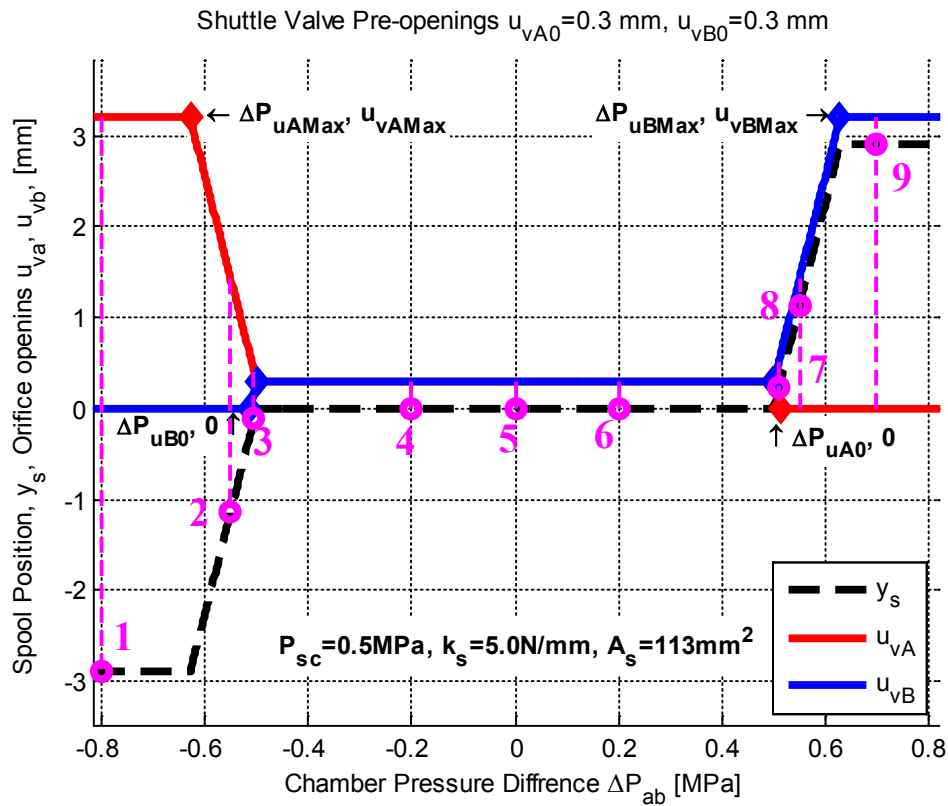


Figure 5-14 Underlapped shuttle valve orifice openings and test points

As it is seen from the figure, at test points 1 & 9 the shuttle valve is fully opened. In Table 5-3, the calculated transformer ratios for the 1<sup>st</sup> and 9<sup>th</sup> test points are  $0.6 \text{ mm/rad}$  and  $0.45 \text{ mm/rad}$  respectively. Note that the calculated values correspond to minimum and maximum TR defined by equations (5-27) and (5-28), respectively. For 4<sup>th</sup>, 5<sup>th</sup> and 6<sup>th</sup> test inputs the spool is centered. It is seen that for the 4<sup>th</sup> and 6<sup>th</sup> test inputs the desired speed is the same,  $-20 \text{ mm/s}$ . However the calculated transformer ratios are, different  $0.404 \text{ mm/rad}$  and  $0.706 \text{ mm/rad}$ , respectively. This difference is due to the different signs of the relative chamber pressures. These two test points correspond to the circulating leakage flow region that is shown previously by Figure 5-9. However, the 5<sup>th</sup> test point is outside the circulating leakage flow region, and therefore, its TR is  $0.515 \text{ mm/rad}$ , which is consistent by Eq.(5-33). The 2<sup>nd</sup> and 8<sup>th</sup> test points correspond to partially opened spool position with one orifice is opened only. It is seen that the corresponding TR's are  $0.6 \text{ mm/}$

rad and 0.45 mm/rad respectively; this is an expected result since there is no conduit between the two chambers. Lastly, the 3<sup>rd</sup> and 7<sup>th</sup> test points correspond to partially opened spool with two orifices are open. It is seen that the TR's are in between 0.6 mm/rad and 0.45 mm/rad .

Table 5-3 Simulation test points and corresponding simulation inputs  $\omega$  and  $F_L$

Simulation Test points, defined by desired, $\Delta P_{ab}$ and $v$										
$\Delta P_{ab}$	MPa	-0.8	-0.55	-0.505	-0.2	0	0.2	0.51	0.55	0.7
$v_A$	mm/s	100	-100	100	-20	50	-20	-150	100	-100
Calculated, spool position and orifice openings, also shown in Figure 5-14										
$y_s$	mm	-2.9	-1.13	-0.11	0	0	0	0.22	1.13	2.9
$u_{va}$	mm	3.2	1.43	0.41	0.3	0.3	0.3	0.073	0	0
$u_{vb}$	mm	0	0	0.187	0.3	0.3	0.3	0.53	1.43	3.2
Calculated pump drive speed, external load, and relative load pressure										
$\omega$	rpm	1590	-1590	1658	-472	927	-270	-3128	2120	-2120
TR	mm/rad	0.6	0.6	0.575	0.404	0.514	0.706	0.457	0.45	0.45
$F_L$	N	-229	1628	-57	1814	1700	2803	5122	3007	4753
$\Delta P_L$	MPa	-0.60	-0.41	-0.54	-0.15	-0.03	0.2	0.71	0.54	0.70

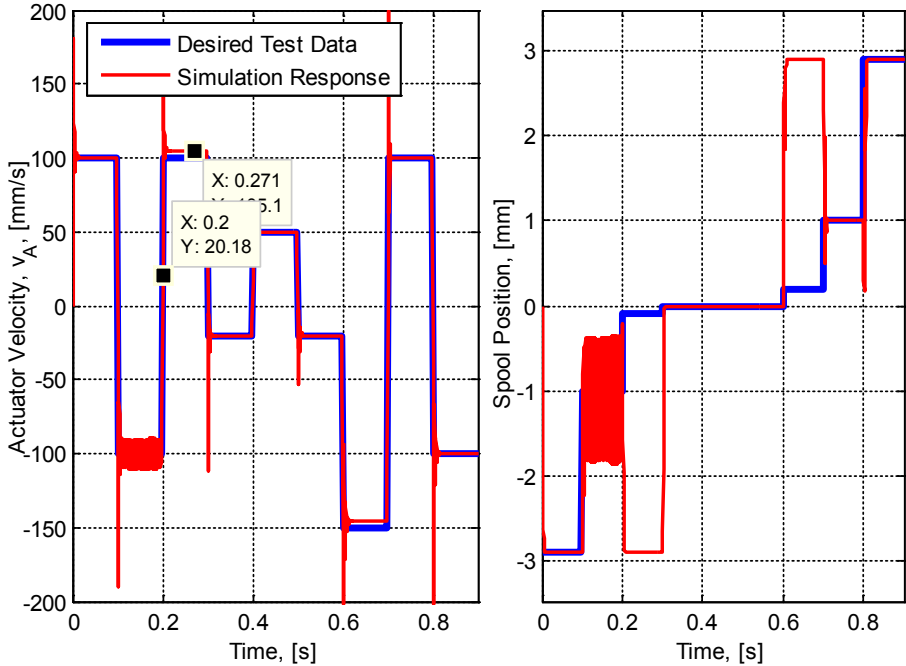


Figure 5-15 Open loop response, where inverse kinematic model is off-line

In the first part of the simulation the calculated pump drive speed  $\omega$  and  $F_L$  inputs are applied to the numerical model. The corresponding actuator velocity and spool position responses are given in Figure 5-15. From the figure it is seen that the desired actuator speeds are achieved, and the calculated spool positions,  $y_s$  are consistent with the simulation results, except for the 3<sup>rd</sup> and 7<sup>th</sup> test points. Furthermore, an oscillatory response is seen for the 2<sup>nd</sup> test point. The 3<sup>rd</sup> and 7<sup>th</sup> test points corresponds to partially opened spool position with two orifices, as seen from the figure, the spools are not partially but fully opened. Furthermore, the 2<sup>nd</sup> response corresponds to partially opened spool with single orifice, the oscillatory response during retraction is an expected result as mentioned in the previous chapter.

In the second part of the numerical simulation tests, the required pump speed  $\omega$  is calculated on-line, instead of off-line calculation. For that reason the MATLAB function used to calculate pump speed  $\omega$  is inserted into the Simulink Model. Different from the first test, this time the desired actuator speed  $v_A$  and the calculated lexternal load  $F_L$  are the input of the simulations model. The actuator speed and the spool position responses are given in Figure 5-16.

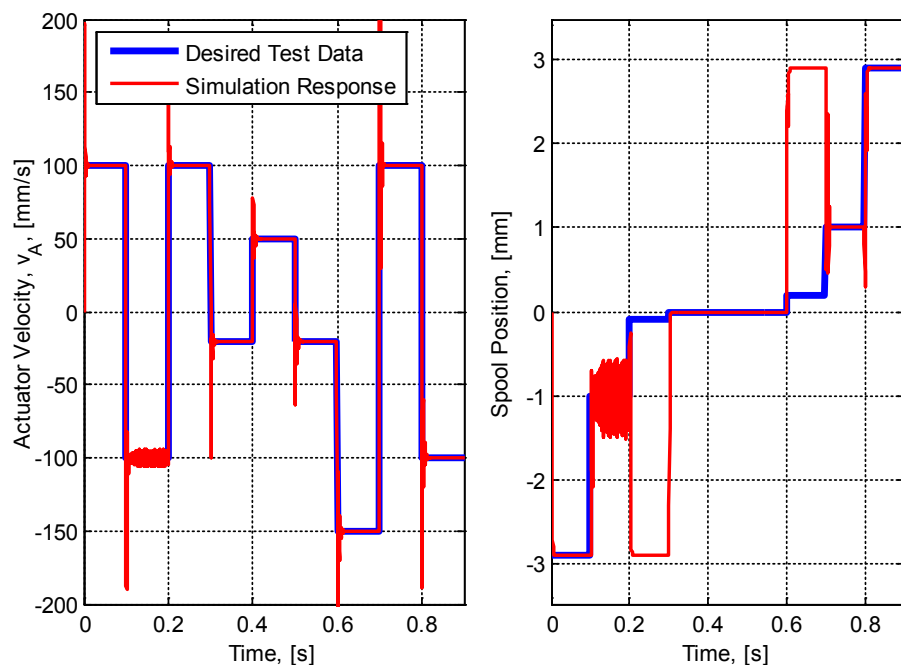


Figure 5-16 OL model response, where inverse kinematic model is activate

In Figure 5-16, it is seen that all the desired speeds are achieved, for both test points, including the 3<sup>rd</sup> and 7<sup>th</sup> test points. However, the spool position calculated for the 3<sup>rd</sup> and 7<sup>th</sup> test points are not the same with Table 5-3. Furthermore, the 2<sup>nd</sup> test point response is still oscillatory.

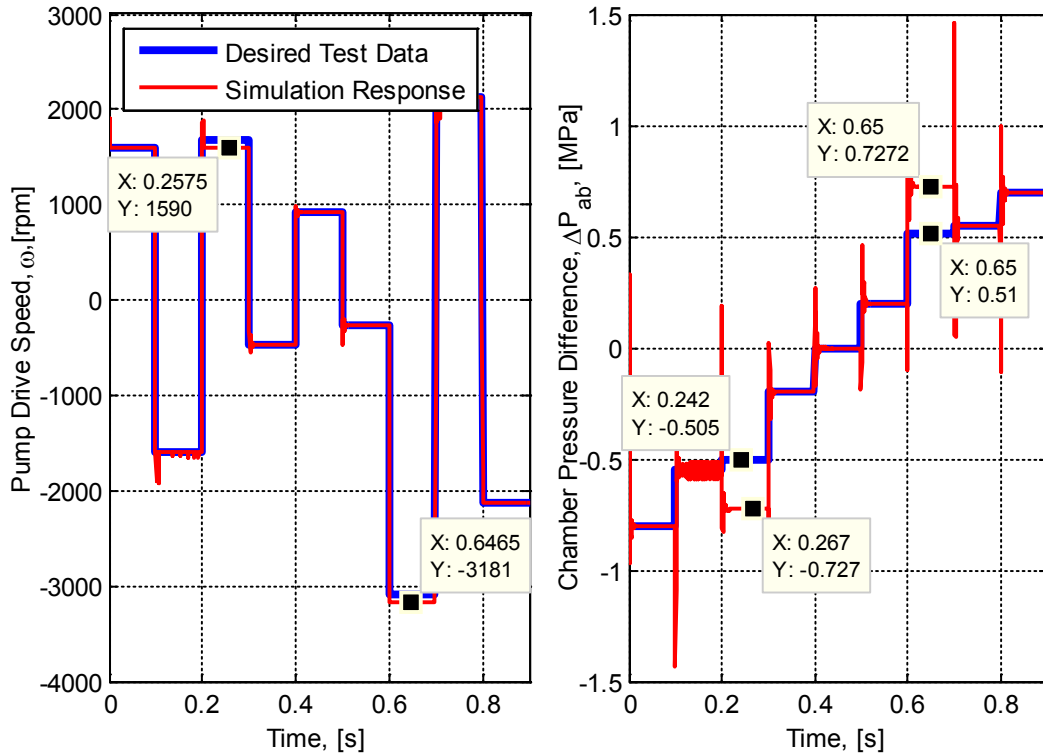


Figure 5-17 OL  $\omega_M$  and  $\Delta P_L$  responses, where inverse kinematic model is on-line

In order to investigate this behavior, the calculated pump speeds,  $\omega$ , during the simulation and the difference of the chamber pressure  $\Delta P_{ab}$ , responses are given Figure 5-17. It is seen that for the 3<sup>rd</sup> and 7<sup>th</sup> test points, the calculated pump drive speeds are different than the first case, which was calculated off-line. This is an expected result, in the second case, instead of calculating the pump drive speed  $\omega$  for the desired spool position, it is online calculated according to model response, i.e. for the fully opened position, therefore applying a different pump speed the desired actuator speed is achieved. As seen in the right side of Figure 5-17, the difference of chamber pressures response,  $\Delta P_{ab}$ , of the 3<sup>rd</sup> and 7<sup>th</sup> points are different from the desired ones given in Table 5-3. For the 3<sup>rd</sup> and 7<sup>th</sup> test points, it can be concluded

that the desired actuator velocity under an external load calculated for a pre-determined  $\Delta P_{ab}$  is achieved, by a different pump drive speed and pilot pressure.

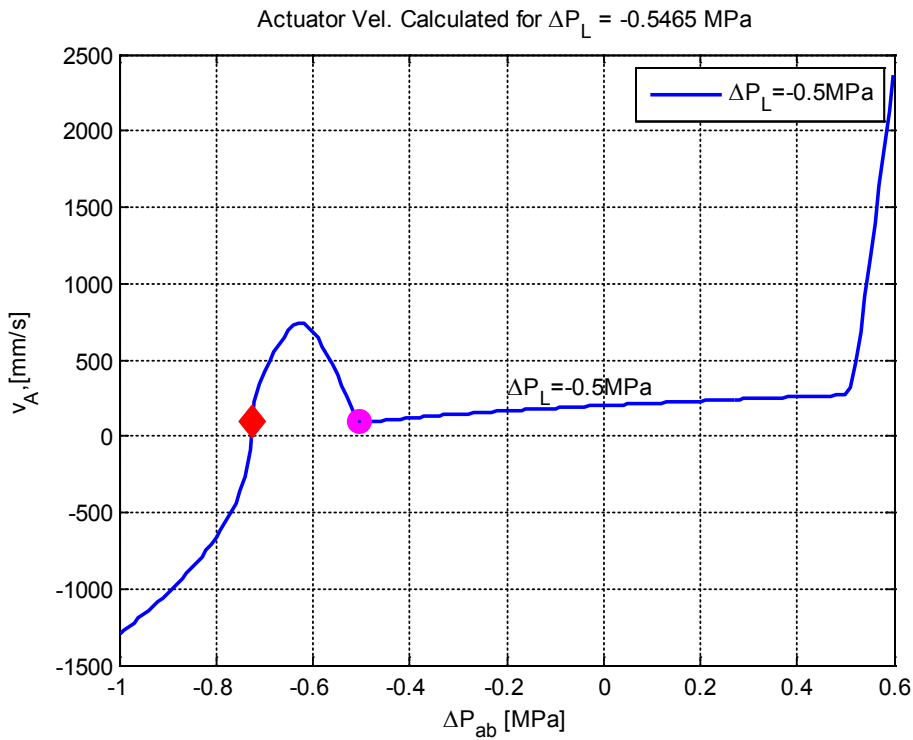


Figure 5-18 Pilot pressure vs. actuator velocity for a load pressure of 0.54 MPa

The system behavior observed for the 3<sup>rd</sup> and 7<sup>th</sup> test points are further investigated by considering the  $\Delta P_{ab} - v_A$  relation. In the 3<sup>rd</sup> test point the relative load pressure response of the simulation model is  $\Delta P_L = -0.54646 \text{ MPa}$ . The  $\Delta P_L$  response is consistent with Table 5-3, since the same load is applied and the desired speed is achieved as seen in Figure 5-16. In order to draw a  $\Delta P_{ab} - v$  curve, first, the relative load pressure is taken as constant  $\Delta P_L = -0.54 \text{ MPa}$ , then several relative chamber pressures  $\Delta P_a$  and  $\Delta P_b$  are calculated by varying the pilot pressure in the range of  $\Delta P_{ab} \in (-1.0, 0.6) \text{ MPa}$ . The resulting actuator velocity  $v_A$  is plotted on the  $\Delta P_{ab} - v_A$  plane as shown in Figure 5-18. This figure shows that the function between the  $\Delta P_{ab}$  and the actuator velocity  $v_A$  is not bijective. This figure explains the system behavior, seen in the 3<sup>rd</sup> and 7<sup>th</sup> test points, where the spool is partially opened, with two orifices. The desired pilot pressure  $\Delta P_{ab}$  of the 3<sup>rd</sup> point was  $-0.505 \text{ MPa}$ , when the off-line calculated pump speed is applied, the desired velocity cannot be reached for that point (magenta-circular dot). However, when the

pump speed calculation is made online, i.e. the inverse model is integrated into the simulation model, then the desired actuator speed is achieved by different pump speed and different  $\Delta P_{ab} = -0.727 \text{ MPa}$ , (red-diamond dot). It should be noted, that the desired test point magenta-circular dot in Figure 5-18 is an unstable equilibrium point, therefore, the desired, speed is achieved, with a different spool position (red-diamond point) which is stable. The stability of the system for the partially opened spool position will be investigated in the subsequent section.

As a conclusion, in this section the kinematic model and the related formulations is validated by the numerical Simulation model developed in MATLAB<sup>®</sup>/Simhydraulics<sup>®</sup> environment. The test points are selected for various positions of the shuttle valve spool. From the simulation results it is seen that for the centered and fully opened spool cases, the inverse model and the transformer ratio formulations works well and are consistent with the simulation model response. However, for the partially opened, spool positions, there occurs differences. This is due to the non-bijective property between  $\Delta P_{ab}$  and  $v_a$ . In Figure 5-18 it is shown that, for range of  $\Delta P_{ab}$  values which correspond to partially opened spool positions, the desired speed can be achieved with different spool positions.

#### 5.4 Asymmetric Shuttle Valve Spool Solution

In the previous section, it is shown that, if an underlapped valve is utilized, the transformer ratio between the pump drive speed input and the actuator speed output is not constant for the centered spool position. Therefore, an inverse kinematic model is utilized in order to predict the transformation ratio. Using the inverse kinematic model as a feed forward term for the control of the EHA is a solution, for the compensation of the dead pump speed and the circulating leakage flow rate. However, since the circulating leakage flow is not eliminated, there will be energy losses. Theoretically it was shown that, a  $0.3\text{ mm}$  underlap shuttle valve spool, creates dead pump speeds up to  $200\text{ rpm}$ . Note that the dead pump speed in the previous section is calculated by neglecting pump flow losses. Moreover, the discharge flow coefficient is taken to be constant for all orifice openings. Therefore, practically the dead pump speeds will be much higher than these values. Furthermore, if the hydraulic accumulator is integrated on the EHA, then, there is no way to replace the hydraulic fluid inside the EHA. The energy losses become much more important, since the circulating leakage flows will heat up the fluid.

In this section it is aimed to modify the shuttle valve spool structure, so that the circulating leakage flow rates and the dead pump speed are eliminated. In order to eliminate the circulating leakage flow rates the conduit between the two hydraulic chambers should be removed. For that reason, instead of providing spool underlap at two ports, it is proposed to provide an asymmetric valve spool underlap, i.e. provide spool pre-opening at the BC port, and provide a critically lapped (zero lapped) or overlapped spool opening at the AC port. The spool position and orifice opening relations of the proposed asymmetric spool are given in Figure 5-19.

As seen from the Figure 5-19, at the centered spool position, only the rod-side chamber is connected to the accumulator, through the pre-opening  $u_{vB_0}$ . At the centered position, there is no conduit between the two chambers; therefore no circulating leakage flow rate is formed. The two chambers are connected to each other, only during the positioning from center to left end stroke. Circulating leakage flow rate may form during this interval, however, it corresponds to a relatively small

pressure interval,  $\Delta P_{ab} = 0.12 \text{ MPa}$ . The shuttle valve parameters that are used are given in Table 5-4. The given data is based on the Bucher Hydraulics shuttle valve.

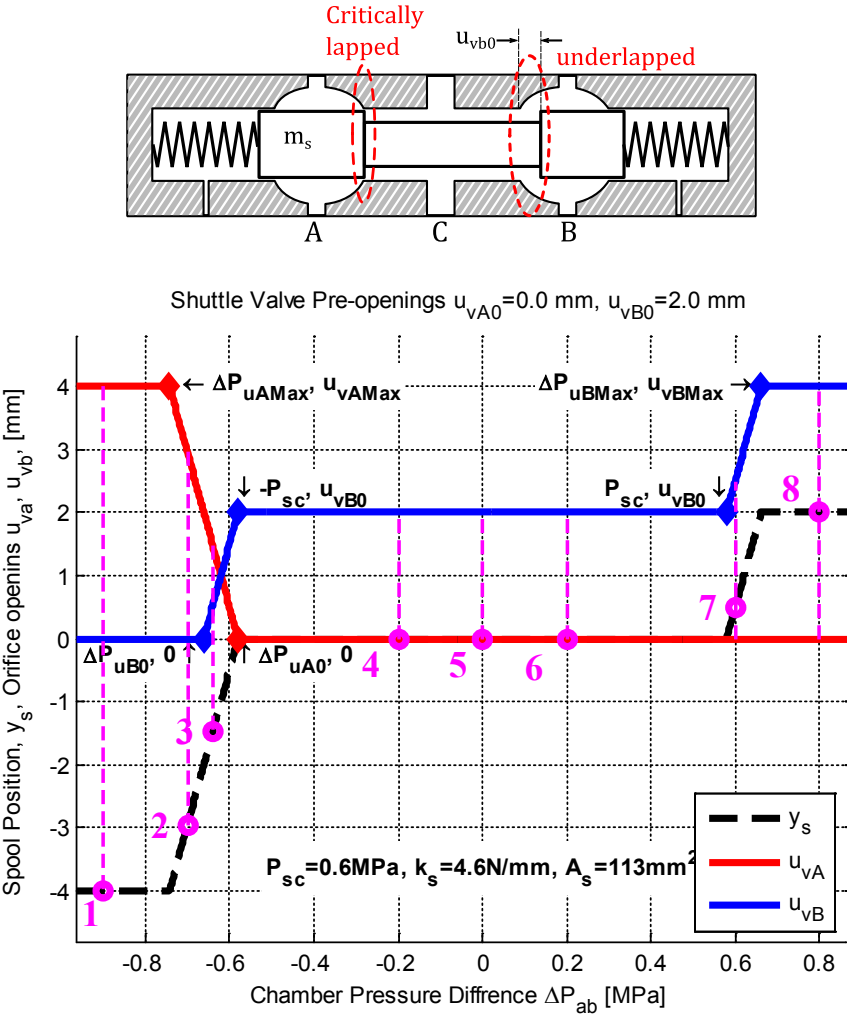


Figure 5-19 Asymmetric shuttle valve solution, orifice opening vs. pilot pressure

The superiorities of the asymmetric spool structure to the underlapped valve is the hydraulic conductance at the centered position. Since,  $u_{va0} = 0$  and no circulating leakage flow rate is possible to form, the spool underlap at port BC,  $u_{vb0}$  becomes a free parameter to increase. When compared with Table 5-2, where the underlapped shuttle valve parameters are given, it is seen in Table 5-4, that the hydraulic conductance is increase 10 times by increasing the overlap from  $0.3 \text{ mm}$  to  $2.0 \text{ mm}$ . The increased hydraulic conductance means the energy losses due to throttling losses that at the centered shuttle valve spool position is decreased .

Table 5-4 Shuttle valve parameter, with asymmetric spool

Shuttle valve design parameters			
$u_{va_0}, u_{vb_0}$	Spool underlapped,	0.0, 2.0	mm
$P_{sc}$	Cracking pressure	5.8	MPa
$k_s$	Spring stiffness is	4.62	N/mm
$A_s$	Pilot area, in	113	mm <sup>2</sup>
$n_h$	Number of holes on valve sleeve	6	
$r_h$	Hole radius	2	mm
$C_d$	Flow coefficient	0.325	
Calculated parameters			
$u_{va_{Max}}, u_{vb_{Max}}$	Maximum opening,	4, 4	mm
$A_{va_0}, A_{vb_0}$	Initial orifice area	0.0, 37.7	mm <sup>2</sup>
$A_{va_{Max}}, A_{vb_{Max}}$	Maximum orifice area	75.4, 75.4	mm <sup>2</sup>
$G_{a_0}, G_{b_0}$	Hydraulic conductance at center	0.0, $5.48 \cdot 10^5$	mm <sup>3</sup> /√MPa

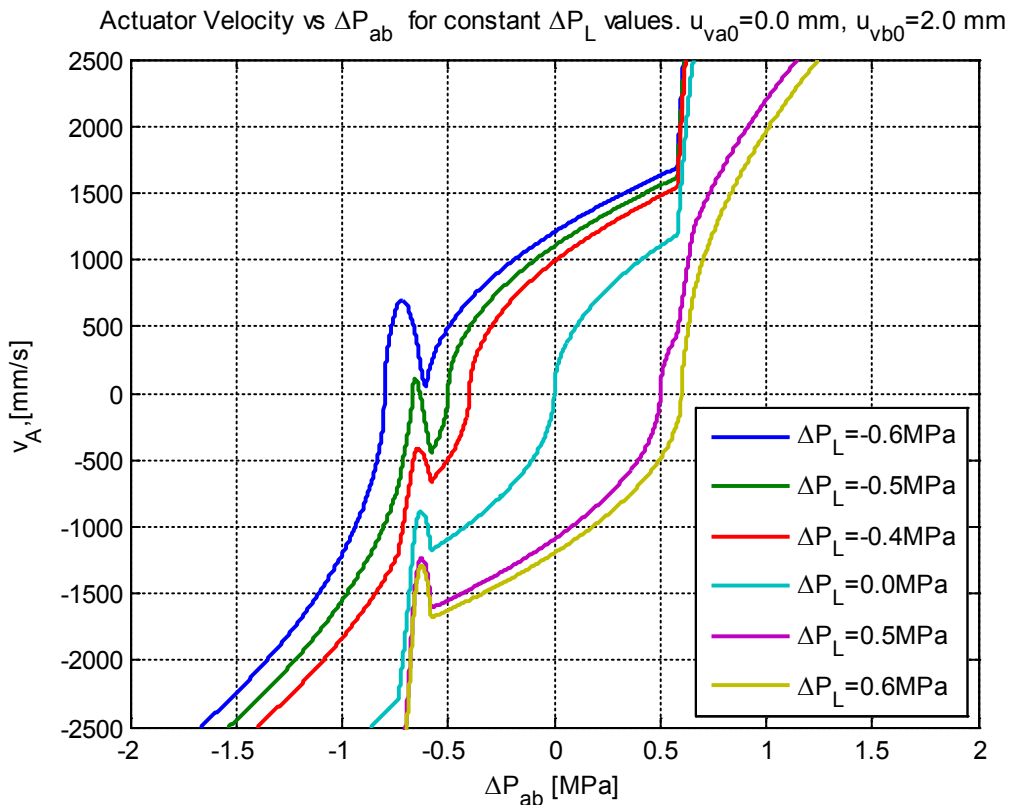


Figure 5-20 Actuator velocity vs pilot pressure  $\Delta P_{ab}$  relation for different values of  $\Delta P_L$

In Figure 5-19 for  $\Delta P_{ab} \in (\Delta P_{uA_{Max}}, -P_{sc})$ , both the two orifices are opened, likewise the underlapped valve given in Figure 5-14. The pressure interval of the spool position transtion is higher than the underlapped valve, since the spool underlap is increased. On the other hand, for  $\Delta P_{ab} \in (P_{sc}, \Delta P_{uB_{Max}})$  only the orifice at port BC is partially opened,  $u_{vb} \in (u_{vb_0}, u_{vb_{Max}})$ , and the orifice at port AC is zero,  $u_{va} = 0 \text{ mm}$ .

The actuator velocity versus pilot pressure  $\Delta P_{ab}$  relation for different values of  $\Delta P_L$  are given in Figure 5-20, when compared with the underlapped valve, given in Figure 5-13, it seen that the non-bijective relation between  $\Delta P_{ab}$  and  $v$  still exist for the region  $\Delta P_{ab} \in (P_{sc}, \Delta P_{uB_{Max}})$ . However, for the region  $\Delta P_{ab} \in (P_{sc}, \Delta P_{uB_{Max}})$ , there is a one-to-one mapping between  $\Delta P_{ab}$  and  $v$ .

The proposed asymmetric spool solution is tested with the same numerical model that is used in the previous chapter. The desired speeds are selected to be the same, and the same responses are investigated. The simulation test points are given in Table 5-5. Furthermore, the orifice openings and spool position calculated for these desired test points are shown in Figure 5-19 . The accumulator pressure  $P_c$  is assumed to be constant at  $3.0 \text{ MPa}$ . The calculated pump drive speeds together with the external loads are given at the end of Table 5-5

In Table 5-5, it is seen that, with the use of asymmetric spool solution, the circulating leakage flow rates are eliminated and the transformer ratio is made constant for the centered position of the spool. The TR for the 4<sup>th</sup> 5<sup>th</sup> and 6<sup>th</sup> inputs are calculated to be  $0.45 \text{ rad/mm}$ . This is an expected result, since only BC port is open the TR at center position is the same with the fully opened BC port.

A similar test procedure is applied as in the previous section. First the off-line calculated pump drive speeds and the external loads are given as the inputs of the simulation model. The resulting actuator velocity and the spool positions are given in Figure 5-21. It is seen that only for the partially opened spool positions, 2<sup>nd</sup> and 3<sup>rd</sup> test points, the desired actuator velocity cannot be reached.

**Table 5-5 Simulation test points and corresponding simulation inputs  $\omega$  and  $F_L$**

Simulation Test points, defined by desired, $\Delta P_{ab}$ and $v$									
$\Delta P_{ab}$	MPa	-0.9	-0.7	-0.6	-0.2	0	0.2	0.6	0.8
$v$	mm/s	100	-100	100	-20	50	-20	-100	100
Calculated, spool position and orifice openings, also shown in Figure 5-19									
$y_s$	mm	-4.0	-2.94	-1.47	0	0	0	0.49	2
$u_{va}$	mm	4	2.94	1.47	0	0	0	0	0
$u_{vb}$	mm	0	0	0.52	2	2	2	2.5	4
Calculated pump drive speed, external load, and relative load pressure									
$\omega$	rpm	1590	-1590	1133	-424	1060	-424	-2120	2120
$TR$	mm/rad	0.6	0.6	0.84	0.45	0.45	0.45	0.45	0.45
$F_L$	N	-440	1291	22.4	1685	1793	2816	4474	3730
$\Delta P_L$	MPa	-0.67	-0.52	-0.51	-0.2	-0.001	0.2	0.6	0.8

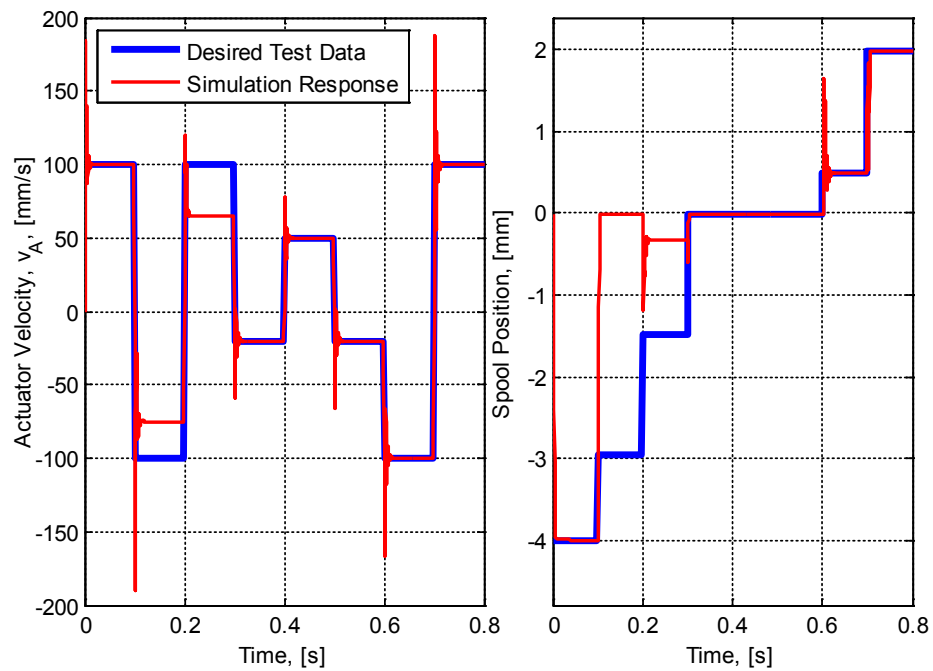


**Figure 5-21 OL model responses, where the inverse kinematic model is off-line**

Similar to the test procedure applied in the previous section, in the second tests, the inverse model is integrated into the simulation. This time the desired actuator velocity is the input of the simulation model, and the required pump speeds are calculated during the simulation. The remaining input, which is the external load

acting on the actuator is not changed. The response of the simulation model is given in Figure 5-22. It is seen that all the desired actuator velocities are achieved. However, the spool positions of the 2<sup>nd</sup> and 3<sup>rd</sup> input set are different from the ones calculated in Table 5-5. Similar to the previous case, the reason of this behavior is the non-bijective function between the  $\Delta P_{ab}$  and  $v$ . As shown in Figure 5-20, for the  $\Delta P_{ab}$  range that corresponds to partially opened orifice, two different  $\Delta P_{ab}$  solutions exist for a given actuator velocity and load pressure. When the inverse model is utilized, the equilibrium speed is achieved, by fully opening the spool instead of opening it partially. It should be noted, that the partially opened spool position, may result in an unstable equilibrium point, however, fully opened spool positions always result in a stable equilibrium position. The stability of the equilibrium points are investigated in detail in the subsequent section.

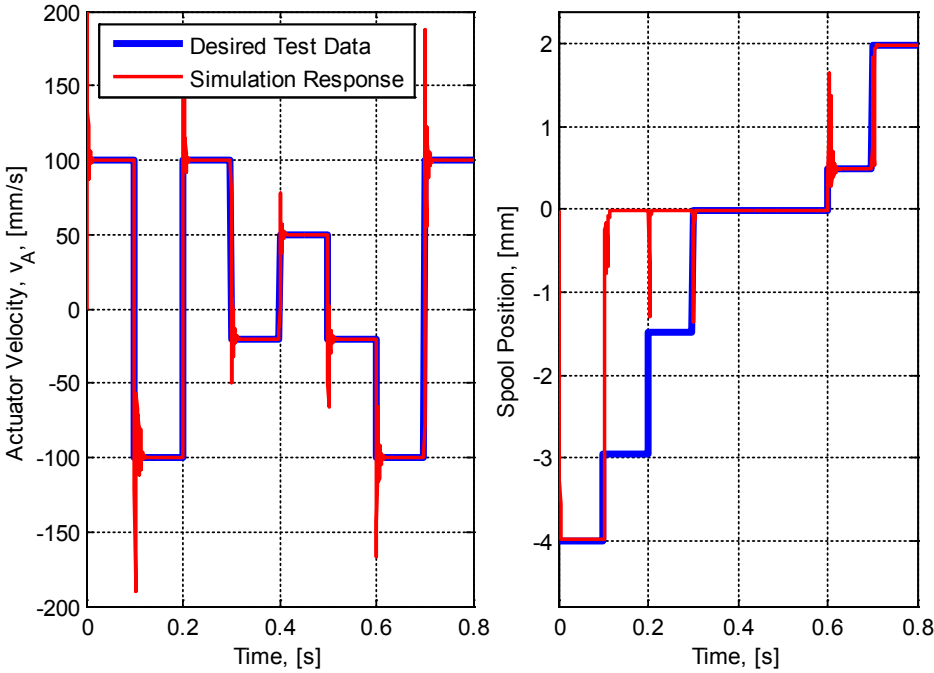


Figure 5-22 OL model responses, where the inverse kinematic model is on-line

### 5.5 Extended Stability Analysis

In the previous chapter the stability of the system is investigated for the partially opened spool position, and it is assumed that only one port is partially opened, while the other is closed. If an overlapped (or closed center) shuttle valve is utilized, this is

the only possible case. However, if an underlapped valve is used, or the spool structure is modified as mentioned in the previous section, then the two ports can be partially opened at the same time. Therefore, in this section a generalized stability analysis is done. Throughout the stability analysis, a similar method is applied. First the shuttle valve flow rates are linearized, then the roots of the characteristic polynomial is investigated. Different from the previous chapter, for the linearization of shuttle valve flow rates, besides assuming proportional orifice opening and area relation, the non-linearity due to circular orifice geometry is also considered. Furthermore, instead of analytical treatment, numerical analysis is done, and unstable regions for different spool structures are shown on  $\Delta P_{ab} - v$  plane.

### 5.5.1 Linearized Valve Coefficients with Linear Orifice Geometry

The relative chamber pressure variables, defined in this chapter, are used in the linearization. The shuttle valve flow rates are linearized around an equilibrium point  $\Delta P_{a_{eq}}$  and  $\Delta P_{b_{eq}}$ . For completeness and consistency with the previous chapter, in the first step it is assumed that the orifice area is proportional with the orifice opening, which is given in Eq.(5-53). Then in the second step, the flow gains are calculated by considering the non-linearity due to the circular orifice geometry. The latter gives closer results when compared with the non-linear numerical model.

$$A_v = A_{vA_{Max}} \frac{u_v}{u_{vMax}} \quad (5-53)$$

#### 5.5.1.1 Shuttle valve flow rate $Q_{a \rightarrow c}$

The orifice opening of the AC port in terms of chamber pressures is defined by Eq.(5-17), inserting into Eq.(5-53), the orifice area in terms of chamber pressure variables,  $\Delta P_{ab}$  is define as follows.

$$A_{vb} = \frac{A_{vA_{Max}}}{u_{vA_{Max}}} \frac{A_s}{k_s} \left( -\Delta P_{ab} + P_{sc} \text{sgn}(\Delta P_{ab}) + u_{vA_0} \frac{k_s}{A_s} \right) \quad (5-54)$$

Inserting the orifice area equation into hydraulic conductance and then into flow rate equations, (5-23) and (5-21) respectively, the flow term  $Q_{b \rightarrow c}$  is defined as follows.

$$Q_{a \rightarrow c} = C_d \sqrt{\frac{2 A_{vA_{Max}} A_s}{\rho u_{vA_{Max}} k_s}} \left( -\Delta P_{ab} + P_{sc} \operatorname{sgn}(\Delta P_{ab}) + u_{vA_0} \frac{k_s}{A_s} \right) \sqrt{|\Delta P_a|} \operatorname{sgn}(\Delta P_a) \quad (5-55)$$

Simplifying with  $P_{a0} = u_{vA_0} \frac{k_s}{A_s}$  and  $K_V = C_d \sqrt{\frac{2 A_{vA_{Max}} A_s}{\rho u_{vA_{Max}} k_s}}$

$$Q_{a \rightarrow c} = K_V (-\Delta P_{ab} + P_{sc} \operatorname{sgn}(\Delta P_{ab}) + P_{a0}) \sqrt{|\Delta P_a|} \operatorname{sgn}(\Delta P_a) \quad (5-56)$$

If the spool has positive pre-opening  $u_{vA_0} > 0$  then Eq. (5-56) is valid for  $\Delta P_{ab} \in (\Delta P_{uA_{Max}}, -P_{sc})$  and  $\Delta P_{ab} \in (P_{sc}, \Delta P_{uA_0})$ . If the spool has negative pre-opening  $u_{vA_0} < 0$ , the Eq. (5-56) is valid only for  $\Delta P_{ab} \in (\Delta P_{uB_{Max}}, \Delta P_{uA_0})$  where and  $\Delta P_{ab}$  are negative.

Note that since the accumulator pressure is constant, the variation of accumulator pressure is zero,  $\delta P_c = 0$ . Therefore, the variation of the relative chamber pressure is equal to the variation of chamber pressure  $\delta(\Delta P_a) = \delta P_a$ .

The Eq. (5-56) is linearized around an equilibrium point  $\Delta P_{b_{eq}}$  and  $\Delta P_{a_{eq}}$  as follows.

$$Q_{a \rightarrow c} = K_{a1} \delta P_a + K_{a2} \delta P_b \quad (5-57)$$

where

$$K_{a1} = \left. \frac{\partial Q_{a \rightarrow c}}{\partial (\Delta P_a)} \right|_{\substack{\Delta P_a = \Delta P_{a_{eq}} \\ \Delta P_b = \Delta P_{a_{eq}}}} \quad \text{and} \quad K_{a2} = \left. \frac{\partial Q_{a \rightarrow c}}{\partial (\Delta P_b)} \right|_{\substack{\Delta P_a = \Delta P_{a_{eq}} \\ \Delta P_b = \Delta P_{a_{eq}}}}$$

for  $\Delta P_a > 0$

$$Q_{a \rightarrow c} = K_V [(\Delta P_b + P_{sc} \operatorname{sgn}(\Delta P_{ab}) + P_{a0}) - \Delta P_a] \sqrt{\Delta P_a}$$

$$K_{a2} = K_V \sqrt{\Delta P_{a_{eq}}}$$

$$K_{a1} = K_V \left[ \left( \Delta P_{b_{eq}} + P_{sc} \operatorname{sgn}(\Delta P_{ab_{eq}}) + P_{a0} \right) \frac{1}{2 \sqrt{\Delta P_{a_{eq}}}} - \left( \sqrt{\Delta P_{a_{eq}}} + \Delta P_{a_{eq}} \frac{1}{2 \sqrt{\Delta P_{a_{eq}}}} \right) \right]$$

for  $\Delta P_a < 0$

$$Q_{b \rightarrow c} = -K_V [(\Delta P_b + P_{sc} \operatorname{sgn}(\Delta P_{ab}) + P_{a0}) - \Delta P_a] \sqrt{-\Delta P_a}$$

$$K_{a2} = -K_V \sqrt{-\Delta P_{aeq}}$$

$$K_{a1} = -K_V \left[ (\Delta P_{beq} + P_{sc} \operatorname{sgn}(\Delta P_{abeq}) + P_{a0}) \frac{-1}{2\sqrt{-\Delta P_{aeq}}} - \left( \sqrt{-\Delta P_{aeq}} + \frac{-\Delta P_{aeq}}{2\sqrt{-\Delta P_{aeq}}} \right) \right]$$

Note that the same result is obtained both for  $\Delta P_a > 0$  or  $\Delta P_a < 0$ ., the shuttle valve flow gains defined in Eq. (5-57) are defined as follows.

$$K_{a2} = K_V \sqrt{|\Delta P_{aeq}|} \quad (5-58)$$

$$K_{a1} = K_V \left[ \frac{\Delta P_{beq} + P_{sc} \operatorname{sgn}(\Delta P_{abeq}) + P_{a0} - 3\Delta P_{aeq}}{2\sqrt{|\Delta P_{aeq}|}} \right] \quad (5-59)$$

In the previous chapter, the shuttle valve flow rates are linearized for  $\Delta P_a > 0$  and  $\Delta P_{ab} < 0$ . Therefore, considering the previous chapter definition  $Q_{a \rightarrow c} = Q_{a \rightarrow c_{SS}} - K_1 \delta P_a + K_2 \delta P_b$ , the gains are the same, with the following relation  $-K_{a1} = K_1$  and  $K_{a2} = K_2$ .

$$K_1 = -K_V \frac{P_{beq} - P_{op} + 2P_c - 3P_{aeq}}{2\sqrt{P_{aeq} - P_c}} \quad (4-57)$$

$$K_2 = K_V \sqrt{P_{aeq} - P_c} \quad (4-58)$$

### 5.5.1.2 Shuttle valve flow rate $Q_{b \rightarrow c}$

The orifice opening of the BC port in terms of chamber pressures is defined by Eq. (5-18), inserting in to Eq.(5-53), the orifice area in terms of chamber pressure variables,  $\Delta P_{ab}$  is define as follows.

$$A_{vb} = \frac{A_{vB_{Max}} A_s}{u_{vB_{Max}} k_s} \left( \Delta P_{ab} - P_{sc} \text{sgn}(\Delta P_{ab}) + u_{vB_0} \frac{k_s}{A_s} \right) \quad (5-60)$$

Inserting the orifice area equation into hydraulic conductance and then flow rate equations, (5-24) and (5-22) respectively, the flow term  $Q_{b \rightarrow c}$  is defined as follows.

$$Q_{b \rightarrow c} = C_d \sqrt{\frac{2 A_{vB_{Max}} A_s}{\rho u_{vB_{Max}} k_s} \left( \Delta P_{ab} - P_{sc} \text{sgn}(\Delta P_{ab}) + u_{vB_0} \frac{k_s}{A_s} \right) \sqrt{|\Delta P_b|} \text{sgn}(\Delta P_b)} \quad (5-61)$$

Simplifying with  $P_{b0} = u_{vB_0} \frac{k_s}{A_s}$  and  $K_V = C_d \sqrt{\frac{2 A_{vB_{Max}} A_s}{\rho u_{vB_{Max}} k_s}}$

$$Q_{b \rightarrow c} = K_V (\Delta P_{ab} - P_{sc} \text{sgn}(\Delta P_{ab}) + P_{b0}) \sqrt{|\Delta P_b|} \text{sgn}(\Delta P_b) \quad (5-62)$$

If the spool has positive pre-opening  $u_{vB_0} > 0$  then Eq. (5-62) is valid for  $\Delta P_{ab} \in (P_{sc}, \Delta P_{uB_{Max}})$  and  $\Delta P_{ab} \in (\Delta P_{uB_0}, -P_{sc})$ . If the spool has negative pre-opening  $u_{vB_0} < 0$ , the Eq. (5-62) is valid only for  $\Delta P_{ab} \in (\Delta P_{uB_0}, \Delta P_{uB_{Max}})$  where  $\Delta P_{uB_0}$  and  $\Delta P_{ab} > 0$  are positive.

The Eq. (5-62) is linearized around an equilibrium point  $\Delta P_{ab_{eq}}$  and  $\Delta P_{b_{eq}}$  as follows.

$$\delta Q_{b \rightarrow c} = K_{b1} \delta P_a + K_{b2} \delta P_b \quad (5-63)$$

where

$$K_{b1} = \left. \frac{\partial Q_{b \rightarrow c}}{\partial (\Delta P_a)} \right|_{\substack{\Delta P_a = \Delta P_{a_{eq}} \\ \Delta P_b = \Delta P_{b_{eq}}}} \quad \text{and} \quad K_{b2} = \left. \frac{\partial Q_{b \rightarrow c}}{\partial (\Delta P_b)} \right|_{\substack{\Delta P_a = \Delta P_{a_{eq}} \\ \Delta P_b = \Delta P_{b_{eq}}}}$$

for  $\Delta P_b > 0$

$$Q_{b \rightarrow c} = K_V [(\Delta P_a - P_{sc} \text{sgn}(\Delta P_{ab}) + P_{b0}) - \Delta P_b] \sqrt{\Delta P_b}$$

$$K_{b1} = K_V \sqrt{\Delta P_{b_{eq}}}$$

$$K_{b2} = K_V \left[ \left( \Delta P_{aeq} - P_{sc} \text{sign}(\Delta P_{abeq}) + P_{b0} \right) \frac{1}{2\sqrt{\Delta P_{beq}}} - \left( \sqrt{\Delta P_{beq}} + \frac{\Delta P_{beq}}{2\sqrt{\Delta P_{beq}}} \right) \right]$$

for  $\Delta P_b < 0$

$$Q_{b \rightarrow c} = -K_V [(\Delta P_a - P_{sc} \text{sgn}(\Delta P_{ab}) + P_{b0}) - \Delta P_b] \sqrt{-\Delta P_b}$$

$$K_{b1} = -K_V \sqrt{-\Delta P_{beq}}$$

$$K_{b2} = -K_V \left[ \left( \Delta P_{aeq} - P_{sc} \text{sgn}(\Delta P_{abeq}) + P_{b0} \right) \frac{-1}{2\sqrt{-\Delta P_{beq}}} - \left( \sqrt{-\Delta P_{beq}} + \frac{-\Delta P_{beq}}{2\sqrt{-\Delta P_{beq}}} \right) \right]$$

Note that the same result is obtained both for  $\Delta P_b > 0$  or  $\Delta P_b < 0$ , the shuttle valve flow gains defined in Eq.(5-63) are given as follows.

$$K_{b1} = K_V \sqrt{|\Delta P_{beq}|} \quad (5-64)$$

$$K_{b2} = K_V \left[ \frac{\Delta P_{aeq} - P_{sc} \text{sgn}(\Delta P_{abeq}) + P_{b0} - 3\Delta P_{beq}}{2\sqrt{|\Delta P_{beq}|}} \right] \quad (5-65)$$

In the previous chapter, the shuttle valve flow rates is linearized for  $\Delta P_{ab} > 0$  and  $\Delta P_b < 0$ , that is  $P_c > P_b$ . When compared with the previous chapter defined as,  $Q_{c \rightarrow b} = K_1 \delta P_a - K_2 \delta P_b = -Q_{b \rightarrow c} = -(K_{b1} \delta P_a + K_{b2} \delta P_b)$ . The resulting gains are related as follows:  $-K_{b1} = K_1$  and  $K_{b2} = K_2$ .

$$K_1 = K_V \sqrt{P_c - P_{beq}} \quad (4-49)$$

$$K_2 = K_V \frac{P_{aeq} - P_{op} + 2P_c - 3P_{beq}}{2\sqrt{P_c - P_{beq}}} \quad (4-50)$$

## 5.5.2 Linearized Valve Coefficients with Non-Linear Orifice Geometry

The shuttle valve used in the scope of this study is of cartridge type. The orifice area is formed by the circular holes drilled on the valve sleeve. Therefore there exists a non-linear relationship between the orifice area and opening. This relation is formulated in section 3.2.3. In this section the shuttle valve flow rate is linearized considering this circular hole geometry.

Note that, in the linearization procedure, given in the previous chapter and the previous section is valid only for pressure intervals that correspond to partially opened orifice opening. On the other, the linearization procedures given in this sub section is valid for all pressure intervals.

### 5.5.2.1 Shuttle valve flow rate $Q_{a \rightarrow c}$

The shuttle valve flow rate is defined as follows.

$$Q_{a \rightarrow c} = C_d \sqrt{\frac{2}{\rho}} A_{va} (\Delta P_{ab}) \sqrt{|\Delta P_a|} \text{sgn}(\Delta P_a) \quad (5-66)$$

The absolute value of the flow rate,  $Q_{a \rightarrow c}$ , can be calculated, by first finding the orifice opening for a given pilot pressure  $\Delta P_{ab}$  by using Eq.(5-17), and then calculating the resulting orifice area  $A_{va}$  by using Eq.(5-19).

On the other hand, the variation of the shuttle valve flow rate  $\delta Q_{a \rightarrow c}$ , around an equilibrium point  $\Delta P_{ab_{eq}}$ ,  $\Delta P_{a_{eq}}$ , can be defined as follows.

$$\delta Q_{a \rightarrow c} = C_d \sqrt{\frac{2}{\rho}} \left( A_{va_{eq}} \frac{1}{2 \sqrt{|\Delta P_{a_{eq}}|}} \delta(\Delta P_a) + \sqrt{|\Delta P_{a_{eq}}|} \text{sgn}(\Delta P_{a_{eq}}) \delta A_{va} \right) \quad (5-67)$$

Here the term  $\delta A_{va}$  represents the variation of the orifice area. Considering the hole geometry as given in Figure 3-10. The orifice area variation can be represented by the variation of spool position as follows.

$$\delta A_{va} = n_h h_{aeq} \delta u_{va} \cdot \text{Cond}_h \quad (5-68)$$

In Eq. (5-68), the term  $n_h$  is the number of holes,  $h_{aeq}$  is the chord of the orifice hole formed by the spool surface for a given equilibrium point  $\Delta P_{ab_{eq}}$ , and is shown in Figure 3-10. The chord of the hole given in Figure 3-10 can be found as follows.

$$h_{aeq} = 2 \left| r_h \sin(\theta_{aeq}) \right| \quad (5-69)$$

Where,  $r_h$  is the hole radius and  $\theta_{aeq}$  is the angle calculated at an operating point  $\Delta P_{ab_{eq}}$  through Eq. (5-20), which is defined for all orifice openings  $u_v \in [0, u_{vMax}]$ . Note that according to the definition of the angle  $\theta_v$  given in Eq. (5-20) or Eq. (3-26): if the orifice is closed, i.e.  $u_v = 0$ , then the angle  $\theta_v = 0$  or if fully opened i.e.  $u_v = u_{vMax}$ , then  $\theta_v = \pi$ . Therefore, in Eq. (5-69), the chord length  $h_{aeq} = 0$  for  $\Delta P_{ab} \notin [\Delta P_{uA_0}, \Delta P_{uAMax}]$ .

Special attention should be given for the centered spool case, i.e.  $\Delta P_{ab} \in [-P_{sc}, P_{sc}]$ . In that interval, if there exist a spool underlap  $u_{v0} > 0$ , the angle  $\theta_v \neq 0$  and the chord length  $h_a \neq 0$  have a fine value. However, the spool is stationary, which means that mean  $\delta u_v = \delta A_v = \delta h_v = 0$ . In order to represent this condition a condition operator  $\text{Cond}_h$  is included in Eq. (5-68). Therefore, the condition operator is defined as  $\text{Cond}_h = 0$  for the pressure interval  $\Delta P_{ab} \in [-P_{sc}, P_{sc}]$ , and  $\text{Cond}_h = 1$  for all other pressure ranges.

$$\text{Cond}_h = \begin{cases} 0 & \text{for } \Delta P_{ab} \in [-P_{sc}, P_{sc}] \\ 1 & \Delta P_{ab} \notin [-P_{sc}, P_{sc}] \end{cases} \quad (5-70)$$

In Eq. (5-68), the remaining term,  $\delta u_{va}$  is the variation of the orifice opening. If the valve spool is not centered or saturated, then the orifice opening,  $u_{va}$ , is determined by the pilot pressure  $\Delta P_{ab}$ , as given in Eq.(5-17). Considering small variations, the orifice opening is can be defined as follows.

$$\delta u_{va} = \frac{A_s}{k_s} (\delta P_b - \delta P_a) \quad (5-71)$$

Note that since the accumulator pressure is constant, the variation of accumulator pressure is zero,  $\delta P_c = 0$ . Therefore, the variation of the relative chamber pressure is equal to the variation of chamber pressure  $\delta(\Delta P_a) = \delta P_a$ . Inserting Eq. (5-71) into Eq.(5-68) then inserting the resulting Eq. (5-67), the shuttle valve flow rate is linearized as follows.

$$\delta Q_{a \rightarrow c} = K_{a1} \delta P_a + K_{a2} \delta P_b \quad (5-72)$$

where, the flow gains  $K_{a1}$  and  $K_{a2}$  are calculated for an operating point,  $\Delta P_{abeq}$  and  $\Delta P_{aeq}$  as follows.

$$K_{a1} = C_d \sqrt{\frac{2}{\rho}} \left( \frac{A_{va_{eq}}}{2\sqrt{|\Delta P_{aeq}|}} - 2n_h |r_h \sin(\theta_{aeq})| \frac{A_s \sqrt{|\Delta P_{aeq}|} \operatorname{sgn}(\Delta P_{aeq})}{k_s} \operatorname{Cond}_h \right) \quad (5-73)$$

$$K_{a2} = C_d \sqrt{\frac{2}{\rho}} n_h 2 |r_h \sin(\theta_{aeq})| \frac{A_s \sqrt{|\Delta P_{aeq}|} \operatorname{sgn}(\Delta P_{aeq})}{k_s} \operatorname{Cond}_h \quad (5-74)$$

### 5.5.2.2 Shuttle valve flow rate $Q_{b \rightarrow c}$

The shuttle valve flow rate  $Q_{b \rightarrow c}$  is linearized with a similar procedure. The variation of the flow rate  $Q_{b \rightarrow c}$  around an equilibrium point  $\Delta P_{abeq}$ ,  $\Delta P_{beq}$  can be written as follows.

$$\delta Q_{b \rightarrow c} = K_{b1} \delta P_a + K_{b2} \delta P_b \quad (5-75)$$

where, the gains  $K_{b1}$  and  $K_{b2}$  are calculated as follows,

$$K_{b2} = C_d \sqrt{\frac{2}{\rho}} \left( \frac{A_{vb_{eq}}}{2\sqrt{|\Delta P_{b_{eq}}|}} - n_h 2 |r_h \sin(\theta_{b_{eq}})| \frac{A_s \sqrt{|\Delta P_{b_{eq}}|} \operatorname{sgn}(\Delta P_{b_{eq}})}{k_s} \operatorname{Cond}_h \right) \quad (5-76)$$

$$K_{b1} = C_d \sqrt{\frac{2}{\rho}} n_h 2 |r_h \sin(\theta_{b_{eq}})| \frac{A_s \sqrt{|\Delta P_{b_{eq}}|} \operatorname{sgn}(\Delta P_{b_{eq}})}{k_s} \operatorname{Cond}_h \quad (5-77)$$

where, the angle  $\theta_{b_{eq}}$  and the orifice area  $A_{vb_{eq}}$  are calculated at an operating point  $\Delta P_{ab_{eq}}$  and  $\Delta P_{b_{eq}}$ . Given that,  $\Delta P_{ab_{eq}} = \Delta P_{a_{eq}} - \Delta P_{b_{eq}}$ , first the related orifice opening is found by using the Eqs (5-15)–(5-18), then, the angle  $\theta_{v_{eq}}$  and the orifice area  $A_{v_{eq}}$  is calculated by using Eqs.(5-19) and (5-20).

Different from the previous case , where the orifice area is assume to be proportional to orifice opening, the coefficient calculations given in this section,  $K_{a1}$ ,  $K_{a2}$ ,  $K_{b1}$ ,  $K_{b2}$ , are valid for all pressure intervals. However, for the pressure ranges corresponding to static orifice openings, the computation effort of  $A_{v_{eq}}$  and  $\theta_{v_{eq}}$  can be avoided.

For the below defined conditions, the orifice area  $A_{v_{eq}}$  can be directly found as follows.

- For  $\Delta P_{ab_{eq}} \geq \Delta P_{uB_{Max}}$  and  $\Delta P_{ab_{eq}} \leq \Delta P_{uA_{Max}}$ , the related orifice is fully opened, therefore  $A_{v_{eq}} = A_{v_{Max}}$ .
- For  $\Delta P_{ab_{eq}} \leq \Delta P_{uB_0}$  and  $\Delta P_{ab_{eq}} \geq \Delta P_{uA_0}$  the related orifice is closed, therefore,  $A_{v_{eq}} = 0$ .
- For  $-P_{sc} \leq \Delta P_{ab_{eq}} \leq P_{sc}$  the spool is centered, therefore,  $A_{v_{eq}} = A_{v_0}$ .

For the conditions defined below, the calculation of the angle  $\theta_{v_{eq}}$  can be avoided, since for  $\theta_{v_{eq}} = 0$  or  $\theta_{v_{eq}} = \pi$  and  $\operatorname{Cond}_h = 0$ , the second terms of the coefficients  $K_{a1}$  and  $K_{b2}$  becomes zero, together with  $K_{a2} = K_{b1} = 0$ .

- For  $\Delta P_{ab_{eq}} \geq \Delta P_{uB_{Max}}$  and  $\Delta P_{ab_{eq}} \leq \Delta P_{uA_{Max}}$ , the related orifice is fully opened, therefore Eq. (5-20) gives  $\theta_{v_{eq}} = \pi$
- For  $\Delta P_{ab_{eq}} \leq \Delta P_{uB_0}$  and  $\Delta P_{ab_{eq}} \geq \Delta P_{uA_0}$  the related orifice is closed, therefore, Eq. (5-20) gives  $\theta_{v_{eq}} = 0$ .
- For  $-P_{sc} \leq \Delta P_{ab_{eq}} \leq P_{sc}$  the spool is centered,  $\theta_{v_{eq}}$  has a finite value, however since  $\delta A_v = 0$ , by definition given in Eq.(5-68) the condition operator  $\text{Cond}_h = 0$ .

## 5.6 Linearized State Equations

In the first part the state equations of the linearized system are written by neglecting the shuttle valve dynamics, i.e. there exists a static relation between spool position and pilot pressure. In the second part, the state matrix of the linearized system is augmented with a first order shuttle valve spool dynamics equation. A time constant is utilized to represent the overall effects of the pilot pressure line losses, and frictional losses.

### 5.6.1 Without Shuttle Valve Dynamics

By using the shuttle valve flow rates defined in Eqs. (5-57) and (5-63), the state equations defining the state variations  $\delta v, \delta P_a, \delta P_b$  around an equilibrium point  $v_{eq}, \Delta P_{a_{eq}}, \Delta P_{b_{eq}}$  is written as follows.

$$m\delta \dot{v}_A = A\delta P_a - \alpha A\delta P_b - \delta F_L \quad (5-78)$$

$$C_a\delta \dot{P}_a = D_p\delta \omega - A\delta v_A - (K_{a2}\delta P_b + K_{a1}\delta P_a) \quad (5-79)$$

$$C_b\delta \dot{P}_b = \alpha A\delta v_A - D_p\delta \omega - (K_{b1}\delta P_a + K_{b2}\delta P_b) \quad (5-80)$$

The linearized system represented in state space form is given as follows.

$$\begin{bmatrix} \delta \dot{v}_A \\ \delta \dot{P}_a \\ \delta \dot{P}_b \end{bmatrix} = \begin{bmatrix} -\frac{b}{m} & \frac{A}{m} & \frac{-\alpha A}{m} \\ -\frac{A}{C_a} & -\frac{K_{a1}}{C_a} & -\frac{K_{a2}}{C_a} \\ \frac{\alpha A}{C_b} & -\frac{K_{b1}}{C_b} & -\frac{K_{b2}}{C_b} \end{bmatrix} \begin{bmatrix} \delta v_A \\ \delta P_a \\ \delta P_b \end{bmatrix} + \begin{bmatrix} -\frac{1}{m} & 0 \\ \frac{D_p}{C_b} & 0 \\ 0 & -\frac{D_p}{C_b} \end{bmatrix} \begin{bmatrix} \delta F_L \\ \delta \omega \end{bmatrix} \quad (5-81)$$

The stability can be checked by checking the eigen values of the state matrix or the roots of the characteristic equation given as follows.

$$a_3 s^3 + a_2 s^2 + a_1 s + a_0 = 0 \quad (5-82)$$

where

$$a_3 = m C_a C_b$$

$$a_2 = m(K_{b2} C_a + K_{a1} C_b) + b C_a C_b$$

$$a_1 = m(K_{a1} K_{b2} - K_{b1} K_{a2}) + b(K_{b2} C_a + K_{a1} C_b) + A^2(C_b + \alpha^2 C_a)$$

$$a_0 = b(K_{a1} K_{b2} - K_{b1} K_{a2}) + A^2(K_{b2} + \alpha K_{a2} + \alpha^2 K_{a1} + \alpha K_{b1})$$

At that point it should be noted that the characteristic polynomial defined in Eq.(5-82) is written for the generalized case and covers the characteristic polynomials, written in the previous chapter. Remembering that, only one port open condition is considered, Eq.(4-54) and Eq. (4-62) written in previous chapter, are the simplified forms of Eq.(5-82). Therefore considering the sign definitions, and inserting  $-K_{a1} = K_1$  and  $K_{a2} = K_2$ , and  $K_{b1} = K_{b2} = 0$ , Eq.(5-82) reduces to Eq. (4-62). Similarly, Eq.(4-54) can be obtained if it is inserted,  $K_{b1} = K_{b2} = 0$  and  $-K_{b1} = K_1$  and  $K_{b2} = K_2$ .

Note that although the stability condition of the characteristic polynomial Eq.(5-82) is simple, i.e., all positive coefficients  $a_2$ ,  $a_1$ ,  $a_0$ , and  $a_2 a_1 > a_3 a_0$ , it is not easy to make an analytical treatment as in the previous chapter, since both shuttle valve flow rates are considered. Therefore, numerical treatment is considered in the subsequent sections.

## 5.6.2 With Shuttle Valve Dynamics

The shuttle valve dynamics is given in detail in section 3.2.3. In that part the pilot pressure lines, pilot pressure chamber capacitances, valve spool mass, centering spring stiffness and the viscous friction effects are considered. Including all the terms increases the order of the model. The aim of this part is to construct a linear system model, in order to investigate the effects of valve dynamics on system stability. Therefore, first order transfer function with time constant  $T_{sv}$  is utilized in order to represent the overall effects of capacitive and frictional losses.

$$T_{sv}\dot{y}_s + y_s = \frac{A_s}{k_s} (P_a - P_b - P_{sc} \text{sign}(P_a - P_b)) \quad (5-83)$$

Physically, increasing the pilot pressure resistance or pilot pressure chamber volume corresponds to increasing the time constant  $T_{sv}$ . A similar relation between the sum of the pilot and port pressures is given in Eq. (3-17).

The linearized shuttle valve flow equations have to be modified. Since, the spool position  $y_s$ , is related with pilot pressure  $\Delta P_{ab}$  over a low pass filter, the Eq. (5-71) defining a static relationship between orifice opening and the pressure difference  $\delta u_{va} = (\delta P_b - \delta P_a)A_s/k_s$  is not valid. Therefore, by using the direction definitions given in Figure 3-9, the variation of orifice openings,  $\delta u_{va}$  and  $\delta u_{vb}$ , are directly related with the variation of spool positions,  $\delta y_s$  as follows.

$$\delta u_{va} = -\delta y_s \quad (5-84)$$

$$\delta u_{vb} = \delta y_s \quad (5-85)$$

The new linearized shuttle valve flow rate is written as follows.

$$\delta Q_{a \rightarrow c} = K'_{a1} \delta P_a + K'_{a2} (-\delta y_s) \quad (5-86)$$

where, the flow gains  $K'_{a1}$  and  $K'_{a2}$  that are calculated for the operating point,  $\Delta P_{ab_{eq}}$  and  $\Delta P_{a_{eq}}$  are given as follows.

$$K'_{a1} = C_d \sqrt{\frac{2}{\rho}} \left( \frac{1}{2 \sqrt{|\Delta P_{aeq}|}} A_{va_{eq}} \right) \quad (5-87)$$

$$K'_{a2} = C_d \sqrt{\frac{2}{\rho}} n_h 2 |r_h \sin(\theta_{aeq})| \sqrt{|\Delta P_{aeq}|} \operatorname{sgn}(\Delta P_{aeq}) \operatorname{Cond}_h \quad (5-88)$$

Since the orifice opening is defined as  $\delta u_{va} = -\delta y_s$ , instead of  $\delta u_{va} = (\delta P_b - \delta P_a)A_s/k_s$ , the new flow coefficients  $K'_{a1}$  and  $K'_{a2}$  are found by removing the  $A_s/k_s$  terms in the previous coefficient equations (5-73) and (5-74) which are for  $K_{a1}$  and  $K_{a2}$ , respectively.

Similarly the linearized shuttle valve flow rate  $Q_{b \rightarrow c}$  is re-written as follows.

$$\delta Q_{b \rightarrow c} = K'_{b1}(\delta y_s) + K'_{b2} \delta P_b \quad (5-89)$$

where, the gains  $K'_{b1}$  and  $K'_{b2}$  are calculated as follows,

$$K'_{b2} = C_d \sqrt{\frac{2}{\rho}} \left( A_{vb_{eq}} \frac{1}{2 \sqrt{|\Delta P_{beq}|}} \right) \quad (5-90)$$

$$K'_{b1} = C_d \sqrt{\frac{2}{\rho}} n_h 2 |r_h \sin(\theta_{beq})| \sqrt{|\Delta P_{beq}|} \operatorname{sgn}(\Delta P_{beq}) \operatorname{Cond}_h \quad (5-91)$$

Since the orifice opening is defined as  $\delta u_{vb} = \delta y_s$ , instead of  $\delta u_{vb} = (\delta P_a - \delta P_b)A_s/k_s$ , the new flow coefficients  $K'_{b1}$  and  $K'_{b2}$  are found by removing the  $A_s/k_s$  terms in the previous coefficient equations (5-76) and (5-77), written for  $K_{b1}$  and  $K_{b2}$ , respectively.

Similar to the previous linearization case which is given in Section 5.5.2, the equilibrium angles  $\theta_{aeq}$ ,  $\theta_{beq}$  and the orifice areas  $A_{va_{eq}}$ ,  $A_{vb_{eq}}$  given in Eqs. (5-87) – (5-91) are calculated for a given operating point  $\Delta P_{aeq}$ ,  $\Delta P_{beq}$ . Given

that,  $\Delta P_{ab_{eq}} = \Delta P_{a_{eq}} - \Delta P_{b_{eq}}$ , first the related orifice opening is found by using the Eqs. (5-15)–(5-18), then, the angle  $\theta_{v_{eq}}$  and the orifice area  $A_{v_{eq}}$  is calculated by using Eqs. (5-19) and (5-20).

It should be noted that, the coefficient equations given above are valid for all possible pressure intervals. However, for some pressure intervals, the following comments can be applied in order to avoid the computational effort of the angle  $\theta_{v_{eq}}$  and the orifice area  $A_{v_{eq}}$ .

In the calculation of flow coefficients  $K'_{a1}$  and  $K'_{b2}$ , the orifice area  $A_{v_{eq}}$  can be directly found as follows.

- For  $\Delta P_{ab_{eq}} \geq \Delta P_{uB_{Max}}$  and  $\Delta P_{ab_{eq}} \leq \Delta P_{uA_{Max}}$ , the related orifice is fully opened, therefore  $A_{v_{eq}} = A_{v_{Max}}$ .
- For  $\Delta P_{ab_{eq}} \leq \Delta P_{uB_0}$  and  $\Delta P_{ab_{eq}} \geq \Delta P_{uA_0}$  the related orifice is closed, therefore,  $A_{v_{eq}} = 0$ .
- For  $-P_{sc} \leq \Delta P_{ab_{eq}} \leq P_{sc}$  the spool is centered, therefore,  $A_{v_{eq}} = A_{v_0}$ .

Similarly, there is no need to calculate the angle  $\theta_{v_{eq}}$  shown in flow coefficients  $K'_{a2}, K'_{b1}$  for all pressure intervals. The flow coefficients, can be directly equated to zero,  $K'_{a2} = K'_{b1} = 0$ , in the below defined conditions.

- For  $\Delta P_{ab_{eq}} \geq \Delta P_{uB_{Max}}$  and  $\Delta P_{ab_{eq}} \leq \Delta P_{uA_{Max}}$ , the related orifice is fully opened, therefore Eq. (5-20) gives  $\theta_{v_{eq}} = \pi$ .
- For  $\Delta P_{ab_{eq}} \leq \Delta P_{uB_0}$  and  $\Delta P_{ab_{eq}} \geq \Delta P_{uA_0}$  the related orifice is closed, therefore, Eq. (5-20) gives  $\theta_{v_{eq}} = 0$ .
- For  $-P_{sc} \leq \Delta P_{ab_{eq}} \leq P_{sc}$  the spool is centered,  $\theta_{v_{eq}}$  has a finite value, however since  $\delta A_v = 0$ , by definition given in Eq.(5-68) the condition operator  $\text{Cond}_h = 0$ .

Using the new linearized flow coefficients and the equation of motion of the spool the state space representation of the system is written as follows.

$$\begin{bmatrix} \delta \dot{v}_A \\ \delta \dot{P}_a \\ \delta \dot{P}_b \\ \delta \dot{y}_s \end{bmatrix} = \begin{bmatrix} \frac{-b}{m} & \frac{A}{m} & \frac{-\alpha A}{m} & 0 \\ \frac{-A}{C_a} & \frac{-K'_{a1}}{C_a} & 0 & \frac{K'_{a2}}{C_a} \\ \frac{\alpha A}{C_b} & 0 & \frac{-K'_{b2}}{C_b} & \frac{-K'_{b1}}{C_b} \\ 0 & \frac{A_s}{k_s T_{sv}} & \frac{-A_s}{k_s T_{sv}} & \frac{-1}{T_{sv}} \end{bmatrix} \begin{bmatrix} \delta v_A \\ \delta P_a \\ \delta P_b \\ \delta y_s \end{bmatrix} + \begin{bmatrix} \frac{-1}{m} & 0 \\ \frac{D_p}{C_b} & 0 \\ 0 & \frac{-D_p}{C_b} \\ 0 & 0 \end{bmatrix} \begin{bmatrix} \delta F_L \\ \delta \omega \end{bmatrix} \quad (5-92)$$

As a conclusion, by neglecting the spool dynamics, the effect of spool structure i.e. underlap/overlap values on the system stability can be investigated, by checking the eigenvalues of the state matrix given at Eq. (5-81). On the other hand, in order to investigate the effect of the spool dynamics on system stability the eigenvalues of the state matrix given at Eq. (5-92) can be checked.

## 5.7 Numerical Stability Analysis Program

The numerical stability analysis model is shown schematically in Figure 5-23. The input of the program is the desired actuator velocity array,  $v_A \in [v_{Min}, v_{Max}]$ , and the pilot pressure array,  $\Delta P_{ab} \in [\Delta P_{abMin}, \Delta P_{abMax}]$ , together with the system parameters.

The shuttle valve related variables are function of  $\Delta P_{ab}$  only. Therefore for each  $\Delta P_{ab}$  input, orifice openings, orifice area, and hydraulic conductance of the two metering orifices are calculated, based on the equations that given in Sections 5.1.1 and 5.1.2. The calculated, hydraulic conductance values are utilized in the inverse model. For each  $v$ ,  $\Delta P_{ab}$  input set, the corresponding relative chamber pressures  $\Delta P_a$  and  $\Delta P_b$  are calculated, based on the inverse model given in Section 5.3. After finding the relative chamber pressures, the linearized shuttle valve flow coefficients are found. If the shuttle valve is assumed as ideal, then the coefficients defined in the flow equations (5-72) and (5-75) are calculated. On the other hand if the shuttle valve dynamics is considered, then the coefficients of the linearized flow equations (5-86) and (5-89) are calculated. In the next step, the related state matrix is formed and the eigen values are check, by using the system parameters and the flow coefficients. In the last step, the equilibrium points are plotted on the  $\Delta P_L - v_A$  and  $\Delta P_{ab} - v_A$  plane.

The stable equilibrium points are shown with cyan colored dot markers, while the unstable equilibrium points are shown with red colored star markers. A secondary orifice opening axis is included into the  $\Delta P_{ab} - v_A$  plane, in order to show the direct relation between the spool opening and the instability region.

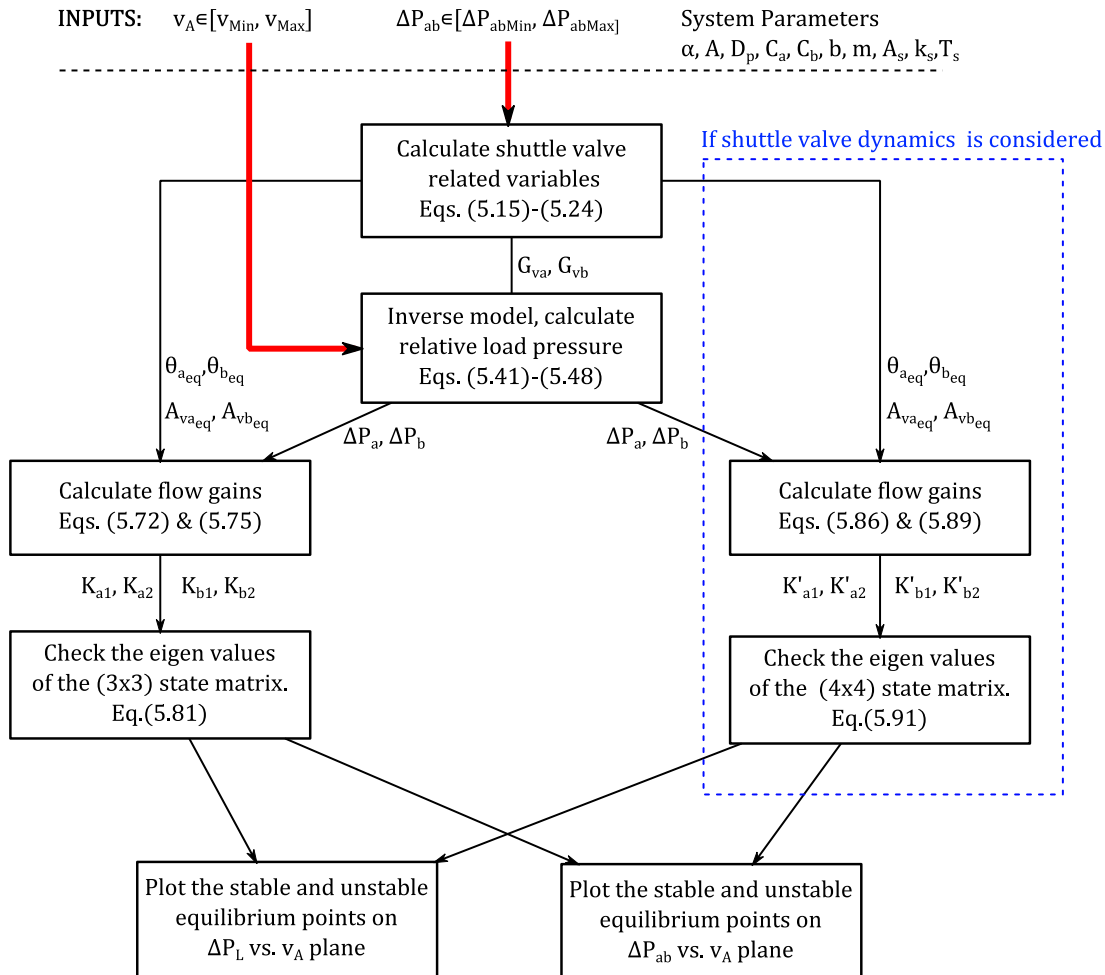


Figure 5-23 Structure of the numerical stability analysis program

By using the numerical stability analysis model several spool structures is analyzed. When running the numerical model, only the shuttle valve spool related parameters are changed and the remaining system parameters are kept constant. The system parameters used in the numerical model, i.e. actuator piston area  $A$ , actuator area ratio  $\alpha$ , pump displacement  $D_p$ , and hydraulic fluid density  $\rho$ , are given in Table 5-1. These parameters are related with the kinematic model. The remaining system parameters required for the dynamic model is given in Table 5-6.

**Table 5-6 System parameters used in dynamic modeling**

Shuttle valve design parameters			
$m$	Hydraulic actuator moving mass	9.36	$kg$
$b$	Hydraulic actuator viscous friction coefficient	6.3	$Ns/mm$
$y_{A_{in}}$	Operating point of the hydraulic actuator	0.75	$mm$
$E$	Bulk modulus	1100	$MPa$
$T_{sv}$	Spool time constant	$1 \cdot 10^{-3}$	$s$
Calculated parameters			
$C_a$	cap-side chamber capacitance	302.5	$mm^3/MPa$
$C_b$	rod-side chamber capacitance	238.2	$mm^3/MPa$

In all numerical stability analysis the input velocity array is formed in between  $[-500,500] mm/s$ . The electro hydraulic actuator used in this thesis is designed for  $\pm 200 mm/s$  velocity interval. Therefore physically, it cannot achieve the input velocity array limits. The higher velocity limits are selected in the in order to see the behavior of the instability region. The array of the difference of the chamber pressures is selected to cover the all possible orifice opening arrangements. Therefore the input pressure array is selected to be  $[\Delta P_{uA_{Max}}, \Delta P_{uB_{Max}}] \cdot 1.5$ .

### 5.7.1 Underlapped Shuttle Valve

The numerical stability analysis model is first used to investigate the underlapped shuttle valve. The underlapped shuttle valve has pre openings on both AC and BC ports, and is investigated in section 5.3.1. The same shuttle valve parameters given in Table 5-2 are used in the numerical stability analysis model. The stable and unstable operating points are shown in  $\Delta P_{ab} - v_A$  and  $\Delta P_L - v_A$  plane given in Figure 5-25, and Figure 5-24, respectively. Furthermore, test points used in section 5.3.1 are also plotted on the two figures.

In Figure 5-25 it is clearly seen that the equilibrium points that corresponds to the centered and fully opened spool positions are stable, cyan colored dot markers. However, the partially opened spool positions are unstable, red colored star markers. The instability region depends on the actuator velocity, as well as orifice openings. For the extension of the actuator  $v_A > 0$ , the equilibrium points are unstable only for

a limited opening on the AC port. However, for the retraction of the actuator  $v_A < 0$ , the equilibrium points are unstable for all partially opened spool positions.

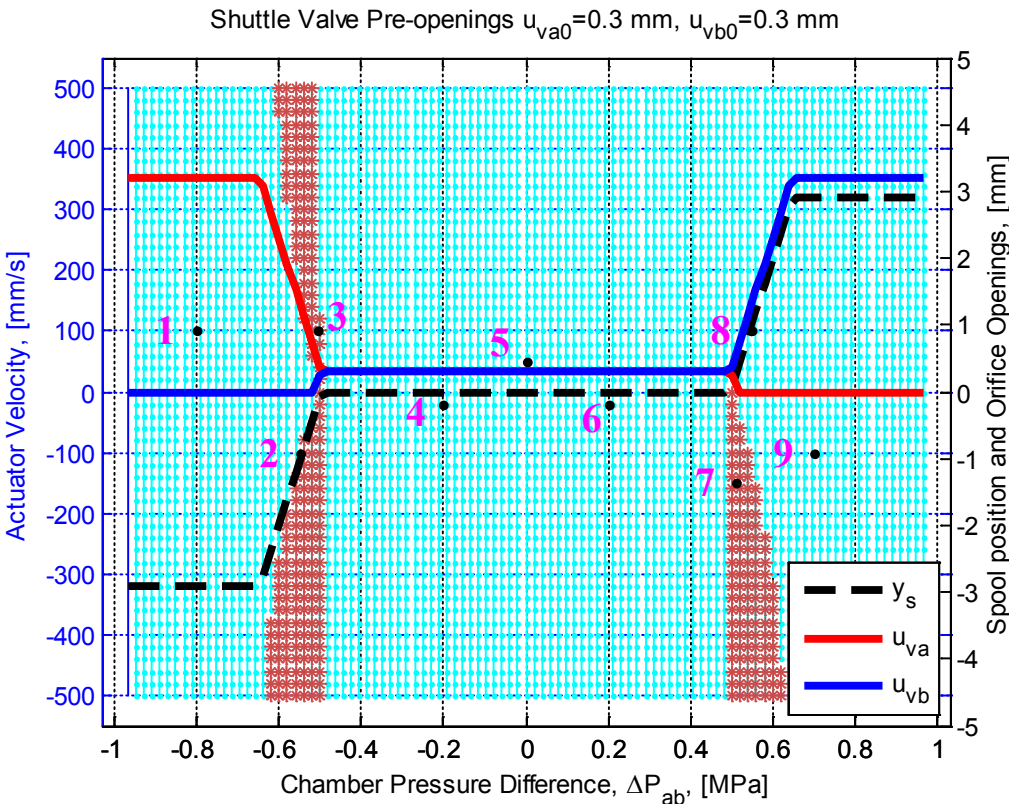
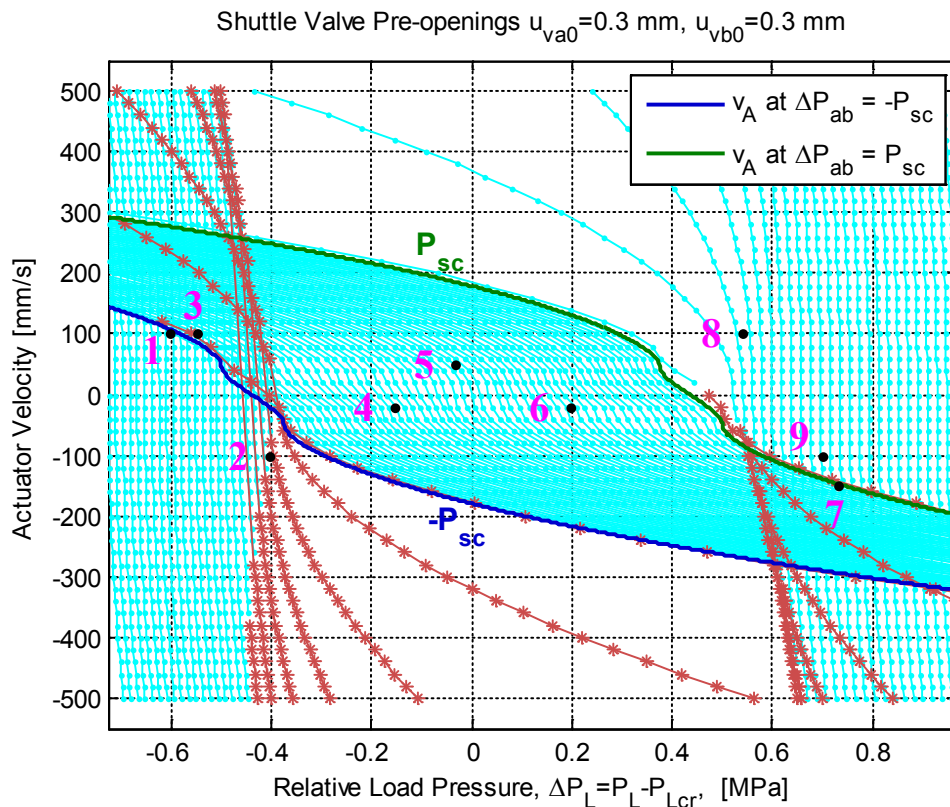


Figure 5-24 Stability of the underlapped shuttle valve on  $\Delta P_{ab} - v_A$  plane

In Section 5.3.1, the non-linear simulation model developed in MATLAB<sup>®</sup>/SimHydraulics<sup>®</sup> is used to investigate the system response, at the given test points. In Figure 5-25 it is seen that the 2<sup>nd</sup>, 3<sup>rd</sup> and 7<sup>th</sup> test points are located inside the instability region. However, in Section 5.3.1 it is shown with the simulation response that, only the 2<sup>nd</sup> test point is unstable, while the 3<sup>rd</sup> and 7<sup>th</sup> points are stable but achieved, with a different pump speed and spool opening than the calculated ones with the inverse model. The non-bijective relation between the pilot pressure and the actuator velocity is shown in Figure 5-18. This behavior can be well understood if the stability region on  $\Delta P_L - v_A$ , which is given in Figure 5-24, is investigated. The points on this plane are found by mapping the  $\Delta P_{ab}$  and  $v$  input arrays to the  $\Delta P_L$  and  $v_A$ , through the inverse model.



**Figure 5-25 Stability of the underlapped shuttle valve on  $\Delta P_L - v_A$  plane**

In Figure 5-24, it is seen that for the centered and fully opened spool positions the mapping is one to one. However, some of the  $\Delta P_{ab}$  points that correspond to partially opened spool positions are mapped to the same  $\Delta P_L$  region that corresponds to the fully opened spool position. In those overlapped region there exists a non-bijective  $\Delta P_{ab} - v_A$  relation. This means that an equilibrium speed  $v_{Aeq}$  under an equilibrium load  $p_{Leq}$  can be achieved by two different spool positions. The 3<sup>rd</sup> and 7<sup>th</sup> test points are located in such an overlapped region. In  $\Delta P_{ab} - v_A$  plane these two points corresponds to partially opened spool position and are seen to be unstable. However, in  $\Delta P_L - v_A$  plane, it is seen that the two test points can also be achieved by the fully opened spool position which is stable. The same relation is not true for the 2<sup>nd</sup> test point. This point cannot be achieved by fully opening the spool. In Figure 5-24, it is seen that the 2<sup>nd</sup> test point is located at the pure instability region.

### 5.7.2 Asymmetric Spool Shuttle Valve

The circulating leakage flow rates of the underlapped shuttle valve are eliminated by modifying the shuttle valve spool. In section 5.4 it is proposed to provide a spool underlap at BC port and zero underlap at AC port. In the non-linear simulation model responses it is seen that the circulating leakage flow rates are eliminated. Furthermore, different from the underlapped valve no instability is observed at the partially opened spool position. In the numerical stability analysis model the same shuttle valve parameters given in Table 5-4 are used. The stable and unstable operating points are shown in  $\Delta P_{ab} - v_A$  and  $\Delta P_L - v_A$  plane given in Figure 5-26 and Figure 5-27, respectively. Furthermore, test points used in section 5.4 are also plotted on the two figures.

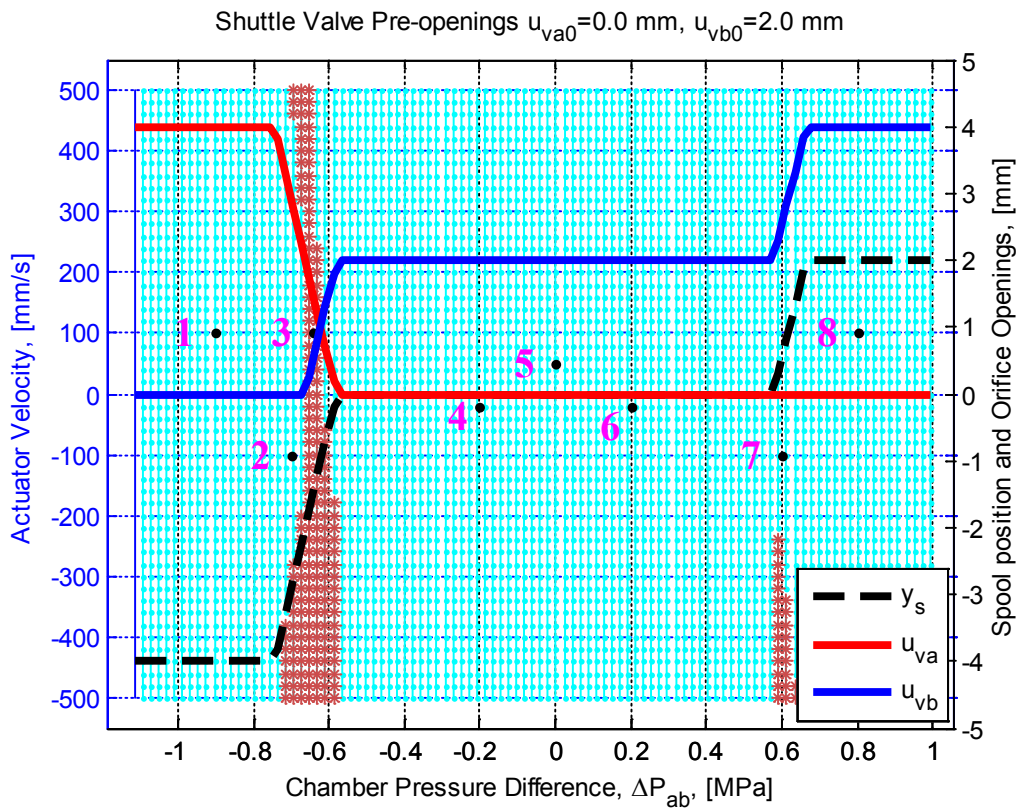


Figure 5-26 Stability of the asymmetric shuttle valve on  $\Delta P_{ab} - v_A$  plane

In Figure 5-26, unstable operating points, red colored star markers, are seen for a range of partially opened orifice openings. The instability at port AC is much higher than at BC, where instability is seen only at high retraction speeds for a small range of spool position.

By using the inverse model the input  $\Delta P_{ab}$  and  $v_A$  points are mapped on the  $\Delta P_L - v_A$  plane and is given in Figure 5-27. When compared with the underlapped spool case, in this proposed solution, the pure instability region in  $\Delta P_L - v_A$  plane is removed. On the  $\Delta P_L - v$  plane there exists no operating point that can only be achieved by a partially opened orifice opening.

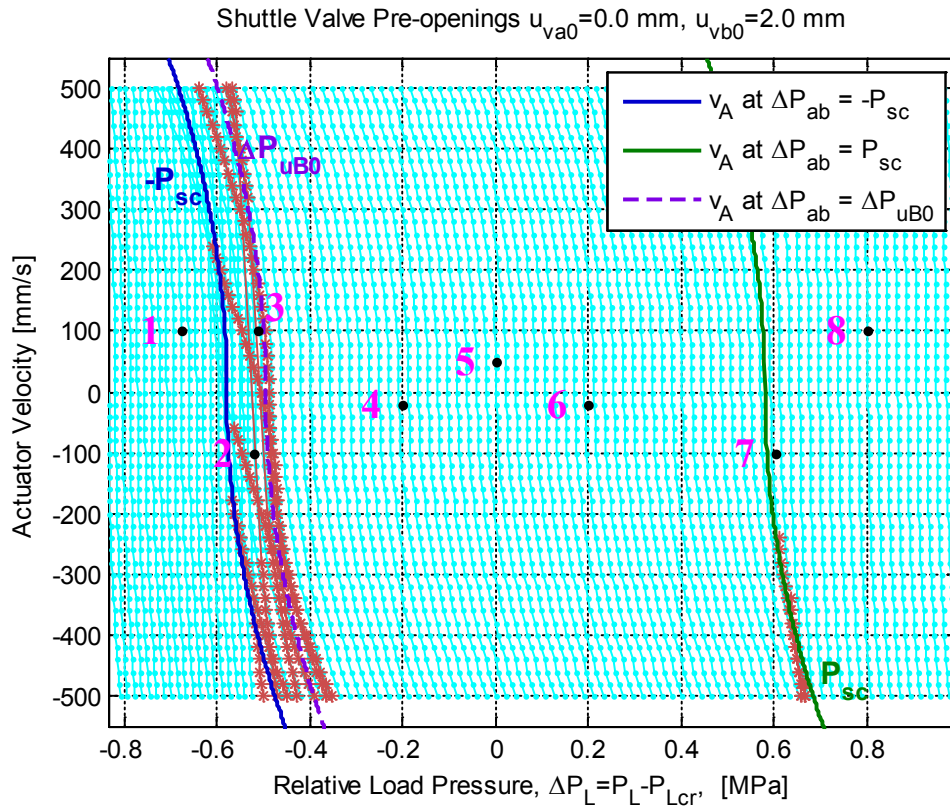


Figure 5-27 Stability of the asymmetric shuttle valve on  $\Delta P_L - v_A$  plane

The unstable equilibrium points on  $\Delta P_{ab} - v_A$  plane are seen for the partially opened orifice case. In section 5.4 it is mentioned at partially opened spool position, the function between the  $\Delta P_{ab}$  and  $v_A$  is non-bijective i.e., an equilibrium point defined by  $[\Delta P_L, v_A]$  can be satisfied by different spool positions or  $\Delta P_{ab}$  value. Due to this property, the unstable equilibrium points are overlapped on the stable equilibrium points found for fully opened spool position. This region is roughly in between the blue line and purple lines, that represents the actuator velocity calculated for valve cracking pressure  $\Delta P_{ab} = -P_{sc}$  and orifice opening pressure,  $\Delta P_{ab} = \Delta P_{uB0}$ , respectively.

On  $\Delta P_{ab} - v_A$  plane it is seen that 3<sup>rd</sup> test point corresponds to partially opened spool position and is unstable. However, on  $\Delta P_L - v_A$  plane this point is located at the overlapped mapping region. Therefore, the desired speed and load pressure defined by the 3<sup>rd</sup> test point is achieved by fully opening the spool and which is stable. The 2<sup>nd</sup> test point is not located at the instability region on  $\Delta P_{ab} - v_A$  plane, however it corresponds to the overlapped mapping region of  $\Delta P_L - v_A$  plane. Therefore, the 2<sup>nd</sup> test point speed is achieved, for the fully opened spool position, rather than the calculated partially opened spool position, and is also stable.

It can be concluded that, besides eliminating the circulating leakage flow rate and dead pump speeds, the proposed asymmetric shuttle valve spool solution is superior to the underlapped valve, since it eliminates the pure instability region on  $\Delta P_L - v_A$  plane.

## 5.8 Second Shuttle Valve Solution and Comments on Stability

In the previous sections, it is shown that the underlapped valve have unstable equilibrium points, corresponding to particular chamber pressure ranges, where the metering orifices are partially opened. Besides, eliminating the dead pump speed, and circulating leakage flow rates, the proposed shuttle valve spool solution, with pre-opening at BC port  $u_{vb_0} > 0$ , and zero opening at AC port  $u_{va_0} = 0$ , solves the instability problem. The numerical stability analysis reveals that the equilibrium points corresponding to partially opened orifice openings are unstable. However, these equilibrium points can be achieved, by a different spool opening, due to the non-bijective relationship between  $\Delta P_{ab}$  and  $v_A$ . The non-bijective mapping between the  $\Delta P_{ab} - v_A$  and  $\Delta P_L - v_A$  planes can be seen as a benefit. However, it is problematic in control perspective. The feedforward motor speed cannot be calculated, if the spool position is not known. When compared with the whole operation region of the actuator, the region that requires a partially opened orifice opening is relatively small. However, it is certain that the spool is passing from this region while moving from one end position to the other end position. During this transition, undesired velocity oscillations occur.

Therefore, in this section it is aimed to find a shuttle valve solution, that will provide a stable operation region as well as will provide a one to one mapping between the  $\Delta P_{ab} - v_A$  and  $\Delta P_L - v_A$  planes.

In this section the effects of several shuttle valve parameters on system stability will be shown by using the numerical stability analysis program developed in section 5.7. The shuttle valve parameters that will be used in this section are given in Table 5-4, some of these parameters are selected as design parameters and changed during the analysis. The design parameters that will be investigated are listed as follows.

- Orifice pre-openings,  $u_{va_0}$  and  $u_{vb_0}$
- Spool time constant,  $T_{sv}$
- Flow discharge coefficient,  $C_d$
- Pilot pressure sensitive surface area  $A_s$
- Spring stiffness,  $k_s$

During the iteration running on the developed numerical stability analysis model, it is observed that the non-bijective relation highly depends on the pre-compression force of the spool centering springs. Therefore the pre-compression force is removed, i.e., the cracking pressure is zero,  $P_{sc} = 0$ . Furthermore, a spool underlap that corresponds to the half of the maximum orifice is provided both at the AC and BC ports.

The resulting orifice openings and spool positions are shown in Figure 5-28-(a). It is seen that the orifice openings  $u_{va}$  and  $u_{vb}$  are symmetry according to pilot pressure,  $\Delta P_{ab}$  and spool position,  $y_s$  axes. When the operating points on the  $\Delta P_{ab} - v_A$  plane are mapped on the  $\Delta P_L$  plane as shown in Figure 5-28-(b), no overlapping occurs, i.e. the function between  $\Delta P_{ab}$  and  $v_A$  are bijective. This spool configuration satisfies one to one mapping between the two planes, however, it suffers from the instability region, which is relatively high when compared with the previous solutions.

As the next step, the effect of spool dynamics on system stability is shown by assuming the spool is ideal. Note that since the shuttle valve dynamics is neglected, the stability analysis program uses the 3x3 state matrix defined in (5-81). The resulting stability region is given in Figure 5-28-(c) on  $\Delta P_L - v_A$  plane. When compared with the sub figure (a), with time constant 1ms, it is seen that the instability region is increased up to 500 mm/s extension speeds, moreover, during the retraction of the actuator  $v_A < 0$ , most of the operating points that corresponds to partial orifice opening became unstable. Similarly, Figure 5-28-(d) is drawn, with time constant  $T_{sv} = 0.5 \text{ ms}$ , it is seen that the instability region is reduced with respect to ideal shuttle valve. However, it should be noted that there is not a proportional relation between the spool time constant and stability. The stability region of a shuttle valve with time constant of  $T_{sv} = 10 \text{ ms}$  is also similar to the region satisfied by the shuttle valve with 1ms time constant as shown in sub figure (b). Increasing the time constant is not a solution for the stability problem. Therefore, the effects of the orifice openings are investigated.

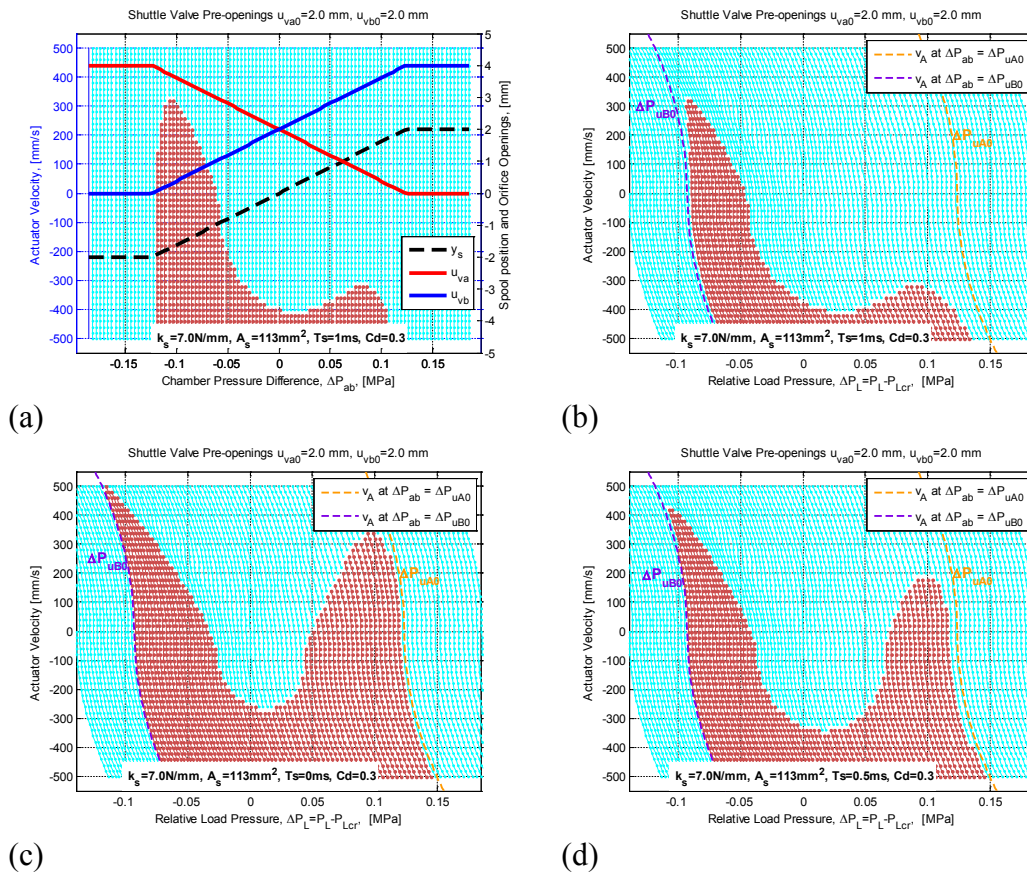


Figure 5-28 Shuttle Valve without spring pre load, and effect of time constant

The stability is directly related with the orifice openings. In the spool configuration given in Figure 5-29-(a), the spool underlap is decreased both at AC and BC ports,  $u_{va} = 1 \text{ mm}$  and  $u_{vb} = 1 \text{ mm}$  respectively. Figure 5-29-(a) & (b), it is seen that providing a small spool underlap decreases the instability region. However, different from the symmetric orifice opening structure, it is seen that the operating points are overlapped, when mapped on the  $\Delta P_L - v_A$  plane, as shown in Figure 5-29-(b). However, this non-bijective property is seen at high velocities,  $v_A > 300 \text{ mm/s}$ . As a next step, the orifice opening is further reduced,  $u_{va} = 0.5 \text{ mm}$  and  $u_{vb} = 0.5 \text{ mm}$ . The resulting stability region is shown in  $\Delta P_{ab} - v_A$  and  $\Delta P_L - v_A$  planes in In Figure 5-29-(c) and (d), respectively. It is seen that the sized of both the instability region and the overlapped mapping region is increased. This result shows that a stable operation region cannot be achieved by just decreasing the orifice pre-openings.

The flow discharge coefficient is an important parameter that defines the hydraulic conductance. Throughout this thesis study the flow discharge coefficient is taken as constant, and its value is found from  $P - Q$  diagram supplied by the manufacturer. During the orifice opening, the value of flow coefficient may differ from the one calculated for fully opened spool position. Therefore, its effect on stability is investigated by changing its value two times.

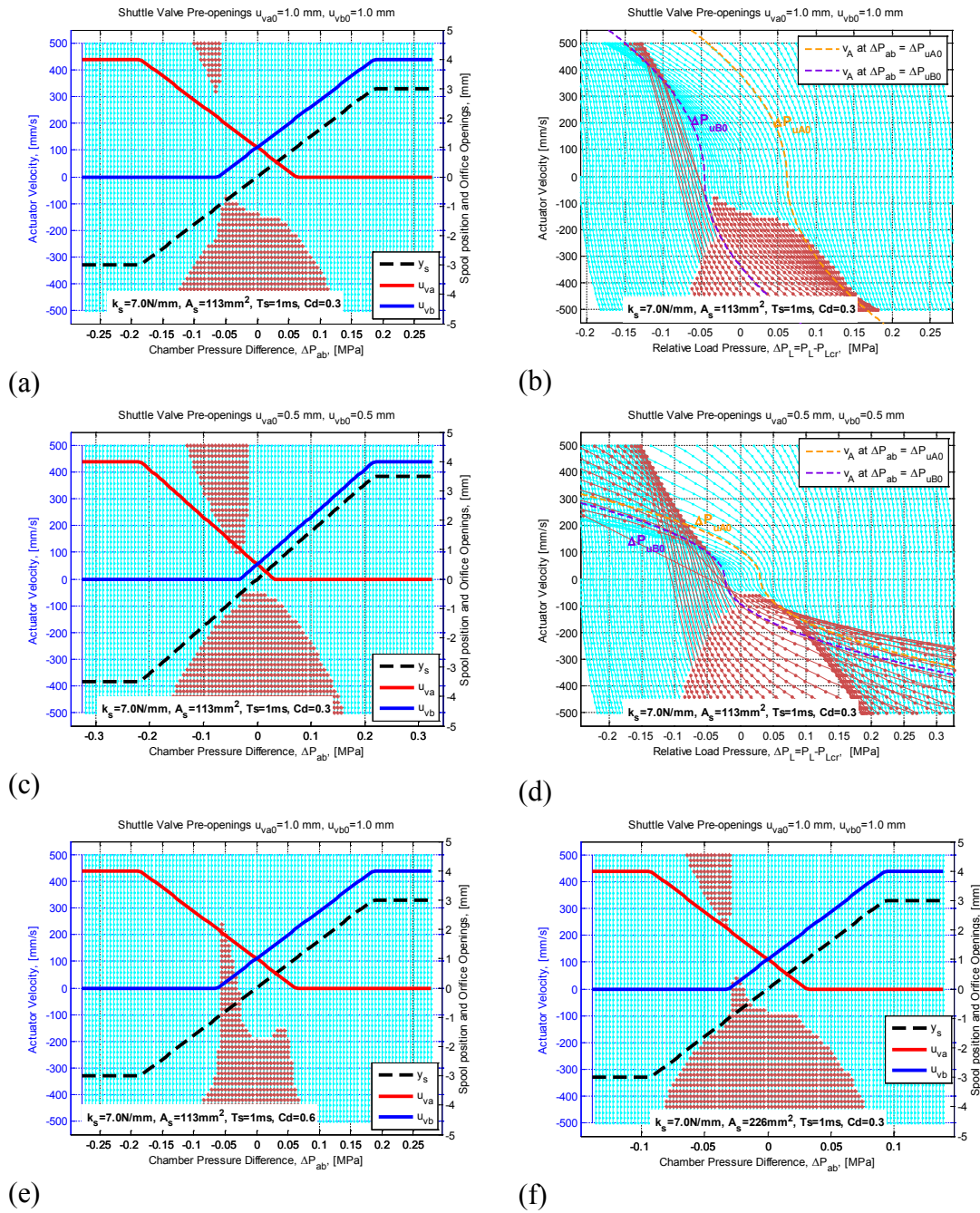


Figure 5-29 Stability relations of orifice opening, flow coefficient and pilot area

The stability region for the flow coefficient  $C_s = 0.6$  is given in Figure 5-29-(e). When compared with sub figure (a), which has  $C_d = 0.3$  and the same orifice pre-openings, it is clearly seen that, the size of instability region is increased, especially in the pressure interval that corresponds to opened AC orifice. Similar to discharge coefficient, the pilot pressure sensitive surface area of the spool  $A_s$ , adversely affects the stability. Increasing the pilot area, two times increases the instability region as shown in Figure 5-29-(f).

Different from the discharge coefficient  $C_d$  and surface area  $A_s$ , the spring stiffness positively affects the stability. This is an expected result, unlike pilot area  $A_s$ , the stiffness  $k_s$  term appears at the denominator of the equation, that defines the relation between the orifice opening and pilot pressures.

In Figure 5-30, the stable operation region that can be achieved by increasing the spring stiffness 2.5 times is shown. The orifices pre-openings are taken to be  $u_{va0} = u_{vb0} = 1 \text{ mm}$ , and all the other parameters are the same with the valve configuration given in Figure 5-29-(a). It is seen that instability is eliminated up to  $300 \text{ mm/s}$  retraction speed. Furthermore, the roughly below  $300 \text{ mm/s}$  extension speeds, there exist a one to one mapping between the  $\Delta P_L - v_A$  and  $\Delta P_{ab} - v_A$  planes.

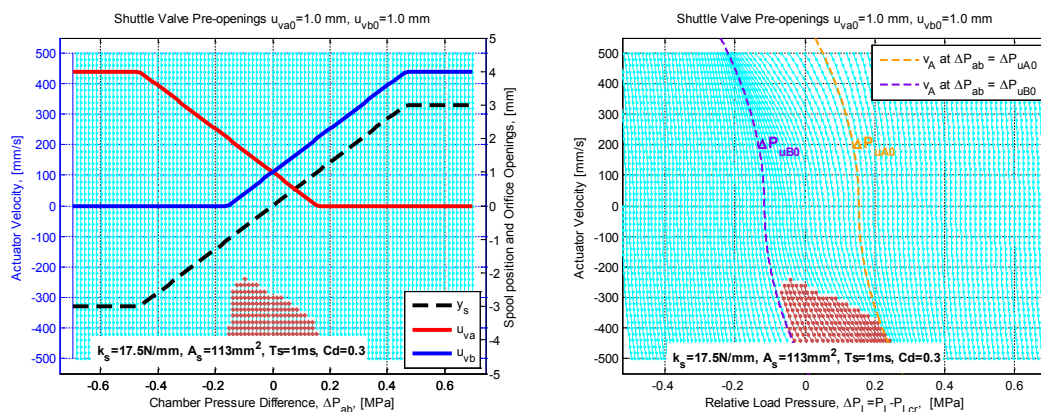


Figure 5-30 Proposed shuttle valve solution, the spring pre-loading is removed, and the stiffness is increased.

## 5.9 The Proposed Shuttle Valve Solutions

The two shuttle valve solutions, proposed in this chapter are shown in Figure 5-31. The two solutions are realized by the modification of closed center Bucher Hydraulics shuttle valves. The parameters of this valve are given in Table 5-4. The spool shown at the top is the asymmetric spool structure proposed in section 5.4. The spool is modified to provide 2 mm pre-opening between B-C ports, and A-C port is closed. On the other hand, the spool shown at the bottom is the one that is proposed in section 5.8. Both the AC and BC ports are modified to have a 1.5 mm pre-opening. Furthermore, the pre-compression force of the centering spring is removed and stiffness is increased by shortening the spring length.



**Figure 5-31 Proposed shuttle valve spool structures, a-) AC port underlapped, BC port closed, b-) spring pre-load removed, AC and BC ports are underlapped**

In the experimental performance tests only the spool shown at the top is implemented. The spool solution shown at the bottom cannot be implemented due to practical reasons. In the last spool solution, the desired spring stiffness cannot be achieved by just shortening the original valve spring. Therefore, it is decided to replace the spring and increase the wire diameter. However, a backlash free spring valve arrangement assembly cannot be succeeded; furthermore, the increased wire

diameter resulted in assembly problems at the valve heading. Therefore, although the last solution is superior to the first one, it is not implemented.

The hydraulic circuit solution that is implemented and tested on the experimental test set up is shown in Figure 5-32.

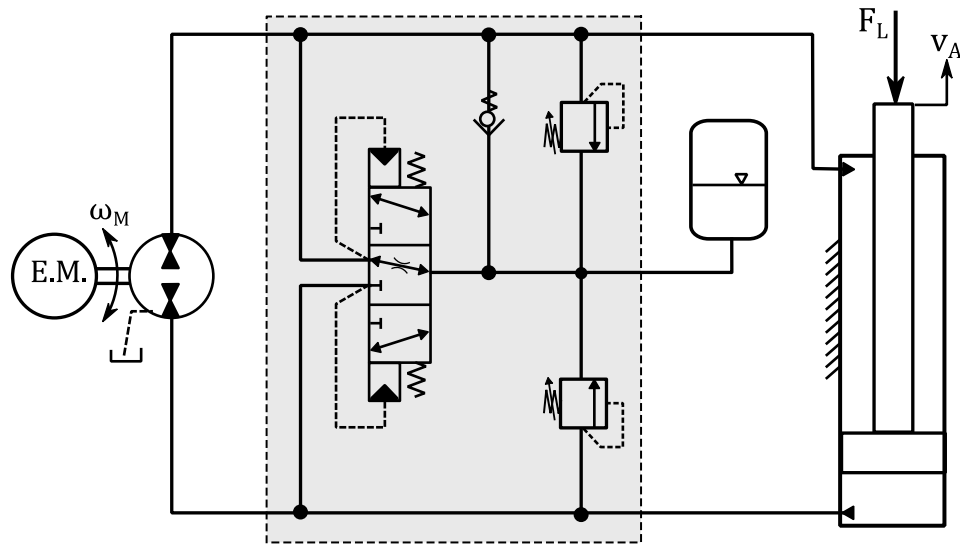


Figure 5-32 Proposed hydraulic circuit solution

## 5.10 Conclusion

In the previous chapter, as opposed to the general use of closed center shuttle valve in literature, an underlapped shuttle valve is proposed to provide a stable operation region in the critical load pressure plane. However, this valve solution leads to circulating leakage flow rates.

In this section, the deficiencies of the underlapped shuttle valve are investigated, in terms of transformer ratio and dead pump speeds. In order to make a theoretical analysis, a kinematic model, neglecting the all the dynamics of the moving masses, compressibility of the fluid, and flow losses is constructed. The pressure states are defined with respect to the accumulator pressure. In that way representation of the system equations are simplified. Furthermore, besides the cracking pressure four more pressure constants are defined, in order to determine the shuttle valve state.

Based on the kinematic model, first the transformer ratio and dead pump speeds are investigated. It is concluded that a shuttle valve with relatively high cracking pressure will be problematic since it will increase the critical load pressure region. The closed loop performance of an EHA may degrade if the load loci enter into that region, since the transformer ratio between pump speed input and actuator speed output is probable to vary between infinity or zero.

As a first solution the compensation of dead pump is proposed, which requires the knowledge of the spool position or the difference between the chamber pressures. As a second solution, elimination of the circulating leakage flow region by modifying the shuttle valve spool is proposed. The shuttle valve spool is modified to provide an orifice pre-opening only in between the AC ports. In this way, since the BC port is closed the circulating leakage flow rates are eliminated at the centered shuttle valve spool position.

The numerical simulations, which are done for the underlapped valve and asymmetric shuttle valve solution, revealed that the function between the spool position and the actuator velocity is not bijective, i.e. a desired actuator velocity can be achieved with two different spool positions. In order to investigate the effect of this non-bijective relationship, the stability analysis is extended. Different from the stability analysis given in Chapter 4, which considers the single partially opened orifice only, in this chapter the stability analysis is extended to cover all possible orifice structures, i.e. all possible spool positions. Furthermore, in the linearization of the shuttle valve flow rates, instead of assuming a proportional relation between the spool position and orifice opening, the geometric non-linearity of the metering orifices which are formed by the circular holes on the valve sleeve is considered. Lastly, besides assuming a static relationship between pilot pressure  $\Delta P_{ab}$  and spool position,  $y_s$ , the valve dynamics is also considered with a time constant. As a result, by using the kinematic model and the linearized state equations a numerical stability analysis model is developed.

The numerical stability analysis model is run for an array of pilot pressure,  $\Delta P_{ab}$ , and actuator velocity,  $v_A$ , inputs. The pilot pressure array is selected to cover all possible shuttle valve spool positions and actuator velocity array is selected to cover all

possible actuator velocities. In this numerical model first the corresponding  $[\Delta P_L, v_A]$  point is found for each  $[\Delta P_{ab}, v_A]$  input point. Then, the system is linearized around this equilibrium point and the stability is determined by checking the roots of the linearized model.

First the underlapped valve solution is investigated by this numerical stability analysis model. The results revealed that on  $\Delta P_L$  versus  $v_A$  plane an equilibrium point requiring a partially opened spool position is unstable during the retraction of the actuator. This result is consistent with the stability analysis given in the previous chapter. On the other hand numerical model further revealed that, during the extension of the actuator, the equilibrium point requiring a partially opened spool position is also unstable. However, the desired actuator velocity can be satisfied by a different spool position which correspond a stable  $[\Delta P_{ab}, v_A]$  point. The non-bijective relation between the spool position and the actuator velocity is illustrated by showing the unstable equilibrium points both on  $\Delta P_{ab} - v_A$  and  $\Delta P_L - v_A$  planes.

The stability of the asymmetric shuttle valve spool is also investigated by the numerical stability analysis model is used to investigated position. The results revealed that the equilibrium points requiring partially opened spool position are unstable. However, different from the underlapped valve solution,  $\Delta P_L - v_A$  every unstable point can be satisfied by a stable  $[\Delta P_{ab}, v_A]$  point, which corresponds to a fully opened spool position.

The numerical stability analysis model is further utilized to investigate the effects of shuttle valve parameters on stability. The simulation model is run for different orifice pre-opening, flow discharge coefficient, valve time constant and spring stiffness values. At the end of the simulations a second novel shuttle valve solution is proposed. This solution proposes to remove the pre-compression force of the centering springs and increase its stiffness and provides spool underlap both at AC and BC ports. It is shown that if the shuttle valve parameters like spring stiffness and flow coefficient are well adjusted, up to certain actuator speeds, a stable operation region can be achieved, for all possible spool openings.



## CHAPTER 6

### LINEARIZED SYSTEM MODEL

In the previous stability analysis sections, the linearized models of the EHA system are derived by considering the hydraulic pump as an ideal flow rate source, i.e. it is assumed to be driven by an ideal velocity source. Although a servo motor provides a relatively high bandwidth, in controller design model the dynamics of the servo motor has to be considered. This situation can be well understood by simply calculating the equivalent inertia of the moving mass of the hydraulic actuator. For example, the mass of the piston-rod assembly is  $9.4 \text{ kg}$ , considering the transformer ratio  $\frac{D_p}{A} = 0.45 \frac{\text{mm}}{\text{rad}}$ , the equivalent inertia of the actuator mass on the electric motor is  $m(D_p/A)^2 = 1.9 \cdot 10^{-4} \text{ kg} \cdot \text{m}^2$ , on the other hand the inertia of the rotor of the servo motor is  $27.3 \cdot 10^{-4} \text{ kg} \cdot \text{m}^2$ . In this chapter the linearized model of the whole system is derived and it is shown that the poles due to servo motor dynamics are close to the poles due to chamber pressure dynamics.

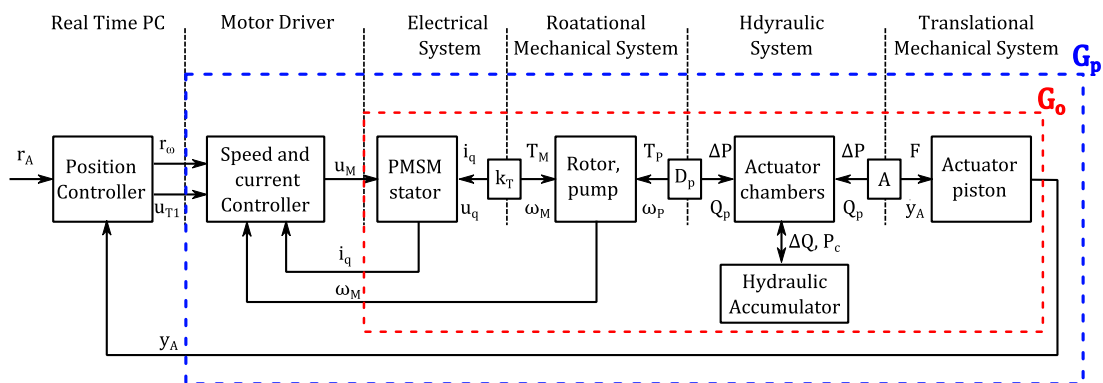


**Figure 6-1** The physical systems that constitute the EHA and their interactions

In order to give an insight into the system dynamics, the electrical, rotational mechanical, hydraulic and the translational mechanical systems are considered in the design plant model of the controller, and the state space representation of the whole

system is derived. Then, the roots related with each sub system is investigated, and the system is simplified, for the controller design.

The physical systems that constitute the EHA and their relationships are given in Figure 6-1. The control system constitutes of three parts, position, motor speed and current controllers. In the scope of this thesis study the position controller is designed and implemented on a real time PC. The motor speed and current controllers are an integral part of a servo motor. The red dashed line rectangle represents the open loop plant,  $G_o$ . The servo motor controllers can be tuned by using this plant model. On the other hand, the blue dashed line rectangle represent the design plant model,  $G_p$ , of the position controller. Note that the hydraulic accumulator includes the thermal domain, the thermal system is considered in the subsequent sections but for simplicity it is not shown in the Figure 6-1.

## 6.1 Electrical and Rotational Mechanical System

In mathematical modeling of electric motor, in section 3.2.4, it is mentioned that the 3-phase currents and voltages can be represented in an equivalent d-q axis rotor reference frame. The q-axis stator current creates reaction torque. On the other hand the d-axis current creates reluctance torque, thus, it is regulated with zero reference input. In this section, it is assumed that the d-axis current is zero, therefore the torque and current are related with a torque constant,  $T = \frac{3}{2} n_p \lambda_m i_q = k_T i_q$ . In the linearized model, the d-axis current equation (3-39) is neglected. The q-axis current equation (3-40) is re-written in terms of torque constant. The resulting state equation resembles a dc machine and written as follows.

$$L_q \frac{di_q}{dt} = u_q - R_s i_q - \frac{2}{3} k_T \omega_M \quad (6-1)$$

The electric motor and the hydraulic pump are assumed to be coupled through a rigid coupling. Therefore, the pump inertia together with the frictional losses is lumped into electric motor dynamics. The resulting torque continuity equation on the motor shaft is written as follows.

$$k_T i_q = (J'_M) \dot{\omega}_M + (b'_M) \omega_M + D_p (P_a - P_b) \cdot 10^{-3} \quad (6-2)$$

where,  $J'_M = J_M + J_P$  and  $b'_M = b_M + b_P$  are the total effective inertia and friction coefficients, respectively.

The first term of Eq. (6-2) represents the electric torque generated by the q-axis current, while the last component represents the hydraulic torque. Note that, for unit conversion purposes, the last component is multiplied by  $10^{-3}$ , since the  $D_p \Delta P$  multiplication produces torque in  $Nmm$ .

The block diagram representation of the electrical and rotational mechanical system is shown in the MATLAB<sup>®</sup>/Simulink<sup>®</sup> model as given in Figure 6-2.

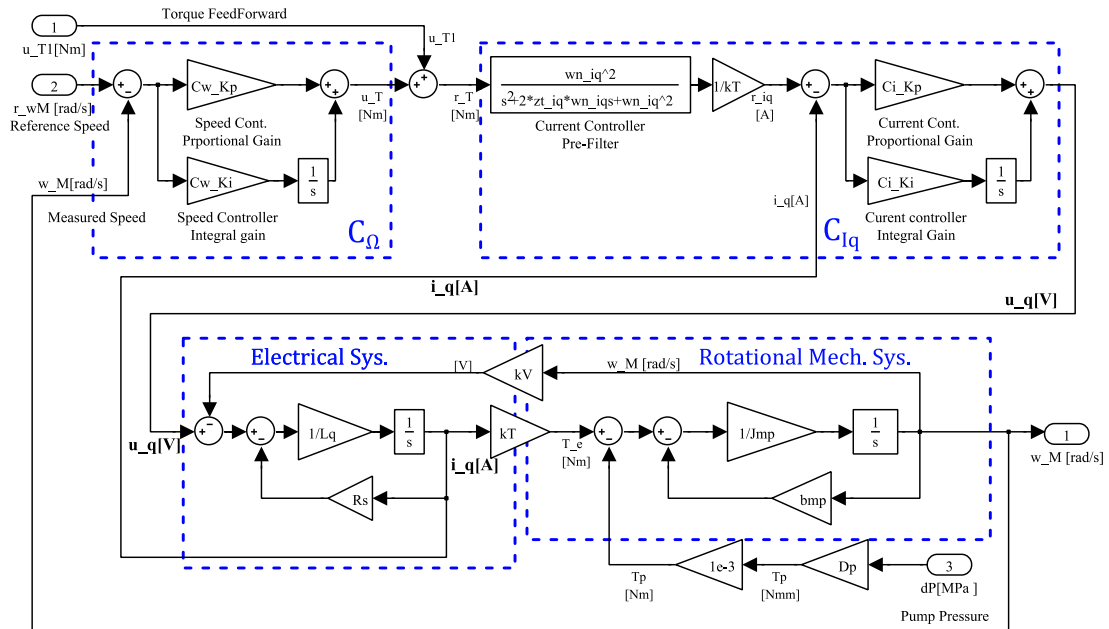


Figure 6-2 Block diagram representation of the linearized servo motor model

## 6.2 Hydraulic and Translational Mechanical System

The linearized model of the hydraulic actuator is derived in the previous chapters. In the linearized model of the actuator only the viscous type of friction is considered. Since relatively short hoses are utilized, the transmission lines are assumed to be lossless. However, in order to represent the effects of hydraulic capacitance, the transmission line volumes together with the dead volumes of the hydraulic manifold

and block are lumped into the hydraulic actuator chambers. Furthermore, in order to consider the effects hydraulic inertance, the mass of the circulating fluid, in between the pump and actuator, is lumped into the moving mass of the actuator.

The equation of motion for the actuator is written as follows,

$$m\delta\ddot{y}_A + b\delta\dot{y}_A + F_L = A(\delta P_a - \alpha\delta P_b) \quad (6-3)$$

where,

$y_A$  = actuator position, in  $mm$

$F_L$  = external load, in  $N$

The block diagram representation of the translational mechanical system is shown in the MATLAB<sup>®</sup>/Simulink<sup>®</sup> model as given in Figure 6-3.

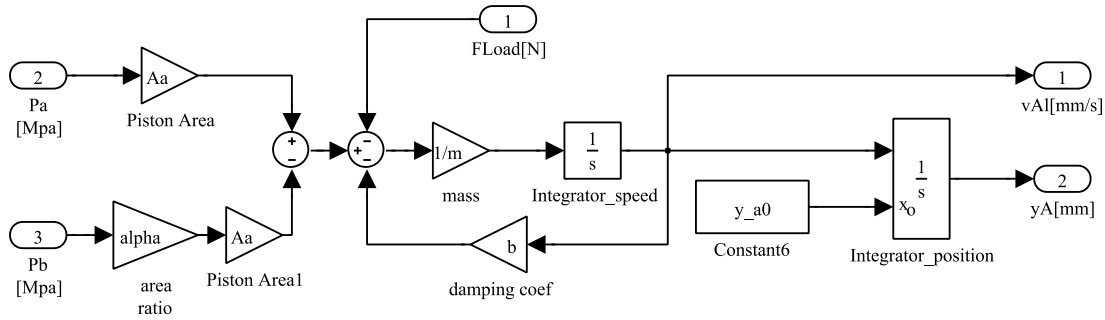


**Figure 6-3 Block diagram representation of the translational mechanical system**

The leakage flow between the actuator chambers is lumped in to the internal leakage flow of the pump. The internal and external leakage coefficients of the pump are assumed to be constant at a defined operating pressure difference.

$$C_a\delta\dot{P}_a = D_p\delta\omega_M - A\delta\dot{y}_A - H_e\delta P_a - H_i(P_a - P_b) - (K'_{a1}(\delta P_a - \delta P_c) - K'_{a2}\delta y_s) \quad (6-4)$$

$$C_b\delta\dot{P}_b = \alpha A\delta\dot{y}_A - D_p\delta\omega_M - H_e\delta P_a + H_i(P_a - P_b) - (K'_{b1}\delta y_s + K'_{b2}(\delta P_a - \delta P_c)) \quad (6-5)$$

where  $D_p$  is the pump displacement,  $H_e$  and  $H_i$  are external and internal leakage coefficients of the pump, and  $\omega_M$  is the motor speed driving the pump.

In the flow continuity equations of the hydraulic chambers, the last terms written in parenthesis represent the shuttle valve flow rates  $\delta Q_{a \rightarrow c}$  and  $\delta Q_{b \rightarrow c}$ , which are defined in Eq.(5-86) and Eq.(5-89), respectively.

Note that in the previous chapter since the accumulator pressure is assumed to be constant,  $\delta P_c = 0$ , the variation of the relative chamber pressures are assumed to be equal to the variation of chamber pressures  $\delta(\Delta P_a = P_a - P_c) = \delta P_a$  and  $\delta(\Delta P_b) = \delta P_b$ . However, in this section since the accumulator dynamics is considered,  $\delta P_c \neq 0$ . Therefore the accumulator pressure variation is also multiplied with the flow coefficients  $K'_{a1}$  and  $K'_{b2}$ .

The flow coefficients  $K'_{a1}$  and  $K'_{b2}$  are previously defined in section 5.6.2. The equation of the flow coefficients given in Eq. (5-87) and Eq. (5-90) can be considered in two parts and represented as follows.

$$K'_{a1} = G_{va}(A_{va_{eq}}) \frac{1}{2\sqrt{|\Delta P_{a_{eq}}|}} \quad (6-6)$$

$$K'_{b2} = G_{vb}(A_{vb_{eq}}) \frac{1}{2\sqrt{|\Delta P_{b_{eq}}|}} \quad (6-7)$$

The first part is the hydraulic conductance calculated at an equilibrium orifice area  $A_{v_{eq}}$ , and the second part is the gain calculated at the operating pressure. In Section 5.6.2, the calculation procedure of the orifice area for a given operating point  $P_{a_{eq}}$  and  $P_{b_{eq}}$  is explained. Furthermore, it is mentioned that for certain pressure intervals, that corresponds to fully opened/closed or centered spool positions there is no need to calculate the orifice area, since it is constant and known. For completeness these conditions are given in terms of hydraulic conductance as follows.

$$G_{va} = \begin{cases} G_{vaMax} & \text{for } \Delta P_{ab} \leq \Delta P_{uAMax} \\ G_{va0} & \text{for } -P_{sc} \leq \Delta P_{ab} \leq P_{sc} \\ C_d \sqrt{\frac{2}{\rho}} A_{vaeq} & \text{for } \Delta P_{uAMax} < \Delta P_{ab} < \Delta P_{uA0} \\ 0 & \text{for } \Delta P_{ab} \geq \Delta P_{uA0} \end{cases} \quad (6-8)$$

$$G_{vb} = \begin{cases} 0 & \text{for } \Delta P_{ab} \leq \Delta P_{uB0} \\ C_d \sqrt{\frac{2}{\rho}} A_{vbeq} & \text{for } \Delta P_{uB0} < \Delta P_{ab} < \Delta P_{uBMax} \\ G_{vb0} & \text{for } -P_{sc} \leq \Delta P_{ab} \leq P_{sc} \\ G_{vbMax} & \text{for } \Delta P_{ab} \geq \Delta P_{uBMax} \end{cases} \quad (6-9)$$

Similarly, in Section 5.6.2 it is mentioned that, there is no need to calculate the flow coefficients,  $K'_{a2}$  and  $K'_{b1}$ , at all pressure intervals since, the coefficient will be zero if the spool is centered, or fully opened/closed. For completeness, the coefficients are given as follows.

$$K'_{a2} = \begin{cases} 0 & \text{for } \begin{array}{l} \Delta P_{ab} \leq \Delta P_{uAMax} \quad \theta_a = 0 \\ -P_{sc} \leq \Delta P_{ab} \leq P_{sc} \quad \text{Cond}_h = 0 \\ \Delta P_{ab} \geq \Delta P_{uA0} \quad \theta_a = \pi \end{array} \\ C_d \sqrt{\frac{2}{\rho}} n_h 2 |r_h \sin(\theta_{aeq})| \sqrt{|\Delta P_{aeq}|} \text{sgn}(\Delta P_{aeq}) \end{cases} \quad (6-10)$$

$$K'_{b1} = \begin{cases} 0 & \text{for } \begin{array}{l} \Delta P_{ab} \leq \Delta P_{uB0} \quad \theta_b = 0 \\ -P_{sc} \leq \Delta P_{ab} \leq P_{sc} \quad \text{Cond}_h = 0 \\ \Delta P_{ab} \geq \Delta P_{uBMax} \quad \theta_b = \pi \end{array} \\ C_d \sqrt{\frac{2}{\rho}} n_h 2 |r_h \sin(\theta_{beq})| \sqrt{|\Delta P_{beq}|} \text{sgn}(\Delta P_{beq}) \end{cases} \quad (6-11)$$

The hydraulic accumulator constitutes of thermal and hydraulic domain. The non-linear model of the accumulator is given in 3.2.5. In that section the constitutive equations are also linearized and the related linear graph is given in Figure 3-22.

The accumulator flow rate is the sum of the shuttle valve flow rates,  $Q_c = Q_{a \rightarrow c} + Q_{b \rightarrow c}$ . Inserting the linearized shuttle valve flow rates into Eq.(3-81), the state

equation of the accumulator charge gas in terms of state variations can be written as follows.

$$\delta \dot{T}_g = -\frac{\delta T_g}{\tau_g} + \frac{T_{g0}}{V_{g0}}(k-1)\delta Q_c \quad (6-12)$$

where, the accumulator flow rate is as follows.

$$\delta Q_c = K'_{a1}(\delta P_a - \delta P_c) + K'_{b2}(\delta P_b - \delta P_c) + (-K'_{a2} + K'_{b1})\delta y_s \quad (6-13)$$

Inserting Eq.(3-81) into Eq.(3-83), the charge gas pressure dynamics in terms of state variations is written as follows.

$$\delta \dot{P}_c = -\frac{P_{g0}}{\tau_g \cdot T_{g0}} \delta T_g + k \frac{P_{g0}}{V_{g0}} \delta Q_c \quad (6-14)$$

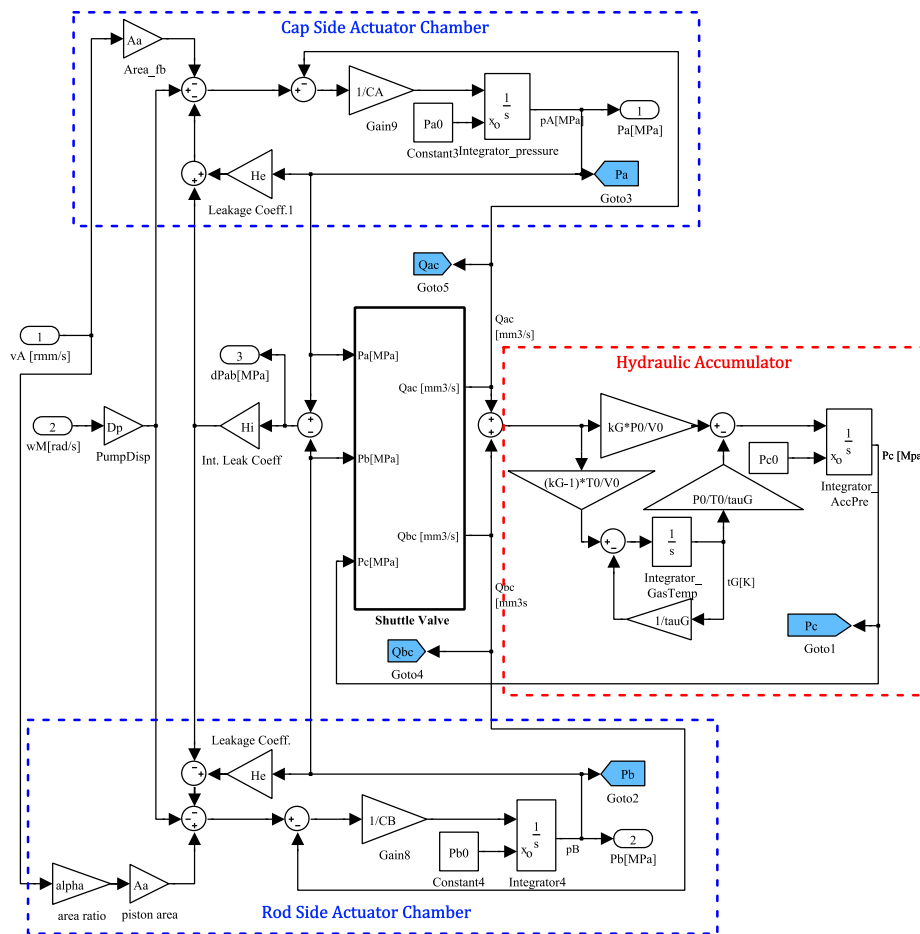


Figure 6-4 Block diagram representation of the hydraulic system

The block diagram representation of the hydraulic sub-system is shown in Figure 6-4, as a MATLAB<sup>®</sup>/Simulink<sup>®</sup> model. The upper most rectangle represents the cap side chamber pressure dynamics and formed by Eq. (6-4), while the lower most part is the rod side chamber pressure dynamics as defined by Eq. (6-5). The thermal and hydraulic domain equations, (6-12) and (6-14), of the accumulator is implemented in the right most part. The shuttle valve flow rate equations are implemented inside the subsystem, shown in the middle.

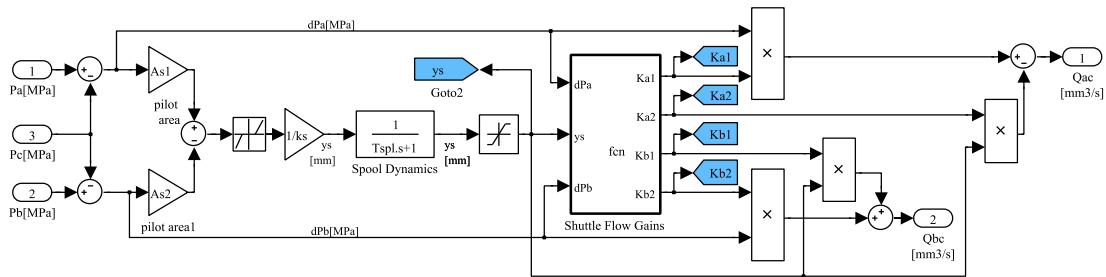


Figure 6-5 Shuttle valve model with linearized flow gains

The shuttle valve sub-system model based on the linearized flow gains is constructed in MATLAB<sup>®</sup>/Simulink<sup>®</sup> environment as given in Figure 6-5. A MATLAB<sup>®</sup> function is used to calculate the flow gains defined in Eqs.(6-6) – (6-11).

### 6.3 State Space Representation of the Open Loop Plant, $G_o$

The states are selected as follows.

$$\mathbf{x}_o = [y_A \quad \dot{y}_A \quad P_a \quad P_b \quad T_g \quad P_c \quad y_s \quad i_q \quad \omega_M] \quad (6-15)$$

The state equation of the electro hydraulic system is given as follows.

$$\mathbf{x}_o = \mathbf{A}_o \mathbf{x}_o + \mathbf{B}_o \mathbf{u}_o \quad (6-16)$$

where, the state matrix  $\mathbf{A}_o$  is,

$$\mathbf{A}_o = \begin{bmatrix}
\delta y_A & \delta \dot{y}_A & \delta P_a & \delta P_b & \delta T_g & \delta P_c & \delta y_s & \delta i_q & \delta \omega_M \\
0 & 1 & 0 & 0 & 0 & 0 & 0 & 0 & 0 \\
0 & \frac{-b}{m} & \frac{A}{m} & \frac{-\alpha A}{m} & 0 & 0 & 0 & 0 & 0 \\
0 & \frac{-A}{C_a} & \frac{-H_{ei} - K'_{a1}}{C_a} & \frac{H_i}{C_a} & 0 & \frac{K'_{a1}}{C_a} & \frac{K'_{a2}}{C_a} & 0 & \frac{D_p}{C_a} \\
0 & \frac{\alpha A}{C_b} & \frac{H_i}{C_b} & \frac{-H_{ei} - K'_{b2}}{C_b} & 0 & \frac{K'_{b2}}{C_b} & \frac{-K'_{b1}}{C_b} & 0 & \frac{-D_p}{C_b} \\
0 & 0 & \frac{K'_{a1}}{TQ} & \frac{K'_{b2}}{TQ} & \frac{-1}{\tau_g} & -\frac{K'_{a1} + K'_{b2}}{TQ} & \frac{K'_{b1} - K'_{a2}}{TQ} & 0 & 0 \\
0 & 0 & \frac{K'_{a1}}{PQ} & \frac{K'_{b2}}{PQ} & \frac{-P_{g0}}{V_{g0}\tau_g} & -\frac{K'_{a1} + K'_{b2}}{PQ} & \frac{K'_{b1} - K'_{a2}}{PQ} & 0 & 0 \\
0 & 0 & \frac{A_s}{k_s T_{sv}} & \frac{-A_s}{k_s T_{sv}} & 0 & 0 & \frac{-1}{T_{sv}} & 0 & 0 \\
0 & 0 & 0 & 0 & 0 & 0 & 0 & \frac{-R_s}{L_q} & \frac{-k_V}{L_q} \\
0 & 0 & \frac{-D_p}{J'_M} 10^3 & \frac{D_p}{J'_M} 10^3 & 0 & 0 & 0 & \frac{k_T}{J'_M} & \frac{-b'_M}{J'_M}
\end{bmatrix} \quad (6-17)$$

where the coefficient  $\frac{1}{TQ} = \frac{T_{g0}}{V_{g0}}(k - 1)$  defined in Eq.(6-12) and  $\frac{1}{PQ} = k \frac{P_{g0}}{V_{g0}}$  defined in Eq. (6-14), and  $H_{ei} = H_e + H_i$

The input matrix,  $\mathbf{B}_o$  is,

$$\mathbf{B}_o = \begin{bmatrix}
0 & 0 & 0 & 0 & 0 & 0 & 0 & \frac{-1}{L_q} & 0 \\
0 & \frac{-1}{m} & 0 & 0 & 0 & 0 & 0 & 0 & 0
\end{bmatrix}^T \quad (6-18)$$

with the motor voltage  $u_M$  and external load  $F_L$  inputs given as follows,

$$\mathbf{u}_o = \begin{bmatrix} u_M \\ F_L \end{bmatrix} \quad (6-19)$$

The system mode given in Eq. (6-16) can be used for the design of the motor speed and current controller. However, in order to design a position controller of the EHA, the state space representation should be augmented with the servo motor controllers.

#### 6.4 Servo Motor Control System

The servo motor controller consists of three parts, namely: speed compensator, current pre-filter, and the current compensator. The servo motor controllers are

shown in the upper most part of Figure 6-2. A PI regulator is utilized as the speed controller, and its equation is given as follows.

$$u_T = \left( K_{p\omega} + \frac{K_{i\omega}}{s} \right) (r_\omega - \omega_M) \quad (6-20)$$

where,

$K_{p\omega}$  = proportional gain, in  $Nm \cdot s/rad$

$K_{i\omega}$  = integral gain, in  $Nm/rad$

$r_\omega$  = motor reference speed, in  $rad/s$

$u_T$  = manipulated output, motor torque, in  $Nm$

The torque output of the speed compensator,  $u_T$ , together with the supplementary torque input,  $u_{T1}$ , are converted to reference current,  $r_{i_q}$ , through a low pass current filter whose equation is written as follows.

$$\ddot{r}_{i_q} + 2\zeta_{fI}\omega_{fI}\dot{r}_{i_q} + r_{i_q}\omega_{fI}^2 = \omega_{fI}^2 \frac{1}{k_T} (u_T + u_{T1}) \quad (6-21)$$

where,

$k_T$  = motor torque constant, in  $Nm/A$

$\omega_{fI}$  = natural frequency of the low pass current filter, in  $rad/s$

$\zeta_{fI}$  = damping coefficient of the low pass current filter

A PI regulator is utilized as the q-axis current controller, and its equation is given as follows.

$$u_M = \left( K_{pIq} + \frac{K_{iIq}}{s} \right) (r_{i_q} - i_q) \quad (6-22)$$

where,

$K_{pIq}$  = proportional gain, in  $V/A$

$K_{iIq}$  = integral gain, in  $V/A \cdot s$

$r_{i_q}$  = motor reference current, in  $A$

$u_M$  = manipulated output motor voltage, in  $V$

The state space model of the servo motor, without current pre filter and independent of the hydraulic drive system can be written as follows.

$$\begin{bmatrix} ie_{\omega_M} \\ ie_{i_q} \\ i_q \\ \omega_M \end{bmatrix} = \begin{bmatrix} 0 & 0 & 0 & -1 \\ \frac{K_{i\omega}}{kT} & 0 & -1 & -\frac{K_{p\omega}}{k_T} \\ \frac{K_{pIq}K_{i\omega}}{k_T L_q} & \frac{K_{iIq}}{L_q} & \frac{K_{pIq} - R_s}{L_q} & -\frac{k_V}{L_q} - \frac{K_{pIq}K_{p\omega}}{k_T L_q} \\ 0 & 0 & \frac{k_T}{J'_M} & -\frac{b'_M}{J'_M} \end{bmatrix} \begin{bmatrix} ie_{\omega_M} \\ ie_{i_q} \\ i_q \\ \omega_M \end{bmatrix} + \begin{bmatrix} 1 \\ \frac{K_{p\omega}}{k_T} \\ \frac{K_{pIq}K_{p\omega}}{k_T L_q} \\ 0 \end{bmatrix} r_\omega \quad (6-23)$$

### 6.5 State Space Representation of the Motor Speed Controlled Plant, $G_p$

The controller equations are converted to state equations in order to derive the state space representation of the EHA system. The design plant model  $G_{po}$  of the position controller is formed by augmenting the plant model  $G_o$  with the servo motor current and speed controllers.

The motor controller states are selected are given below.

$$\mathbf{x}_c = [ie_{\omega_M} \quad r_{i_q} \quad \dot{r}_{i_q} \quad ie_{i_q}] \quad (6-24)$$

where,

- $ie_{\omega_M}$  = integral of motor speed error, in *rad*
- $r_{i_q}$  = reference q-axis current, in *A*
- $\dot{r}_{i_q}$  = derivative of the reference q-axis current, in *A/s*
- $ie_{i_q}$  = integral of q-axis current error, in *As*

The state equations of the EHA system augmented with the servo motor controller is written as follows.

$$\begin{bmatrix} \dot{\mathbf{x}}_c \\ \dot{\mathbf{x}}_o \end{bmatrix} = \left( \mathbf{A}_c + \begin{bmatrix} \mathbf{0}_{4 \times 4} & \mathbf{0}_{4 \times 9} \\ \mathbf{0}_{9 \times 4} & \mathbf{A}_o \end{bmatrix} \right) \begin{bmatrix} \mathbf{x}_c \\ \mathbf{x}_o \end{bmatrix} + \mathbf{B}_c \begin{bmatrix} r_\omega \\ u_{T1} \\ F_L \end{bmatrix} \quad (6-25)$$

where, the inputs  $r_\omega$ ,  $u_{T1}$  and  $F_L$  are the reference motor speed, supplementary torque and external load acting on the EHA, respectively, and are shown in Figure 7-1.

The state matrix  $\mathbf{A}_c$  and the input matrix  $\mathbf{B}_c$  are defined as follows.

$$\mathbf{A}_c = \begin{bmatrix} ie_{\omega_M} & r_{i_q} & \dot{r}_{i_q} & ie_{i_q} & \mathbf{x}_{0(1:7)} & i_q & \omega_M \\ \begin{bmatrix} 0 & 0 & 0 & 0 \\ 0 & 0 & 1 & 0 \\ K_{i\omega} \frac{\omega_{fl}^2}{k_T} & -\omega_{fl}^2 & -2\zeta_{fl}\omega_{fl} & 0 \\ 0 & 1 & 0 & 0 \end{bmatrix} & [\mathbf{0}_{4 \times 7}] & \begin{bmatrix} 0 & -1 \\ 0 & 0 \\ 0 & K_{p\omega} \frac{-\omega_{fl}^2}{k_T} \\ -1 & 0 \end{bmatrix} \\ [\mathbf{0}_{7 \times 4}] & [\mathbf{0}_{7 \times 7}] & [\mathbf{0}_{7 \times 2}] \\ \begin{bmatrix} 0 & \frac{K_{pIq}}{L_q} & 0 & \frac{K_{iIq}}{L_q} \end{bmatrix} & [\mathbf{0}_{1 \times 7}] & \begin{bmatrix} -\frac{K_{pIq}}{L_q} & 0 \end{bmatrix} \\ [\mathbf{0}_{1 \times 4}] & [\mathbf{0}_{1 \times 7}] & [\mathbf{0}_{1 \times 2}] \end{bmatrix} \quad (6-26)$$

$$\mathbf{B}_c = \begin{bmatrix} r_{\omega} & u_{T1} & F_L \\ \begin{bmatrix} 1 & 0 & 0 \\ & [\mathbf{0}_{1 \times 3}] \\ K_{p\omega} \frac{\omega_{fl}^2}{k_T} & \frac{\omega_{fl}^2}{k_T} & 0 \end{bmatrix} \\ [\mathbf{0}_{2 \times 3}] \\ \begin{bmatrix} 0 & 0 & -\frac{1}{m} \end{bmatrix} \\ [\mathbf{0}_{7 \times 3}] \end{bmatrix} \quad (6-27)$$

The output equation is defined as follows.

$$\begin{bmatrix} u_T \\ r_T \\ r_{i_q} \\ u_M \\ \mathbf{x}_o \end{bmatrix} = \begin{bmatrix} ie_{\omega_M} & r_{i_q} & \dot{r}_{i_q} & ie_{i_q} & \mathbf{x}_{0(1:7)} & i_q & \omega_M \\ \begin{bmatrix} K_{i\omega} & 0 & 0 & 0 \\ K_{i\omega} & 0 & 0 & 0 \\ 0 & 1 & 0 & 0 \\ 0 & K_{pIq} & 0 & K_{iIq} \end{bmatrix} & [\mathbf{0}_{4 \times 7}] & \begin{bmatrix} 0 & -K_{p\omega} \\ 0 & -K_{p\omega} \\ 0 & 0 \\ -K_{pIq} & 0 \end{bmatrix} & \begin{bmatrix} \mathbf{x}_c \\ \mathbf{x}_o \end{bmatrix} + \begin{bmatrix} K_{p\omega} & 0 & 0 \\ K_{p\omega} & 1 & 0 \\ 0 & 0 & 0 \\ 0 & 0 & 0 \\ [\mathbf{0}_{9 \times 3}] \end{bmatrix} \begin{bmatrix} r_{\omega} \\ u_{T1} \\ F_L \end{bmatrix} \end{bmatrix} \quad (6-28)$$

where,

$u_T$  = torque output of speed controller, in  $Nm$

$r_T$  = reference motor torque, in  $Nm$

$r_{i_q}$  = reference q-axis current, in  $A$

$u_M$  = motor voltage, in  $V$

## 6.6 Comparison with Non-linear Simulink Model

The linearized model of the EHA system is constructed in MATLAB<sup>®</sup>/Simulink<sup>®</sup> environment and is compared with the non-linear simulation model introduced in section 3.3. The linearized model is shown in Figure 6-6. It is constructed by the sub system models given in Figure 6-2 to Figure 6-5.

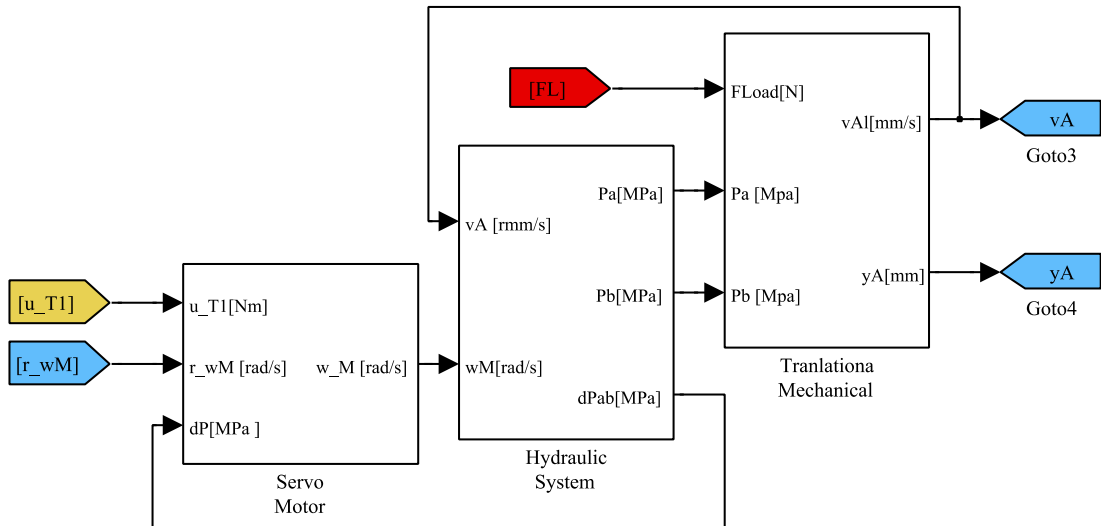


Figure 6-6 Linearized whole system model in MATLAB<sup>®</sup>/Simulink<sup>®</sup> environment

The linearized and nonlinear simulation models are run for the same input set. The reference motor speed,  $r_\omega$  is a sinusoidal signal with  $10 \text{ rad/s}$  amplitude and  $1 \text{ Hz}$  frequency. Furthermore a sinusoidal external load with  $5000 \text{ N}$  amplitude and  $5 \text{ Hz}$  frequency is applied. The velocity responses of the two model are given in Figure 6-7. It is seen that the linearized model response fits well with the non-linear model response. When the external load change signs, the spool change direction, therefore, velocity responses oscillate. The magnitude of velocity oscillations as well as the frequency is similar for the two models. There seems a time delay in the non-linear model. This is due to the rate transitions, of the non-linear SimHydraulics<sup>®</sup> model.

## 6.7 Investigation of the Root Locations

In order to investigate the pole locations of the design plant model,  $G_p$ , the numerical linear model of the system is obtained, by making the linearization at operating point,  $\Delta P_a = 1 \text{ MPa}$ ,  $\Delta P_b = 0.1 \text{ MPa}$ ,  $y_A = 100 \text{ mm}$ , and  $P_c = 3 \text{ MPa}$ . Note that in the

linearized model the shuttle valve proposed in section 5.4 that has a asymmetric spool structure is utilized. This shuttle valve has zero pre-opening at AC port,  $u_{vA_0} = 0 \text{ mm}$  and has a positive spool underlap at BC port  $u_{vB_0} = 2 \text{ mm}$ . The remaining shuttle valve parameters are given in Table 5-4. Furthermore, the parameters of the remaining components are given in Table 3-1 – Table 3-5.

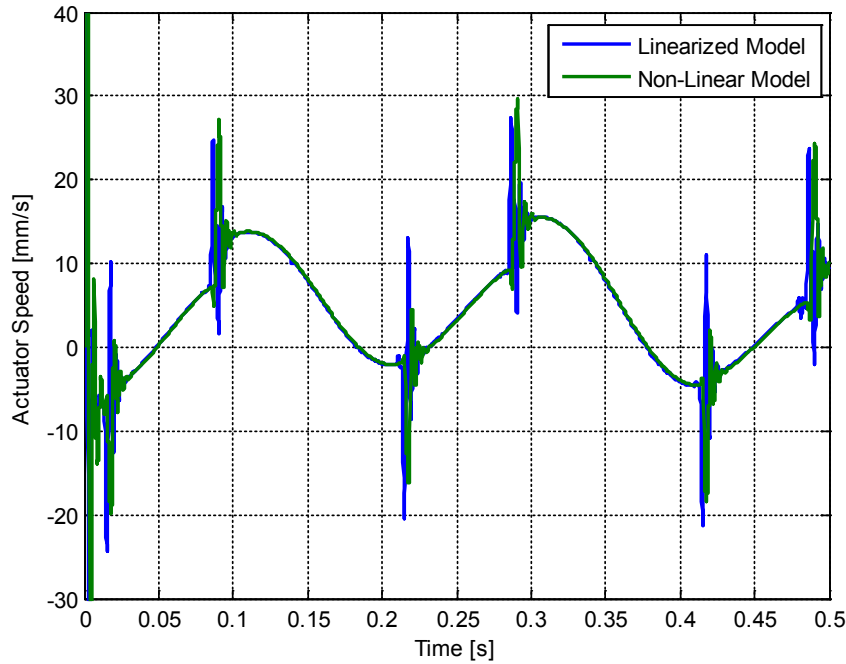


Figure 6-7 Velocity response comparison of the linearized and non-linear models

Using the state space model which is given in Eq.(6-25), the transfer function between the actuator reference speed input and the actuator position output,  $Y_A(s)/R_\omega(s)$ , is found as follows.

$$\frac{Y_A(s)}{R_\omega(s)} = \frac{7.0011 \cdot 10^{20} (s + 3733)}{s (s + 6986) (s^2 + 1000s + 2.95 \cdot 10^6)} \cdot \frac{(s + 0.1492)(s + 4.23 \cdot 10^{-4})}{(s + 0.1493)(s + 4.15 \cdot 10^{-4})} \cdot \frac{(s + 500)(s + 24.17)}{(s + 393.5)(s + 24.77)(s^2 + 2024s + 2.19 \cdot 10^6) (s^2 + 1.78e004s + 1.59 \cdot 10^8)}$$

Note that the dc gain of the above transfer function is  $0.458 \text{ mm/rad} \approx D_p/A$ , since the rod-side chamber is connected to the hydraulic accumulator line for the given operating pressures. In the transfer function of the design plant model, the red

colored components represent the poles and zeros are due to servo motor dynamics. The red polynomial shown a the right most of the denominator represents the poles due to current filter, which has natural frequency 2000 Hz, and damping ratio 0.7. The remaining red colored poles and zeros are due to motor speed and current controllers, as well as the electrical and rotational mechanical system. This will be well understood if the transfer function between the motor speed reference input and the motor speed output  $\Omega_M(s)/R_\omega(s)$  is derived. By using the state space model of the servo motor given by Eq. (6-23), the transfer function  $\Omega_M(s)/R_\omega(s)$  is found as follows.

$$\frac{\Omega_M(s)}{R_\omega(s)} = \frac{1.79 \cdot 10^6 (s + 500) (s + 24.17)}{(s + 393.4)(s + 24.79) (s^2 + 2024s + 2.19 \cdot 10^6)}$$

The blue colored poles and zeros given in the transfer function  $Y_A(s)/R_\omega(s)$  are due to pressure dynamics of the hydraulic chamber together with the translational mechanical system dynamics. In order to see the root locations of the hydraulic and the translational mechanical system, the linearized state space models of the system which assumes the pump as an ideal flow source can be utilized. In the previous chapter Eq. (5-81) defines the state space model without spool dynamics, and Eq. (5-92) defines the state space model with spool dynamic. Both the two model gives the same transfer function since the spool is saturated for the given operating points. The transfer function between the input motor drive speed and the actuator velocity,  $V_A(s)/\Omega_M(s)$ , is found as follows.

$$\frac{V_A(s)}{\Omega_M(s)} = \frac{2.48 \cdot 10^6 (s + 3731)}{(s + 6985)(s^2 + 999.7s + 2.95 \cdot 10^6)}$$

In the transfer function of  $Y_A(s)/R_\omega(s)$  the remaining green colored poles and zeros are due to pressure and temperature dynamics of the hydraulic accumulator. In Section 3.2.5.5, Eq.(3-82) and Eq. (3-84), the transfer functions between the hydraulic accumulator input flow rate  $Q_c$  and the output temperature  $T_g$  and accumulator pressure  $P_c$  is derived. It is easily seen that the roots located at 0.1492 rad/s is directly related with the accumulator time constant  $\tau_g = 6.7 s$  which is given in Table 3-5. The other poles and zeros can be obtained if the

accumulator states equations are augmented to the hydraulic system model without servo motor dynamics, Eq. (5-81). The transfer function  $Y_A(s)/R_\omega(s)$  of the resulting model is given as follows.

$$\frac{Y_A(s)}{R_\omega(s)} = \frac{2.48 \cdot 10^6 (s + 3733)(s + 0.1492)(s + 4.23 \cdot 10^{-4})}{s (s + 6987)(s + 0.1492)(s + 4.52 \cdot 10^{-4})(s^2 + 999.6s + 2.95 \cdot 10^6)}$$

From the above transfer function it is seen that including the hydraulic accumulator does not change the pole locations due to hydraulic actuator chambers and translational mechanical system.

Note that the transfer function  $Y_A(s)/R_\omega(s)$  of the design plant model  $G_p(s)$  has 12 roots, however, the state matrix defined in Eq. (6-26) has 13 states. The remaining root is due to the spool dynamics. For the given operating pressures, the spool is saturated.

In this time, the operating point is changed to  $\Delta P_a = 0.75 \text{ MPa}$  and  $\Delta P_b = 0.1 \text{ MPa}$ . According to Figure 5-19, the shuttle valve is partially opened, where for  $\Delta P_{ab} = 0.65 \text{ MPa}$ , the spool openings are  $u_{va_{eq}} = 0 \text{ mm}$  and  $u_{vb_{eq}} = 3.7 \text{ mm}$ .

The transfer function between  $Y_A(s)/R_\omega(s)$ , of the design plant model  $G_p$  defined in Eq.(6-25) is found as follows.

$$\begin{aligned} \frac{Y_A(s)}{R_\omega(s)} &= \frac{7.0011 \cdot 10^{20} (s + 3876)(s + 741)}{s (s + 7631)(s + 740.3) (s^2 + 390.2s + 2.8 \cdot 10^6)} \cdot \frac{(s + 0.1492)(s + 5.32 \cdot 10^{-4})}{(s + 0.1492)(s + 5.23 \cdot 10^{-4})} \\ &\quad \cdot \frac{(s + 500)(s + 24.17)}{(s + 393.5)(s + 24.76)(s^2 + 2024s + 2.19 \cdot 10^6) (s^2 + 1.78e004s + 1.59 \cdot 10^8)} \end{aligned}$$

It is clearly seen that the root locations due to servo motor (red-colored) and the accumulator (green colored) dynamics remained unchanged. However, the roots locations due to hydraulic actuator chambers and mass have changed (blue colored). Furthermore the order of the numerator is 13, as expected, the root located at  $-740 \text{ rad/s}$  is due to the spool dynamics.

The same result can be obtained if the transfer function  $V_A(s)/\Omega_M(s)$  of the hydraulic system without servo motor dynamic, which is defined by Eq. (5-92) is found as follows.

$$\frac{V_A(s)}{\Omega_M(s)} = \frac{2.48 \cdot 10^6 (s + 3875) (s + 740.9)}{(s + 7630) (s + 740.2) (s^2 + 390s + 2.8 \cdot 10^6)}$$

It should be noted that, inside the pressure interval where the spool is not fully opened (i.e saturated), the spool dynamics together with the spool structure has a considerable effect on system dynamics and stability. Therefore, has to be considered in the design plant model.

In order to illustrate this conclusion the variation of the eigen values of the state matrix given by Eq. (5-92) is shown in Figure 6-8. The flow coefficients,  $K'_{a1}, K'_{a2}, K'_{b1}, K'_{b2}$ , given the state matrix of Eq. (5-92) is calculated for every  $\Delta P_{ab}$  input which are in the range of  $2 \cdot [\Delta P_{uA_{Max}}, \Delta P_{uB_{Max}}]$  and input velocity  $-200 \text{ mm/s}$ . Note that the pressure interval covers all possible spool positions.

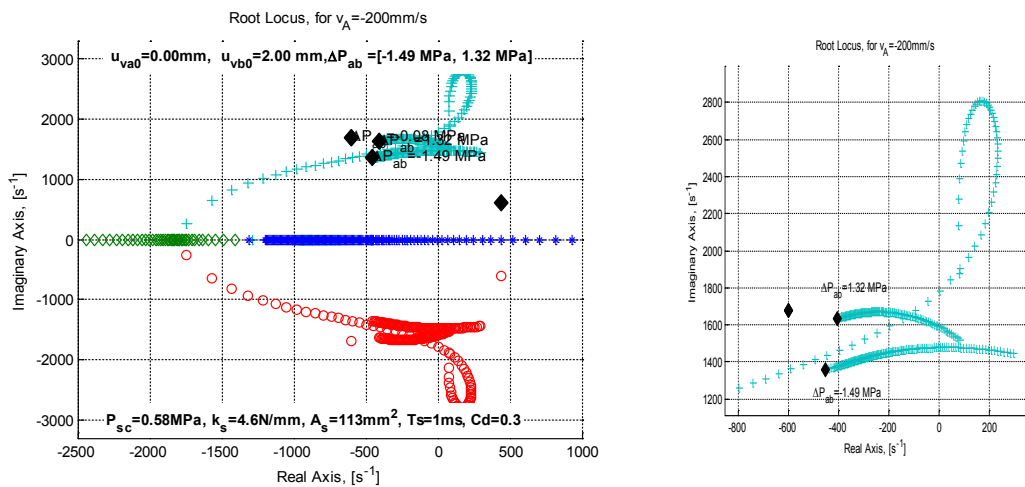


Figure 6-8 Root locations during the asymmetric spool switching

It is seen that for the fully opened spool position,  $\Delta P_{ab} < \Delta P_{uA_{Max}}$ , the roots due to chamber pressure dynamics are located at  $\approx -400 \pm 1350i$ . Furthermore, for the fully opened spool position that corresponds to  $\Delta P_{ab} > \Delta P_{uB_{Max}}$  the roots are located at,  $\approx -450 \pm 1650i$ . These two locations can be considered as the origin. For the pressure intervals where the spool is not fully opened, the eigen values change in

between these two origins. Note that some roots have positive real parts. In section 5.4, it was mentioned that this valve has unstable operating points. These regions are further considered in section **Error! Reference source not found.**

The root locus for the proposed shuttle valve solution in Section 5.8 is shown in Figure 6-8. Note that similar to the previous shuttle valve, for the pressure intervals where the spool is fully opened the complex conjugate roots converge to  $\approx -400 \pm 1350i$  and  $\approx -450 \pm 1650i$ . This is an expected results since the shuttle valve dynamics have no effect on system stability if the spool is saturated. Since  $\delta y_s = 0$ , the flow coefficients,  $K'_{a2}$  and  $K'_{b1}$  becomes zero.

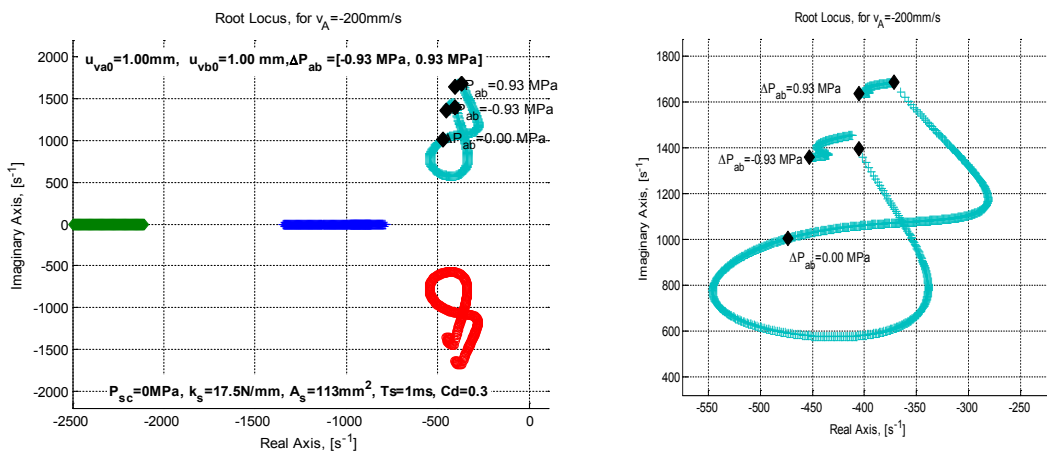


Figure 6-9 Root locations, when the shuttle valve proposed in Section 5.8 is utilized.

## 6.8 Simplified Plant Model

The accumulator pressure and temperature responses are considerably slow, with respect to other sub systems. Furthermore, the electric motor current dynamics is very fast. Therefore, the accumulator pressure, temperature and motor current dynamics are neglected in the design plant model of the position controller.

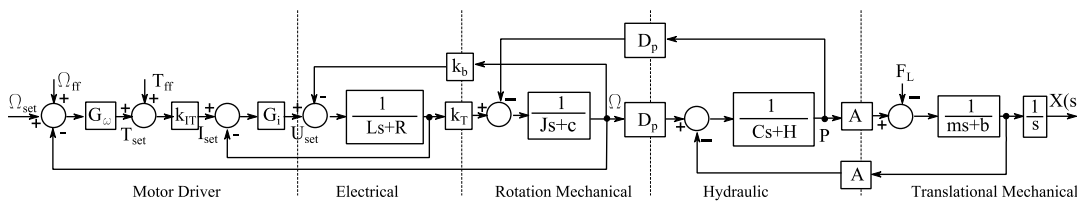


Figure 6-10 Block diagram representation of the plant

### 6.8.1 State Space Model with Fully Opened Valve Considerations

If the shuttle valve is fully opened, then there is no need to consider spool dynamics, since the spool is saturated at the end position  $\delta y_s = 0$ . In such a case, only one hydraulic chamber determines the pressure dynamics since the hydraulic accumulator capacitance together with the hydraulic conductance of the shuttle valve are considerably high. In other words, for the case  $\Delta P_{ab} > \Delta P_{uBMax}$ , since  $\delta P_b \approx \delta P_c \approx 0$ , the pressure dynamics is  $\delta P_L = \delta P_a$ . For the case,  $\Delta P_{ab} < \Delta P_{uAMax}$ , since  $\delta P_a \approx \delta P_c \approx 0$ , the pressure dynamics is  $\delta P_L = -\alpha \delta P_b$ .

Therefore, the design plant model of the position controller can be formed by augmenting the state matrix given in section 4.5, Eq. (4-20). The states of the simplified open loop plant model are defined as follows.

$$\mathbf{x}_o^* = [y_A \quad \dot{y}_A \quad P_L \quad \omega_M] \quad (6-29)$$

The rotational mechanical systems equation has to be re-written considering the load pressure state,  $\delta P_L$ . In Eq.(6-2), the hydraulic torque on the motor shaft is represented by  $T_p = D_p(P_a - P_b)$ . For the fully opened valve positions, variation of the hydraulic torque  $\delta T_p$ , in terms of load pressure, ( $P_L = P_a - \alpha P_b$ ), will be  $D_p \delta P_L$  and  $\frac{1}{\alpha} \delta P_L$  for  $\delta P_b \approx 0$  and  $\delta P_a \approx 0$  respectively. Considering the current loop is very fast, such that the torque set point is equal to the electric torque,  $\delta u_T = K_T \delta i_q$ , the torque continuity equation on the electric motor shaft is re-written as follows.

$$u_T = (J'_M) \ddot{\omega}_M + (b'_M) \dot{\omega}_M + D_p \delta P_L \cdot \Gamma_T \cdot 10^{-3} \quad (6-30)$$

where,  $\Gamma_T$  is the condition operator. For the fully opened valve cases,  $\Gamma_T$  is equal to 1 and  $1/\alpha$ , for  $\Delta P_{ab} > \Delta P_{uBMax}$  and  $\Delta P_{ab} < \Delta P_{uAMax}$  respectively.

The state space representation of the open loop simplified plant is defined as follows

$$\begin{bmatrix} \delta y_A \\ \delta \dot{v}_A \\ \delta \dot{p}_L \\ \delta \dot{\omega} \end{bmatrix} = \begin{bmatrix} 0 & 1 & 0 & 0 \\ 0 & -\frac{b}{m} & \frac{A}{m} & 0 \\ 0 & -\Gamma_v \frac{A}{C} & -\frac{H}{C} & \Gamma_\omega \frac{D_p}{C} \\ 0 & 0 & -\Gamma_T \frac{D_p}{J'_M} & -\frac{b'_M}{J'_M} \end{bmatrix} \begin{bmatrix} \delta y_A \\ \delta v_A \\ \delta p_L \\ \delta \omega \end{bmatrix} + \begin{bmatrix} 0 & 0 \\ -\frac{1}{m} & 0 \\ 0 & 0 \\ 0 & \frac{1}{J'_M} \end{bmatrix} \begin{bmatrix} \delta F_L \\ \delta u_T \end{bmatrix} \quad (6-31)$$

where, the conditions of the coefficients are as follows.

$$\begin{aligned} \Gamma_v &= \begin{cases} \alpha^2 & \Delta P_{ab} \leq \Delta P_{uA_{Max}} (\delta P_a \approx 0) \\ 1 & \Delta P_{ab} \geq \Delta P_{uB_{Max}} (\delta P_b \approx 0) \end{cases} \\ \Gamma_\omega &= \begin{cases} \alpha & \Delta P_{ab} \leq \Delta P_{uA_{Max}} (\delta P_a \approx 0) \\ 1 & \Delta P_{ab} \geq \Delta P_{uB_{Max}} (\delta P_b \approx 0) \end{cases} \\ \Gamma_T &= \begin{cases} \frac{1}{\alpha} & \Delta P_{ab} \leq \Delta P_{uA_{Max}} (\delta P_a \approx 0) \\ 1 & \Delta P_{ab} \geq \Delta P_{uB_{Max}} (\delta P_b \approx 0) \end{cases} \\ C &= \begin{cases} C_b & \Delta P_{ab} \leq \Delta P_{uA_{Max}} \\ C_a & \Delta P_{ab} \geq \Delta P_{uB_{Max}} \end{cases} \end{aligned} \quad (6-32)$$

Augmenting the open loop system with the motor speed controller, the state space representation of the design plant model of the position controller is defined as follows.

$$\begin{bmatrix} \delta \dot{y}_A \\ \delta \dot{v}_A \\ \delta \dot{p}_L \\ \delta \dot{\omega}_M \\ \delta i \dot{e}_\omega \end{bmatrix} = \begin{bmatrix} 0 & 1 & 0 & 0 & 0 \\ 0 & -\frac{b}{m} & \frac{A}{m} & 0 & 0 \\ 0 & -\Gamma_v \frac{A}{C} & -\frac{H}{C} & \Gamma_\omega \frac{D_p}{C} & 0 \\ 0 & 0 & -\Gamma_T \frac{D_p}{J'_M} & -\frac{b'_M + K_{\omega p}}{J'_M} & \frac{K_{\omega i}}{J} \\ 0 & 0 & 0 & -1 & 0 \end{bmatrix} \begin{bmatrix} \delta y_A \\ \delta v_A \\ \delta p_L \\ \delta \omega \\ \delta i e_\omega \end{bmatrix} + \begin{bmatrix} 0 & 0 & 0 \\ -\frac{1}{m} & 0 & 0 \\ 0 & 0 & 0 \\ 0 & \frac{1}{J'_M} & \frac{K_{\omega p}}{J'_M} \\ 0 & 0 & 1 \end{bmatrix} \begin{bmatrix} \delta f_L \\ \delta u_{T1} \\ \delta r_\omega \end{bmatrix} \quad (6-33)$$

In Eq. (6-33) the state variable,  $i e_\omega$ , represents the integral of the error between the reference and output motor speeds,  $(\int (r_\omega - \omega_M) dt)$ . The control inputs of the system are the reference motor speed  $r_\omega$  and the supplementary torque  $u_{T1}$ ,

furthermore, the disturbance input is the external load acting on the hydraulic actuator  $F_L$ .

### 6.8.2 State Space Model with Partially Opened Valve Considerations

In that case, the pressure dynamics of the two hydraulic actuator chambers are included to the design plant model. Furthermore, the spool dynamics is also considered, since it affects the stability as mentioned in Section 5.8.

In this case, the states of the simplified open loop plant model are defined as follows.

$$\mathbf{x}_o^{**} = [y_A \quad \dot{y}_A \quad P_a \quad P_b \quad y_s \quad \omega_M] \quad (6-34)$$

The state space representation of the open loop plant is as follows.

$$\dot{\mathbf{x}}_o^{**} = \begin{bmatrix} 0 & 1 & 0 & 0 & 0 & 0 \\ 0 & -\frac{b}{m} & \frac{A}{m} & -\frac{\alpha A}{m} & 0 & 0 \\ 0 & \frac{-A}{C_a} & -\frac{H_{ei} + K'_{a1}}{C_a} & \frac{H_i}{C_a} & \frac{K'_{a2}}{C_a} & \frac{D_p}{C_a} \\ 0 & \frac{\alpha A}{C_b} & \frac{H_i}{C_b} & -\frac{H_{ei} + K'_{b2}}{C_b} & \frac{-K'_{b1}}{C_b} & -\frac{D_p}{C_b} \\ 0 & 0 & \frac{A_s}{k_s T_{sv}} & -\frac{A_s}{k_s T_{sv}} & \frac{-1}{T_{sv}} & 0 \\ 0 & 0 & -\frac{D_p}{J'_M} & \frac{D_p}{J'_M} & 0 & -\frac{b'_M}{J'_M} \end{bmatrix} \mathbf{x}_o^{**} + \begin{bmatrix} 0 & 0 \\ -\frac{1}{m} & 0 \\ 0 & 0 \\ 0 & 0 \\ 0 & 0 \\ 0 & \frac{1}{J'_M} \end{bmatrix} \begin{bmatrix} \delta F_L \\ \delta u_T \end{bmatrix} \quad (6-35)$$

Augmenting the open loop system with the speed controller, the state space representation of the design plant model of the position controller is defined as follows.

$$\dot{\mathbf{x}}_p^{**} = \begin{bmatrix} 0 & 1 & 0 & 0 & 0 & 0 & 0 \\ 0 & -\frac{b}{m} & \frac{A}{m} & -\frac{\alpha A}{m} & 0 & 0 & 0 \\ 0 & \frac{-A}{C_a} & -\frac{H_{ei} + K'_{a1}}{C_a} & \frac{H_i}{C_a} & \frac{K'_{a2}}{C_a} & \frac{D_p}{C_a} & 0 \\ 0 & \frac{\alpha A}{C_b} & \frac{H_i}{C_b} & -\frac{H_{ei} + K'_{b2}}{C_b} & \frac{-K'_{b1}}{C_b} & -\frac{D_p}{C_b} & 0 \\ 0 & 0 & \frac{A_s}{k_s T_{sv}} & -\frac{A_s}{k_s T_{sv}} & \frac{-1}{T_{sv}} & 0 & 0 \\ 0 & 0 & -\frac{D_p}{J'_M} & \frac{D_p}{J'_M} & 0 & -\frac{b'_M + K_{\omega p}}{J'_M} & \frac{K_{\omega i}}{J'_M} \\ 0 & 0 & 0 & 0 & 0 & -1 & 0 \end{bmatrix} \begin{bmatrix} \delta y_A \\ \delta v_A \\ \delta P_a \\ \delta P_b \\ \delta y_s \\ \delta \omega_M \\ \delta i e_{\omega} \end{bmatrix} + \begin{bmatrix} 0 & 0 & 0 \\ -\frac{1}{m} & 0 & 0 \\ 0 & 0 & 0 \\ 0 & 0 & 0 \\ 0 & 0 & 0 \\ 0 & \frac{1}{J'_M} & \frac{K_{\omega p}}{J'_M} \\ 0 & 0 & 1 \end{bmatrix} \begin{bmatrix} \delta f_L \\ \delta u_{T1} \\ \delta r_{\omega} \end{bmatrix} \quad (6-36)$$

## 6.9 Comparison of the Design Plant Models

The simplified design plant models, Eq.(6-33) and Eq.(6-36) , are compared with the full order system model, Eq.(6-28). Furthermore, the response of the system model that assumes the servo motor as an ideal velocity source, Eq. (5-81), is also provided.

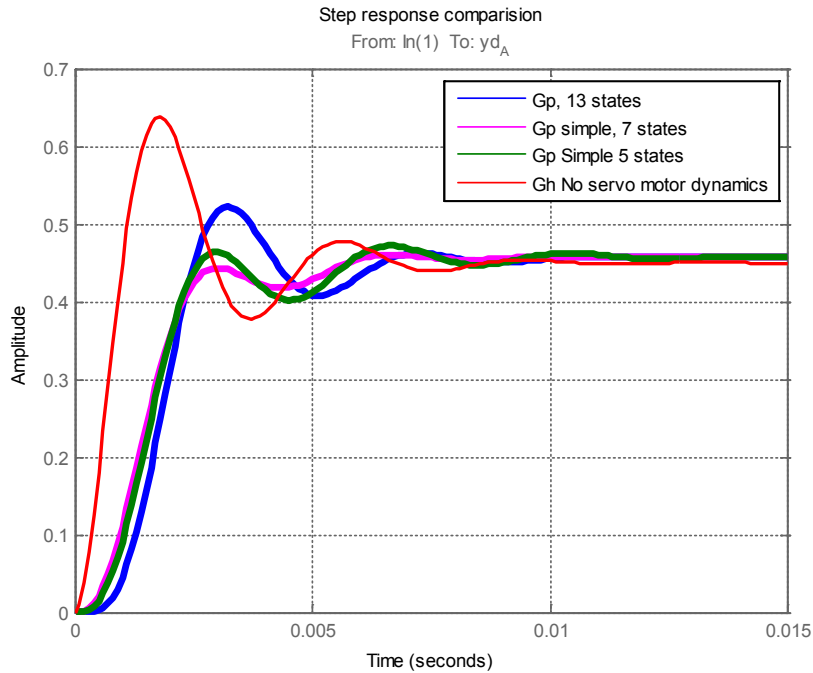


Figure 6-11 Step response comparison of the design plant models

The system is linearized for  $\Delta P_a = 1 \text{ MPa}$ , and  $\Delta P_b = 0.1 \text{ MPa}$ . Note that  $\Delta P_{ab} > \Delta P_{uB_{Max}}$ , therefore, the shuttle valve is fully opened, connecting the rod side chamber to the accumulator line.

The step responses are shown in Figure 6-11. The solid blue line is the full order model response given by Eq. (6-28). It is seen that if the servo motor dynamics is neglected and assumed to be an ideal velocity source, as in Eq. (5-81), then the response of the simplified system, solid red line, differs from the full order model. On the other hand, the green and magenta lines represent the simplified plant model responses defined in Eq. (6-33) and Eq. (6-36). It is seen that when the servo motor dynamics is considered, the simplified model response is consistent with the full order model response.

## CHAPTER 7

### CONTROLLER DESIGN AND PERFORMANCE TESTS

This chapter addresses the position control system design of the electro hydrostatic actuator (EHA) and its implementation. A combined feedback and feedforward control strategy is utilized. The feedback compensators have a three layer cascade structure. The inner layers are the motor speed and current compensators and are implemented on the servo motor control unit. These two inner compensators are tuned by the automatic commissioning toolbox of the servo motor control software.

On the other hand the design of the outermost layer which is the position controller is mainly addressed in the scope of this thesis study. The position controller consists of feedback and feedforward compensators, trajectory generator and supervisory finite state machine. The two compensators are designed based on the simplified model and are implemented on the real time control PC. The designed controllers together with the proposed asymmetric shuttle valve spool are tested experimentally on the load simulator test set up. The proposed EHA is experimentally evaluated in terms of tracking, disturbance rejection and steady state error performance.

#### 7.1 Controller Structure

The controller structure of the EHA is shown in Figure 7-1. Considering the cascade servo motor controllers as a part of the process, a two degree of freedom architecture is applied for the position control of the EHA. The first degree of freedom is the feedback position compensator,  $C_p(s)$ , and the second degree of freedom is the reference feedforward compensators  $F_{\Omega R}(s)$  and  $F_{TR}(s)$ . The feedback compensator is designed to shape the disturbance response and the feedforward compensators are designed to shape the reference response independently.

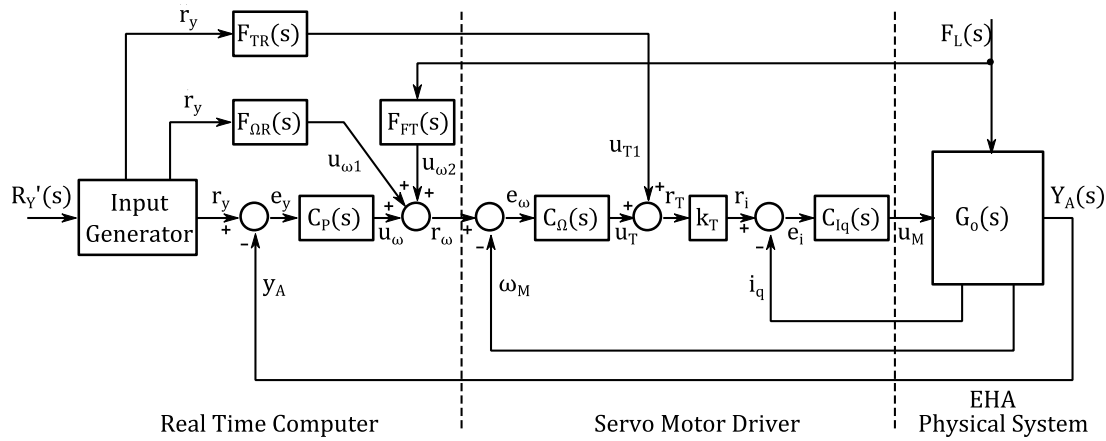


Figure 7-1 Control structure of the EHA

In Figure 7-1, the physical system is represented with  $G_o(s)$ , which is defined in section 6.3. Furthermore, the simplified plant model that will be used in the position controller design is introduced in section 6.8. The block diagram representation of this simplified design plant model is shown in Figure 7-2. In this simplified model, it is assumed that the reference torque output of the motor speed controller is equal to the motor electrical torque,  $r_T \approx T_M$ . Besides, neglecting the current dynamics, the accumulator pressure and temperature dynamics are also neglected, since they have relatively slow responses.

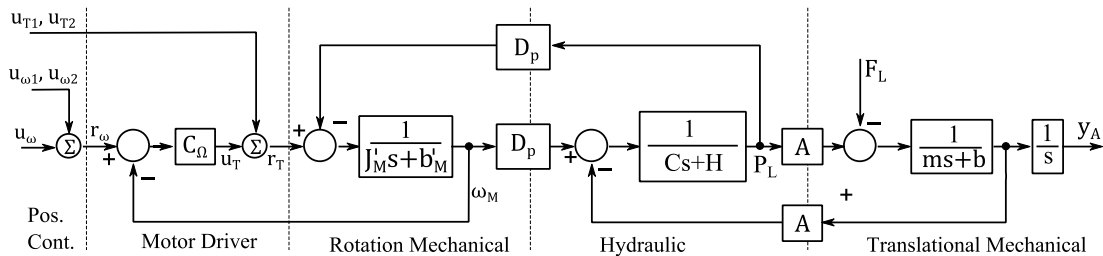


Figure 7-2 Block diagram representation of the simplified design plant model,  $G_p$

The plant model includes the rotational mechanical system together with the speed controller, the hydraulic system of the actuator chambers and the translational mechanical system of the hydraulic piston rod assembly. The block diagram representation of the simplified model is drawn for the fully opened shuttle valve case. Therefore, only one hydraulic actuator chamber is considered to represent the pressure dynamics, since the other one is connected to the accumulator line.

## 7.2 Position Feedback Controller Design

The feedback controller is designed considering the cap side chamber only, i.e. the cap side chamber is pressurized and the rod side is connected to the accumulator. According to the asymmetric shuttle valve spool structure proposed in 5.4, since spool underlap is provided between BC port only, the rod side chamber is connected to the accumulator line for the pressure interval  $\Delta P_{ab} \geq -P_{sc}$ . The velocity constant (dc gain) for this case is  $\frac{D_p}{A} = 0.45 \frac{mm}{rad}$ . On the other hand for the pressure interval  $\Delta P_{ab} \leq \Delta P_{uA_{Max}}$  the cap-side chamber is connected to the accumulator line and the velocity constant is  $\frac{D_p}{\alpha A} = 0.6 \frac{mm}{rad}$ . For the case where the cap-side is connected to the accumulator line, the calculated FB gains are multiplied by  $\alpha$ . Note that no special FB control is utilized for the spool positioning between the two end points, i.e.  $\Delta P_{uA_{Max}} \leq \Delta P_{ab} \leq -P_{sc}$ . The range of this pressure interval is  $\approx 0.1MPa$ . In that interval the feedback gains are switched linearly.

A proportional integral control strategy is utilized, for the feedback position control of the EHA. The type number of the plant transfer function,  $G_p(s)$ , is unity. Therefore, the position response of the close loop system with proportional action has zero steady state error for a reference step input. However, integral action is required in order to remove the steady state error due to disturbance input i.e. external load acting on the actuator.

The simplified design plant model is obtained for the operating points,  $\Delta P_a = 1MPa$  and  $\Delta P_b = 0.1MPa$ . By using the simplified plant model defined by Eq. (6-33), the transfer function between the actuator position and motor reference speed  $G_p = Y_A(s)/R_\omega(s)$ , is defined as follows.

$$G_p(s) = \frac{8.787 \cdot 10^8 \cdot (s + 24.17)}{s(s + 676)(s + 24.7)(s^2 + 950.8s + 2.828 \cdot 10^6)} \quad (7-1)$$

Note that the dc gain of the transfer function is  $\frac{D_p}{A} = \frac{0.45mm}{rad}$ . The zero and pole located at  $\approx 24 rad/s$  are due to servo motor speed controller with proportional and integral gains,  $K_{\omega p} = 2.02 Nms/rad$  and  $K_{\omega i} = 48.8 Nm/rad$ , respectively. Note that the

motor speed controller is tuned by using the auto commissioning toolbox of the servo motor programming software. The servo motor is connected to the EHA during the tuning process. The pole located  $\approx 676 \text{ rad/s}$  is due to servo motor speed control loop. The frequency response of the transfer function between motor speed  $\Omega_M(s)$  and the reference motor speed  $R_\Omega(s)$  is given Figure 7-3. The blue line is drawn by considering the servo motor dynamics only, i.e. using the Eq. (6-23). On the other hand the red line is drawn by considering the whole system dynamics, i.e. Eq. (6-25). It is seen that the close loop pole located at  $676 \text{ rad/s}$  corresponds to  $\approx 45^\circ$  phase angle.

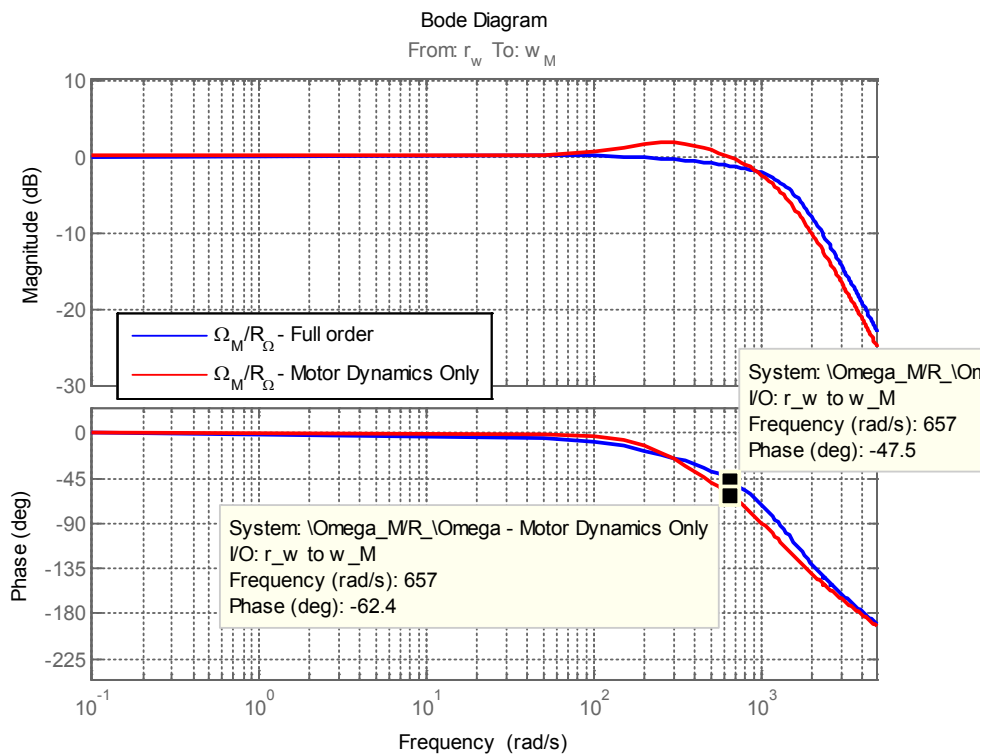


Figure 7-3 Frequency response of the servo motor speed loop

The complex conjugate poles  $-543.56 \pm 1591.6i$  of the transfer function given in Eq.(7-1) are due to hydro-mechanical system dynamics. The real part of the complex pole pair is  $\approx -b/2m$ , while the complex part is  $\approx \sqrt{A^2/C_A}$ .

The root locus of the simplified plant transfer function  $Y_A(s)/R_Y(s)$  defined by Eq.(6-33) and Eq.(7-1) is given in Figure 7-4. Note that the green line represents the transfer function derived from full order system model defined by Eq. (6-25).

Different from the simplified model it has complex conjugate pole pairs located at  $1000 \text{ rad/s}$  which are related with the current dynamics. The damping of the hydraulic system is seen as  $\zeta = 0.28$ , which is relatively high when compared with a conventional hydraulic actuator which have generally a low damping ratio in between  $0.05 - 0.2$ . The high damping ratio is not only due to the high viscous friction coefficient of the hydraulic actuator. The differential flow rate passing from the shuttle valve further increases the damping ratio. Furthermore, since only one chamber is pressurized, the natural frequency is decreased by  $\sqrt{2}$  times when compared with the conventional system with two pressurized chambers. It should be remembered that the pole pairs due to hydraulic system change location while the spool is changing position. The locus of hydraulic pole pairs with the shuttle valve spool position is shown in Figure 6-8 and Figure 6-9. A load pressure feedback can be activated during the shuttle valve spool transition from one end point to the other end. However, the pressure feedback is not applicable on an industrial controller and brings additional costs. Therefore, in the scope of this thesis study no special compensator is designed for the spool switching. The feedback gains are adjusted by considering the fully opened spool positions only.

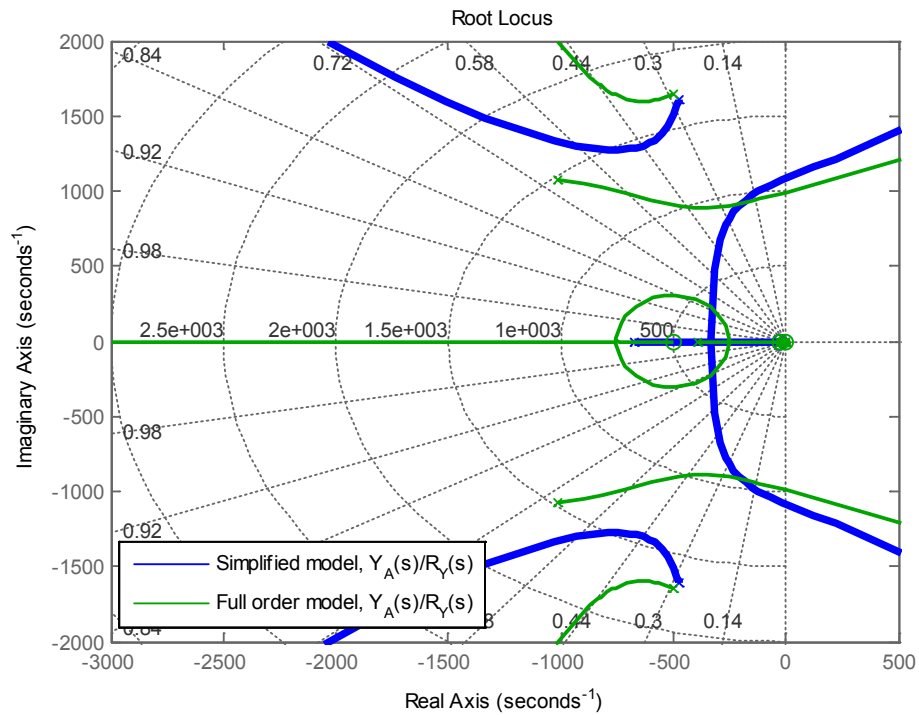


Figure 7-4 Root locus of the plant transfer function

The PI position controller is designed for  $60^\circ$  phase margin and  $10\text{ Hz}$  gain cross over frequency. The specifications of the close loop system are given in Table 7-1. The frequency response of the open loop plant and the compensated system are given in Figure 7-5.

Table 7-1 Specifications of the closed loop system		
Phase margin	[deg]	60
Gain cross over frequency	[Hz]	10
Calculated controller gains		
Proportional gain	[rad/(mm · s)]	125
Integral gain	[rad/(mm · s <sup>2</sup> )]	3510
Properties of the compensated system		
Gain margin	[dB]	24
Bandwidth ( $-3\text{dB}$ )	[Hz]	15

The gain margin of the compensated system is  $-24\text{ dB}$ , which is large enough to compensate for the model uncertainty due to spool dynamics. The bandwidth of the closed loop system is  $15\text{ Hz}$ , which might be considered as sufficient for many industrial applications. The set point tracking performance is be further increased by using feedforward compensators that will be discussed in the subsequent sections.

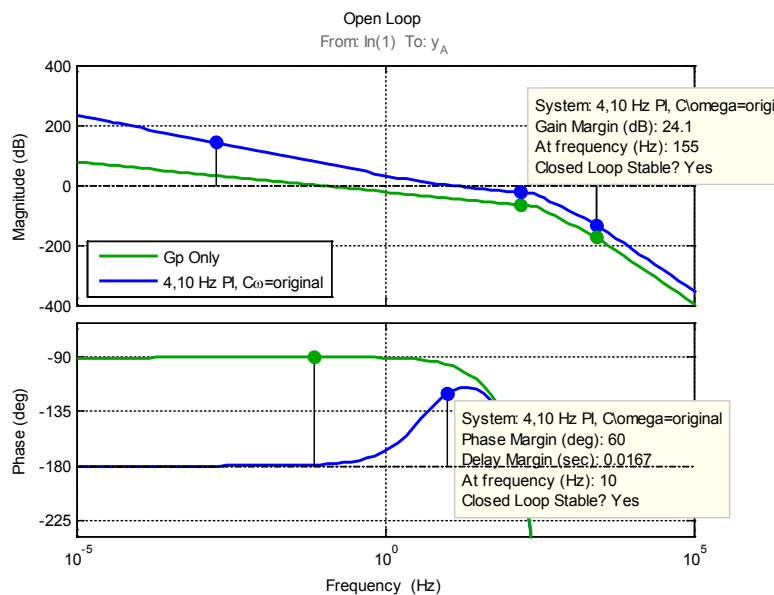


Figure 7-5 Open loop Bode diagram of the compensated and uncompensated systems

The compliance defined by the transfer function between the external load and the actuator position  $Y_A(s)/F_L(s)$  is given in Figure 7-6. The solid green line represents the compliance with the use of PI controller. The dashed blue line is drawn for the P controller that satisfies the same phase margin and gain crossover frequency requirements. It is clear that the steady state error due to external load is removed with the use of integral action. The dashed dotted red line is drawn with the use of semi-integrator that will be discussed in the subsequent section. In Figure 7-6 it is seen that for a 10 Hz disturbance input with 1 kN magnitude, the actuator position response is 0.04 mm. The corresponding actuator stiffness for this high frequency disturbance input is  $\approx 25 \text{ kN/mm}$ . On the other hand for low frequency disturbance inputs ( $\approx 1 \text{ Hz}$ ) the stiffness is 800 kN/mm. Note that the actuator stiffness can be further increases by increasing the controller gains, however the shuttle valve dynamics has to be considered as mentioned previously.

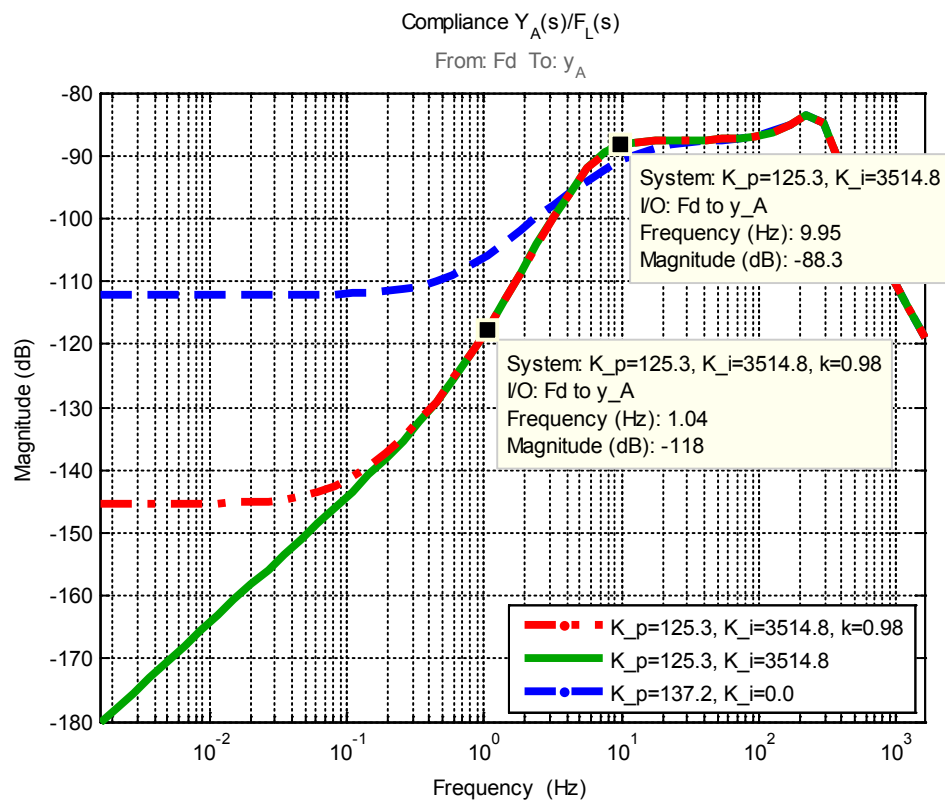


Figure 7-6 Frequency response of the compliance

In practical application, during the positioning of the actuator, the pure integrator may cause limit cycles in case of dry friction. The actuator position oscillates around

the set point with small amplitudes that are in the order of the resolution of the position feedback encoder. In order to prevent this limit cycle behavior the standard PI controller in standard form is modified as given in Table 7-2, where  $T_i$  is the integral time constant,  $T_i = K_p/K_i$ . The modified controller is named as semi-integrator or quasi integrator [96], [38] and is similar to lag compensator. The tuning gain  $k$  is selected in between  $k = 0.95 \dots 1$ . Note that selecting  $k = 1$  results in a pure integrator, with pole located at the origin of the s-plane. The compliance of the system with the use of semi integrator with  $k = 0.98$  is shown by dashed dotted red line in Figure 7-6. The high frequency response is the same with the PI controller in standard form. On the other hand, low frequency response is similar to P controller. In case of static loading state error exists, corresponding to  $-145 \text{ dB}$  compliance. Note that this compliance value corresponds to  $17783 \text{ kN/mm}$  stiffness. Which means that for a  $50 \text{ kN}$  (5 metric ton) static load the steady state error is  $2.8 \mu\text{m}$ , which is smaller than the resolution of standard position encoder  $5 \mu\text{m}$ .

**Table 7-2 PI controller**

Standard PI controller	$C_P(s) = K_p \left( \frac{T_i s + 1}{T_i s} \right)$
PI controller with semi-integrator	$C_P(s) = K_p \left( \frac{T_i s + 1}{T_i s + 1 - k} \right)$

The step response of the closed loop system is given in Figure 7-7. The settling time is  $0.12 \text{ s}$  and the maximum overshoot is  $20\%$ . Note that the step response is drawn by utilizing the linearized system model where no actuator limits and saturations are considered. However, the servo motor of the EHA has a finite power, its maximum speed and current are limited; therefore, the real response of the EHA will be much different than given in Figure 7-7. In the subsequent section the integrator anti wind up strategy that is utilized to cope with servo motor limits is discussed.

### 7.3 Integrator Anti-Windup Strategy

Many aspects of the EHA can be understood and regulators can be designed based on the linearized system model. However, some nonlinear effects should also be

considered. Like all the actuators, the EHA has also physical limitations; the servo motor speed and current are limited by the servo motor driver. Although the desired position trajectory is formed by considering the power limits of the servo motor, it may also happen that the control variables, motor speed and current reach its allowable limits.

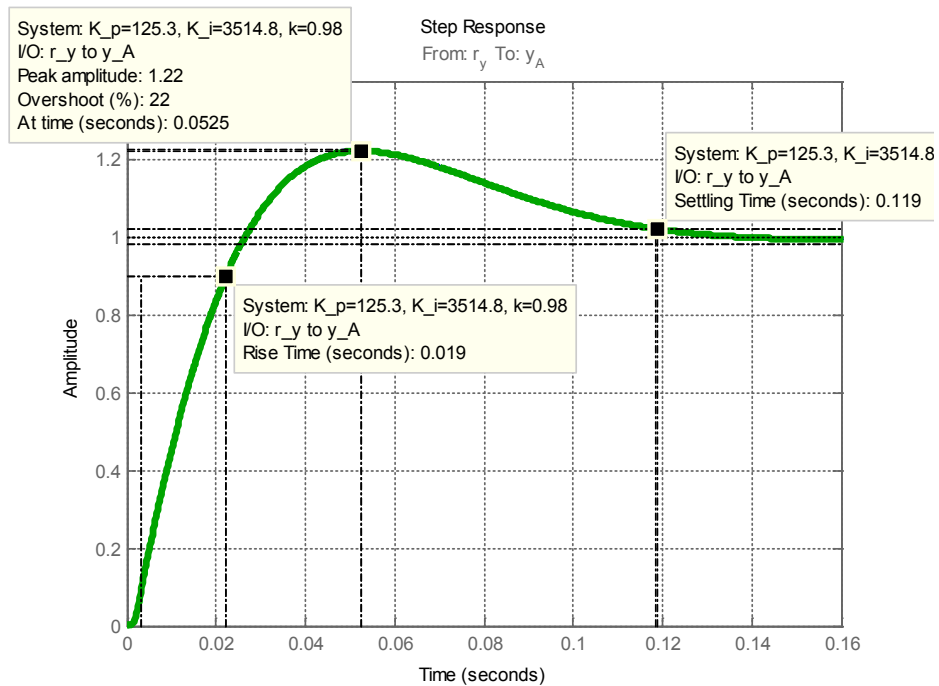


**Figure 7-7 Step response of the close loop system**

Any regulator with integral action may give large transients when the actuator saturates [97]. When the actuator saturates, integrator is likely to build up a large value, and when the input comes out of the limit the initial condition will cause large transients [98].

In all the three layers of the cascade structure of the EHA, the regulators are using integral action. The motor current and speed loops are implemented inside the motor driver. In the scope of this thesis study, there is no need to design an anti-windup algorithm for these two inner loops, since most of the industrial controllers, has their own regulators and not allow to implement or re-shape their anti-windup mechanism. However, for the position loop, running on the target pc, an anti-windup algorithm should be designed, in case the control variable which is the motor speed is saturated.

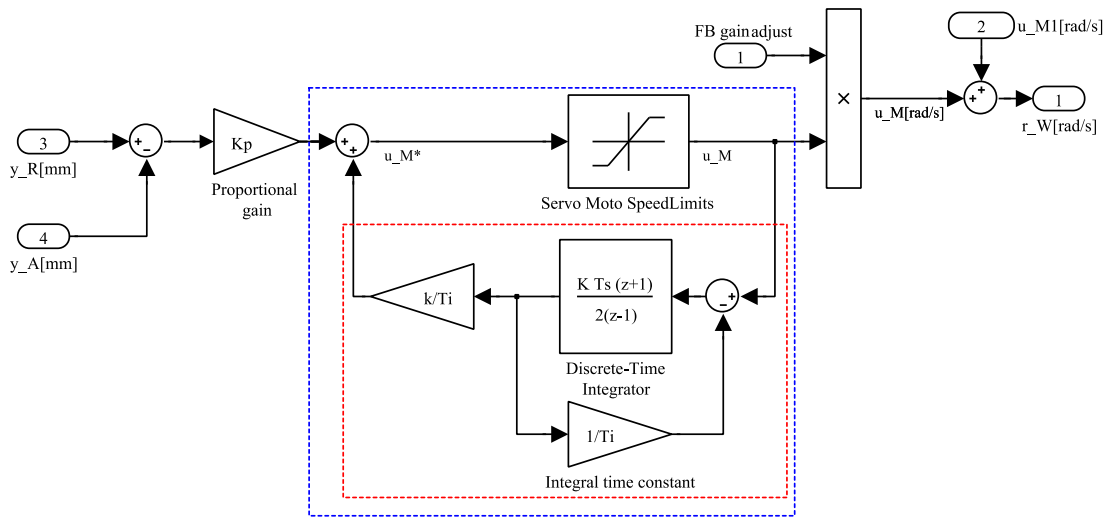


Figure 7-8 Feedback position controller and integral anti wind up strategy

The anti-wind up strategy utilized in the position control loop is shown in Figure 7-8. The transfer function inside the red rectangle is  $\frac{k}{T_i s + 1}$ . If the control variable,  $u_M^*$ , is in between the servo motor maximum and minimum limits, than the saturation block is equal to unity,  $u_M^* = u_M$ , and the controller transfer function becomes.

$$C_p(s) = K_p \left( \frac{1}{1 - \frac{k}{T_i s + 1}} \right) = K_p \frac{T_i s + 1}{T_i s + 1 - k} \quad (7-2)$$

If the control variable is not saturated, then the controller is the same as given in Table 7-2. On the other hand, if the control variable is greater than the servo motor limits, than the control signal is saturated  $\delta u_M = 0$ . In that case the controller becomes a proportional gain  $K_p$ , since the feedback integral component vanishes,  $\delta u_M \cdot \frac{k}{T_i s + 1} = 0$ .

The effect of integrator anti wind up is illustrated by the comparison of the linearized simulation models given in Figure 7-9. The first model is the linearized system model, where no actuator limitations are considered, in the second model, servo motor speed limitations and transportation lag is included to the plant model. On the other hand, no anti-wind up strategy is applied with the PI compensator. In the last part the motor speed saturation is considered in the feedback compensator.

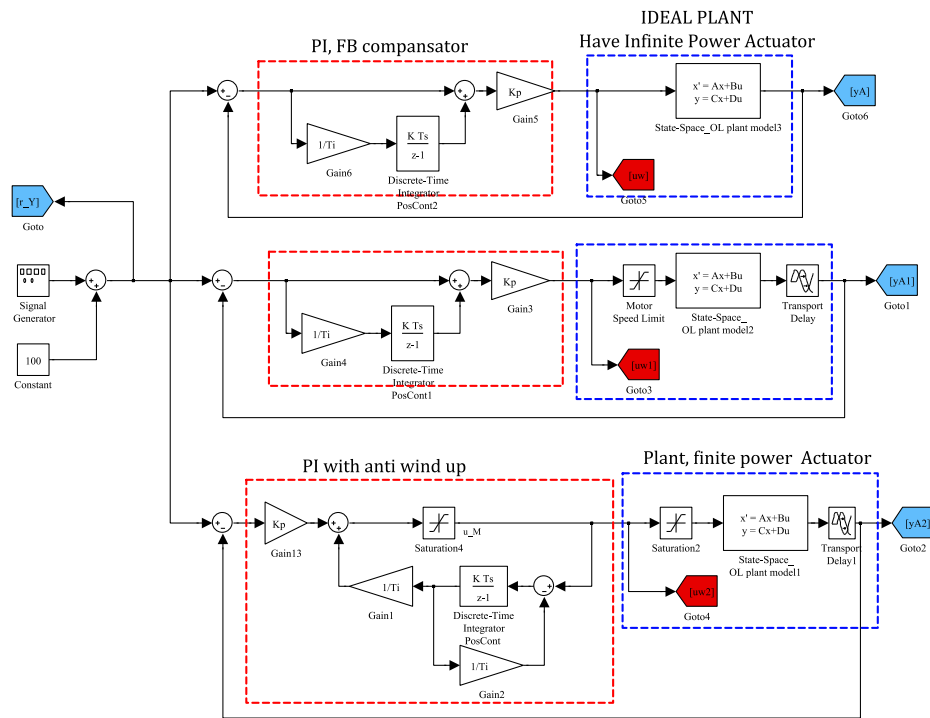


Figure 7-9 Close loop linear system model and the effects of integrator anti-wind up

A reference step input with 10 mm amplitude is applied to the three models given in Figure 7-9. The comparison of position responses together with the control variables are given in Figure 7-10. It is seen that the response of the ideal plant with no physical limitations, blue line, is the same with the one given in Figure 7-7. The reference motor speeds goes up to 2000 rad/s. However, when the servo motor speed is limited with  $\pm 300$  rad/s and if no integrator anti-wind up strategy is applied, large transients occurs, green line. The red line represents the response of when the integrator is limited. It is seen that large transients are eliminated.

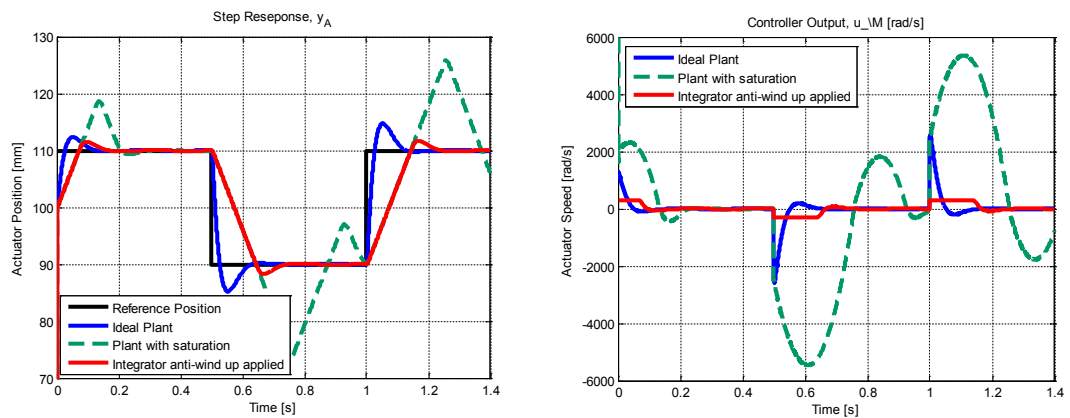


Figure 7-10 Step response with and without saturation and integrator anti windup strategy

## 7.4 Reference Feedforward Controller Design

Feedback is reactive in the sense that there must be an error before control actions are taken. Feedforward is another control concept that is proactive because control actions are taken before the disturbance has generated any errors [99]. In order to increase the speed of the response and set point tracking performance a feedforward controller is design based on the simplified design plant model.

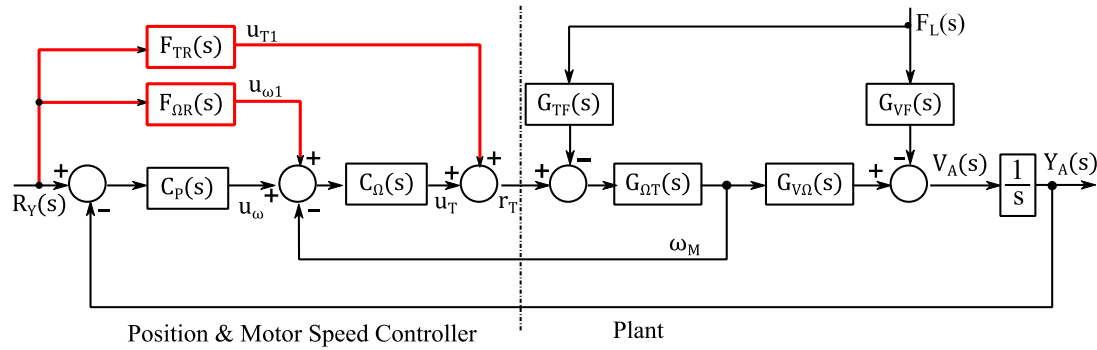


Figure 7-11 Block diagram representation of the reference feedforward

The motor speed,  $F_{\Omega R}(s)$  and torque,  $F_{TR}(s)$ , feedforward controllers are shown in Figure 7-11. In that figure, the plant is represented with two transfer functions  $G_{\Omega T}(s)$  and  $G_{V\Omega}(s)$ , which are in between the motor torque and the speed, and in between motor speed and the actuator speed, respectively. The two transfer functions are found based on the block diagram representation given in Figure 7-2.

The transfer function between motor reference torque input and speed,  $G_{\Omega T}(s)$  is given as follows.

$$G_{\Omega T}(s) = \frac{Cms^2 + (bc + mH)s + bH + A^2}{a_3s^3 + a_2s^2 + a_1s + a_0} \quad (7-3)$$

The transfer function between servo motor speed and the actuator speed,  $G_{V\Omega}(s)$  is given as follows.

$$G_{V\Omega}(s) = \frac{AD_p}{Cms^2 + (bc + mH)s + bH + A^2} \quad (7-4)$$

where,

$$\begin{aligned}
a_3 &= J'_M C m \\
a_2 &= J'_M (bC + mH) + b'_M C m \\
a_1 &= J'_M (Hb + A^2) + b'_M (bC + mH) + mD_p^2 \\
a_0 &= b'_M (Hb + A^2) + bD_p^2
\end{aligned} \tag{7-5}$$

Furthermore, on the feedforward path an equivalent transfer function  $G_{VT}(s) = G_{\Omega T}(s)G_{V\Omega}(s)$  can be written as follows.

$$G_{VT}(s) = \frac{AD_p}{a_3 s^3 + a_2 s^2 + a_1 s + a_0} \tag{7-6}$$

By using the block diagram representation given in Figure 7-11, the equation between the reference position input,  $R_Y(s)$ , and the actuator position output,  $Y_A(s)$ , is written as follows.

$$\left[ \left( (R_Y - Y_A)C_P + R_Y F_{\Omega R} - sY_A \frac{1}{G_{V\Omega}} \right) C_\Omega + R F_{TR} \right] G_{\Omega T} G_{V\Omega} = sY_A \tag{7-7}$$

The Eq.(7-7) is written in explicit form as follows.

$$\begin{aligned}
R_Y (C_P C_\Omega G_{\Omega T} G_{V\Omega} + F_{\Omega R} C_\Omega G_{\Omega T} G_{V\Omega} + F_{TR} G_{\Omega T} G_{V\Omega}) \\
= Y_A (C_P C_\Omega G_{\Omega T} G_{V\Omega} + s C_\Omega G_{\Omega T} + s)
\end{aligned} \tag{7-8}$$

It is desired to find the feedforward transfer functions  $F_{\Omega R}$ ,  $F_{TR}$ , so that  $R_Y(s) = Y_A(s)$ . Therefore, the following relation must hold.

$$F_{\Omega R} C_\Omega G_{\Omega T} G_{V\Omega} = s C_\Omega G_{\Omega T} \tag{7-9}$$

$$F_{TR} G_{\Omega T} G_{V\Omega} = s \tag{7-10}$$

Inserting,  $G_{\Omega T} G_{V\Omega} = G_{VT}$ , and Eq.(7-4) and Eq. (7-6) the motor speed feedforward controller is found as follows

$$F_{\Omega R}(s) = \frac{s}{G_{V\Omega}(s)} = \frac{ms^3 + (bC + mH)s^2 + (bH + A^2)s}{AD_p} \quad (7-11)$$

The motor torque feedforward controller is found as follows

$$F_{TR}(s) = \frac{s}{G_{VT}(s)} = \frac{a_3s^4 + a_2s^3 + a_1s^2 + a_0s}{AD_p} \quad (7-12)$$

Note that, if the friction coefficients  $b$ ,  $b'_M$  and the leakage terms  $H$  are neglected in Eq.(7-11) and Eq. (7-12), then the resulting feedforward gains define the following kinematic relationship.

$$u_{\omega 1} = \frac{A}{D_p} \dot{r}_y \quad (7-13)$$

$$u_{T1} = \left( m \frac{D_p}{A} + J'_M \frac{A}{D_p} \right) \ddot{r}_y \quad (7-14)$$

where  $r_y$  is the reference position input,  $u_{\omega 1}$  is the feedforward motor speed and  $u_{T1}$  is the feedforward motor torque output as shown in Figure 7-1.

The effect of motor speed and torque feed forward is illustrated in the frequency response graph of the closed loop system. In Figure 7-12, the blue line represents the close loop systems with feedback only. It is seen that the bandwidth of the system according to  $-3 \text{ dB}$  criteria is  $15 \text{ Hz}$ . Furthermore, since the PI controller is tuned with  $60$  degree phase margin specification, the close loop system is under damped and the response make overshoots. It is clearly seen that the magnitude ratio is not unity and may go up to  $1.9 \text{ dB}$ . With the addition of speed feedforward,  $F_{\Omega R}(s) = \frac{A}{D_p} \cdot sR_Y(s)$ , it is seen that the bandwidth is increased up to  $300 \text{ Hz}$ , green line. Furthermore, the overshoot of the close loop system is decreased. The performance of the system is more increased with the addition of torque feed forward,  $F_{TR}(s) = \left( m \frac{D_p}{A} + J'_M \frac{A}{D_p} \right) \cdot s^2R_Y(s)$ , red line. It is seen that the magnitude ratio is unity till  $30\text{Hz}$  frequency and the phase lag is close to zero.

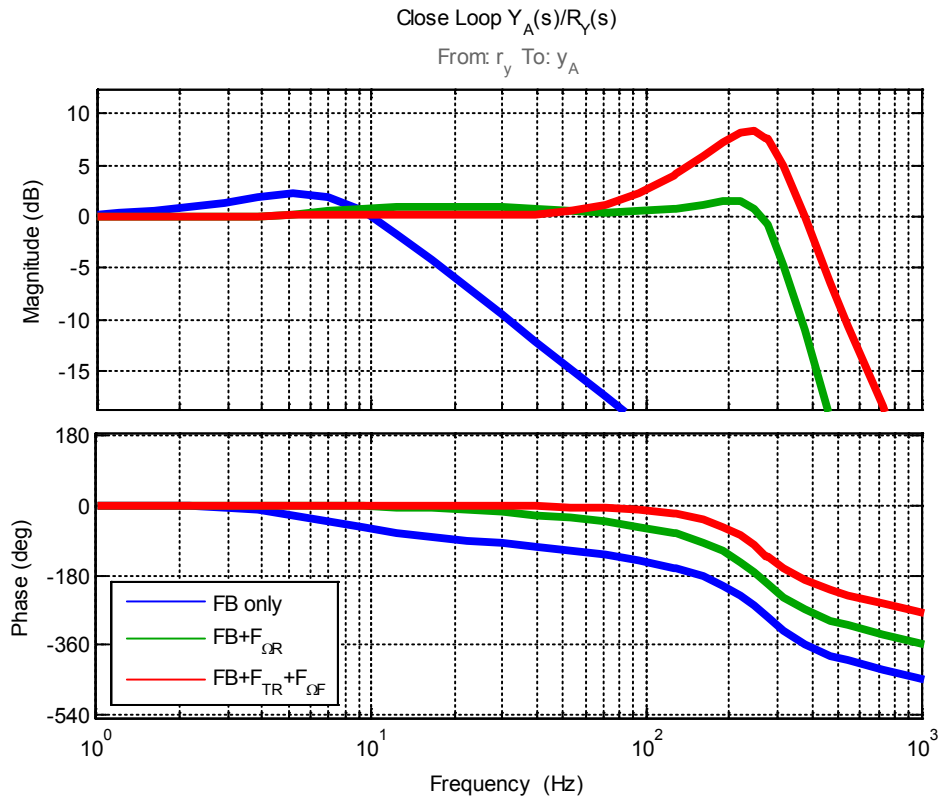


Figure 7-12 Bode diagram of the closed loop system and effects reference feedforward

### 7.5 Pre-Filter Equivalent of the Reference Feedforward Controller

In several books and studies, the feed forward compensation is applied by a pre filter  $H(s)$  as shown in Figure 7-13. If the pre-filter  $H(s)$  is casual then it is advantageous to separate motor speed and torque feed forward terms, since the speed,  $sR_Y(s)$ , and acceleration,  $s^2R_Y(s)$ , information of the reference position together supplementary speed,  $u_{\omega 1}$ , and torque,  $u_{T1}$ , input ports on the motor drive are not required.

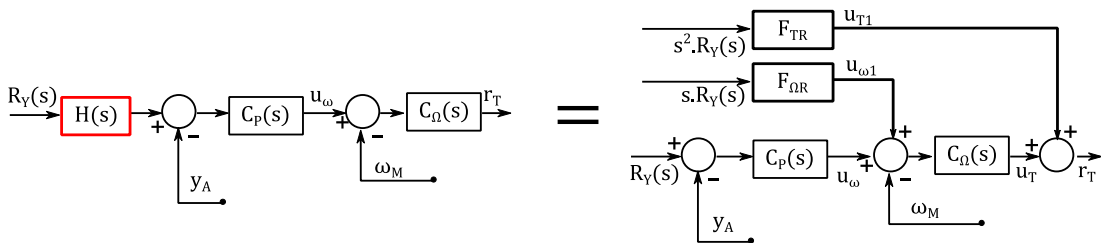


Figure 7-13 The equivalent pre-filter of motor speed and torque feedforward controllers

In this section the pre-filter equivalent of the proposed motor speed and torque feed forward scheme, given in section 7.4, is derived. Note that the equivalent pre-filter

$H(s)$  is not casual moreover includes the position and speed controller parameters. On the other hand, the motor speed and torque feed forward includes system parameters only. Therefore, in practical application the motor speed and torque feed forward is utilized, the pre-filter,  $H(s)$ , is derived only for completeness.

Based on the block diagram representation given in Figure 7-11, the plant transfer function  $G_p(s)$  is written as follows.

$$G_p(s) = \frac{C_\Omega(s)G_{VT}(s)}{1 + C_\Omega(s)G_{\Omega T}(s)} \frac{1}{s} \quad (7-15)$$

Furthermore, the close loop transfer function between  $R_Y(s)$  and  $Y_A(s)$  is defined as follows.

$$G_p(s) = \frac{C_P(s)G_p(s)}{1 + C_P(s)G_p(s)} \left( 1 + \frac{F_{\Omega R}S}{C_P(s)} + \frac{F_{TR}S^2}{C_P(s) \cdot C_\Omega(s)} \right) \quad (7-16)$$

where,  $F_{\Omega R}$  is the motor speed feed forward gain and is equal to  $A/D_p$  and the  $F_{TR}$  is the motor feed forward gain and is equal to  $m \frac{D_p}{A} + J'_M \frac{A}{D_p}$ .

In Eq. (7-16) the last term in the parenthesis is the transfer function of the input filter (pre-filter)  $H(s)$ . Note that; the input filter transfer function is not casual, since the order of the numerator will be higher than the order of the denominator.

$$H(s) = \left( 1 + \frac{F_\omega S}{\frac{K_{py}S + K_{iy}}{s}} + \frac{F_T S^2}{\frac{K_{py}S + K_{iy}}{s} \cdot \frac{K_{p\omega}S + K_{i\omega}}{s}} \right) \quad (7-17)$$

The equivalent pre-filter is derived as follows.

$$H(s) = \frac{F_T S^4 + F_\omega K_{p\omega} S^3 + (K_{py}K_{p\omega} + F_\omega K_{i\omega}) S^2 + (K_{py}K_{i\omega} + K_{p\omega}K_{iy}) S + K_{iy}K_{i\omega}}{K_{py}K_{p\omega} S^2 + (K_{py}K_{i\omega} + K_{p\omega}K_{iy}) S + K_{iy}K_{i\omega}} \quad (7-18)$$

The pre-filter  $H(s)$  is not causal. Similar to the motor speed and torque feedforward compensators, the pre-filter also requires the velocity and acceleration information of

the reference position,  $R_Y(s)$ . However, unlike from the former, it includes the feedback speed and position controller gains, which makes it complicated. Moreover in most of the servo motor drivers the proportional and integral gains are scheduled according to motor speed, this makes the implementation of the pre-filter  $H(s)$  impossible. Therefore, in the practical application the motor speed and torque feedforward is applied as mention in Section 7.4. It should be noted that the feedforward scheme shown in Figure 7-11 does not bring and additional cost, since most of the servo motor drive has a separate supplementary speed,  $u_{M1}$ , and torque,  $u_{T1}$ , input ports.

### 7.6 Disturbance Feedforward Controller Design

The effect of external load  $F_L$  on the actuator position response,  $Y_A(s)$  can be represented by two decoupled transfer function  $G_{TF}(s)$  and  $G_{VF}(s)$ , as shown in Figure 7-14. The  $G_{TF}(s)$  component represents the effect of external load on the motor shaft, and the  $G_{VF}(s)$  component represents the effect on actuator speed.

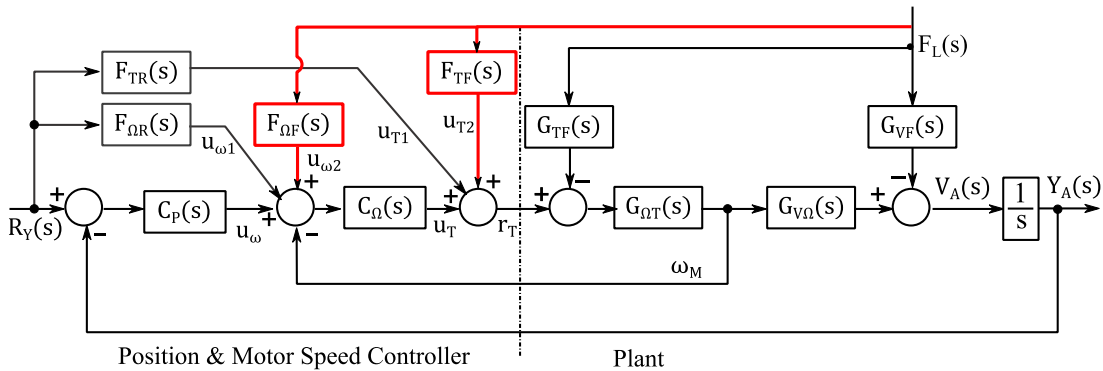


Figure 7-14 Block diagram representation of the disturbance feedforward

By reducing the block diagram given in Figure 7-2, the transfer function between external load input and motor torque,  $G_{TF}(s)$  is found as follows.

$$G_{TF}(s) = G_{V\Omega}(s) = \frac{AD_p}{Cms^2 + (bC + mH)s + bH + A^2} \quad (7-19)$$

Similarly, the transfer function between external load input and actuator speed,  $G_{VF}(s)$  is found as follows.

$$G_{VF}(s) = \frac{Cs + H}{Cms^2 + (bC + mH)s + bH + A^2} \quad (7-20)$$

From Figure 7-14, it is obvious that in order to eliminate the effects of external load input on motor shaft, the feedforward torque controller must be  $F_{TF}(s) = G_{TF}(s)$ .

$$F_{TF}(s) = \frac{AD_p}{Cms^2 + (bC + mH)s + bH + A^2} \quad (7-21)$$

Note that neglecting the friction and capacitance parameters, the torque feedforward controller defines an expected kinematic relationship between the external load and motor torque as follows.

$$u_{T2} = \frac{D_p}{A} F_L \quad (7-22)$$

In order to eliminate the effect of external load on the actuator speed, a feedforward motor speed has to be utilized. In Figure 7-14, assuming the motor speed loop is sufficiently fast,  $\Omega_{set} = \Omega_{mot}$ , the motor speed feedforward controller,  $F_{\Omega F}$ , is defined as follows.

$$F_{\Omega F}(s) = \frac{G_{VF}(s)}{G_{V\Omega}(s)} = \frac{Cs + H}{AD_p} \quad (7-23)$$

The transfer function given in Eq. (7-23), is an expected result. Physically, it implies that, the external load causes flow losses due to pump leakage, with the amount of  $Q_l = \frac{F_L}{A} H$ . In order to compensate the flow losses the pump should be driven with the speed of  $u_{\omega 2} = Q_l/D_p$ . Furthermore, due to compression of the hydraulic oil, flow losses occur with the amount of  $Q_{lc} = \frac{d}{dt} \left( \frac{F_L}{A} \right) \cdot C$ , and in order to compensate the compression losses the pump should be driven with the speed of  $u_{\omega 2} = Q_{lc}/D_p$ .

The effect of disturbance rejection feed forward speed  $F_{\Omega F}(s)$  and torque  $F_{TF}(s)$  controllers are shown on the compliance graph given in Figure 7-15. Note that the frequency response is drawn for standard PI, instead of the semi-integrator. It is seen

that the speed feedforward,  $F_{\Omega F}$ , that only considers the pump leakage losses,  $H$ , improves the low frequency stiffness and has no effect on the mid and high frequency response. On the hand the speed feedforward  $F_{\Omega F}$  that only considers the hydraulic actuator capacitance,  $C$ , improves the mid frequency stiffness. Note that the latter one requires the derivative of the external load as shown in Eq. (7-23). The mid frequency stiffness can be well improves with the use of torque feedforward compensator,  $F_{TF}$ . The disturbance torque feedforward is very effective since it directly eliminates the effect of external load on the motor torque,  $G_{TF}(s)$ , as shown by block diagram representation given in Figure 7-14.

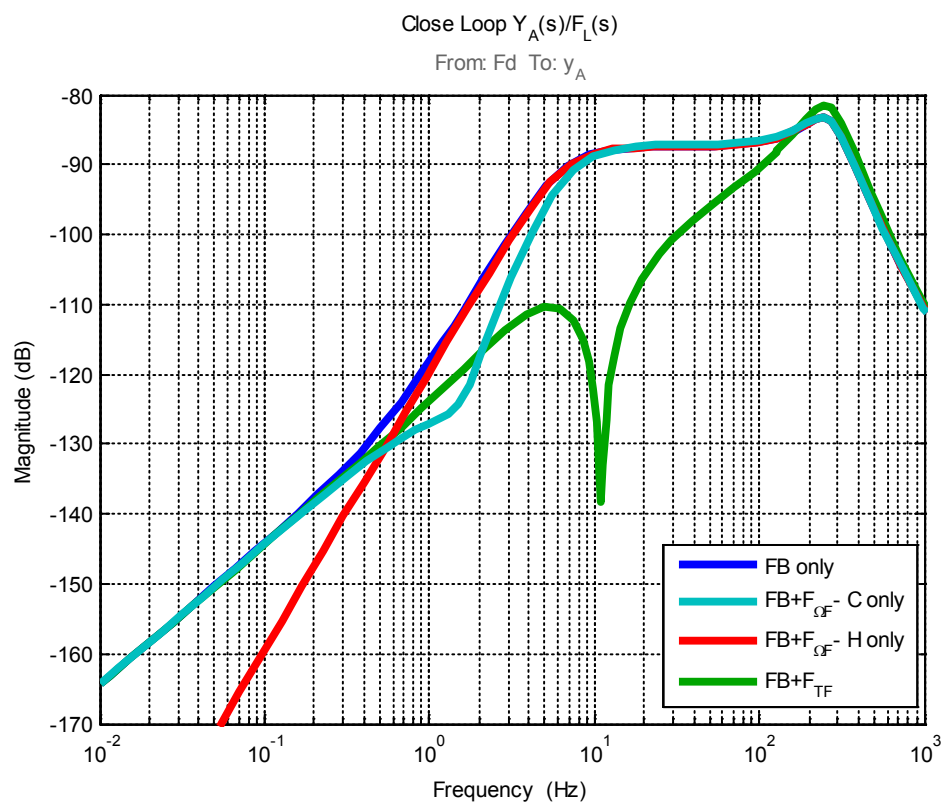


Figure 7-15 Compliance of the close loop system and the effect of disturbance feedforward

In servo mechanisms, generally the set point responses are the predominant factor of concerns, rather than the disturbance rejection (load response). The disturbance rejection capability can be well improved by using large gear ratio,  $A/D_p$ . The disturbance rejection becomes important in direct drive applications, where the servo motor needs to overcome a large load torque directly acting on the motor shaft.

The use of disturbance feedforward should be determined regarding the cost/benefit ratio. The financial cost of new force measurement subsystem, including sensor, signal adaptation and transmission, together with the introduced additional measurement noise, should be considered. Therefore, in the proposed EHA system the disturbance rejection feed forward compensation is not applied, and the compliance obtained by feedback compensation is considered to be sufficient.

### 7.7 Reference Trajectory Generation

The operation region of the EHA, defined on the load versus velocity plane, is mainly determined by the servo motor speed and torque limitations. Therefore the reference position input should be compatible with the velocity and acceleration limits of the actuator. Furthermore, the reference motor speed and torque feed forward controllers require the velocity, and acceleration information of the desired trajectory. For these two reasons a reference input generator is utilized. In most of the servo motor software set point generator (trajectory generator) is available. In the scope of this thesis since the position controller is implemented on a real time controller, the reference input generator is constructed in MATLAB<sup>®</sup>/Simulink<sup>®</sup> environment as shown in Figure 7-16.

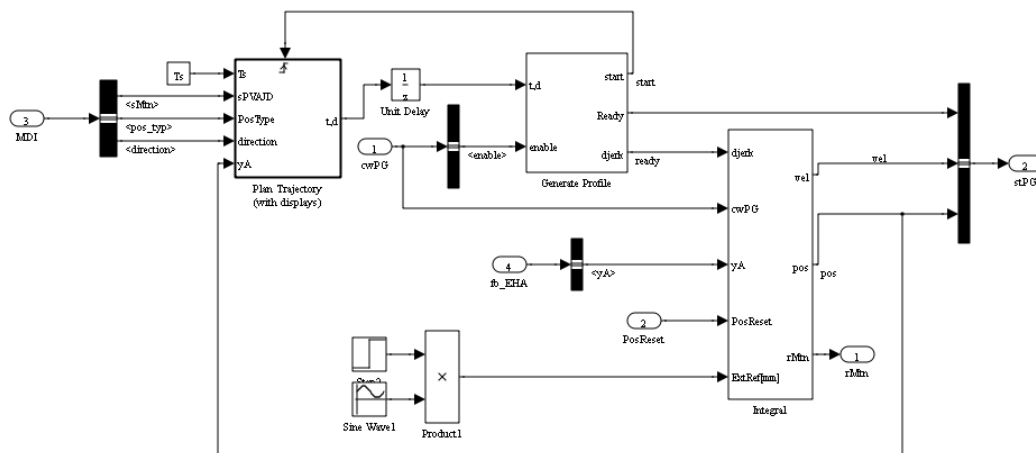


Figure 7-16 Fourth order reference trajectory generator model

The reference input generator is fourth order which means that the desired position is formed by the maximum values of the derivative of jerk, jerk, acceleration and

velocity limitations. The reference trajectory planning utilized in this model are based on Lambrechts's study given in [100]. The output of the reference trajectory generator is shown in Figure 7-17. It is seen that the trajectory for the set point position of 10mm is achieved by considering the maximum acceleration and speed limitation, that are  $3000 \text{ mm/s}^2$  and  $150 \text{ mm/s}$  respectively.

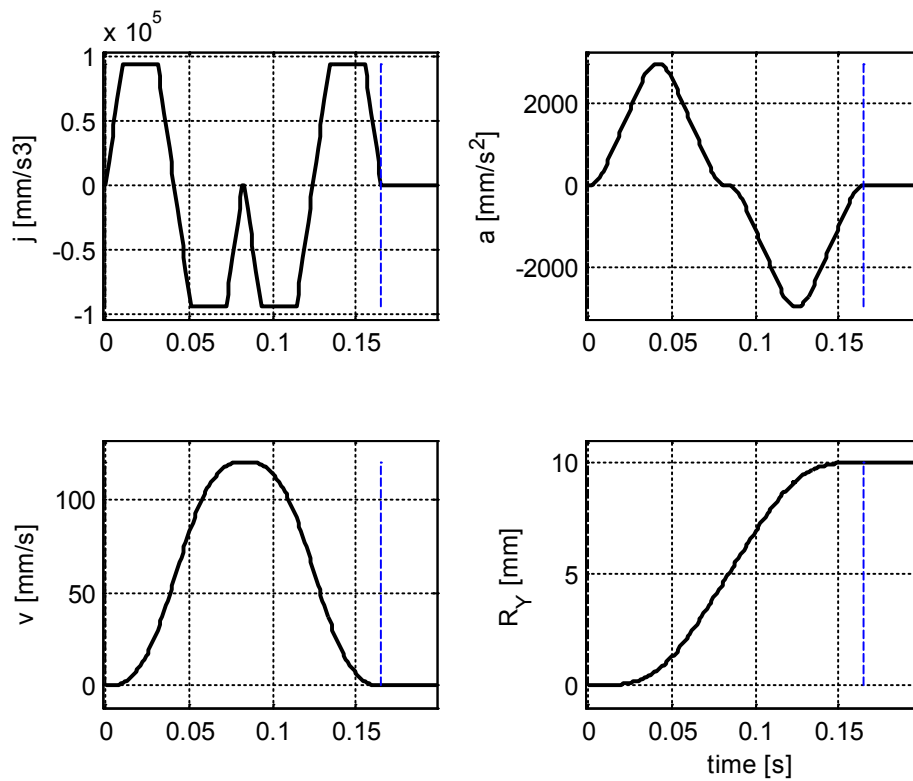


Figure 7-17 Reference trajectory generator output

## 7.8 Supervisory Controller

A finite state machine is design as the supervisory controller. The supervisory controller is responsible for transitions between the standstill and operation-on states. It determines the switching of the drive power, motion controller and reference generator. Furthermore it implies the contingency plan in case of a unexpected error or operation. A fault management system stops the drive in a safe mode. The supervisory controller is designed by using MATLAB<sup>®</sup>/State Flow<sup>®</sup> toolbox and implemented in real time operating PC. The supervisory controller designed as a finite state machine is given in Figure 7-18.

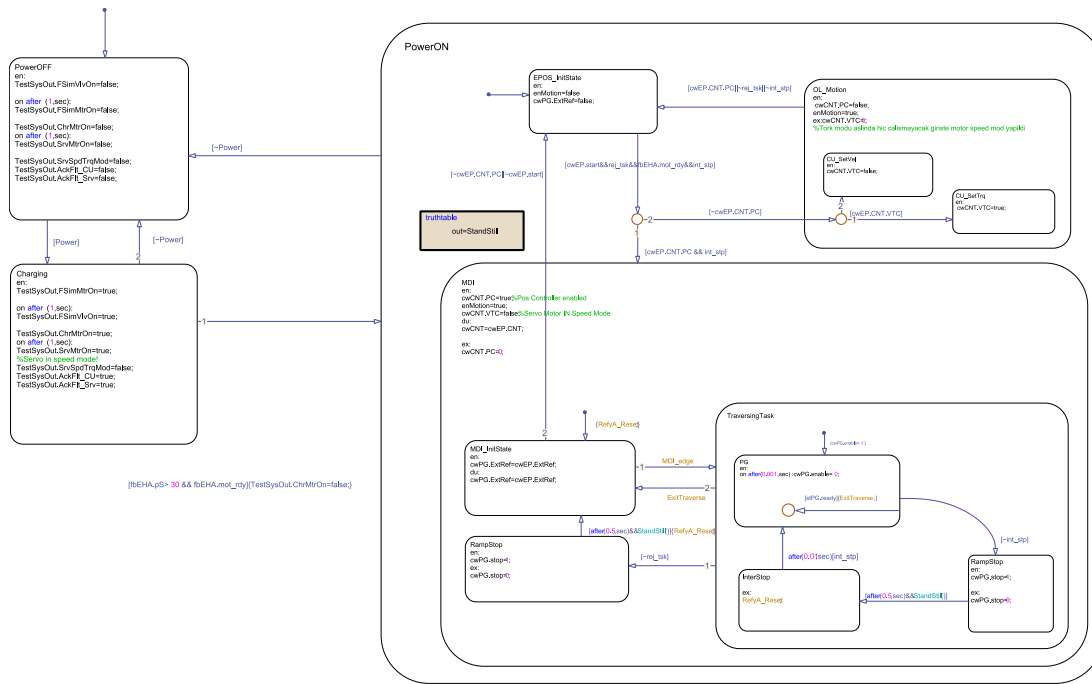


Figure 7-18 Finite state machine of the supervisory control

## 7.9 Performance Evaluation and Experimental Tests

The proposed EHA system together with the asymmetric shuttle valve spool solution and the designed feedback and feedforward controllers are tested in the experimental load simulator test set up, which is introduced in section 3.4. Position controller that consists of supervisory controller, reference trajectory generator, feedback and feedforward controllers are implemented on a MATLAB<sup>®</sup>/Simulink<sup>®</sup> model as shown in Figure 7-19. The Simulink file is compiled and downloaded to the real time target PC. The solver used in the test file is ode4 with fixed step sample time, 1 ms.

In order to evaluate the performance of the proposed EHA system three types of tests are done. In the first tests the positioning of the EHA is evaluated, while in the second tests the set point tracking performance of the EHA is evaluated. Lastly, in the third tests the disturbance rejection capability of the proposed system is evaluated. Each test is carried out with controlled external load input whose magnitude is determined by the desired shuttle valve position. The controlled external load is applied on the EHA by the load simulator.

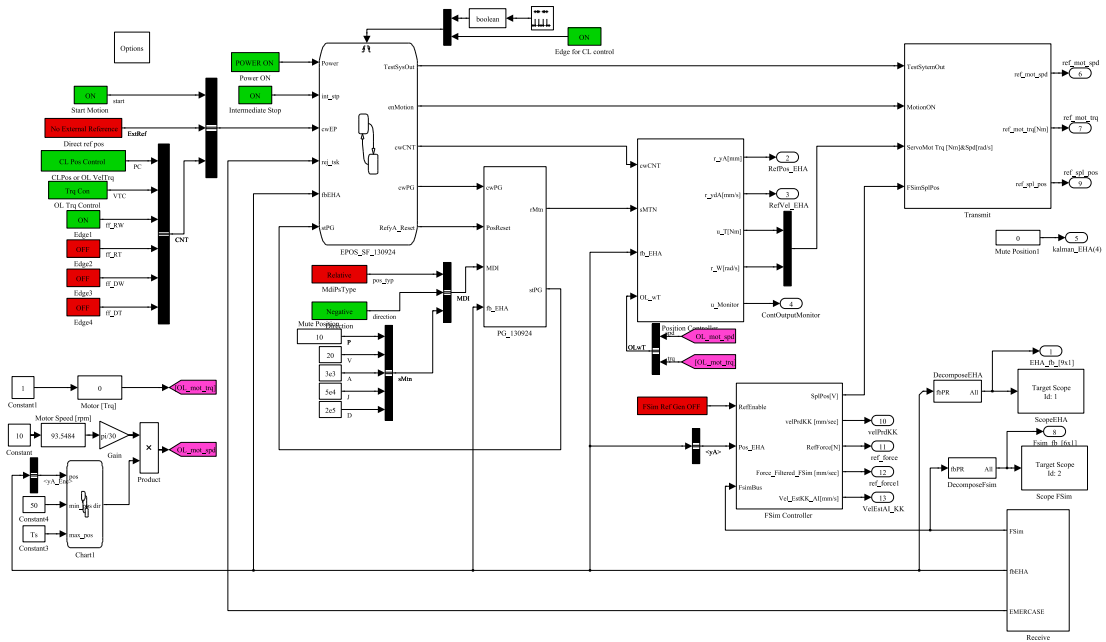


Figure 7-19 The MATLAB®/Simulink® model of the real time EHA controller

## 7.10 Positioning Performance

The position performance of the proposed EHA is first tested for the fully opened spool position. An external load of  $F_L = 7 \text{ kN}$  is applied on the EHA by the load simulator. The applied load and the corresponding chamber pressures are given in Figure 7-20. The pressure difference  $\Delta P_{ab} = P_a - P_b$  between the cap-side and rod side chambers are  $\approx 17 \text{ bar}$ , which is greater than the shuttle valve cracking pressure  $P_{sc} = 5.8 \text{ bar}$ . Therefore, the shuttle valve is fully opened to connect the rod-side chamber to the accumulator line.

Under this loading condition  $60 \text{ mm}$  relative set point is applied. The position response of the system together with the desired trajectory is given in Figure 7-21. It is clearly seen that the positioning accuracy of the system is in the order of  $5 - 10 \mu\text{m}$ , which corresponds to the resolution of the linear encoder. The maximum actuator speed during positioning is  $200 \text{ mm/s}$ . It is seen that during this interval the tracking error is nearly zero. It should be noted that the performance of the velocity tracking is mainly due to the motor speed and torque feedforward compensators.

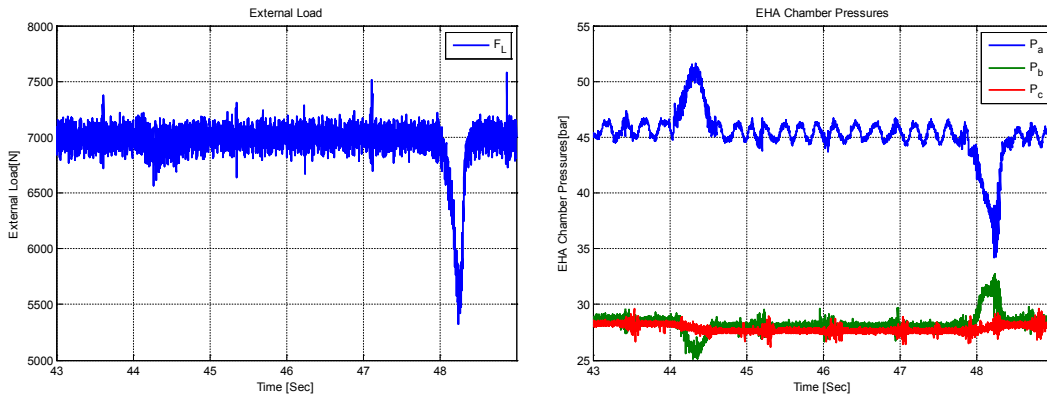


Figure 7-20 Applied external load  $F_L$  and the chamber pressures in positioning tests

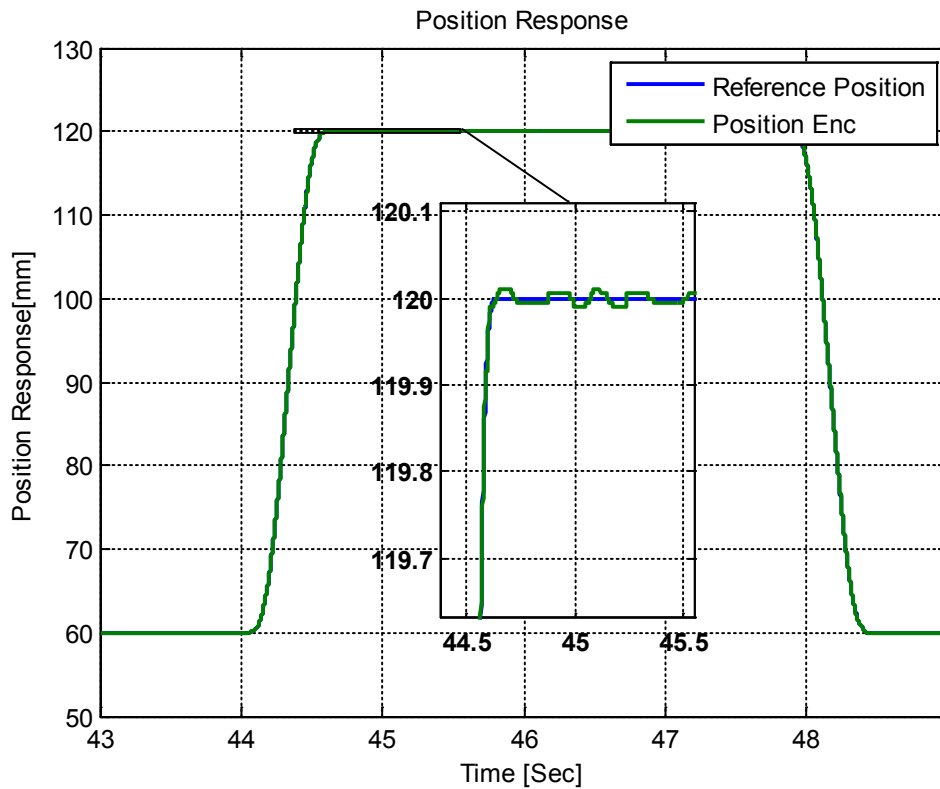
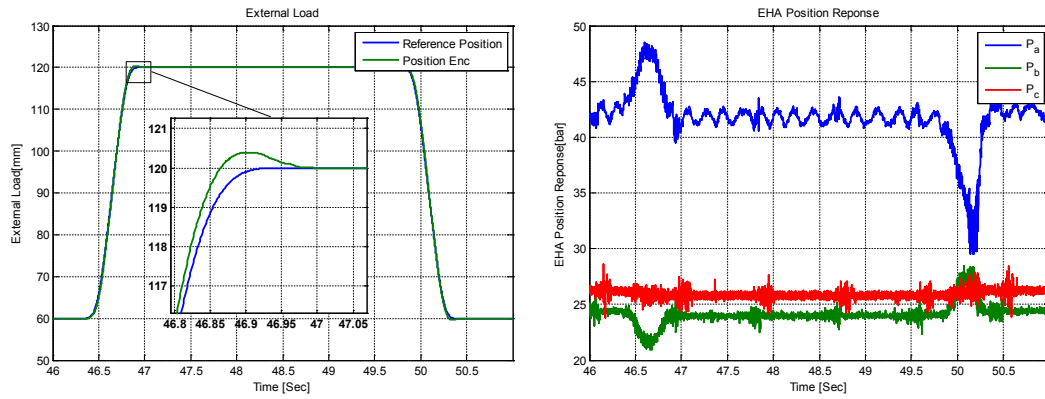


Figure 7-21 Position response for fully opened shuttle valve spool

In Figure 7-22 the two feedforward compensators are disabled. During the positioning from  $Y_A = 60 \text{ mm}$  to  $R_Y = 120 \text{ mm}$  the tracking error is not zero, furthermore, it is seen that the position response overshoots the set point by 0.5 mm.



**Figure 7-22 Position reponse effects of the feed forward compensators**

In the second part, the positioning performance of the EHA is tested inside the critical load pressure region. Therefore an external load of  $F_L = 0.5 \text{ kN}$  is applied on the EHA. The external load together with the chamber pressures are shown in Figure 7-23. In the figure it is seen that the chamber pressures are close to each other. The pilot pressure is nearly  $\Delta P_{ab} \approx -5 \text{ bar}$ , which is very close to the shuttle valve cracking pressure  $P_{sc} = 5.8 \text{ bar}$ .

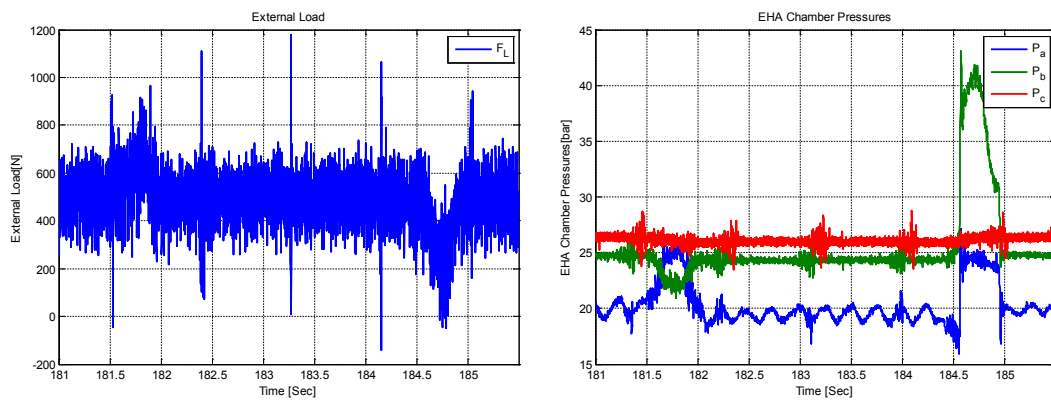


**Figure 7-23 Applied critical external load and pressure responses in positioning tests**

Under this loading condition again  $60 \text{ mm}$  relative set point with  $200 \text{ mm/s}$  maximum velocity is applied. The position response of the system together with the desired trajectory is given in Figure 7-24. Unlike from the previous case, the position response overshoot the desired set point by  $0.15 \text{ mm}$ . This is mainly due to the deficiency of the feedforward compensator. Note that the feedforward gains are calculated by considering the fully opened shuttle valve positions only. In between

the two positions the calculated gains are switched linearly. Not calculating the true transformer ratio for that loading condition, results in a slight overshoot. On the other hand, the steady state error is compatible with the fully opened shuttle valve position. The positioning accuracy of the system is in the orders of  $5 - 10 \mu m$ .

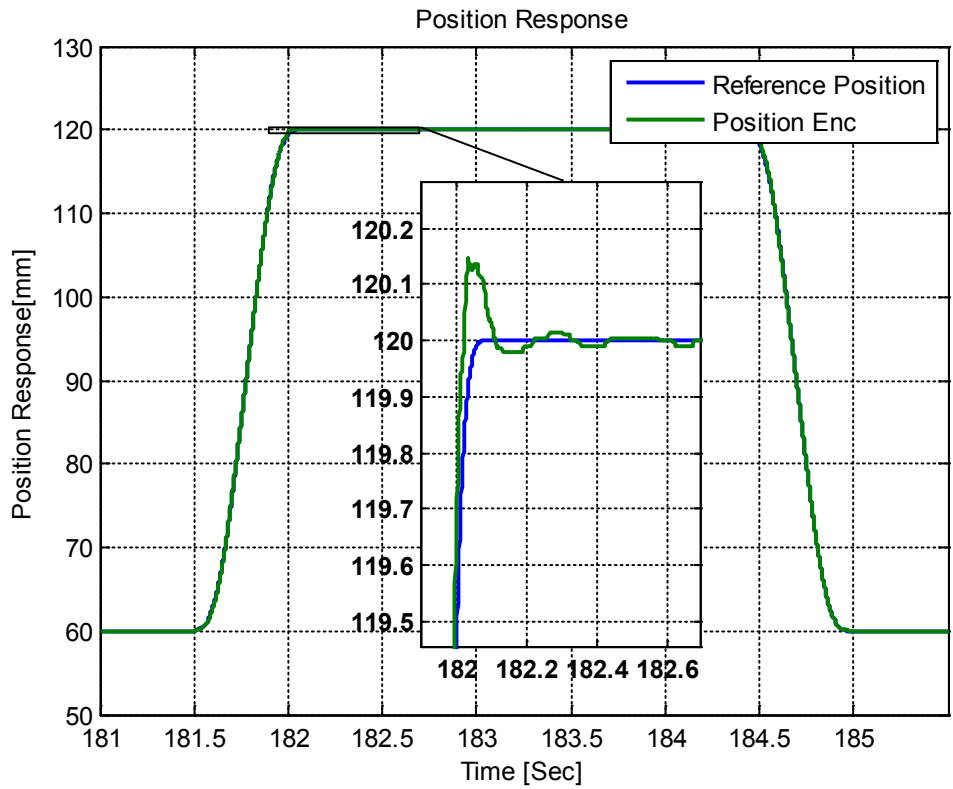


Figure 7-24 Position response under critical external load of 0.6 kN

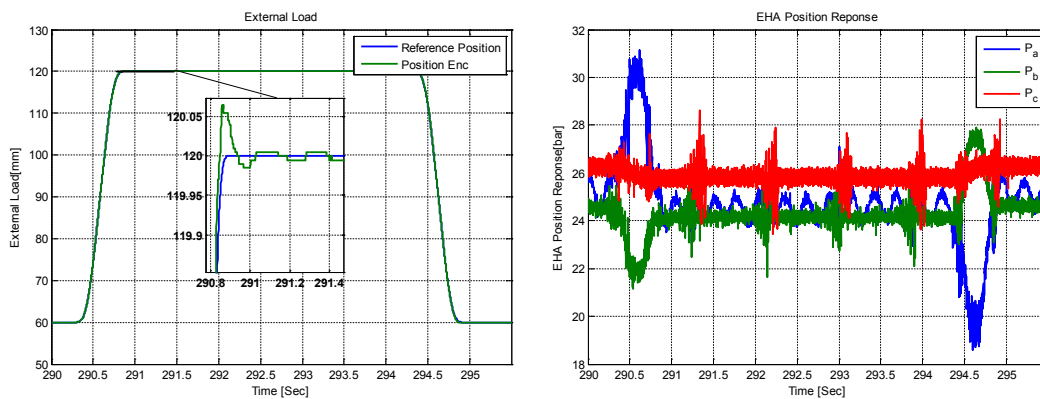


Figure 7-25 Position and pressure response under critical external load of 2 kN

The same positioning test is repeated by increasing the external load to  $F_L = 2 \text{ kN}$ . Chamber pressure responses are given in Figure 7-25. It is seen that the chamber pressures are close to each other, which means that the shuttle valve is centered, and the rod-side chamber is connected to the accumulator line over the pre-opening provided at the BC port. Likewise the previous case, the position response makes an overshoot, but the magnitude of the overshoot is decreased to  $0.05 \text{ mm}$ . Furthermore, the steady state error performance is the same and in the order of encoder resolution.

### 7.11 Set Point Tracking Performance

In this section the set point tracking performance of the proposed EHA system is tested. The first test is done for the fully opened shuttle valve position. The external load applied on the actuator is  $F_L = 7 \text{ kN}$ . In Figure 7-26, the applied force and chamber pressure responses are given. The difference of the chamber pressures clearly reveals that the shuttle valve is fully opened to connect the rod-side chamber to the accumulator line.

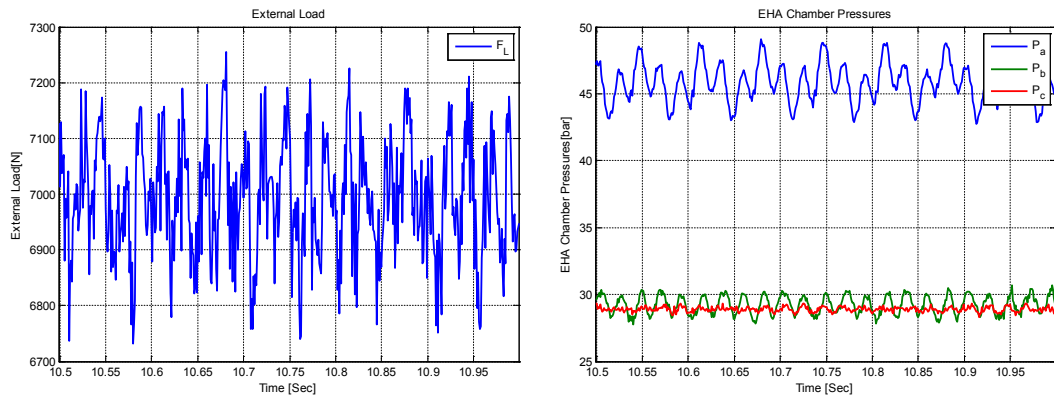


Figure 7-26 Applied external load and pressure responses in set point tracking tests

Under this external load the system tracks a sinusoidal reference input position with amplitude  $0.2 \text{ mm}$  and frequency  $15 \text{ Hz}$ . The position response is given in Figure 7-27. During the test interval both the motor speed and motor torque feedforward compensators are active. It is seen that the magnitude of the response clearly follows the reference input with a phase lag close to zero. In order to show the effect of the

feed forward compensators, the tracking performance with feedback only is given in Figure 7-28.

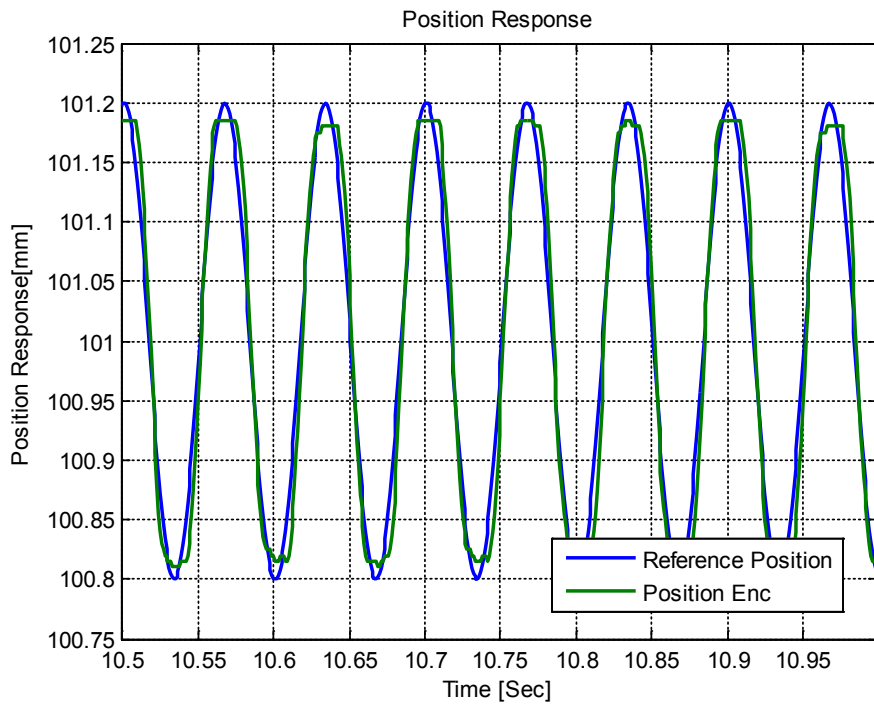


Figure 7-27 Set point tracking performance for fully opened shuttle valve position

When the feedforward compensators are de-activated a phase lag and gain loss occurs. Note that the measured responses are compatible with the frequency response of the closed loop system given in Figure 7-12. In Figure 7-28 the time between the two peak values is 20 ms, which means that the phase lag when considering the period  $\frac{1}{15}$  s, is  $108^\circ$ . Furthermore, the amplitude ratio is  $20\log_{10}\left(\frac{5}{8}\right) = -4$  dB.

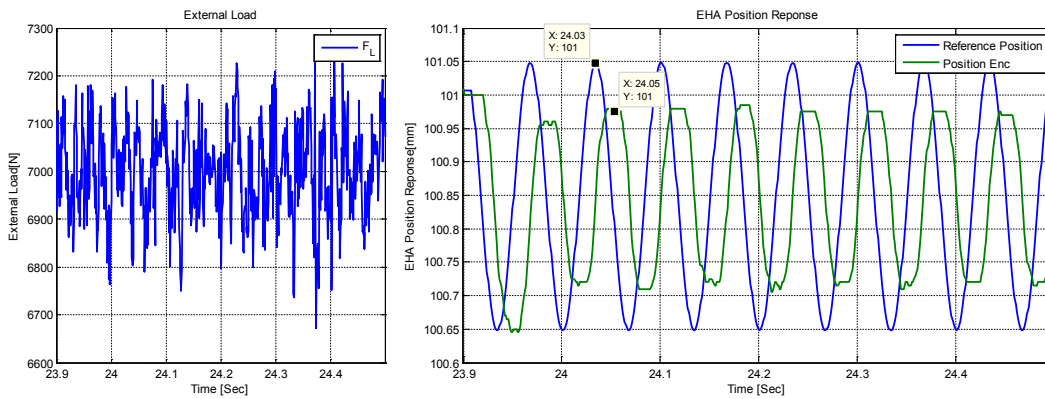


Figure 7-28 Set point tracking performance with feedback compensator only

The set point tracking performance of the EHA is further evaluated in the critical region. For that purpose an external load of  $F_L = 0.8 \text{ kN}$  is applied on the EHA. In Figure 7-29 it is clearly seen that the chamber pressures are close to each other and their difference is smaller than the shuttle valve cracking pressure  $P_{sc} = 5.8 \text{ bar}$ .

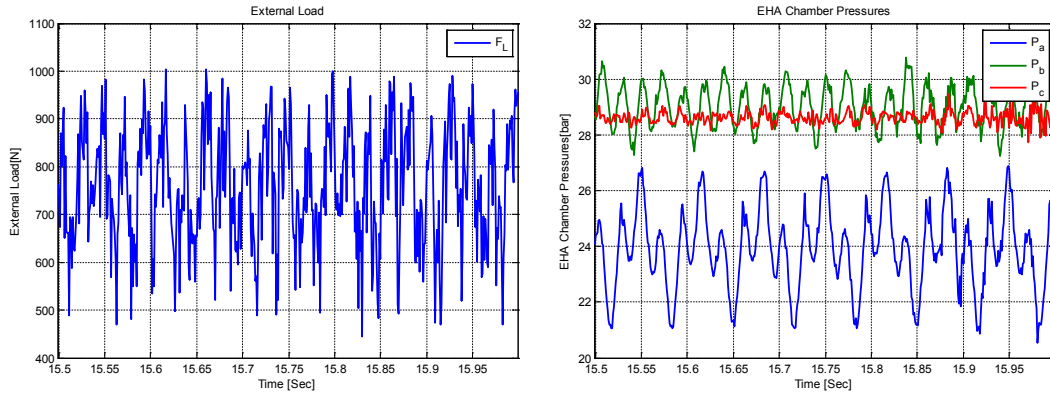


Figure 7-29 Applied critical external load and pressure responses in tracking performance tests

During the test interval both the motor speed and torque feedforward compensators are active. The position response is given Figure 7-32. When compared with the fully opened shuttle valve case, it is seen that the performance degraded slightly; there occurs an amplitude loss. Furthermore, the actuator velocity changes abruptly due to the valve switching.

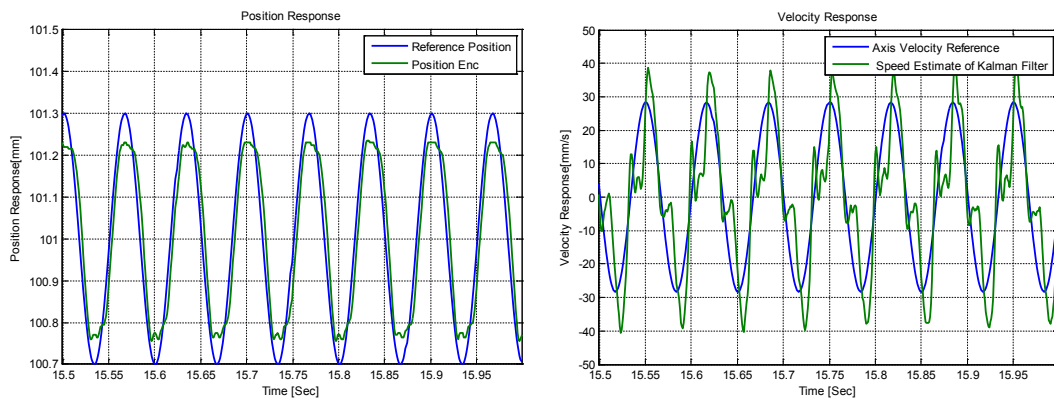


Figure 7-30 Set point tracking performance under critical load of 0.7 kN

## 7.12 Disturbance Rejection Performance

In this section, in order to evaluate the disturbance rejection performance of the EHA step and sinusoidal force inputs are applied on the EHA by the load simulator.

The step force with magnitude  $F_L = 7.5 \pm 2.5 \text{ kN}$  and  $0.5 \text{ Hz}$  frequency is applied on the EHA. From the chamber pressure response of the EHA given in Figure 7-31, it is seen that, under this loading condition, the shuttle valve is fully opened to connect the cap-side chamber to the accumulator line.

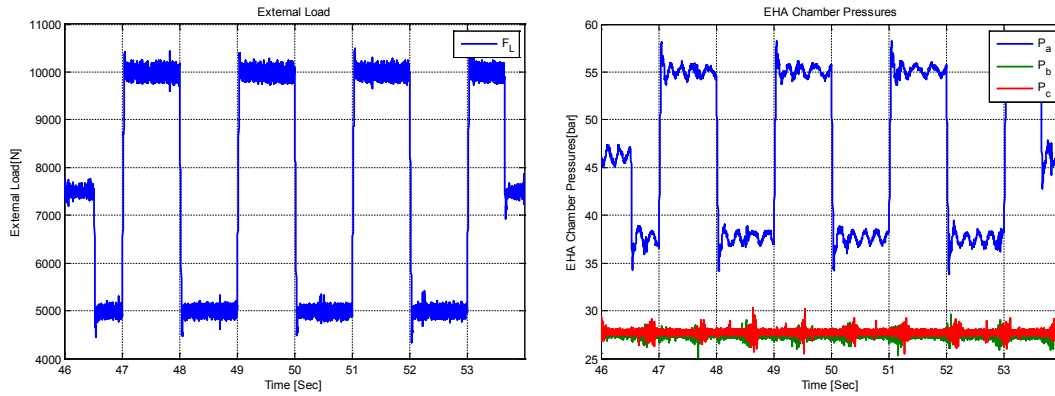


Figure 7-31 External load step input and pressure responses

The position and velocity response of the EHA is given in Figure 7-32. The position error due to  $5.0 \text{ kN}$  amplitude step input is  $0.15 \text{ mm}$ . Furthermore, the position responses settle down to set point  $100 \text{ mm}$  nearly in  $150 \text{ ms}$  time. The steady state errors corresponding to  $5 \text{ kN}$  and  $10 \text{ kN}$  external loads are ranging in between  $5 \mu\text{m}$  and  $10 \mu\text{m}$ . In Figure 7-32, the velocity response is also provided. It is seen that the actuator velocity response for  $5 \text{ kN}$  step disturbance load is  $22 \text{ mm/s}$ .

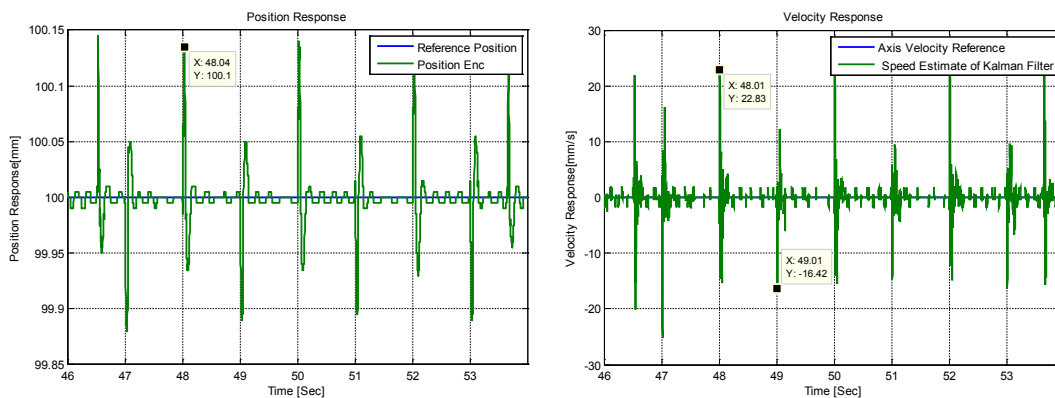
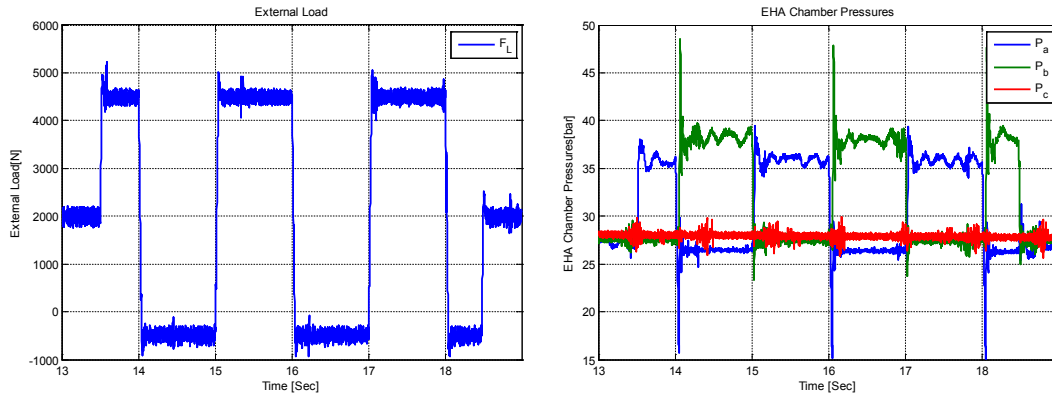


Figure 7-32 Position and velocity response to external load step input

The disturbance rejection performance of the EHA degrades for the external load that corresponds to shuttle valve switching. In order to illustrate it an external load with

magnitude  $F_L = 2 \pm 2.5 \text{ kN}$  is applied on the EHA. From the chamber pressure response of the EHA given in Figure 7-33, it is seen, during time  $t = 15 - 16 \text{ s}$ , the shuttle valve is opened to connect the rod side chamber to the accumulator line, since the pilot pressure is  $\Delta P_{ab} = 9 \text{ bar} > P_{sc} = 5.8 \text{ bar}$ . On the other hand, during time  $t = 16 - 17 \text{ s}$ , the shuttle valve changes position and cap side chamber is connected to the accumulator line, since  $\Delta P_{ab} = -12 \text{ bar} < P_{sc} = -5.8 \text{ bar}$ .



**Figure 7-33 Critical external load step input and pressure responses**

The resulting position and velocity response of the EHA is given in Figure 7-34. It is seen that the position error due to  $5 \text{ kN}$  amplitudes step input is  $0.4 \text{ mm}$ . The steady state errors are not affected by the shuttle valve switching. The positioning error for  $F_L = 4.5 \text{ kN}$  and  $F_L = 0.5 \text{ kN}$  loadings are in between  $\pm 5 \mu\text{m}$ . The shuttle valve switching considerably affects the velocity response. It is seen that the EHA velocity goes up to is  $70 \text{ mm/s}$ . When compared with the fully opened shuttle valve response the velocity response is degraded nearly by three times. For the same amplitude disturbance force input, velocity response increased from  $22 \text{ mm/s}$  to  $70 \text{ mm/s}$ , which is considerably high. On the other hand the effect of spool switching on position response is acceptable. When compare with the fully opened shuttle valve case, it is seen that the error increased from  $0.15 \text{ mm}$  to  $0.4 \text{ mm}$ .

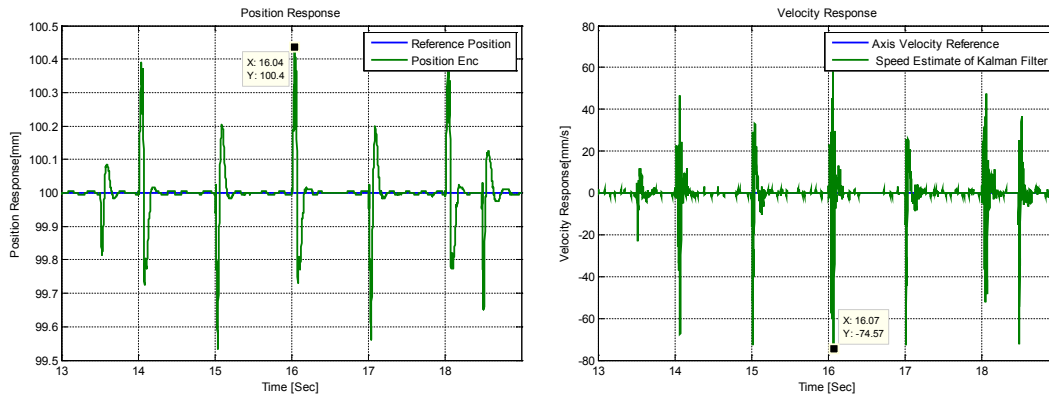


**Figure 7-34 Position and velocity response to critical external load step input**

The sinusoidal external force applied by the load simulator is shown in Figure 7-35. The external load is not an exact sinusoidal since the applied load and frequency is out of the load simulators design limits. The external load has an  $F_L = 2.35 \text{ kN}$  amplitude with  $7.4 \text{ kN}$  bias and  $10 \text{ Hz}$  frequency. Note that from the chamber pressure responses given in Figure 7-35, it is seen that the shuttle valve is fully opened, and the rod-side chamber is connected to the accumulator line.

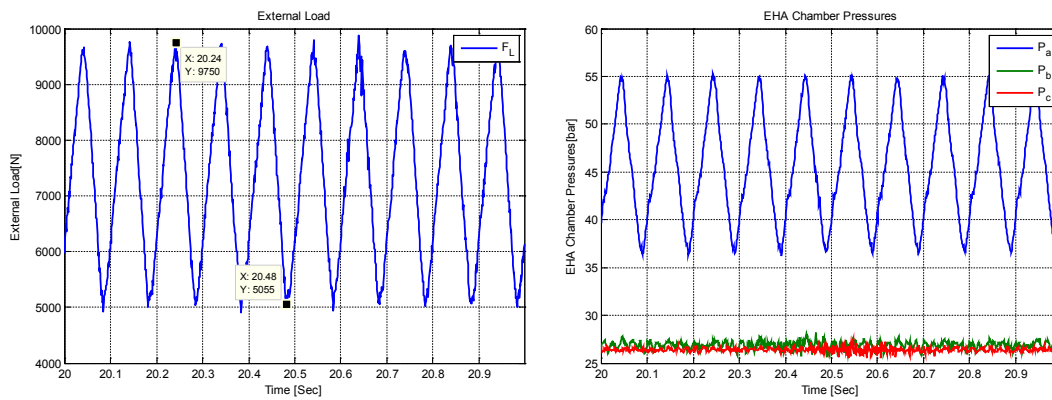


**Figure 7-35 Sinusoidal external load input with 10 Hz frequency, and pressure responses**

The position response is given in Figure 7-36. It is seen that the position error is  $0.12 \text{ mm}$ . By using the force versus position relation, the stiffness of the hydraulic actuator for  $10 \text{ Hz}$  excitation frequency is calculated as  $\approx 20 \text{ kN/mm}$ . Note that the calculated stiffness is compatible with the compliance given in the frequency response of  $F_L(s)/Y_A(s)$  in Figure 7-6. In that figure, the compliance at  $10 \text{ Hz}$

excitation frequency is  $-88 \text{ dB}$  and is compatible with the experimental results  $20 \log_{10} \left( \frac{1}{20 \cdot 10^3} \right) = -86 \text{ dB}$ .

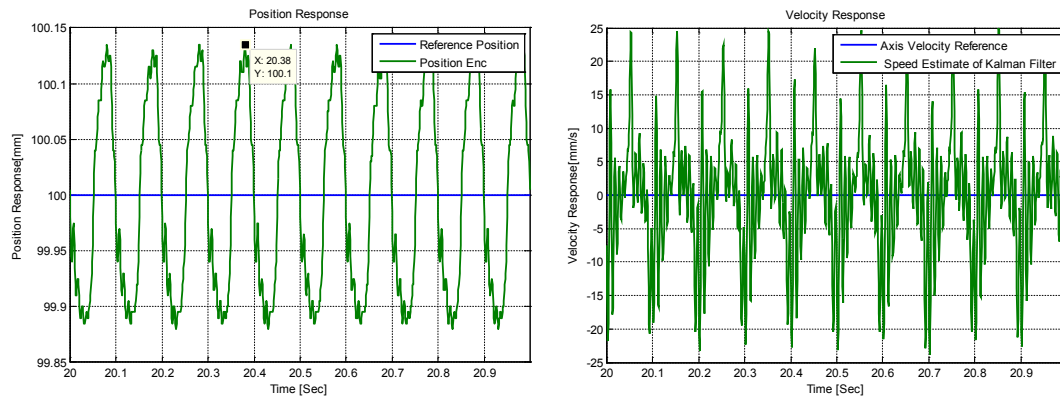


**Figure 7-36 Position and velocity response to sinusoidal external load with 10 Hz frequency**

The same external load is applied by reducing the excitation frequency to 5 Hz. The applied load and the chamber pressure responses are given in Figure 7-37. It is seen that this time the disturbance load profile is sinusoidal; this is an as expected, result since the loading is appropriate for the load simulator design limits.

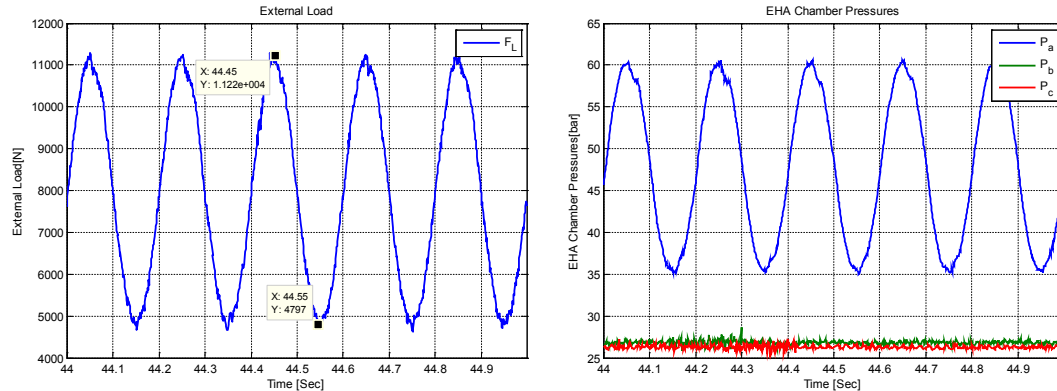


**Figure 7-37 Sinusoidal external load input with 5Hz frequency, and pressure responses**

The position and velocity response of the EHA is given in Figure 7-38. The amplitude of the sinusoidal external load is  $3 \text{ kN}$ . The corresponding actuator position is  $0.12 \text{ mm}$ . Therefore the stiffness of the actuator at 5 Hz excitation frequency is calculated as  $25 \text{ kN/mm}$ . The stiffness has increases by decreasing the excitation frequency, as expected.

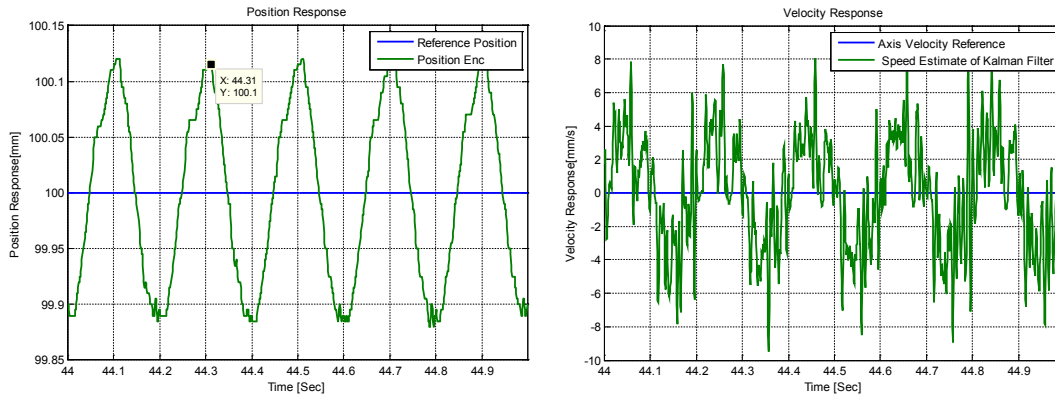


Figure 7-38 Position and velocity response under sinusoidal external load with 5 Hz frequency

The disturbance rejection of the EHA under critical loading is tested by applying the sinusoidal force as shown in Figure 7-39. The external load has 3 kN amplitude and 5 Hz frequency. The chamber pressure response is also provided in Figure 7-39. From the chamber pressure relations  $\Delta P_{ab} = P_a - P_b$  and the cracking pressure  $P_{sc} = 5.8 \text{ bar}$ , it can be concluded that under this loading condition the shuttle valve position is switching in between the two end positions.

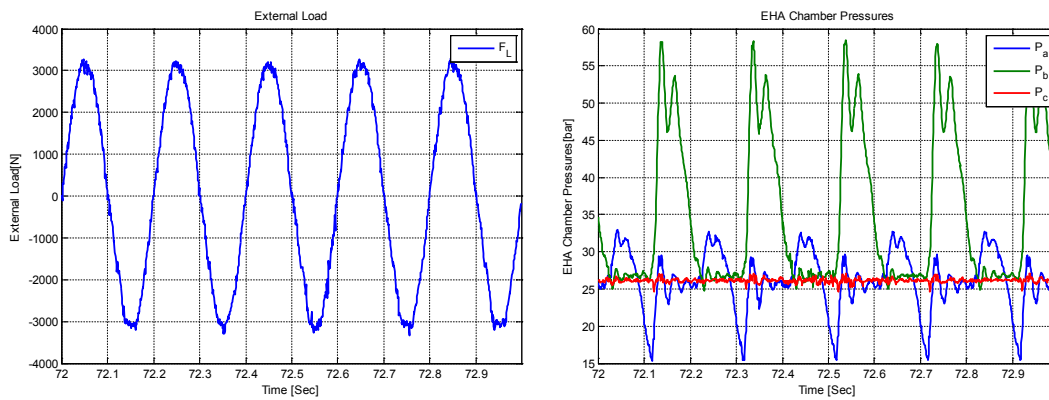
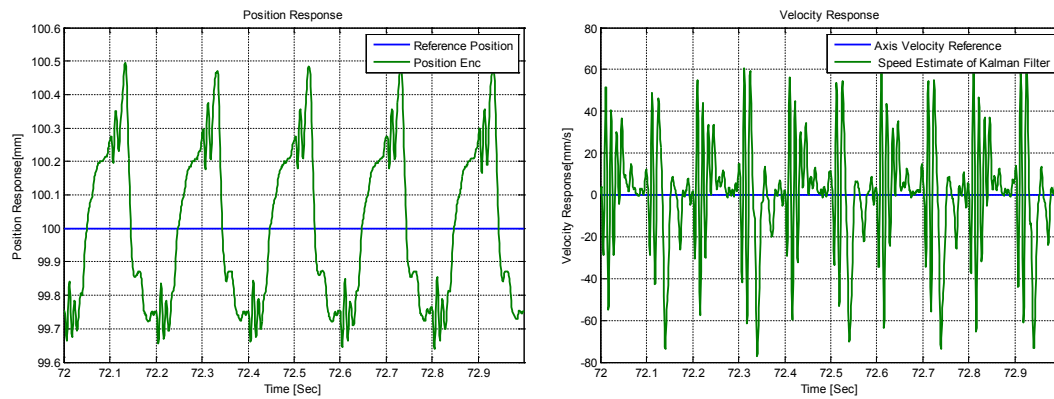


Figure 7-39 Sinusoidal critical external load input and pressure responses

The position response under the critical loading is shown in Figure 7-40. The positioning error is increased to 0.5 mm when compared to 0.12 mm of the previous fully opened valve case. The velocity response also distorted under the critical loading. For the fully opened valve case, the velocity response amplitude is 8 mm/s. Due to valve switching the velocity response for the same amplitude forcing increases up to 60 mm/s.



**Figure 7-40 Position and velocity response under sinusoidal critical external load**

### 7.13 Conclusion

A combined feedback and feedforward control strategy is utilized in the position control system of the electro hydrostatic actuator. The EHA have a three layer cascade control structure. The inner two layers are the PI motor speed and current regulators and they are implemented on the servo motor control unit. These two regulators are tuned by using the commissioning toolbox of the servo motor motion control software. On the other hand the design of the outermost layer which is the position controller is mainly addressed in the scope of this thesis study. A PI regulator with semi integrator is utilized as the feedback position compensator. In order to increase the tracking performance and eliminate the response overshoot to set point changes, motor speed and torque feedforward compensators are designed based on the simplified design plant model. Furthermore, disturbance rejection feedforward compensators are designed and their effects on system stiffness are discussed. The designed feedback and feedforward compensators together with the supervisory motion controllers are implemented on the real time target PC.

The performance of the developed EHA with the proposed asymmetric shuttle valve spool structure is evaluated on the experimental load simulator test set up. The performance of the EHA is evaluated in terms of positioning, set point tracking and disturbance load rejection. The experimental tests are performed under different loading conditions. Controlled external loads are applied on the EHA by the load simulator, and the performance of the EHA is evaluated for different shuttle valve

spool positions. It is shown that the experimental results are compatible with the theoretical results.

Experimentally it is shown that the positioning error of the EHA is in between  $5 - 10 \mu m$ , which is in the order of the linear encoder resolution  $5 \mu m$ . Furthermore, it is shown that the EHA is able to track a sinusoidal signal with  $15 Hz$  frequency without magnitude loss and phase lag. Lastly, the stiffness of the EHA for a sinusoidal external load input with  $10 Hz$  frequency is shown to be  $20 kN/mm$ .

In the scope of this thesis study the controllers are designed by considering the fully opened shuttle valve spool positions. The calculated controller gains are changed linearly in between the two spool positions and no special control effort is applied during the switching of the valve spool. The proposed control strategy is simple and convenient for implementation by a standard market available motion controller. However, it is observed that it cannot eliminate the abrupt velocity response during the shuttle valve switching. In the experimental tests it is shown that under critical external load inputs, which correspond to the centered or partially opened spool position, the performance of the EHA degrades slightly. The actuator velocity changes abruptly due to the shuttle valve switching and the velocity switching distorts the position response. The position distortion is in the order of  $0.1 - 0.5 mm$  and is acceptable for many industrial applications. It should be noted that the proposed valve solution eliminates the instability problem completely and no undesired oscillations are seen due to shuttle valve switching. Lastly it should be mentioned that with the use of load pressure feedback or spool position feedback the effects of spool switching can be suppressed at the expense of increased control effort and hardware cost.

## CHAPTER 8

### SUMMARY, CONCLUSIONS AND RECOMMENDATIONS

#### 8.1 Summary and Conclusions

In this thesis a variable speed pump controlled electro hydrostatic drive system for a single rod actuator is developed. Conventional electro hydrostatic actuators (EHA) and hydrostatic transmission systems utilize hydraulic motors or double rod actuators which have a symmetric structure. The drawback of the single rod actuator in pump control application is the unequal flow rate entering and returning from the actuator due to asymmetric structure of the piston rod assembly.

As mentioned in the literature review, the differential flow compensation can be handled by several ways. Some of these solutions propose the use of a secondary pump and some solutions propose to replace the conventional pump with a three port pump or hydro transformer. Different from these solutions, in the scope of this thesis study the possible solution of the differential flow compensation problem is restricted with the use of a single pump. The hydraulic pump utilized in this solution is a conventional pump, and is able to work in the 4-quadrants of the pressure versus flow plane.

In literature, the single pump hydraulic circuit solutions either utilize pilot operated check valves or a closed center shuttle valve in order to solve the differential flow compensation problem of the single rod hydraulic actuator. Both the two solutions commonly suffer from undesired pressure oscillations, which are named as system internal instability. In order to eliminate this problem, besides the controller related software solutions, addition of on/off valve components together with sensor and actuator hardware are proposed as a physical solution. Besides the solutions to instability, the theoretical investigation of the stability problem is limited in the literature. The current stability analysis studies treat the shuttle valve as an ideal

switching element, i.e. the whole system is investigated as if the shuttle valve is either closed or open.

In the scope of this thesis study an internal pilot operated shuttle valve is utilized to compensate for unequal flow rate compensation. The thesis study mainly covers the non-linear modeling of the EHA, stability analysis that includes the shuttle valve parameters and dynamics, physical solutions to eliminate instability i.e. modification of shuttle valve spools, position controller design and experimental evaluation of the proposed system.

The thesis study start with the non-linear mathematical modeling of the EHA considering all its components namely: the hydraulic pump, the electric motor together with its control unit, shuttle valve, hydraulic accumulator and the hydraulic actuator. Based on the mathematical formulation simulation models are constructed in MATLAB<sup>®</sup>/Simulink<sup>®</sup> and SimHydraulic<sup>®</sup> environments. The simulation models are verified with the measurements taken from an experimental test set up. The experimental test set up is constructed for the development of the EHA and consists of two parts. The first part is the pump speed controlled EHA system under development, and the second part is the valve controlled load simulator. The load simulator is constructed to facilitate the application of controlled external loads on the EHA and is the subject of M.Sc. thesis [16].

After introducing the mathematical modeling, the thesis study addresses the stability problem of the pump controlled asymmetric hydraulic actuators. Unlike from the literature, the reason of system instability is investigated by including the shuttle valve dynamics. Furthermore, different from the previous studies, a simple physical solution which is the use of on underlapped shuttle valve is proposed. The approach given in the stability analysis is not limited with variable speed pump controlled actuator but can be extended to displacement controlled circuits, since the pump is only considered as ideal flow source.

For the stability analysis first a simple linear model of the system is derived. Instead of using individual actuator chamber pressures as separate variables the system model is obtained in the load pressure versus velocity domain. A critical load pressure region is defined in the load pressure versus velocity plane. The location

and size of this region are determined in terms of the accumulator pressure and the shuttle valve opening pressure. In the critical load pressure region, the shuttle valve is whether centered or partially opened, and outside that region it is fully opened.

A common state space representation of the whole system is obtained for both centered and fully opened shuttle valve cases and it is shown that all the possible equilibrium points have stable nature. For the equilibrium points requiring a partially opened valve position, it is shown that a continuous oscillatory response occurs in the critical load pressure region during the retraction of the actuator, commonly termed as instability in earlier work. A mathematical proof of this instability is given by linearizing the flow equations for shuttle valve characteristics. In the critical load pressure region, a close center shuttle valve cannot remain in the centered position but likely to open partially since it has no pre-opening to compensate for the unequal flow rates of the actuator. Therefore, the use of an underlapped shuttle valve is proposed to avoid instability, which remains in the centered position up to a certain retraction speed. A simple relationship between the critical retraction speed limit and the amount of valve underlap is derived for a stable operation.

The theoretical findings are validated by numerical simulations. Furthermore, the instability of the system with the use of a closed center shuttle valve is demonstrated with an experimental study. After replacing the shuttle valve with the underlapped one, the solution to avoid instability is also demonstrated on the same test set up via similar open loop tests. It is shown that in the critical load pressure region, an underlapped shuttle valve provides a stable operation region; however, it decreases the transformer ratio between pump speed input and the actuator speed output. Therefore, a significant emphasis should be given for the selection of the underlapped shuttle valve.

The underlapped shuttle valve spool solution eliminates the instability problem and is a reasonable and simple physical solution. Different from the previous instability solutions that utilize additional hardware components, only the shuttle valve type is changed, i.e. instead of a closed center shuttle valve use an underlapped shuttle valve. However, the deficiency of the underlapped shuttle valve solution is the circulating leakage flow rates that are formed during the centered valve position. In

order to understand this phenomenon a generalized kinematic model is developed. The kinematic model is used to define the transformer ratio between the pump drive speed and actuator speed. The kinematic model neglects the all the dynamics of the moving masses, compressibility of the fluid, and flow losses. The pressure states are defined with respect to the accumulator pressure. In that way representation of the system equations are simplified. Furthermore, besides the cracking pressure four more pressure constants are defined, in order to determine the shuttle valve state.

Based on the kinematic model, first the transformer ratio and dead pump speeds are investigated. It is concluded that a shuttle valve with relatively high cracking pressure will be problematic, since it will increase range of the critical load pressure region. The closed loop performance of an EHA may degrade if the load loci enters into that region, since the transformer ratio between pump speed input and actuator speed output is probable to vary between infinity or zero. As a first solution the compensation of dead pump is proposed, which requires the knowledge of the spool position or the difference between the chamber pressures. Theoretically, it is shown that circulating leakage flow rates can be compensated by using the inverse of the kinematic model.

Although the use of inverse kinematic model for the compensation of circulating leakage flow rates gives satisfactory results in the simulation model, its implementation is not practical since it will require the measurements of the chamber pressure or the spool position. Furthermore inverse model performs extensive numerical calculations that are not applicable on a standard industrial motion controller.

In order to eliminate the circulating leakage flow rates completely, a physical solution is proposed which is the modification of the shuttle valve spool structure. The shuttle valve spool is modified to provide an orifice pre-opening only in between the AC ports. In this way, since the BC port is closed the circulating leakage flow rates are eliminated at the centered shuttle valve spool position.

The numerical simulation model is run both for the underlapped valve and asymmetric shuttle valve spool solutions. The simulation studies revealed that the function between the spool position and the actuator velocity is not bijective, i.e. a

desired actuator velocity can be satisfied for two different spool positions. In order to investigate the effect of this non-bijective relationship the stability analysis is extended. Different from the previous one which considers the partially opened orifice opening at one port only, here the stability analysis is extended to cover all possible orifice structures, i.e. all possible spool positions. Furthermore, in the linearization of the shuttle valve flow rates, instead of assuming the orifice area is proportional to spool position, the geometric non-linearity of the metering orifices which are formed by the circular holes on the valve sleeve is considered. Lastly, besides assuming a static relationship between pilot pressure  $\Delta P_{ab}$  and spool position,  $y_s$ , the valve dynamics is also considered with a time constant. As a result, by using the kinematic model and the linearized state equations a numerical stability analysis model is developed.

The numerical stability analysis model is run for an array of pilot pressure,  $\Delta P_{ab}$ , and actuator velocity,  $v_A$ , inputs. The pilot pressure array is selected to cover all possible shuttle valve spool positions and actuator velocity array is selected to cover all possible actuator velocities. In this numerical model first the corresponding  $[\Delta P_L, v_A]$  point is found for each  $[\Delta P_{ab}, v_A]$  input point. Then, the system is linearized around this equilibrium point and the stability is determined by checking the roots of the linearized model.

First, the underlapped valve solution is investigated by the developed numerical stability analysis model. The results revealed that on  $\Delta P_L$  versus  $v_A$  plane an equilibrium point requiring a partially opened spool position is unstable during the retraction of the actuator. This result is consistent with the stability analysis given in the previous chapter. On the other hand numerical model further revealed that, during the extension of the actuator, the equilibrium point requiring a partially opened spool position is also unstable. However, the desired actuator velocity can be satisfied by a different spool position which correspond a stable  $[\Delta P_{ab}, v_A]$  point. The non-bijective relation between the spool position and the actuator velocity is illustrated by showing the unstable equilibrium points both on  $\Delta P_{ab} - v_A$  and  $\Delta P_L - v_A$  planes.

The stability of the asymmetric shuttle valve spool is also investigated by the numerical stability analysis model. The results revealed that the equilibrium points requiring partially opened spool position are unstable. However, different from the underlapped valve solution, no unstable operation region exists on the  $\Delta P_L - v_A$  plane. All the unstable equilibrium point that exists on the  $\Delta P_L - v_A$  plane can be satisfied by a stable  $[\Delta P_{ab}, v_A]$  point, which corresponds to a fully opened spool position.

The numerical stability analysis model is further utilized to investigate the effects of shuttle valve parameters on system stability. The analysis model is run for different orifice pre-opening, flow discharge coefficient, valve time constant and spring stiffness values. At the end of these simulations a second novel shuttle valve solution is proposed. This solution proposes to remove the pre-compression force of the centering springs, and provides spool underlap both at AC and BC ports. It is shown that if the shuttle valve parameters like spring stiffness and flow coefficient are well adjusted, a stable operation region can be achieved for all possible spool openings.

The last part of this thesis study covers the design a position controller for the proposed EHA structure. For that purpose the whole system is linearized. Different from the stability analysis, the linearized system model includes the dynamics of the hydraulic accumulator, hydraulic pump and the electric motor together its motion control algorithm. The roots of the extended linearized model are investigated and a simplified design plant model is derived for the controller design purposes. It is concluded that the whole system dynamics is dominated by the pressure dynamics of hydraulic actuator and the rotational mechanical system dynamics of the electric motor and pump assembly which is determined by the servo motor speed controller.

A combined feedback and feedforward control strategy is utilized in the position control system of the electro hydrostatic actuator. The feedback controllers have a three layer cascade structure. The inner layers are the PI motor speed and current regulators and are implemented on the servo motor control unit. Therefore, both the two regulators are tuned by using the commissioning toolbox of the servo motor motion control software. On the other hand the design of the outermost layer which is the position controller is mainly addressed in the scope of this thesis study. A PI

regulator with semi integrator is utilized as the feedback position compensator. In order to increase the tracking performance and eliminate the response overshoot, to set point changes, motor speed and torque feedforward compensators are designed based on the simplified design plant model. Furthermore, disturbance rejection feedforward compensators are designed and their effects on system stiffness are discussed. The designed feedback and feedforward compensators together with the supervisory motion controllers are implemented on the real time target PC.

The performance of the developed EHA with the proposed asymmetric shuttle valve spool structure is evaluated on the experimental load simulator test set up. The performance of the EHA is evaluated in terms of positioning, set point tracking and disturbance load rejection.

The experimental tests are performed under different loading conditions. In order to investigate system performance for all possible shuttle valve spool positions, controlled external loads are applied on the EHA by the load simulator. It is shown that the experimental results are compatible with the theoretical results. The motor speed and torque feedforward compensators improve the positioning and set point tracking performance.

The positioning error of the EHA is in the order of encoder resolution,  $5 \mu m$ . The EHA is able to track a sinusoidal signal with  $15 Hz$  frequency without magnitude loss and phase lag. Furthermore, the stiffness of the EHA for  $10 Hz$  external load input is calculated to be  $20 kN/mm$ .

The controllers are designed by considering the fully opened shuttle valve cases only. No special control effort is applied during the spool switching, but the controller gains are change linearly. As a result of this simple control strategy it is seen that, under critical loadings, the performance of the EHA degrades slightly, when compared to the fully opened shuttle valve case. However, since the shuttle valve, proposed in the scope of this thesis study, provides stable operation region on the load pressure versus velocity plane, no instability problems are observed during the spool switching. The degraded performance is acceptable. It is obvious that with the use of load pressure feedback or spool position feedback the effects of spool switching can be eliminated, at the expense of control effort.

## 8.2 Future Recommendations

In the scope of this thesis study, the position controller designed is implemented on a real time operating PC. The developed EHA has a potential to be an industrial product, therefore, the position controller should be implemented inside the servo motor control unit. The feedback and feedforward compensators, designed in this study, are of standard form and are appropriate for industrial implementation. However, it should be noted that the controller gains are switched by checking the pilot pressures. Therefore, in practical implementation, it is required to use a differential pressure sensor. Alternatively the spool position can be directly measured. Note that both the two solutions bring additional costs to the system. Therefore, it is recommended to design an observer for the prediction of shuttle valve spool position. Inserting the observer into the servo motor control unit, the controller gains can be adjusted accordingly.

The thermal properties of the proposed and developed EHA have not been investigated in detail. If an industrial implementation is planned in which the accumulator is integrated on the hydraulic actuator as shown in Figure 3-31, it is strictly recommended to analyze the losses of the servo motor and the hydraulic components. A thermal analyzes should be done to investigate the heating of the hydraulic oil.

In this thesis study the shuttle valve with asymmetric spool structure, proposed in section 5.4, is implemented in the EHA and its performance is evaluated on the load simulator experimental test set up. The asymmetric shuttle valve solution a spool pre-opening that connects only the rod-side chamber to the accumulator line in the centered position. On the other hand the second novel shuttle valve solution proposed in section 5.8 is not tested. This shuttle valve solution proposes to remove the pre-loading of the centering springs and increase its stiffness, and provide spool underlap both at AC and BC ports. Although the simulation studies reveal favorable results, practical problems are faced during the realization of this shuttle valve solution like, spring manufacturing, backlash free mounting and space adjustment in the valve head. Therefore it is not implemented on the EHA. It is recommended that a detailed mechanical design of this shuttle has to be done.

The position controller is designed only considering the fully opened shuttle valve positions. The controller gains calculated for these two positions are changed linearly during the shuttle valve switching. The proposed shuttle valve solution provides a stable operation region on the load pressure versus velocity plane. Therefore, no instability is observed during the shuttle valve switching. However, in the performance evaluation tests, it is observed that for external loads corresponding to critical load region, the position response makes overshoots, and the actuator velocity switches abruptly. As a future study, during the spool switching, the controller gains can be scheduled by considering the shuttle valve dynamics.



## REFERENCES

- [1] C. R. Burrows, "Fluid power systems--some research issues," *Proc. Instn. Mech. Engrs.*, vol. 214, no. C, pp. 203–220, 2000.
- [2] C. R. Burrows, "Fluid power systems design—Bramah's legacy," *Arch. Proc. Inst. Mech. Eng. Part A J. Power Energy 1990-1996 (vols 204-210)*, vol. 210, no. 21, pp. 105–120, 1996.
- [3] F. Blackburn, John, R. Gerhard, and J. L. Shearer, *Fluid Power Control*. New York and London: The technology press of MIT and John Wiley & Sons, Inc., 1960.
- [4] R. H. Maskrey and W. J. Thayer, "A Brief History of Electrohydraulic Servomechanisms," *J. Dyn. Syst. Meas. Control*, vol. 100, no. 2, pp. 110–116, 1978.
- [5] H. Çalışkan, T. Balkan, and B. E. Platin, "Hydraulic Position Control System With Variable Speed Pump," in *ASME 2009 Dynamic Systems and Control Conference, Volume 1*, 2009, pp. 275–282.
- [6] J. Love, Lonnie, E. Lanhe, and P. Alles, "Estimating the Impact (Energy, Emissions and Economics) of the U.S. Fluid Power Industry," in *Oak Ridge National Laboratory, ORNL/TM-2011/14*, 2012.
- [7] S. H. Cho, S. Räcklebe, and S. Helduser, "Position tracking control of a clamp-cylinder for energy-saving injection moulding machines with electric-hydrostatic drives," *Proc. Inst. Mech. Eng. Part I J. Syst. Control Eng.*, vol. 223, no. 4, pp. 479–491, Jun. 2009.
- [8] P. M. Churn, C. J. Maxwell, N. Schofielf, D. Howe, and D. J. Powell, "Elecktro-hydraulic actuation of primary flight control surfaces," in *Proc. IEE Colloq. All Elect. Aircr. (Dig. no. 260)*, 1998, pp. 1–5.
- [9] R. Navarro, "Performance of an Electro-Hydrostatic Actuator on the F-18 Systems Research Aircraft," in *NASA/TM-97-206224*, 1997.
- [10] R. L. Kenyon, D. Scanderbeg, M. E. Nolan, and W. D. Wilkerson, "Electro-hydraulic actuator," EP 0 395 420 B1, 1990.
- [11] Wenping Cao, B. C. Mecrow, G. J. Atkinson, J. W. Bennett, and D. J. Atkinson, "Overview of Electric Motor Technologies Used for More Electric Aircraft (MEA)," *IEEE Trans. Ind. Electron.*, vol. 59, no. 9, pp. 3523–3531, Sep. 2012.

- [12] W. Karam and J.-C. Mare, "Comparision of EMA and HA performance for dynamic load simulators," in *Power Transmission and Motion Control*, 2006, pp. 211–224.
- [13] K. Bridger, V. Cooke Arthur, F. J. Crowne, L. Joseph, M. Sewell, John, and L. Small, George, "Compact Hybrid Actuator," Patent No: US 6,751,954, B2, 2004.
- [14] S. Frischeimer, "Electrohydrostatic Actuators for Aircraft Primary Flight Control-Types, Modelling and Evaluation," in *SICFP'97, Proceedings, 5th Scandinavian International Conference on Fluid Power*, 1997, pp. 1–16.
- [15] "A pre-competitive research agenda for the fluid power industry," *Report from the 2012 NFPA Roadmap Task Force*. pp. 1–16, 2013.
- [16] "Parker Oildyne Compact EHA," *Parker Hannifin Catalog HY22-3101E 7/13*. 2013.
- [17] C. Williamson and M. Ivantysynova, "Pump Mode Prediction for Four-Quadrant Velocity Control of Valveless Hydraulic Actuators," *Proc. JFPS Int. Symp. Fluid Power*, vol. 2008, no. 7–2, pp. 323–328, 2008.
- [18] H. E. Merrit, *Hydraulic Control Systems*, 1st ed. John Wiley & Sons, Inc, 1967.
- [19] J. Watton, *Fundamentals of Fluid Power Control*. Cambridge University Pres, 2009.
- [20] S. Uppal, "Cushin Valve Arrangement," Patent No: 4,040,439, 1977.
- [21] S. H. Gluck, J. A. Baldus, and J. D. Ryken, "Loop Flushing Circuit for Lubricating Rotating Elements in a Hydrostatic Transmission Module," US 6,263,670 B1, 2001.
- [22] X. Dong and J. S. Whitaker, "Hydraulic Device for Smooth Operations of Hydrostatic Transmission," Patent Pub. No: US 2004/0006981 A1, 2004.
- [23] J. Whitaker and X. Dong, "Hydrostatic transmission circuit," Patent No: US,743,0860B2, 2008.
- [24] W. C. Clay and W. Robinson, Curtiss, "Electric Integrated Actuator with Variable Gain Hydraulic Output," Patent No: 4,667,472, 1987.
- [25] R. Chamberlain, Theron, "Electrohydraulic Actuator For Aircraft Control Surfaces," Patent No: 4,630,441, 1986.
- [26] H. Werner, B. Frieder, and H. Hermann, "Electrohydrostatischer Aktuator," *Europaische Patentschrift 0 271 744 B1*, 1992.

- [27] L. Dinca, J. Corcau, and M. A. Lungu, "Electro-hydrostatic Servo-actuators for Aircraft," in *Proceedings of the 7th International Conference on System Science and Simulation in Engineering (ICOSSE'08)*, 2008.
- [28] J. a. Anderson, "Variable displacement electro-hydrostatic actuator," *Proc. IEEE 1991 Natl. Aerosp. Electron. Conf. NAECON 1991*, pp. 529–534, 1991.
- [29] K. R. McCullough, "Design and Characterization of a Dual Electro-Hydrostatic Actuator," McMaster University, Department of Mechanical Engineering, 2011.
- [30] L. Dinca, J. Corcau, M. Lungu, and a Tudosie, "Mathematical Models and numerical simulations for electro-hydrostatic servo-actuators," *Int. J. Circuits, Syst. Signal Process.*, vol. 2, no. 4, pp. 229–238, 2008.
- [31] J. Andersson, P. Krus, K. Nilsson, and K. Strock, "Modelling Electro-Hydrostatic of Heat Generation Systems," in *4th JHPS International Symposium*, 1999, no. C, pp. 537–542.
- [32] E. Wurl and H. Schreiner, "Method of controlling injection molding machine with hydraulic loads," Patent No: US 5093052 A, 1992.
- [33] M.-H. Chiang, C.-C. Chen, and C.-F. J. Kuo, "The high response and high efficiency velocity control of a hydraulic injection molding machine using a variable rotational speed electro-hydraulic pump-controlled system," *Int. J. Adv. Manuf. Technol.*, vol. 43, no. 9–10, pp. 841–851, Aug. 2009.
- [34] S. H. Cho, S. Räcklebe, and S. Helduser, "Position tracking control of a clamp-cylinder for energy-saving injection moulding machines with electric-hydrostatic drives," *Proc. Inst. Mech. Eng. Part I J. Syst. Control Eng.*, vol. 223, no. 4, pp. 479–491, 2009.
- [35] S. Habibi and A. Goldenberg, "Design of a New High Performance ElectroHydraulic Actuator," *IEE/ASME Proc. Mechatronics*, vol. 50, no. 2, pp. 158–164, 2000.
- [36] S. Habibi, R. Burton, and E. Sampson, "High Precision Hydrostatic Actuation Systems for Micro- and Nanomanipulation of Heavy Loads," *J. Dyn. Syst. Meas. Control*, vol. 128, no. 4, p. 778, 2006.
- [37] M. K. Khalil, Bahr, V. Yurkevich, J. Svoboda, and R. B. Bhat, "Implementation of single feedback control loop for constant power regulated swash plate axial piston pumps," *Int. J. Fluid Power*, vol. 3, 2002.
- [38] H. Berg and M. Ivantysynova, "Design and testing of a robust linear controller for secondary controlled hydraulic drive," *Proc. Inst. Mech. Eng. Part I J. Syst. Control Eng.*, vol. 213, no. 5, pp. 375–386, Jan. 1999.

- [39] J. Grabbel and M. Ivantysynova, “An investigation of swash plate control concepts for displacement controlled actuators,” *Int. J. Fluid Power*, vol. 6, no. 2, pp. 19–36, 2005.
- [40] “E-dyn 96 industrial pump.” Artemis- Intelligent Power, a group company of Mitsubishi Heavy Industries, Ltd., V1-April 2015.
- [41] S. Salter and W. H. S. Rampen, “Fluid working machine,” Patent No: US 5,259,738, 1993.
- [42] M. Sasaki, A. Yuge, T. Hayashi, H. Nishino, and M. Uchida, “Large Capacity Hydrostatic Transmission with Variable Displacement,” in *The 9th International Fluid Power conference, 9. IFK*, 2014.
- [43] M. A. Holland, “Design of digital pump/motors and experimental validation of operating strategies,” Ph.D. Thesis, Purdue University, 2012.
- [44] C. C. Locateli, P. L. Teixeira, E. R. De Pieri, P. Krus, and V. J. De Negri, “Digital Hydraulic System Using Pumps and on/off Valves Controlling the Actuator,” in *Proceedings of the 8th FPNI Ph.D Symposium on Fluid Power*, 2014, pp. 1–10.
- [45] M. A. Holland, G. J. Wilfong, K. J. Merrill, and J. H. Lumkes, “Experimental Evaluation of Digital Pump / Motor Operating Strategies with a Single-Piston Pump / Motor,” in *Proceedings of the 52nd National Conference on Fluid Power*, 2011.
- [46] H. Çalışkan, “Modeling And Experimental Evaluation Of Variable Speed Pump And Valve Controlled Hydraulic Servo Drives,” M.Sc. Thesis, Middle East Technical University, Mechanical Engineering Department, 2009.
- [47] Wetzel Dr. E and Tergau, “Hydraulische Anlage,” Patent No: DE 1,601,732 A1, 1970.
- [48] S. Tikkanen, “Hydrostatic Drive Having Volumetric Flow Equalisation,” Patent No: US 8,033,107 B2, 2011.
- [49] J. Dantlgraber, “Hydraulic system for a differential piston type cylinder,” Patent No: 5,179,836, 1993.
- [50] C. Andrew and J. Lennart, “Controlled Electric Pump Drive for Hydraulic Lifting Arrangement with Gas Spring in Motor,” Patent No: 4,961,316, 1990.
- [51] F. Takagi and K. Kunimasa, “Bucket Dredging Device,” JP 1280132 (A), 1989.
- [52] S. Helduser, “Electric-hydrostatic drive—an innovative energy-saving power and motion control system,” *Proc. Inst. Mech. Eng. Part I J. Syst. Control Eng.*, vol. 213, no. 5, pp. 427–437, Jan. 1999.

- [53] Q. Long, T. Neubert, and S. Helduse, "Principle to Closed Loop Control Differential Cylinder with Double Speed Variable Pumps and Single Loop Control Signal," *Chinese J. Mech. Eng.*, vol. 17, pp. 85–88, 2004.
- [54] T. Neubert, "Untersuchungen von drehzahlenveränderbaren Pumpen," Ph.D. Thesis, Technischen Universität Dresden, 2001.
- [55] K. G. Cleasby and A. R. Plummer, "A novel high efficiency electrohydrostatic flight simulator motion system," in *Fluid Power and Motion Control (FPMC 2008)*, 2008, pp. 437–449.
- [56] A. R. Plummer and P. S. Guinzio, "Modal Control of an Electrohydrostatic Flight Simulator Motion System," in *ASME 2009 Dynamic Systems and Control Conference, Volume 2*, 2009, pp. 345–352.
- [57] P. Achten, "What a Difference a Hole Makes – the Commercial Value of the Innas Hydraulic Transformer," *Proc. 6th Scand. Int. Conf. Fluid Power*, pp. 873–876, 1999.
- [58] P. Achten, "Designing the impossible pump," in *Proc. Hydraulikdagarna, Linöping, Sweden*, 2003, pp. 1–16.
- [59] G. Vael, P. Achten, and J. Potma, "Cylinder Control with Floating Cup Hydraulic Transformer," in *The 8th Scandinavian International Conference on Fluid Power, SICFP'03*, 2003.
- [60] P. A. J. Achten, "A serial hydraulic hybrid drive train for off-road vehicles," *Proc. Natl. Conf. fluid power*, vol. 51, pp. 515–521, 2008.
- [61] P. Achten, T. Van Den Brink, J. Potma, M. Schellekens, and G. Vael, "A four-quadrant hydraulic transformer for hybrid vehicles," *11th Scand. Int. Conf. Fluid Power*, no. July, 2009.
- [62] Q. Long, Y. Yang, and X. Hou, "Simulation and experimental research on the axial piston pump with series three-windows in valve plate," *Proc. 2011 Int. Conf. Fluid Power Mechatronics, FPM 2011*, pp. 71–76, 2011.
- [63] J. Huang, L. Quan, and X. Zhang, "Development of a dual-acting axial piston pump for displacement-controlled system," *Proc. Inst. Mech. Eng. Part B J. Eng. Manuf.*, vol. 228, no. 4, pp. 606–616, 2013.
- [64] A. Aly, F. Salem, and T. Hanafy, "Energy Saving Strategies of an Efficient Electro-Hydraulic Circuit (A review)," *Int. J. Control. Autom. Syst.*, vol. 3, no. July 2014, 2014.
- [65] Z. Quan, L. Quan, and J. Zhang, "Review of Energy Efficient Direct Pump Controlled Cylinder Electro-Hydraulic Technology," *Renew. Sustain. Energy Rev.*, vol. 35, pp. 336–346, 2014.

- [66] K. Rydberg, “Energy Efficient Hydraulic Hybrid Drives,” *11th Scand. Int. Conf. Fluid Power, SICFP’09, June 2-4, 2009, Linköping, Sweden*, pp. 1–14, 2009.
- [67] R. K. Gellatly, J. B. Meredith, and R. A. Green, “Hydraulic System with Bi-Rotational Pump with Filter Title,” Patent No: 3,903,698, 1975.
- [68] W. C. Trautman, “Hydraulic System,” Patent No: 2,467,508, 1949.
- [69] E. H. Schanzlin and C. J. Oster, “Hydraulic Control System,” Patent No: 2,657,533, 1953.
- [70] A. J. Hewett, “Hydraulic circuit flow control,” Patent No: A1 2,112,929, 1994.
- [71] R. Rahmfeld and M. Ivantysynova, “Development and Control of Energy Saving Hydraulic Servo Drives,” *Proc. 1st FPNI-PhD Symp.*, pp. 167–180, 2000.
- [72] R. Rahmfeld and M. Ivantysynova, “Displacement controlled linear actuator with differential cylinder- a way to save primary energy in mobile machines.,” *ICFP 2001 Fifth Int. Conf. Fluid Power Transm. Control*, pp. 296–301, 2001.
- [73] R. Rahmfeld, “Development and Control of Energy Saving Hydraulic Servo Drives for Mobile Systems,” *Technischen Universität Hamburg-Harburg*, 2002.
- [74] R. Rahmfeld, M. Ivantysynova, and J. Weber, “Displacement Controlled Wheel Loader – a simple and clever Solution,” *4th IFK (Int. Fluid Power Conf.)*, pp. 183–196, 2004.
- [75] R. Rahmfeld and M. Ivantysynova, “An overview about active oscillation damping of mobile machine structure,” *Int. J. Fluid Power*, vol. 5, no. 2, pp. 5–24, 2004.
- [76] C. Williamson, S. Lee, and M. Ivantysynova, “Active Vibration Damping for an off-road Vehicle with Displacement Controlled Actuators,” *Int. J. Fluid Power*, vol. 10, no. 3, pp. 5–16, 2009.
- [77] R. Hippalgaonkar and M. Ivantysynova, “A Series - Parallel Hydraulic Hybrid Mini - Excavator with Displacement Controlled Actuators 1 Background 2 Simulation of the DC S-P Hybrid,” pp. 31–42, 2013.
- [78] J. Zimmerman, R. Hippalgaonkar, and M. Ivantysynova, “Optimal Control for the Series-Parallel Displacement Controlled Hydraulic Hybrid Excavator,” in *Proceedings of the ASME 2011 Dynamic Systems and Control Conference*, 2011, p. 5996.
- [79] J. Zimmerman, E. Busquets, and M. Ivantysynova, “Forty percent Fuel Savings by Displacement Control Leads to Lower Working Temperatures – A

- Simulation Study and Measurements,” *Proc. 52nd Natl. Conf. Fluid Power 2011*, 2011.
- [80] K. K. Ahn, H. T. C. Nguyen, J. H. Yoon, J. S. Kim, and J. Il Yoon, “A study on a new energy saving load simulator using hybrid actuator and QFT technique,” *2006 SICE-ICASE Int. Jt. Conf.*, pp. 4647–4652, 2006.
- [81] K. K. Ahn and N. H. T. Chau, “Design of a robust force controller for the new mini motion package using quantitative feedback theory,” *Mechatronics*, vol. 17, no. 10, pp. 542–550, 2007.
- [82] D. Q. Truong and K. K. Ahn, “Self-tuning quantitative feedback theory for parallel force/position control of electro-hydrostatic actuators,” *Proc. Inst. Mech. Eng. Part I J. Syst. Control Eng.*, vol. 223, no. 4, pp. 537–556, 2009.
- [83] K. Ahn, N. Thai, and C. Dinh, “Robust force control of a hybrid actuator using quantitative feedback theory,” *J. Mech. Sci. Technol.*, vol. 21, no. 12, pp. 2048–2058, 2007.
- [84] M. Olson and J. Prazak, “Electro-hydraulic actuator,” Patent Pub. No: US 0289912 A1, 2011.
- [85] W. Longke, “Adaptive Robust Control of Variable Displacement Pumps,” Ph.D. Thesis, Georgia Institute of Technology, School of Mechanical Engineering, 2011.
- [86] L. Wang, W. J. Book, and J. D. Huggins, “A Hydraulic Circuit for Single Rod Cylinders,” *J. Dyn. Syst. Meas. Control*, vol. 134, no. 1, p. 011019, 2012.
- [87] L. Wang and W. J. Book, “Using Leakage to Stabilize a Hydraulic Circuit for Pump Controlled Actuators,” *J. Dyn. Syst. Meas. Control*, vol. 135, no. 6, p. 061007, 2013.
- [88] S. Demirer, T. Balkan, and H. Çalışkan, “Energy efficient hydrostatic transmission circuit for an asymmetric actuator utilizing a single 4 - quadrant pump,” Patent Pub. No: WO2013/112109 A1, 2013.
- [89] H. Çalışkan, T. Balkan, and B. E. Platin, “A Complete Analysis and A Novel Solution for Instability in Pump Controlled Asymmetric Actuators,” *J. Dyn. Syst. Meas. Control*, vol. 137, no. September, 2015.
- [90] J. Watton, *Modelling, Monitoring and Diagnostic Techniques for Fluid Power Systems*. Springer, 2007.
- [91] D. W. Novotny and T. A. Lipo, *Vector Control and Dynamics of AC Drives*. Oxford University Press Inc., 1996.

- [92] A. Pourmovahed, N. H. Beachley, and F. J. Fronczak, "Modeling of a Hydraulic Energy Regeneration System: Part I—Analytical Treatment," *J. Dyn. Syst. Meas. Control*, vol. 114, no. 1, p. 160, 1992.
- [93] F. Incropera and D. Dewitt, *Introduction to Heat Transfer*. John Wiley & Sons, Inc, 1985.
- [94] F. T. Brown, *Engineering System Dynamics*. Marcel Dekker, Inc., 2001.
- [95] H. U. Akova, "Design, Contruction and Control of an Electro-Hydraulic Load Simulator for Testing Hydraulic Drives," M.Sc. Thesis, Middle East Technical University, Mechanical Engineering Department, 2014.
- [96] J. Grabbel, "On The Control Of Joint Integrated Servo Actuators For Mobile Handling and Robotic Applications," in *1st FPNI-PhD Symp.*, 2000, pp. 449–465.
- [97] K. J. Astrom, "Advanced Control Methods Survey and Assessment of Possibilities," in *Proceedings of the thirteenth annual Advanced Control Conference*, 1987.
- [98] G. C. Goodwin, S. F. Graebe, and M. E. Salgado, *Control System Design*. Valparaiso, 2000.
- [99] K. J. Astrom and T. Hagglund, *PID Controllers : Theory, Design and Tuning*, 2<sup>nd</sup> ed. 1995.
- [100] P. Lambrechts, M. Boerlage, and M. Steinbuch, "Trajectory planning and feedforward design for electromechanical motion systems," *Control Eng. Pract.*, vol. 13, no. 2, pp. 145–157, 2005.

## CURRICULUM VITAE

### PERSONAL INFORMATION

Surname, Name: ÇALIŞKAN, Hakan  
Nationality: Turkish (TC)  
Date and Place of Birth: 1983, Samsun  
Marital Status: Married  
email: [chakan@metu.edu.tr](mailto:chakan@metu.edu.tr), [hakanc55@gmail.com](mailto:hakanc55@gmail.com)

### Education

Ph.D., Middle East Technical University 2009-2015  
Mechanical Engineering Department  
Development and Control of a Single Rod Electro Hydrostatic Actuator

M.Sc., Middle East Technical University 2006-2009  
Mechanical Engineering Department  
Modeling and Experimental Evaluation of Variable Speed Pump and Valve  
Controlled Hydraulic Servo Drives

B.Sc., Middle East Technical University 2001-2006  
Mechanical Engineering Department

Samsun Anadolu Lisesi 1994-2001  
Math/Science

### Work Experience

ME105 Instructor METU/Mechanical Eng. Dept. 10/2013-2015

Teaching Assistant METU/Mechanical Eng. Dept. 10/2006-10/2013

Research Engineer TÜBİTAK SAGE, Modeling and Sim. Dept. 06-10/2006

Trainee, TÜBİTAK SAGE, Structural Mech. Dept, 2005 Sum., 1.5 month

Trainee, Türk Traktör, Manufacturing, 2006 Sum., 1 month

### Foreign Language

English, German (basic)

### **International Journal**

H. Çalışkan, T. Balkan, and B. E. Platin, "A Complete Analysis and A Novel Solution for Instability in Pump Controlled Asymmetric Actuators," J. Dyn. Syst. Meas. Control, vol. 137, no. September, 2015.

Ergin Kilic, Melik Dolen, Hakan Çalışkan Ahmet Bugra Koku, Tuna Balkan, Pressure prediction on a variable-speed pump controlled hydraulic system using structured recurrent neural networks, Control Engineering Practice, Volume 22, Issue 7, Pages 997-1014, 2014

Ergin Kilic, Melik Dolen, Ahmet Bugra Koku, Hakan Çalışkan, Tuna Balkan, Accurate Pressure Prediction of A Servo-Valve Controlled Hydraulic System Mechatronics, Volume 22, Issue 7, Pages 997-1014, 2012

### **National Journal**

H. Ulaş Akova, Hakan Çalışkan, Tuna Balkan, Bülent Emre Platin, Elektro Hidrolik Yük Simülatörü Tasarımı ve Kontrolü, Mühendis ve Makina, ISSN 1300-3402, Cilt 56, Sayı:662,Sf: 36-48, Mart 2015

Hakan Çalışkan, Tuna Balkan, Bülent Emre Platin, Valf Ve Pompa Denetimli Tek Milli Hidrolik Eyleyici Sistemlerinin Teorik Karşılaştırması, Mühendis ve Makina, ISSN 1300-3402, Cilt 52, Sayı:620,Sf: 40-50, Ekim 2011

Hakan Çalışkan, Tuna Balkan, Bülent Emre Platin, Değişken Devirli Pompa ile Servo Hidrolik Konum Kontrolü, Mühendis ve Makina, ISSN 1300-3402, Cilt 50, Sayı:689,Sf: 2-12, Ocak 2009

### **International Conference**

Hakan Çalışkan, H. Ulaş Akova, Tuna Balkan, Bülent Emre Platin, Electro-Hydraulic Lift System with Single Acting Actuator, ICFP 2013, The Eighth International Conference on Fluid Power Transmission and Control, Hangzhou, China, 2013

Hakan Çalışkan, Tuna Balkan, Bülent Emre Platin, A Control System For Hydraulic Single Axis Durability Test Rig, DSCC 5th Annual Dynamic Systems and Control Conference and 11th Motion and Vibration Conference, Ford Laurderdale, MIA, /2012

Hakan Çalışkan, Tuna Balkan, Bülent Emre Platin, Hydraulic Position Control System with Variable Speed Pump, ASME DSCC and BATH/ASME Symposium on Fluid Power and Motion Control, Los Angeles, CA, USA, 2009

## **National Conference**

Hakan Çalışkan, Tuna Balkan, Bülent Emre Platin, Tek Pompa Denetimli Asimetrik Hidrolik Eyleyici Sistemlerinin İncelenmesi, VII. Ulusal Hidrolik Pnömatik Kongresi, Bildiriler Kitabı, MMO Yayın No: E/2014/627, Sf: 359-376, İstanbul/Türkiye, 2014

Hakan Çalışkan, H. Ulaş Akova, Tuna Balkan, Bülent Emre Platin, Suat Demirer, Abkant presler için enerji verimli hidrolik tahrik sistemi ve kontrolü, VII. Ulusal Hidrolik Pnömatik Kongresi, Bildiriler Kitabı, MMO Yayın No:E/2014/627, Sf: 359-376, İstanbul/Türkiye, 2014

H. Ulaş Akova, Hakan Çalışkan, Tuna Balkan, Bülent Emre Platin, Tek Etkili Eyleyiciler için Enerji Verimli Yük Kaldırma Sistemi, VII. Ulusal Hidrolik Pnömatik Kongresi, Bildiriler Kitabı, MMO Yayın No: E/2014/627, Sf: 393-406, İstanbul/Türkiye, 2014

H. Ulaş Akova, Hakan Çalışkan, Tuna Balkan, Bülent Emre Platin, Elektrohidrolik Abkant Pres Tasarımı - I : Modelleme ve Benzetim, TOK 2013, İnönü Üniversitesi, Malatya/Türkiye, 2013

Hakan Çalışkan, H. Ulaş Akova, Tuna Balkan, Bülent Emre Platin, Elektrohidrolik Abkant Pres Tasarımı - II : Kontrol Sistemi, TOK 2013, İnönü Üniversitesi, Malatya/Türkiye, 2013

Hakan Çalışkan, H. Ulaş Akova, Tuna Balkan, Bülent Emre Platin, Elektro-Hidrostatik Tahrikli Bir Hareket Taklitçisinin Alt Sistemlerinin Ortak Benzetimi, USMOS 2013, ODTÜ, Ankara/Türkiye, 2013

Hakan Çalışkan, Tuna Balkan, Bülent Emre Platin, Valf Ve Pompa Denetimli Tek Milli Hidrolik Eyleyici Sistemlerinin Teorik Karşılaştırması, VI. Ulusal Hidrolik Pnömatik Kongresi, Bildiriler Kitabı, MMO Yayın No: E/2011/561, Sf: 367-381, İzmir/Türkiye 10/2011

Hakan Çalışkan, Tuna Balkan, Bülent Emre Platin, İlhan Konukseven, Tek Eksenli Yorulma Test Düzeneği İçin Konum Denetleyicisi Tasarımı, VI. Ulusal Hidrolik Pnömatik Kongresi, Bildiriler Kitabı, MMO Yayın No: E/2011/561, Sf: 519-535, İzmir/Türkiye 10/2011

Hakan Çalışkan, Ulaş Yaman, Rasim A. Dilan, Tuna Balkan, Suat Demirer, Pompa Denetimli Asimetrik Hidrolik Eyleyici Sistemleri, VI. Ulusal Hidrolik Pnömatik Kongresi, Bildiriler Kitabı, MMO Yayın No: E/2011/561, Sf: 479-490, İzmir/Türkiye, 2011

Rasim A. Dilan, Ulaş Yaman, Hakan Çalışkan, Tuna Balkan, Suat Demirer, 3 Serbestlik Derecesine Sahip Bir Hareket Taklitçisinin Mafsal Uzayı Eniyilemesi Ve

Çözüm Analizi, VI. Ulusal Hidrolik Pnömatik Kongresi, Bildiriler Kitabı, MMO Yayın No:E/2011/561, Sf: 539-552, İzmir/Türkiye, 2011

Ergin Kılıç, Hakan Çalışkan, Melik Dölen, A. Buğra Koku, Tuna Balkan, Yapay Sinir Ağ Modellerinin Valf Denetimli Hidrolik Bir Sistemin Uzun Süreli Basınç Tahmininde Kullanılması, VI. Ulusal Hidrolik Pnömatik Kongresi, Bildiriler Kitabı, MMO Yayın No:E/2011/561, Sf: 211-225, İzmir/Türkiye, 10/2011

Tuna Balkan, İlhan Konukseven, Hakan Çalışkan, Ufuk Dursun, A Control System For Vehicle Durability Test Rigs, OTEKON, Bursa/Türkiye, 06/2010

Hakan Çalışkan, Tuna Balkan, Bülent Emre Platin, Değişken Devirli Pompa ile Servo Hidrolik Konum Kontrolü, V. Ulusal Hidrolik Pnömatik Kongresi, Bildiriler Kitabı, MMO Yayın No:E/2008/487, Sf: 359-375, İzmir/Türkiye, 10/2008

### **Patents**

S. Demirer, T. Balkan, and H. Çalışkan, “Energy efficient hydrostatic transmission circuit for an asymmetric actuator utilizing a single 4 - quadrant pump,” WO2013112109 (A1), 2013.

H. Çalışkan, Shuttle valve embodiment for compensating differential flow rate of single-rod actuators in hydrostatic systems, 2014

### **Projects**

Design and control of energy efficient hydraulic system, for press brake manufacturers, DTSIS-KOSGEB, 2012-2013

Design of a 3 dof motion simulator, DTSIS-KOSGEB, 2011-2012

Design of a single axis durability test rig, BIAS, 2010

Thrust vector control, TUBITAK-SAGE, 2009